CATALYTIC CONVERSION OF ETHANE TO ETHYLENE BY CARBON DIOXIDE OXIDATIVE DEHYDROGENATION

Submitted in partial fulfillment of the requirements for the award of the degree of

DOCTOR OF PHILOSOPHY

In

CHEMICAL ENGINEERING

by

Mrs. P. THIRUMALA BAI
(Roll No. 714150)

Supervisor

Dr. S.SRINATH
Associate Professor

DEPARTMENT OF CHEMICAL ENGINEERING
NATIONAL INSTITUTE OF TECHNOLOGY
WARANGAL-506 004,TELANGANA, INDIA
MARCH 2019

Dedicated to my beloved Parents

NATIONAL INSTITUTE OF TECHNOLOGY- WARANGAL

CERTIFICATE

This is to certify that the thesis entitled "**Catalytic conversion of Ethane to Ethylene by Carbon Dioxide Oxidative Dehydrogenation"** being submitted by **Mrs. P. THIRUMALA BAI** in partial fulfillment for the award of the degree of Doctor of Philosophy (Ph.D) to the Department of Chemical Engineering, National Institute of Technology, Warangal, India, is a record of the bonafide research work carried out by her under my supervision. The thesis has fulfilled the requirements according to the regulations of this Institute and in my opinion has reached the standards for submission. The results embodied in the thesis have not been submitted to any other University or Institute for the award of any degree or diploma.

Date:

Dr. S. SRINATH
Supervisor
Department of Chemical Engineering,
National Institute of Technology, Warangal.

DECLARATION

This is to certify that the work presented in the thesis entitled "**Catalytic Conversion of Ethane to Ethylene by Carbon Dioxide Oxidative Dehydrogenation"** is a bonafide work done by me under the supervision of Dr**. S.SRINATH** and was not submitted elsewhere for award of any degree.

I declare that this written submission represents my ideas in my own words and where other's ideas or words have been included, I have adequately cited and referenced the original sources. I also declare that I have adhered to all principles of academic honesty and integrity and have not misrepresented or fabricated or falsified any idea/data/fact/source in my submission. I understand that any violation of the above will be a cause for disciplinary action by the institute and can also evoke penal action from the sources which have thus not been properly cited or from whom proper permission has not been taken when needed.

Mrs. P.THIRUMALA BAI
(Roll No. 714150)

ACKNOWLEDGMENTS

It gives me immense pleasure and great opportunity to express my profound sense of gratitude and indebtedness to my supervisor, **Dr. S. Srinath,** Associate Professor, NIT Warangal, for his guidance, unfailing attention and constant encouragement throughout the execution of research work embodied in this thesis.

I express my profound regards to **Dr .P. S. Sai Prasad,** Emeritus Scientist, I& PC Division, for his inspiring discussions and suggestions throughout the research work.

I whole- heartedly thank **Prof. N.V. Ramana Rao**, Director, of NITW permitting me to utilize the facilities in NIT and allowing me to submit this research work in the form of a thesis.

I would like to express my sincere thanks to **Prof. Shirish H.Sonawane,** HOD, Chemical Engineering, National Institute of Technology, Warangal for his continuous support towards carrying out research work.

I would like to express my sincere and whole hearted thanks and gratitude to my Doctoral Scrutiny Committee (DSC) members **Prof. Y. Pydi setty** Department of Chemical Engineering, **Dr. A. Seshagiri Rao,** Associate Professor, Department of Chemical Engineering, **Dr. Venkatathri Narayanan,** Associate Professor, Department of Chemistry, National Institute of Technology, Warangal for their kind help, encouragement and valuable suggestions for successful completion of research work.

I would like to extend my sincere thanks to all the faculty members of Chemical Engineering Department for their valuable suggestions and encouragement.

I wish to express my thanks to **Dr. N. Lingaiah,** Principal Scientist,IICT for his support in characterizing the materials using different techniques.

I appreciate the cooperation rendered by my colleagues **Dr. B. Hari Babu, Manokaran, Kalakuntla.Raju , Dr. K. Upender, Mr. Y. Ramesh, , Dr.M. Srinivas, Dr. G. Ravindra, Dr. M. Surender, , Dr.T.Vikram Sagar, B.Srinu, Dhanalakshmi, D.Padmakar, N.Raju,** for their lively company, moral support, motivation, encouragement and help.

I thank MHRD, New Delhi for financial assistance in the form of Ph.D Fellowship. I express my sincere regards to all my family members and well-wishers for their moral support, motivation and encouragement.

P.THIRUMALA BAI

ABSTRACT

The consumption of olefins and olefin derived products is increasing year by year. Particularly the demand for ethylene is increasing as it is the preferred raw material for the manufacture of numerous industrially significant products. The global production of ethylene has increased to approximately 160 million tons per year with a growth rate of 4% per year. A majority of industries in the world produce ethylene commercially by dehydrogenation of hydrocarbons feedstock like natural gas and naphtha by steam cracking. This process is energy intensive as it is endothermic in nature. The process operating at high temperatures also has thermodynamic limitations in the paraffin conversions. Besides, it leads to coke formation. To overcome these difficulties Catalytic oxidative dehydrogenation (ODH) using various oxidants especially oxygen has emerged as an extremely attractive alternative for ethylene. This process eliminates thermodynamic limitations in the paraffin conversion and this it can be executed at reasonably low temperatures and it also requires less energy when compared to traditional production routes. Coke formation is also reduced and as a consequence the frequency of catalyst regeneration is diminished. Even though the ODH with oxygen is environmentally friendly, it requires an air separation unit which increases the cost of the process. Due to the exothermic nature the reaction is also associated with some major drawbacks like thermal run-away of reaction and the difficulty in controlling the selectivity of ethylene due to the formation of unwanted oxides of carbon because of over oxidation. Another alternative is the utilization of N_2O as the oxidant, wherein high conversions could be realized due to the formation of O^- radical species, but the limited availability of the oxidant and low ethylene selectivity at high conversions make this methodology of ethylene generation less attractive.

Over the past decades, much attention has been paid on limiting the emissions of carbon dioxide into the atmosphere as it is a greenhouse gas and is recognized as a major culprit for global warming. In recent years, carbon dioxide capture and its sequestration has been given immense importance. Instead of looking it as a waste, it is now considered as a cheap raw material in chemical production. It can be used as a non-traditional oxygen source or a mild oxidant for ethylene production in the dehydrogenation of ethane due to its huge advantages in containing the exothermicity of the reaction. It also acts as a diluents to achieve great equilibrium conversion of light alkanes, thus giving way to high selectivity towards ethylene formation. Coke formation on the catalyst can also be reduced and the catalytic activity can be maintained over a longer period

of time. An extensive gamut of catalysts with wide variety of supports has been studied for the oxidative dehydrogenation of ethane using different oxidants. Among them supported chromium catalysts are highly active for ODH of ethane and are found to offer superior CO_2 conversion. The nature of chromium species formed and their distribution on the support surface play important role in the activity and selectivity of the catalyst. The activity of catalysts and selectivity of supported chromium catalysts are considerably influenced by the type of supports due to their different physico–chemical characteristics like acid-base properties, thermal stability, surface areas, active-phase –support interactions, oxidant (oxygen) storage capacity, reducibility and so on. This observation emphasizes the need for identification of a proper support. It is well known that mixed oxide supports combine good textural and mechanical properties and establish different types of interaction with the active component. It is noticed that sulfation of silica has a positive effect on the catalyst material while strong basic promoters (alkali metal oxides) suppress the catalytic activity. It is required to study the influence of sulfate modification of mesoporous silica supported chromium oxide catalysts in view of their beneficial effects in controlling the aggregation phenomena.

In view of the importance of chromium based catalysts this thesis is proposed to study the preparation, characterization, and evaluation of chromium based catalysts with different support materials i.e. non silica (metal oxides) and silica materials for the Oxidative Dehydrogenation of ethane to ethylene. Carbon dioxide oxidative dehydrogenation of ethane was successfully carried out over the chromium based catalysts. All the chromium based catalysts with different supports were prepared by impregnation technique. The catalysts were characterized by different physico – chemical methods like BET surface area, X-ray diffraction, temperature programmed reduction and X-ray photoelectron spectroscopy for better understanding of their properties and to know the nature of interaction of Cr_2O_3 with the supports. The characterization results revealed that the chromium can be stabilized on supports with its higher oxidation states along with its highly stable oxidation state (Cr^{+6}, Cr^{+5} and Cr^{+3}) and also inferred that the redox couples (Cr^{+6}/Cr^{+5} to Cr^{+3}) are responsible for carbon di oxide oxidative dehydrogenation of ethane. The performance of these catalysts with different supports was evaluated for the Oxidative Dehydrogenation of Ethane in a fixed bed quartz down flow reactor at 550 – 650 ˚C. The main focus is devoted to deeper insights on nature and type of catalysts and their physico-chemical characteristics in relation to their performance properties.

For metal oxide supported Cr_2O_3 catalysts with varying Cr_2O_3 contents (5-20 wt%) , it has been observed that the performance of catalyst and selectivity are strongly depend on the nature of chromium oxide species formed and the surface enrichment of chromium in the near surface region, The content of chromium in turn strongly influence these two properties. Among all, the 15 wt% chromium loading is necessary to obtain reasonable ethane and carbon dioxide Conversions due to clear enrichment of chromium in the near –surface region and formation of optimum amount of CrO_x species. Based on this result 15wt% Cr_2O_3 has been considered as an optimum loading and it is used for further studies.

It is generally accepted that a mixed oxide support has an edge over its component single oxides as support in combining their good textural and mechanical properties. The performance of mixed i.e Al_2O_3& ZrO_2 supports at different combinations were evaluated for ODH of ethane. Equal compositions of mixed oxide i.e. 15 wt% Cr_2O_3/Al_2O_3-ZrO_2 (1:1) catalyst showed the best catalytic activity among all the catalysts used in this study. The selectivity of ethylene mainly depends on the oxidizing atmosphere, which can be clearly explained by the C_2H_4 temperature programmed desorption. The performance of silica supported catalysts was also evaluated with special emphasis to sulfate modifications of the catalysts. The catalytic activity and selectivity over metal oxide and silica material supported chromium based catalysts with varying compositions were found to depend strongly on the nature of support and chromium oxide species formed and the surface enrichment of chromium in the near-surface region. Among all, sulfated SBA-15 supported chromium based catalyst has displayed the superior performance.

In heterogeneous catalytic reactions the heat and mass transfer play a vital role in affecting the rate of a reaction. In the study of intrinsic rates of reaction both the diffusion mechanism should be negligible prior to the kinetic studies. Kinetic parameters were evaluated at different feed conditions. The rate of C_2H_4 and CO_2 formations were measured by varying the total flow rate of the reactants, temperature and Catalyst particle size. The oxidative dehydrogenation of ethane using CO_2 is kinetically modeled by various models for mixed supported chromium based catalyst and it is found that the ethane and CO_2 decomposition rates are given by LHHW model. The parameters obtained from the model are checked for thermodynamic and statistical consistency.

The response surface methodology is formulated for different independent variables and the corresponding surface plots and contour plots are plotted to check for optimum conditions. The optimum results are in good agreement with the experimental values.

CONTENTS

CHAPTER 3

CHAPTER 4

LIST OF FIGURES

LIST OF TABLES

LIST OF ABBREVIATIONS/SYMBOLS

BET	Brunauer-Emmett-Teller
CO_2 (g)	Carbon dioxide
CO (g)	Carbon monoxide
C_2H_6 (g)	Ethane
C_2H_4 (g)	Ethylene
CH_4 (g)	Methane
GC	Gas Chromatograph
He (g)	Helium
MFC	Mass Flow Controllers
ODH	Oxidative Dehydrogenation of Ethane
P	Pressure (atm or bar)
PID	Proportional Integral Derivative Controller
T	Temperature (^oC or K)
TCD	Thermal Conductivity Detector
TPD	Temperature Programmed Desorption
TPR	Temperature Programmed Reduction
XPS	X-ray Photoelectron Spectroscopy
XRD	X-Ray Diffraction
LHHW	Langmuir Hinshelwood Model
MVK	Mars Van Krevelen Model
ER	Eley Rideal Model
RSM	Response Surface Methodology
ANOVA	Analysis of variance

X C_2H_6	Conversion of Ethane
X CO_2	Conversion of Carbon dioxide
S C_2H_4	Selectivity of Ethylene
S CH_4	Selectivity of Methane
Y C_2H_4	Yield of Ethylene
GC	gas chromatography
TEM	transmission electron microscopy
XRD	X-ray diffraction
MoO_x	Molybdenum oxide
Cr_2O_3/ Al_2O_3	Cr/Al
Cr_2O_3 /ZrO_2	Cr/Zr
Cr_2O_3/Al_2O_3-ZrO_2	Cr/Al Zr
Cr_2O_3/SiO_2	Cr/Sio
Cr_2O_3/SO_4.SiO_2	Cr/S.Sio
Cr_2O_3 / SBA-15	Cr/S15
Cr_2O_3 / SO_4.SBA-15	Cr/S.S15
Cr_2O_3 / SBA-16	Cr/S16
Cr_2O_3 / SO_4.SBA-16	Cr/S.S16

CHAPTER -1

INTRODUCTION

1.0. General:

The conversion of alkanes to olefins is very popular in chemical industry. Particularly, the process of ethane dehydrogenation to ethylene is in large demand due to the enormous applications of ethylene such as the production of polyethylene, ethylene dichloride, ethylene oxide etc. The world ethylene capacity and the demand for the chemical in 2016 are provided in Figures 1.1 & 1.2, respectively. World's total ethylene production in that year was 146 MMT. China, Middle East and United States are the major ethylene producing regions in the world. They have 15%, 19% and 18% share of ethylene production, respectively. The production of ethylene is expected to grow in the range of 3-6% in the above said countries over the next ten years.

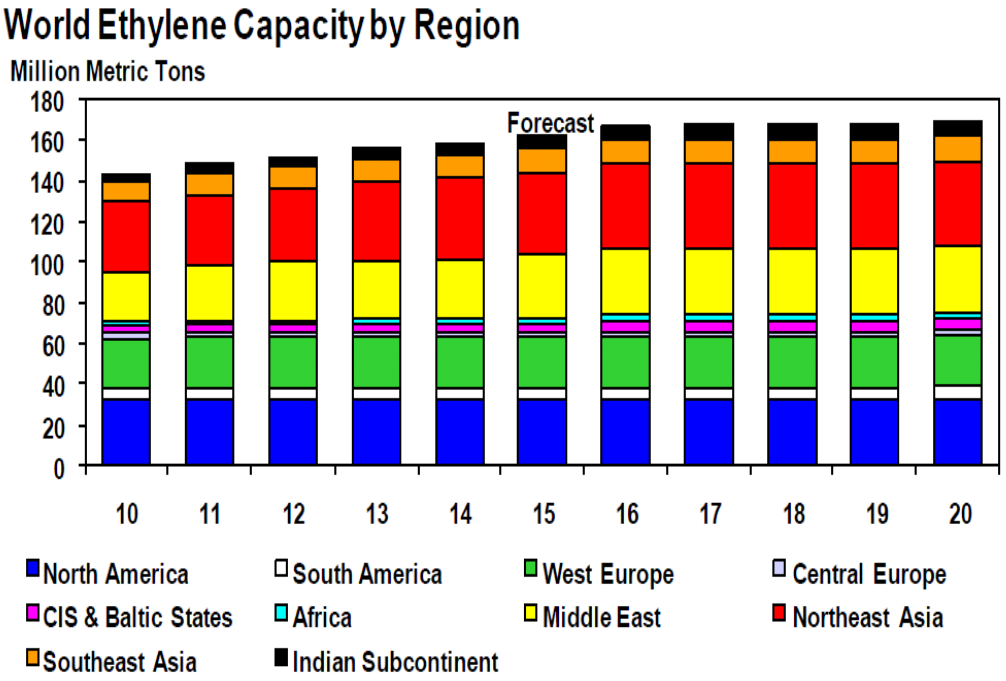

Figure.1.1. World ethylene capacity (Source:Global Data, Petrochemicals etrack**)**

1.1. Methods of ethylene production:

Depending upon the operating temperature, the technologies of ethylene production can be divided into two categories, (i) high temperature processes and (ii) Low Temperature Processes. The high temperature processes mainly include the conventional Thermal and Steam Cracking processes, whereas the low temperature processes are the new technologies like the ethane oxidative dehydrogenation.

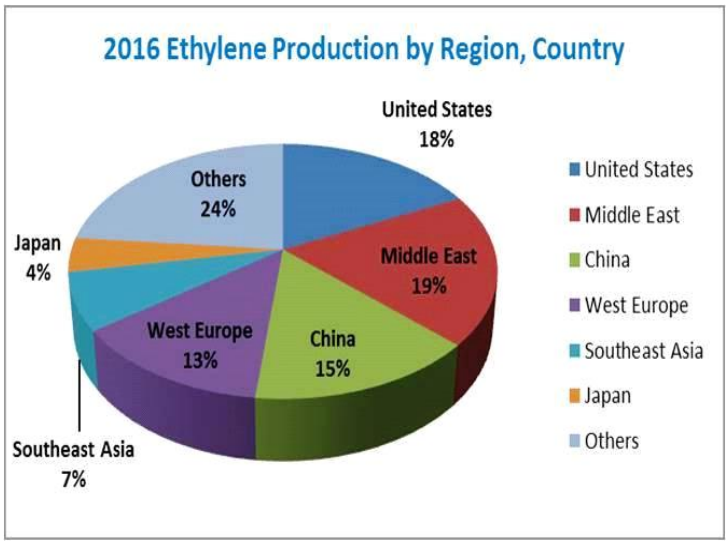

Figure.1.2. Ethylene Production by Region/Country in 2016

1.1.1. Thermal cracking:

Thermal cracking process was developed by William Merriam Burton in the year 1912.The process was operated at a pressure of 6 atm and at 370-400 ℃. Presently, moderate temperatures (450–750 ℃) [1] and high pressure (70 atm) are applied to crack the hydrocarbon molecules. To obtain high-degree conversions, it is required to operate thermal dehydrogenation process at high temperatures because the process is endothermic in nature. To attain the cracking temperature, the feed oil is sent through the heating tubes of the cracking furnace [6]. As a result, high costs are required to maintain the high reaction temperatures [7]. Thermal cracking proceeds in two ways; in one of the procedure, cracking occurs in the cracking furnace heating tubes and partly in the pipelines which lead to the process steps following cracking. In this cracking procedure, the delay is relatively short in the order of one minute. The pressure in the furnace varies greatly along the length of the furnace.

In the second procedure, first, the hydrocarbon feed is heated to a desired reaction temperature in cracking furnace, while the main cracking reaction happens in the reaction zone, in which the time delay is very high when compared to the previous method, i.e., in the order of 10–30 min. The flow direction in the reaction zone is either downward from above or upward from below. The product is collected finally after cooling and separation.

1.1.2. Steam cracking:

The large amount of commercial ethylene production is based on pyrolysis generally called as steam cracking. Steam cracking leads to break down of saturated hydrocarbons into smaller/unsaturated hydrocarbons. For lighter alkenes (ethylene and propylene), it is the major industrial method for production. Hydrocarbon feed stream is heated to cracking temperature,

i.e., 500–680 ℃, with flue gas which is mixed with steam in the convection section. Further feed steam is heated under controlled residence time to cracking temperature 750–875 ℃ for 0.1–0.5 s in a fired tubular reactor, where feedstock hydrocarbons are split into smaller molecules in this short reaction time. It requires high energy for the conversion of saturated hydrocarbons to highly endothermic olefins in the radiant tube. The products of the reaction leaving at 800–850 ℃ from the radiant tube are cooled to 550–650 ℃ within very short time, i.e., 0.02–0.1 s in order prevent degradation by secondary reactions. Further the cracked gas can be cooled by vaporizing the high-pressure boiler feed water.

1.2. Carbon dioxide mitigation:

The studies on the behavior of carbon dioxide as a soft oxidant were investigated by Park et al [3]. Since the early 50's, as regular measurements of the atmospheric concentrations of CO_2 were started, it has been conclusively established that these concentrations are increasing rapidly, driven by human activities. The concentration of CO_2 in the earth's atmosphere was about 280 parts per million by volume (ppmv) in 1750, before the industrial revolution began. By 1994 it was 358 ppmv and rising by about 1.5 ppmv per year. If the emission of CO_2 continued as per the rate observed in the 1994, the concentration will be around 500 ppmv, nearly double the preindustrial level, by the end of the 21^{st} century. The average temperature of the Earth's surface as increased by an estimated 0.6 ^oC in the 20^{th} century. According to the most recent projections of the Intergovernmental Panel on Climate Change, the temperature could rise 1.4 to 5.8 ^oC above the 1990 average by 2100. According to India's National Action Plan on Climate Change (IPCC), multi-model averages show that the temperature increases during 2090 - 2099 relative to 1980 - 1999 may range from 1.1 to 6.4 ^oC and sea level rise from 0.18 to 0.59 meters. These could lead to impacts on freshwater availability, oceanic acidification, food production, flooding of coastal areas and increased diseases associated with extreme weather events. Because of these huge detriments, most of the researchers have been working for the development of technologies which can reduce the production of major greenhouse gas (CO_2) and the CO_2 in atmosphere can be reduced by CO_2 fixation i.e. CO_2 separation and recovery, utilization, dissolution and disposal.

1.3. Disadvantages of conventional methodologies of ethylene production:

1.3.1. Thermal cracking:

1. The reaction is extremely endothermic (ΔH 590 ℃ = +143 kJ/mol).
2. The operating pressure is excessive (70 atm).
3. This method produces large quantities of solid and unwanted coke.

1.3.2. Steam cracking:

1. The reaction is extremely endothermic.
2. The time of residence is in the order of milliseconds, causing a drop in the pressure.
3. Coking is a major problem in the furnace as well as in the transfer line exchanger.
4. Catalyst activity decreases because of coke formation and catalyst regeneration measure is required
5. Formation of coke reduces product yields, shortens the span of coil service life and increases energy consumption.
6. The heavier the feed stocks more are the undesired products.

1.4. Alternative Method: Oxidative dehydrogenation of ethane:

As explained above the conventional processes have several disadvantages. One of the essential shortcomings is endothermic nature of the alkane dehydrogenation reaction. As per Le Chatlier's principle, high temperature is required for higher conversions. The temperatures for 50% conversion of alkane to corresponding alkenes are in the range of about 720 ℃ [2]. An improvement on this method is the catalytic dehydrogenation process. However, environmental issues along with high operational costs have made this conversion profitable only on a very large scale. To overcome this drawback a new technology called "Catalytic Oxidative Dehydrogenation (ODH)" has been pursued vigorously. The reaction of ethane with oxygen, Nitrous oxide or carbon dioxide in the presence of suitable catalyst offers lots of advantages that include execution at low temperatures by overcoming the equilibrium restrictions.

Ethane oxidative dehydrogenation has the following advantages.

1. Eliminates thermodynamic limitations in the ethane conversion.
2. It is an exothermic reaction and economically feasible.
3. Relatively operates at low reaction temperatures (350–600 ℃).
4. Catalyst regeneration.
5. It enables one to achieve total conversion at much lower temperatures.

1.4.1. Oxidative dehydrogenation using O_2 as oxidant:

In recent times the ODH reaction has gained remarkable interest. Consequently, a large number of researchers have been studying the reaction particularly on catalytic ODH of ethane. It was found that vanadium-based catalyst activity is very high when compared to other catalysts. In the case of mesoporous alumina supported vanadium catalysts Concepcion et al [3] observed that the activity depends on V-loading. The catalyst with a V-coverage of 20%, showed 30% ethane conversion with 63.4% ethylene selectivity at 570 ℃. Other

catalysts like vanadium-exchanged Ti, Zr, and Sn cubic pyrophosphates were also found to be active [4]. Novel materials such as the micro-structured catalysts i.e CeO_2-NiO-Al_2O_3/Ni-foam were discovered to be highly active and selective with promising stability [5]. However, the desired selectivity has not been reached so far.

$$C_2H_6 + 0.5O_2 \rightarrow C_2H_4 + CO + H_2O \quad -----1.1$$

$$C_2H_6 + 3.5O_2 \rightarrow 2CO_2 + 3H_2O \quad -----1.2$$

1.4.2. Oxidative dehydrogenation using nitrous oxide (N_2O) as oxidant:

N_2O is a waste by product and an environmental pollutant generated mainly from industrial processes such as adipic acid and nitric acid plants. Its global warming potential is 300 times more than that of CO_2 and it also causes ozone depletion [6]. However, it is also a good oxidant. When N_2O is used, the activation energy of re-oxidation of the reduced catalyst falls closer to the apparent ODH activation energy making it a good oxidant. The reaction proceeds as follows:

$$C_2H_6 + N_2O \rightarrow C_2H_4 + N_2 + H_2O \quad -----1.3$$

Lunsford et al. [7,8] suggested that N_2O is predominantly dissociated to produce O-species that are exchanged with oxide ions in the lattice of (Molybdinum oxide on silica supported catalyst) MoO_x/SiO_2 catalysts [9]. They reported high activities and selectivities during ethane ODH with N_2O than using molecular oxygen [8]. However, usage reduces the significance of the O_2^- species during ethane ODH.

1.4.3. Oxidative dehydrogenation using CO_2 as oxidant:

Globally about 35 billion tons per annum of CO_2 is emitted into the atmosphere. A major portion of these emissions comes from burning of fossil fuels in the process of deriving energy. CO_2 is one of the most important greenhouse gases. The mitigation of CO_2 emission from various sources has been a worldwide objective. The CO_2 recovered from various sources such as flue gases of coal or gas oil fired plants and other industrial processes is mainly sequestered in underground locations or deep under the sea. The trend is to not consider this gas as a pollutant anymore but as a single carbon,oxygen (O), carbon dioxide or carbon monoxide sources.It has been recognized that enhancing the capacities of CO_2 usage could have a significant role in addressing the global warming problem. Already technologies like urea production make use of CO_2. However, the extent of chemical utilization (totalling 300 MT) so far is a small fraction of the huge emissions. Therefore, continued efforts have been made to identify more and more processes that can utilize CO_2 in large quantity.

In recent years oxidation reactions have become an alternative way to synthesize the low molecular weight paraffin's. Ethane is the second major component of natural gas, which

makes it a potential source for ethylene [10, 11]. In the ODH reaction the main aim is the conversion of cheaper ethane into valuable ethylene simultaneously adopting CO_2 as an oxidant.

Technically, this soft oxidant could help improve ethylene selectivity and offer stabilization of the activity and the prolongation of catalyst lifetime.

The reactions involved when CO_2 is used as oxidizing agent are as follows:

Main reaction	$C_2H_6 + CO_2 \rightarrow C_2H_4 + CO + H_2O$	1.4
Side reactions	$C_2H_6 \rightarrow C_2H_4 + H_2$	1.5
	$C_2H_6 + 2CO_2 \rightarrow 4CO + 3H_2$	1.6
	$H_2 + CO_2 \rightarrow CO + H_2O$	1.7
	$C_2H_6 + H_2 \rightarrow 2CH_4$	1.8

All the above reactions are endothermic in nature but the CO_2 - ODH reaction is favourable due to thermodynamic constraints. Ethylene is produced through direct dehydrogenation (Reaction-1.5) and also by the oxidative dehydrogenation process (Reaction-1.4). Reverse water gas shift (Reaction-1.7) aids in dehydrogenation of alkanes resulting in the formation of alkene. Equations 1.6 and 1.8 represent the reforming and hydro cracking, respectively. The lower oxidizing ability of CO_2 suppresses the formation of unwanted total oxidation products [12] and can also increase the ethylene selectivity by poisoning the catalyst's non selective sites , which contribute essentially to the formation of by-products (CO, CH_4) [13]. Wang and his colleagues [14] first found the promoting effects of CO_2, either formed during the course of the reaction or physically added to the system in the ODH process. Subsequently, there has been a tremendous improvement in the catalytic ODH of ethane using CO_2.

1.5. Advantages of ODH of ethane using CO_2:

Alkenes like ethylene and propylene can be produced through non-oxidative dehydrogenation of the respective alkanes. Reactions of non-oxidative dehydrogenation are endothermic in nature and results in the concurrent formation of alkanes with lower molecular weight and carbon, both of them decreases alkenes yields. ODH offers an attractive route to the alkenes, because the reaction is exothermic and prevents the thermodynamic non-oxidative routes constraints by producing water as a by-product. Along with that, carbon depositions eliminated during ODH, results in stable catalytic activity. Ethane ODH using O_2 as oxidant has higher conversion of ethane but the ethylene selectivity is very low because of the formation of secondary oxidation products such as CO, CO_2. However, the alkenes combustion to CO and CO_2 limits the yield of alkenes obtained by ODH on most catalysts [12, 13]. Also

the reverse water gas shift reaction aids in the ethylene formation by dehydrogenation of ethane. With the successful ODH development, higher yields of olefins can be obtained even at much smaller volumes of alkanes. ODH could decrease the costs, reduce emissions of greenhouse gas, and save energy. By removing the need for a furnace and for decoking shutdowns, reducing operating temperatures, reducing material requirements, reducing maintenance operations, and using a greater proportion of the alkanes in the olefin conversion process results in capital and operational efficiency gain. The major advantages of using CO_2 as a oxidant in ODH process are summarized below.

- Using CO_2 as oxidant it prevents hot spots in the reactor it helps to get higher alkane equilibrium conversion.
- Lesser coke formation on the catalyst.
- Higher ethylene selectivity.
- Extended catalyst life.

1.6. Catalyst development for ODH of ethane using CO_2:

The catalytic system for ODH of ethane can be classified into three groups:

• Catalytic systems based on oxides and ions of group I A and II A metals dispersed on inactive supports (e.g., Li, Na/MgO or Li/metal chlorides).

• Rare earth metals oxides (La_2O_3, Sm_2O_3, CeO_2).

• Transition metal oxides, containing Mo, Cr, Ga, and V.

The metal catalysts from groups I A and II A are usually active at temperatures higher than 600 ℃. They were previously found to be active in the reaction of oxidative methane coupling, OCM [15]. radical O– generated on a catalyst surface on a Li^+–O– centre. Gas-phase reaction initiation is the role of metal catalyst. The catalyst activity can be extensively enhanced by adding small amounts of chlorine or chlorine-containing compounds (e.g., tetrachloro methane or HCl), or halides directly added to the catalyst in the initial stage of preparation [16]. It is suggested that chlorine radicals are responsible for the decomposition of the ethyl radical to ethene. Among all these catalysts, the most successful one is the Cl– Li/MgO. The yield of ethane is found to be in the range of 30–40%, while the ethylene selectivity is of 70–80% at 40–60% conversions [17, 18].

The second group of catalysts for ODH of ethane comprises oxides of rare earth metals (La_2O_3, Sm_2O_3, CeO_2, and Pr_6O_{11}). The rare earth metal oxides are active and stable even at high temperature, i.e. 500–700 ℃. The mechanism of these catalysts is similar to first group catalysts, i.e. group I A and II A metals. The good catalytic performances in ODH of ethane have been obtained with La_2O_3 and Sm_2O_3; however, the best system contained La_2O_3 in a

mixture with Fe_2O_3 supported on a-Al_2O_3. The yields 40–80% with selectivity between 70 and 90% conversions was reported [22-24].

The third class of catalysts is based on oxides of transition metals, containing in particular Mo and V. They can activate ethane at temperatures usually 400–550 ℃ and operate most probably by a redox mechanism. Among them, Mo–V–O system promoted with Sb, Nb, active at relatively low temperatures 400 ℃ gives a yield of 50% with selectivity to ethane about 70% [25, 26]. Vanadium oxides dispersed on different supports, magnesium vanadates, or molybdates, which are active in ODH of higher alkanes, show relatively poor performance in the reaction of ethane (ethane yields usually below 10%) [18,19]. The overall conversions of ethane to ethylene for chromia on mixed oxide supported catalyst (Cr_2O_3/Al_2O_3+ ZrO_2) depends not only on the basicity of the surface but also on the redox property of chromia. These two properties might have attained their optimum values by combining Al_2O_3 and ZrO_2. [27]

Among all supported chromium catalysts were found to be more active for ethane ODH in terms of superior ethane and CO_2 conversions. Particularly, two types of supports were used for Cr_2O_3; the non-silica supported and silica supported systems, respectively. Whereas Cr_2O_3/Al_2O_3, Cr_2O_3/ZrO_2, Cr_2O_3/TiO_2 [21,22], modified Cr_2O_3/ZrO_2 and nano-composite [23] catalysts fell in the first category, Cr_2O_3/SiO_2, Cr_2O_3/SBA-15/Al_2O_3 FeCrAl monoliths [24] came in the second category. Apart from these two, there were few reports on mixed catalyst/support systems like Cr-O, Cr-V-O oxide [19] catalysts. Very few systems like the Ga_2O_3 containing catalysts supported on HZSM-5 and silicalite [20] were also found in the literature, but they showed low conversion of the light alkane and CO_2 apart from undergoing drastic deactivation within a few hours on stream. By and large, all the catalysts operated at 650 ℃ offering about 50% conversion of ethane and 80% selectivity towards ethylene. Shaobin Wang et al. [28] reported the results on ODH of ethane into ethylene after sulfate modification of Cr_2O_3/SiO_2 [29,30]. The silica sulfation influence the catalyst behaviour based on the sulfate amount. Cr_2O_3/6wt% SO_4^-–SiO_2 catalysts exhibited magnificent performance, providing an ethylene yield of 55% with 67% conversion of ethane at 650 ℃. The catalyst characterization indicated that the inclusion of sulfate changes the surface and bulk properties of Cr_2O_3/SiO_2 in support of catalytic activity.

1.7. The importance of studying the mixed oxide and SiO_2 based supported Cr_2O_3 catalysts:

Catalytic oxidative dehydrogenation has emerged as a better technology to combat the disadvantages of the cracking processes such as high energy requirement and thermodynamic

limitations.Cr_2O_3 catalyst with non-silica based supports emerged as superior catalysts. Nevertheless, a great deal of work is required to improve ethane and CO_2 conversions, enhancing selectivity of ethylene, apart from containing deactivation of catalyst. It is generally accepted that a mixed oxide support has an edge over its component single oxides as support for Cr_2O_3 in combining their good textural and mechanical properties. Anyhow, these catalysts were not thoroughly studied. Literature is abundant with the performance data on a variety of single oxide supported catalysts such as Al_2O_3, TiO_2 and ZrO_2 supported Cr_2O_3 catalysts. The catalytic activity dependency on the distribution of CrO_x and the Cr structure species on the mixed oxide surface has not been reported so far. Compared to oxygen, CO_2 in the feed has been shown to facilitate dehydrogenation by improving ethane conversion, in addition to increasing ethylene yield and significantly retarding coke deposition on the catalyst. The chromium, such as Cr^{6+}on the surface is found to be the active species in its high oxidation [31]. Reducibility is one more parameter that determines the rate of dehydrogenation of ethane [32,33]. Thus, it is necessary to study Cr_2O_3 supported on mixed oxide catalysts [35].

Catalytic performance of silica-supported chromium oxide catalysts in carbon dioxide with dehydrogenation of ethane is most favourable**.** However, Cr_2O_3 was reported to aggregate on SiO_2 and the catalyst behaviour during the ODH (oxidative dehydrogenation) reaction has negative influence [36]. SBA-15 is a better support to overcome the problem of aggregation [37]. The interaction between Cr_2O_3 and SBA-15 is suggested to prevent aggregation, especially during the reduction-oxidation cycle between $Cr^{3+}$and Cr^{6+}species. Wang et al. [38] has been reported that the silica support sulfate modification is beneficial in preparing more active chromia catalysts for the ODE reaction in the existence of CO_2. It is observed that silica sulfation has a positive impact on the catalyst while strong fundamental promoters (alkali metal oxides) undermine the catalytic activity [39,40]. Zirconia sulfate modification is also tried in the ODE related studies to achieve good results [41]. Thus, it is imminent to study the influence of Cr_2O_3/SBA-15 sulfate modification in view of the beneficial effects of SBA-15 in controlling the aggregation phenomenon.

In this thesis the influence of mixed oxides as supports for Cr_2O_3 and the effect of sulfate modification of SBA-15 support in enhancing the activity and selectivity of supported Cr_2O_3 catalysts has been studied and the results are reported in terms of their physic-chemical properties. A comparison has been made between for the catalytic functionalities of the un-modified and the modified supported catalysts.

1.8. Studies on reaction modelling:

1.8.1. Heat & mass transfer effects:

Reactants transfer from bulk fluid to the surface of catalyst particles depends on the difference in concentration that is affected by the velocity pattern of fluid near the catalyst surface, fluid's physical properties and chemical reactions intrinsic rate. While the property of fluid affect the mass transfer between catalyst surface and fluid, the catalyst properties and condition determines the intrinsic rate. Diffusion of reactants into the catalyst play vital role while determining the kinetics of the reaction. Prior to kinetic studies it is important to study the diffusion of reactants from the bulk phase to the catalyst particle surface, and afterwards from the surface to the inside of the particle. External and internal diffusion plays an important role in the reactants transfer rate to heterogeneous catalysts.

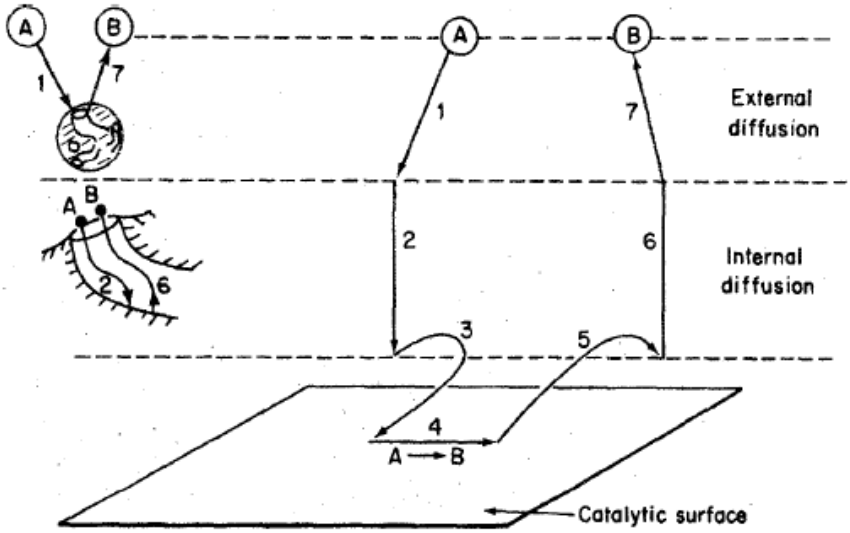

Figure.1.3. Steps involved in Heterogeneous Reactions (42)

The steps 1 and 7 are dependent on fluid flow characteristics of the system. These steps depend on the mass velocity of the feed, diffusion of various components in the catalyst surface and particle size. These steps limit the observed rates only when the mass transfer is slow and the reaction is rapid in nature.

The steps 2 and 6 are dependent on the pore size of the catalyst as the reactant gases diffuses into the catalyst surface during the reaction. Three modes of diffusion are present depending on the pore size. If the pore diffusion exceeds the mean free path of gas bulk diffusion happens. Similarly when the pore diameter and mean free gas path are same, molecules diffuse by Knudsen diffusion. When the diameter of pore is same as size of reactant molecule can only diffuse in the pores by staying constantly in contact with the walls of pore (configurational or surface diffusion). The effects of diffusion can be neglected when the mass transfer is very fast.

1.8.2. Mass transfer limitations:

In heterogeneous catalytic reactions the gas diffusion from the bulk to the surface of catalyst (External diffusion) and from the surface to the catalyst interior (Internal diffusion) plays an important role in rate of reaction. These diffusion mechanisms act as resistances which affect the rate of reaction and it should not be neglected. The figure below gives the steps taking place in a porous catalytic particle

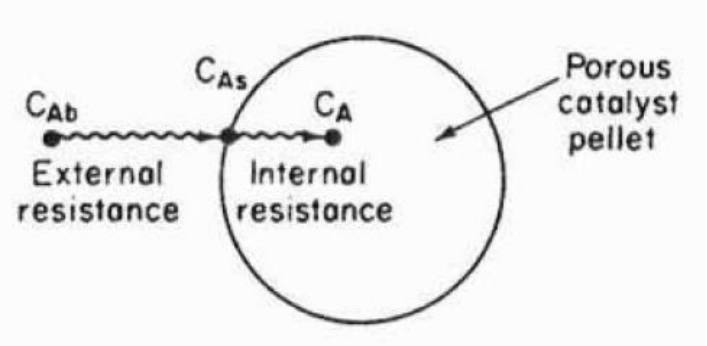

Figure.1.4. Internal and external diffusion in a porous catalyst (42)

Shell mass balance on catalyst pellet.

The material balance across an element of the reactor can be described as follows

[Input mass rate of A] - [Output mass rate of A] + [A's Disappearance Rate within the element, Δr] = 0

$$[4\pi R^2 N_A]_r - [4\pi R^2 N_A]_{r+\Delta r} + \left[-r_A^{'}\rho_c 4\pi R^2 \Delta r\right] = 0 \qquad \text{- - - - (1.9)}$$

$$\frac{d(N_A r^2)}{dr} - r_A^{'}\rho_c r^2 = 0 \qquad \text{- - - - (1.10)}$$

The molar flux of A by molecular diffusion is given by

$$N_A = -D_e \frac{dC_A}{dr} \qquad \text{- - - - (1.11)}$$

where D_e is effective diffusivity given by

$$D_e = \frac{D_{AB}\,\phi\,\sigma}{\tau} \qquad \text{- - - - (1.12)}$$

where D_{AB} is nothing but bulk or A's Knudsen diffusivity in B, ϕ is the porosity of pellet and σ is the constriction factor. The σ value is taken as 1 for many cases and the tortuosity [43] of catalyst is calculated from porosity by

$$\tau = 1 - 0.5\ ln\ \phi \qquad \text{- - - - (1.13)}$$

Thiele modulus ϕ_1 of 1st reaction order is given by

$$\phi_1 = \frac{surface\ reaction\ rate}{diffusion\ rate} = R\sqrt{\frac{k_1^{''} S_a \rho_c}{D_e}} \qquad \text{- - - - (1.14)}$$

where $k_1^{''}$ is the rate constant per unit catalyst surface, S_a is the catalyst surface area

and ρ_c is the density of catalyst.

When the Thiele modulus is extremely high , the mass transfer controls the reaction and when it is low, the surface reaction is the rate limiting step. We can also use the internal efficiency factor η to verify whether internal diffusion is the rate limiting step.

$$\eta = \frac{(\text{actual reaction rate within the pore})}{(\textit{reaction rate if not slowed by diffusion})} \qquad \text{- - - - (1.15)}$$

The internal efficiency factor is dependent on order of reaction as well as shape of the catalyst. For a first order of reaction on a spherical catalyst the internal efficiency factor is given by

$$\eta = \frac{3}{\phi_1^2}(\phi_1 \coth\phi_1 - 1) \qquad \text{- - - - (1.16)}$$

Where ϕ_1 is the Thiele modulus Ƞ is the efficiency factor

The internal efficiency factor η is nearly equal to 1 when internal diffusion in the catalyst is negligible. The variation of effectiveness factor for various values of Thiele modulus for different reaction orders in a spherical catalyst is given by

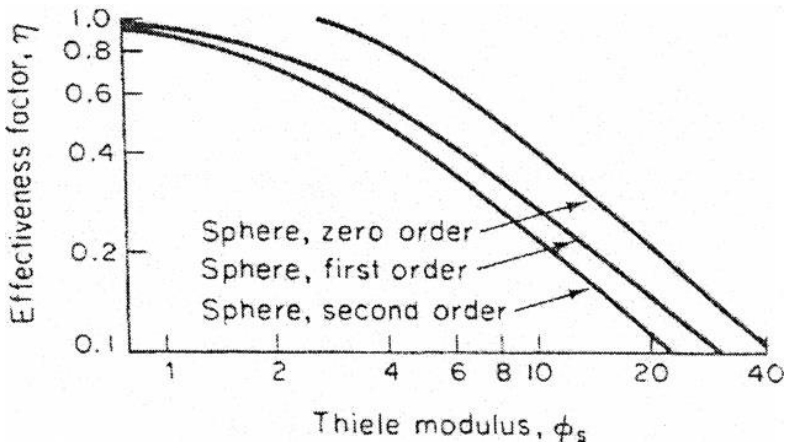

Figure.1.5: Thiele modulus versus effectiveness factor for spherical particles for different reaction order

Weisz Prater criterion [44] is used to check whether the reaction is diffusion limited or not.

$$C_{wp} = \frac{-r_A' \rho_c R^2}{D_e C_{As}} < 1 \qquad \text{- - - (1.17)}$$

C_{wp} =Actual reaction rate/Actual diffusion rate

Where r_A is the reaction rate observed

ρ_c is the catalyst pellet density

R is the radius of the catalyst particle

D_e is the effective diffusivity of the particle

C_{As} is the concentration of A the surface

D_{Ai} is the diffusivity of A in the mixture of gas into catalyst

The Internal diffusion is negligible when C_{wp} is <<1 and vice versa

1.8.3. Heat transfer effects in the catalyst:

Ethane oxidative dehydrogenation with CO_2 is exothermic in nature. Non isothermal effects in the catalyst are much higher as the particle is cooler than the surrounding fluid when compared with endothermic reactions. The difference between these two temperatures, ΔT within the particle of catalyst is provided by Prater for any particle geometry and kinetics.

The Laplace equation is used to represent temperature and concentration within the particle and therefore its corresponding distribution curves must at any point in the pellet x have the same shape.

$$-\lambda_{eff}\frac{dT}{dx} = -D_e\frac{dC_A}{dx}(-\Delta H_r) \quad \text{- - - -} \quad (1.18)$$

Where λ_{eff} is the efficient thermal conductivity

$-\Delta H_r$ is the reaction heat.

The efficient thermal conductivity λ_{eff} [44] is in turn calculated by

$$\lambda_{eff} = \lambda_s^{1-\phi}\lambda_f^{\phi} = \lambda_s\left(\frac{\lambda_f}{\lambda_s}\right)^{\phi} \quad \text{- - - -} \quad (1.19)$$

For the catalyst pellet as a whole is given by

$$\Delta T_{Particle} = \frac{D_e(C_{As}-C_{A,centre})(-\Delta H_r)}{\lambda_{eff}} \quad \text{- - - -} \quad (1.20)$$

The maximum temperature at the centre of the catalyst is when $C_{A,centre}$ is equal to zero. The ΔT_{max} / T is equal to β, for various values of ϕ_1 and β the effectiveness factor is shown below.

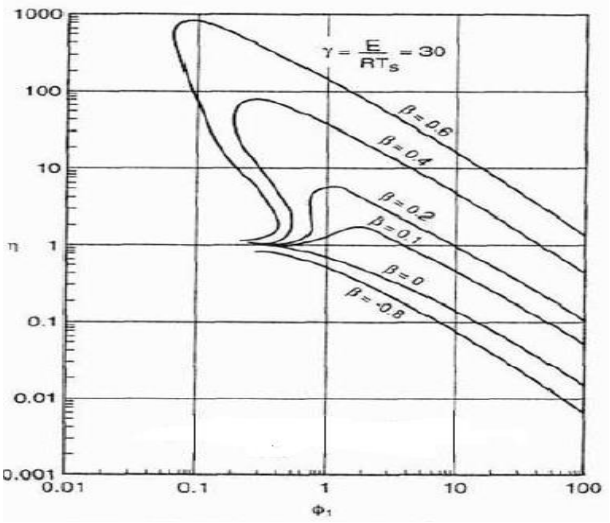

Figure.1.6. Non Isothermal effectiveness factor curve for temperature variation within the particle

The ΔT within the particle is almost zero hence the nature catalytic reaction is isothermal. The fixed bed reactor to be modelled the above studies to simplify the reactor model that is the diffusion effects are negligible for the given catalyst particle size and flow rate. Also the Fixed bed reactor is assumed to be isothermal in nature.

1.8.4. Reaction modelling:

Different models are available in the literature for reaction modelling. In the Law of Power model, the reaction order with respect to individual reactants is found by varying either the partial pressure or volumetric flow rate of one reactant keeping this condition of other reactants at constant value. The rate at which each reactant reacts is plotted against the concentration of reactant at different temperatures and the kinetic parameters are evaluated. The model, Langmuir-Hinshelwood-Hougen-Watson (LHHW) is on the basis of assumptions that there is one type of active sites over the whole surface of catalyst; reactants and products on the catalytic surface are competitively adsorbed; molecular adsorption of reactant gases and the surface reaction is the rate controlling mechanism. Similarly, in Eley Rideal model one of the gaseous components adsorbs on the catalyst active site while the other component reacts from bulk gaseous phase. Based on the properties of catalyst surface the adsorbing component changes and the model is created. In this work ethane is assumed to be the adsorbed molecule while CO_2 reacts from the bulk gas phase. In an yet another model called the Mars van Krevlen mechanism the catalyst which is a metal oxide is decreased by hydrocarbon and is again regenerated by CO_2 which re oxidises the reduced catalyst. Krylov [45,46] proposed a model equation for ethane oxidative dehydrogenation. Any study attempting to evaluate the intrinsic reaction parameters necessarily fit the reaction data and identifies the bet model.

Estimation in differential or algebraic equations which are nonlinear in their parameters can be carried out by reducing the objective function by methods such as Newton-Gauss, Marquardt algorithm and steepest descent. These methods are explained elsewhere [47-49]. The Marquardt method was considered for this thesis. Similarly, for the thermodynamic validation, Boudart and co-authors [50,51] proposed well established rules to test the suitability of the estimated parameter values for final rate equations. In this work, adsorption enthalpies and entropies are tested by the constraint rules of Boudart et al.[51] and Boudart [52]. The model validity is finally compared to the experimental results.

1.9. Response Surface Methodology:

This is a statistical technique used to find the optimum conditions for a process of interest. In RSM a relationship is found between the variables involved in the process and the response variable which is usually unknown. When the relationship between variables involved and the

response is approximated by using low order approximations such as linear functions of independent variables the model is said to be a first order model.

For example if $x_1 \ldots x_n$ are variables which affect the dependent variable y, the first order is given by

$$y = \beta_0 + \beta_1 x_1 + \beta_2 x_2 \ldots \ldots \beta_n x_n \qquad \text{- - - - (1.21)}$$

where β_i are the coefficients of the various variables.

Similarly, if there is a curvature in the system, the higher order polynomial can be used to approximate the response as shown below.

$$y = \beta_0 + \sum_{i=1}^{n} \beta_i x_i + \sum_{i=1}^{n} \beta_{ii} x_i^{\,2} + \sum_i \sum_j \beta_{ij} x_i x_j \; i < j \qquad \text{- - - - (1.22)}$$

The steepest ascent or descent method is used to identify the optimum conditions of independent attributes. In this method we move in the direction normal to the contours of response variable y and the experiment response is observed for changes. This process gives the optimum conditions of independent variables with several additional experiments. In our case the independent variables which affect the response (ethane conversion, ethane selectivity and methane selectivity) are the temperature and volumetric flow rates of CO_2.

1.10. Scope of the thesis work:

The scope of the present thesis includes:

- Preparation of non-silica based (Al_2O_3, ZrO_2 & Mixed oxide) and silica based (SiO_2, SBA-15 and SBA-16) supported Cr_2O_3 catalysts.
- Preparation of silica based supported sulphate modified Cr_2O_3 catalysts**.**
- Detailed characterization of the prepared catalysts using XRD, XPS, Raman, and IR and BET surface area. Determining their acid-base characteristics by FTIR and reducibility by H_2-TPR and TPD of adsorbed ethane.
- Evaluation of the catalysts by Oxidative dehydrogenation of ethane using carbon dioxide in a packed bed reactor.
- Reaction modelling using established models for the identification of the best model. Evaluation of the optimum parameters and checking them for thermodynamic and statistical consistency.
- Application of response surface methodology to identify the optimum conditions for the process.

1.11. Thesis Organization:

The thesis consists of seven chapters so as to make the contents more comprehensible. The seven chapters include; introduction, literature review, materials and methods, results and discussion-metal oxide supported chromia catalysts, results and discussion- silica based

material supported chromia catalysts, kinetic modelling , Optimisation using response surface methodology and conclusions.

Chapter 1.Deals with the importance and manufacturing methods of ethylene and comparison of methods. Development of catalysts and various oxidants used for oxidative dehydrogenation method. Discussion about reaction modelling.

Chapter 2.Presents exhaustive review of literature on the previous works related to various catalysts and oxidants used for the synthesis of ethylene using oxidative dehydrogenation method and kinetic modelling and optimisation of the process using response surface methodology

Chapter 3.Presents materials and methods adopted for preparation of the catalysts and detailed experimental evaluation procedures with sample calculation methodology

Chapter 4. Deals with results and discussion of metal oxide supported chromia catalysts. Preparation methods, analysis of prepared catalysts and measurement of catalytic activity.

Chapter 5. Deals with results and discussion of silica based material supported chromia catalysts. Preparation methods, analysis of prepared catalysts and measurement of catalytic activity.

Chapter 6. Presents kinetic modelling of the best catalyst selected from metal oxide supports i.e mixed oxide supported chromia catalyst (15wt% Cr_2O_3/ Al_2O_3 - ZrO_2 (1:1). development and validations kinetic models.

Chapter 7.Deals with optimisation of process parameters for ODH of ethane for the best catalyst from metal oxide supports i.e mixed oxide supported chromia catalyst 15wt% Cr_2O_3/ Al_2O_3 - ZrO_2 (1:1).

Chapter 8. Includes over all conclusions of the research work and Scope for future work

REFERENCES:

1. Finashina, E. D., Kucherov, A. V., Kustov, L. M., Cai, H., & Krzywicki, A. (2017). Effect of feedstock impurities on activity and selectivity of V-Mo-Nb-Te-Ox catalyst in ethane oxidative dehydrogenation. Journal of Advanced Oxidation Technologies, 20(2).
2. Pieck CL, Banares MA, Fierro JLG (2004) Propane oxidative dehydrogenation on VOx/ZrO_2 catalysts. J Catal 224(1):1–7
3. Cavani F, Ballarini N, Cericola A (2007) Oxidative dehydrogenation of ethane and propane: how far from commercial implementation? Catal Today 127(1–4):113–131.
4. Heracleous E, Lee AF, Wilson K, Lemonidou AA (2005) Investigation of Ni-based alumina-supported catalysts for the oxidative dehydrogenation of ethane to ethylene: structural characterization and reactivity studies. J Catal 231(1):159–171.
5. Heracleous E, Lemonidou AA (2006) Ni–Nb–O mixed oxides as highly active and selective catalysts for ethene production via ethane oxidative dehydrogenation. Part I: Characterization and catalytic performance. J Catal 237(1):162–174.
6. Kondratenko, E.V.; Ovsitser, O. Angew. Chem. Int. Ed. 2008, 47, 3227–3229.
7. Ward, M. B., Lin, M. J., & Lunsford, J. H. (1977). The oxidative dehydrogenation of ethane by nitrous oxide over molybdenum oxide supported on silica gel. Journal of Catalysis, 50(2), 306-318.
8. Liu, H. F., Liu, R. S., Liew, K. Y., Johnson, R. E., & Lunsford, J. H. (1984). Partial oxidation of methane by nitrous oxide over molybdenum on silica. Journal of American Chemical Society, 106(15), 4117-4121.
9. Taarit, Y. B., & Lunsford, J. H. (1973). EPR evidence for $17O^-$ on molybdenum oxide supported by silica-gel. Chemical Physics Letters, 19(3), 348-350.
10. Martinez-Huerta, M. V., Gao, X., Tian, H., Wachs, I. E., Fierro, J. L. G., &Banares, M. A. (2006). Oxidative dehydrogenation of ethane to ethylene over alumina-supported vanadium oxide catalysts: Relationship between molecular structures and chemical reactivity. Catalysis Today, 118(3-4), 279-287.
11. Grudzien, R. M., Grabicka, B. E., & Jaroniec, M. (2006). Effective method for removal of polymeric template from SBA-16 silica combining extraction and temperature-controlled calcination. Journal of Materials Chemistry, 16(9), 819-823.
12. .Yoo, J. S. (1998). Selective gas-phase oxidation at oxide nanoparticles on microporous materials. Catalysis Today, 41(4), 409-432.

13. Yoo, J. S., Lin, P. S., & Elfline, S. D. (1993). Gas-phase oxygen oxidations of alkylaromatics over CVD Fe/Mo/borosilicate molecular sieve. II. The role of carbon dioxide as a co-oxidant. Applied Catalysis A: General, 106(2), 259-273.
14. Wang, D., Xu, M., Shi, C., & Lunsford, J. H. (1993). Effect of carbon dioxide on the selectivities obtained during the partial oxidation of methane and ethane over Li+/MgO catalysts. Catalysis letters, 18(4), 323-328.
15. Gao X, Wachs IE (2000) Investigation of surface structures of supported vanadium oxide catalysts by UV–vis–NIR diffuse reflectance spectroscopy. J Phys Chem B 104(6):1261–1268.
16. Watson RB, Lashbrook SL, Ozkan US (2004) Chlorine modification of Mo/silica-titania mixed-oxide catalysts for the oxidative dehydrogenation of ethane. J Mol Catal A Chem 208 (1–2):233–244.
17. Jones A (2014) Tempature-programmed reduction for solid materials characterization. CRC Press, Boca Rotan.
18. Malet P, Caballero A (1988) The selection of experimental conditions in temperature-programmed reduction experiments. J Chem Soc Faraday Trans 1 Phys Chem Condens Phases 84(7):2369–2375.
19. Tran K, Hanning-Lee MA, Biswas A, Stiegman AE, Scott GW (1995) Electronic structure of discrete pseudotetrahedraloxovanadiumcenters dispersed in a silica xerogel matrix: implications for catalysis and photocatalysis. J Am Chem Soc 117(9):2618–2626.
20. Haber J (1994) Supported vanadium oxide catalysts: molecular structural characterization and reactivity properties. Crit Rev Surf Chem 4(3/4):141–187.
21. Newbury DE, Joy DC, Echlin P, Fiori CE, Goldstein JI (1986) Electron channeling contrast inthe SEM. In: Advanced scanning electron microscopy and X-ray microanalysis. Springer,Boston, MA, pp 87–145.
22. McDonald AM (1998) Environmental scanning electron microscopy. Mater World 6:399–401.
23. Koeppel RA, Nickl J, Baiker A (1994) 5 Characterization of V_2O_5/TiO_2 Eurocat samples by temperature-programmed reduction. Catal Today 20(1):45–52
24. Hurst NW, Gentry SJ, Jones A, McNicol BD (1982) Temperature programmed reduction. Catal Rev SciEng 24(2):233–309.
25. Monti DA, Baiker A (1983) Temperature-programmed reduction. Parametric sensitivity and estimation of kinetic parameters. J Catal 83(2):323–335.

26. RJ, Amenomiya Y (1972) A temperature programmed desorption technique forinvestigation of practical catalysts. Catal Rev 6(1):21–48.
27. Ramesh, Y., Bai, P. T., Babu, B. H., Lingaiah, N., Rao, K. R., & Prasad, P. S. (2014). Oxidative dehydrogenation of ethane to ethylene on Cr_2O_3 / Al_2O_3 -ZrO_2 catalysts: the influence of oxidizing agent on ethylene selectivity. Applied Petrochemical Research, 4(3), 247-252.
28. Shaobin Wang ,K. Murata T. Hayakawa S. Hamakawa K. Suzuki November 1999, Volume 63, Issue 1–2, pp 59–64.
29. Talati, Azadeh; Haghighi, Mohamma Advanced Powder Technology (2016), 27(4), 1195-1206.
30. Asghari, Elmira; Haghighi, Mohammad; Rahmani, FarhadFrom Journal of Molecular Catalysis A: Chemical (2016), 418-419, 115-124.
31. Iglesia, E., Spivey, J. J., Fleisch, T. H., Schmidt, L. D., Bell, A. T., Zhang, Y.& Ma, D. (2001). Natural Gas Conversion VI. Amsterdam: Elsevier.
32. Mimura, N., Okamoto, M., Yamashita, H., Oyama, S. T., & Murata, K. (2006). Oxidative dehydrogenation of ethane over Cr/ZSM-5 catalysts using CO2 as an oxidant. The Journal of Physical Chemistry B, 110 (43), 21764-21770.
33. Bi, Y. L., Corberán, V. C., Zhuang, H., & Zhen, K. J. (2004). Oxidehydrogenation of Ethane with CO_2 over transition metal doped MCM-41 mesoporous catalysts. In Studies in Surface Science and Catalysis (Vol. 153, pp. 343-346).
34. Karamullaoglu, G., & Dogu, T. (2007). Oxidative dehydrogenation of ethane over chromium− vanadium mixed oxide and chromium oxide catalysts. Industrial & Engineering Chemistry Research, 46 (22), 7079-7086.
35. Wang, Shaobin, K. Murata, T. Hayakawa, S. Hamakawa, and fK Suzuki. "Dehydrogenation of ethane with carbon dioxide over supported chromium oxide catalysts." Applied Catalysis A: General 196, no. 1 (2000): 1-8.
36. Ge, X., Zhu, M., & Shen, J. (2002). Catalytic performance of silica-supported chromium oxide catalysts in ethane dehydrogenation with carbon dioxide. Reaction Kinetics and Catalysis Letters, 77(1), 103-108.
37. Zhao, X., & Wang, X. (2010). Characterizations and catalytic properties of chromium silicalite-2 prepared by direct hydrothermal synthesis and impregnation. Catalysis letters, 135(3-4), 233-240.

38. Shi, X., Ji, S., Wang, K., & Li, C. (2008). Oxidative dehydrogenation of ethane with CO_2 over novel Cr/SBA-15/Al_2O_3/FeCrAl monolithic catalysts. Energy & Fuels, 22(6), 3631-3638.
39. Wang, S., Murata, K., Hayakawa, T., Hamakawa, S., & Suzuki, K. (1999). Oxidative dehydrogenation of ethane by carbon dioxide over sulphate modified Cr_2O_3/SiO_2 catalysts. Catalysis letters, 63(1-2), 59-64.
40. Wang, S., Murata, K., Hayakawa, T., Hamakawa, S., & Suzuki, K. (1999). Oxidative dehydrogenation of ethane with carbon dioxide over sulfated zirconia supported metal oxides catalysts. Reaction Kinetics and Catalysis Letters, 68(2), 265-270.
41. Wang, S., Murata, K., Hayakawa, T., Hamakawa, S., & Suzuki, K. (2001). Effect of promoters on catalytic performance of Cr/SiO_2 catalysts in oxidative dehydrogenation of ethane with carbon dioxide. Catalysis letters, 73(2-4), 107-111.
42. Fogler, H. S. (1999). Elements of chemical reaction engineering.
43. Abbas, M. N. (2011). Modelling of porosity equation for water flow through packed bed of mono size spherical packing. Journal of Engineering and Sustainable Development, 15(4), 205-226.
44. Fogler, S. H. (2006). Elements of Chemical Reaction Engineering, Prentice Hall International Series in the Physical and Chemical Engineering Sciences.
45. Krylov O.V, Mamedov A.A, Mirzabekova A.K. 'The regularities in the interaction of alkanes with CO_2 on oxide catalysts'**,** Catal. Today 24 (1995)371-375
46. Krylov, O. V, Mamedov A. K, Mirzabekova S. R.' (1995) Oxidation of Hydrocarbons and Alcohols by Carbon Dioxide on Oxide Catalysts' Ind. Eng.Chem. Res. 34 474-482.
47. Froment, G. F. (1975). 'Model Discrimination and Parameter Estimation in Heterogeneous Catalysis'. AIChE J.**,** 21, 1041-1057
48. Constantinides, A.; Mostoufi, N. Numerical Methods for Chemical Engineers with MATLAB Applications; Prentice Hall Inc.: Upper Saddle River, N. J., 1999
49. Edgar, T. F.; Himmelblau, D. M.(2001).Optimization of Chemical Processes, 2nd ed.; McGraw-Hill: New York,
50. Marquardt, D. W.'(1963) An Algorithm for Least-Squares Estimation of Nonlinear Parameters'. J. Soc. Indust. Appl. Math
51. Boudart, M., & Djéga-Mariadassou, G. (2014). Kinetics of heterogeneous catalytic reactions. Princeton University Press.
52. Boudart, M. (1972). Two step catalytic reactions. Aiche journal, 18(3), 465-478.

CHAPTER -2

LITERATURE REVIEW

2. LITERATURE REVIEW

Ethane oxidative dehydration with CO_2 has been successfully performed over metal oxide based catalysts especially chromium based catalysts. A detailed survey has been made on previous work to identify gaps in literature with regard to characterization, synthesis and catalytic functionalities of silica and chromia catalysts supported by metal oxide used for ethane oxidative dehydrogenation and kinetic aspects of Oxidative Dehydrogenation process.

2.1. Catalyst development:

2.1.1. Oxidative dehydrogenation of ethane using O_2 as oxidant:

Concepción et al [1] studied mesoporous alumina supported vanadium catalysts for ethane oxidative dehydrogenation of ethane to ethylene. The catalysts behavior was dependent on the catalyst V-loading. On a V-coverage of 20% the catalyst has shown 30 % of ethane conversion with 63.4 % ethylene selectivity at 570 ℃. The activity of this catalyst was explained as due to relatively high dispersion of vanadium because of which the deep oxidation of ethane and ethylene reduced. Vanadium-phosphorous catalysts, e.g. V-exchanged pyrophosphates Zr, Sn and Ti were tested for oxidative ethane dehydrogenation from 550 to700 ℃ [2]. Micro structured CeO_2-NiO-Al_2O_3/Ni-foam catalysts have been reported to be very active and selective with highly promising stability [3].

2.1.2. Ethane oxidative dehydrogenation using N_2O as oxidant:

A molybdenum oxide catalyst supported by Silica−Titania has been tested for its ethane ODH activity with N_2O as an oxidant. The ethylene selectivity decreased significantly slower when N_2O was used as an oxidant. Ethane Oxidative dehydrogenation activity was periodically tested from 0.46 - 1.0 mg min/cm^{-3}. N_2O was observed to give greater the selectivity of ethylene at a known conversion of ethane exceeding oxygen, tested at all periodic times [4] The reaction was investigated by oxidizing nitrous oxide over partially reduced silica supported MoO_3 at temperatures of 280–350 ℃. The formation rate of C_2H_4 was substantially constant even if the carbon dioxide mole fraction increased over time. The early rate of C_2H_4 formation was high on a new catalyst. The coke inhibited the reaction and at 280 ℃ a steady state was observed. The N_2O breakdown over the partially reduced MoO_3/SiO_2 resulted in the creation of O− ions, which reacted quickly with ethane in order to generate C_2H_4 [5]. Nitrous oxide introduced into the reaction medium was partly utilized for ethane oxidation and it was also directly decomposed to N_2 and O_2 over iron modified catalysts. [6]. Iron modified ZSM-5 showed high selectivity towards ethene (in the range from 55% to 87%), while Fe-mordenite and Fe-Y catalysed mainly for the total oxidation process. These results indicated that the

zeolite structure played an important role in the formation of iron complexes active for oxydehydrogenation reaction [6].

2.1.3. Catalytic systems used for oxidative ethane dehydrogenation with CO_2 as oxidant

Impregnation versus co-precipitation method of preparation was pursued to identify the effect of Cr dispersion over ZrO_2 and nano-catalysts in ethane ODH to ethylene by oxidizing carbon dioxide [7]. Catalytic tests have shown that Cr-based catalysts produced by co-precipitation have a high conversion of ethane and yield of ethylene than those produced by impregnation. Mimura et al [8] has reported the CO_2 effects on dehydrogenation of ethane on catalysts Cr / H-ZSM-5. At 650 ℃, the Cr / H-ZSM-5 catalyst (SiO_2/Al_2O_3) resulted in 51.6 % conversion of ethane and 79.1 % selectivity of ethylene. It has been declared that CO_2 has maintained catalyst activity by removing the coke from the catalyst surface. Shaobin Wang et al[9] has reported oxidative ethane dehydrogenation by carbon dioxide over nanocatalyst Cr_2O_3,Cr / TiO_2-ZrO_2, Cr_2O_3/SiO_2 and a list of sulfate-modified catalysts Cr_2O_3/SiO_2 [10]. The results have shown that Cr_2O_3/SiO_2 was an efficient catalyst for the ethane dehydrogenation and CO_2 in the feed where catalytic activity was promoted. Cr_2O_3/SiO_2 's catalytic behavior depending on the quantity of sulfate added was influenced by silica sulfate.Cr_2O_3/ 6wt % SO_4–SiO_2 catalysts have shown excellent performance, delivering 55 % ethylene output at 67 % conversion of ethane at 650 °C. Characteristics suggested that the sulfate inclusion actually changes the Cr_2O_3/SiO_2 surface and bulk properties, promoting the decrease of Cr^{6+} to Cr^{3+} in turn in favor of catalytic activity.

Wang with his colleagues reported first on the CO_2 positive impact in the C_2H_6 ODH [11]. They eventually found that Carbon Dioxide, that either produced or getting added to the system, actually the desired hydrocarbon products oxygen reactivity increased over Li^+/MgO catalysts during the CH_4 oxidative coupling and C_2H_6 ODH. Krylov et al. carried out research on the C_1-C_7 CO_2 catalytic ODH of several oxide catalysts, such as Cr_2O_3, Fe_2O_3, MnO_2, as well as their multi - component systems. For C_2H_6 ODH with 800 ° C CO_2, MnO_2-based catalysts showed high levels of activity. Further improvements can be made if promoters such as Cr and K modified the catalyst. Azadeh Talati [12] had used TiO_2–ZrO_2 mixed oxide supports and a slightly different compositions scale between 0 and 100 wt % of ZrO_2 was co-precipitated and Cr_2O_3 was impregnated with 5 wt %. PSD, FTIR, EDX, FESEM, BET and XRD techniques were used to characterize synthesized catalysts. Characterization studies have shown that the mixture of various quantities of ZrO_2 and TiO_2 in the substrates has a clear effect on the molecular structure, texture and activity of catalyst in the ethane oxidative dehydration to ethylene by CO_2 as a smooth oxidant. BET outcomes showed a large area of Cr

/ TiO_2–ZrO_2 nanocatalysts. The largest catalytic yield and behavior (46 % C_2H_4 yield and ethylene selectivity of 95 % at 700ºC) was acquired when 25 wt % of ZrO_2 and 75 wt % of TiO_2 were used as support. Ca-doped ThO_2, synthesized using the solution combustion method, ethane dehydrogenation with CO_2 in the range of 600–750 ºC was tested. It gave 97 % selectivity to ethane with 46% ethane conversion. ThO_2 Ca-doping greatly improved ethane yield. Ethane thermal dehydrogenation occurred above 700 ºC, resulting in a lower selectivity. Krylov et al, et al. Studied 17% MnO / SiO_2 catalyst attaining a 73.1% C_2H_6 conversion and also a 49 % CO_2 conversion at 800 °C. The most active and the most selective catalyst for production of C_2H_4 have been found to be 5.5% Cr-17 % Mn- O / SiO_2.

Table.2.1. Activity of different catalysts for ODH of ethane

S.No	Catalyst Name	T(℃)	X-C_2H_6	S-C_2H_4	Y-C_2H_4	Ref/Author /Year
1.	MoO_3 Nanoclusters Decorated on TiO_2 Nanorods	700	-	-	50.7	Sarkar, Bipul; Goyal, Reena Applied Catalysis, B: Environmental (2017)
2.	Mg_6MnO_8	700	-	89.2	68.2	Yusuff, Seif; Neal, ACS Catalysis (2017)
3.	V_2O_5/MgO-ZrO_2	700	79	-	48	Taghavinezhad, Parisa (2017) American Chemical Society
4.	NiO/ZrO_2(x)-MgO (100-x) nano catalyst	650	66.35	-	56.9	Delir Kheyrollahi Nezhad Journal of Sol-Gel Science and Technology (2016)
5.	Mo-V-Te-Nb-O	400	37	85		Mishanin, I. I Russian Journal of Physical Chemistry A (2016)
6.	Ni-Nb-M-O	650	26	65	32	Qiao, AiLing Catalysis Today (2016)
7.	Cr/clinoptilolite nano catalyst	700	-	98.8	39.3	Rahmani, Farhad Journal of Industrial and Engineering Chemistry (2015)
8.	MoVNbTeOx	650	73	85	-	Chu, Bozhao(2015) Catalysis Science & Technology.
9.	Ga-Loaded TiO_2	700	57	38	-	Koirala, Rajesh ACS Catalysis (2015)
10.	Alkali Chloride Catalysts	-	70	98	-	Gaertner, Christian A Topics in Catalysis (2014)
11.	Mo-V-Te-Nb oxide	400	40	95	-	Hartmann, D DGMK Tagungsbericht (2013)
12.	MPA/Al_2O_3	60-0	24	65		Sri Hari Kumar Kinetics and Catalysis (2013)
13.	MoVTeNb Mixed-Oxide		85	76		Valente, Jaime S Industrial & Engineering Chemistry Research (2014)
14.	RE-NiO	-		56	29	Zhou, Qin Journal of Rare Earths (2013)

15.	VO_x/Al_2O_3	-	27.6	84.5	-	Al-Ghamdi, Sameer A Industrial & Engineering Chemistry Research (2013)
16.	MoO_3/V_2O_5-Al_2O_3	-	35	65	-	Sri Hari Kumar Catalysis Communications (2013)
17.	V_2O_5/Nb_2O_5	600	28	38	-	Qiao, A Catalysis Communications (2013)
18.	Ni-Zr-O nanoparticles	-	60	66	-	Wu, Ying Applied Surface Science (2012)
19.	Nb_2P_4O	-	75	85	-	Weng, Weihao Physical Chemistry Chemical Physics (2011)
20.	$Na_2WO_4/Mn/SiO_2$	750	50.5	94.2	47.6	Jianqiang Zhu, Song Qin,Catalysis Today 148 (2009) 310–315
21.	5Cr–10Ce/SBA-15	700	55.0	96.0	33.9	Xuejun Shi, Catal Lett (2008) 125:331–339.
22.	Ni(19)Ce(8)-M.	450	35	80.0	18.62	Catalysis Today 273 (2016) 259–265

2.1.4. The importance of silica support for chromium catalyst:

Xuejun Shi revealed [13] 99.5 % ethylene selectivity and 66.5 % ethane conversion with a 750 ℃ monolithic catalyst loaded at 5.0% Cr. The hexagonal mesoporous design of SBA-15 was still present even after 1130 h of reaction and the SBA-15 pore walls prohibited the accumulation of the Cr species. Cr interactions with Al_2O_3/FeCrAl and SBA-15 altered the redox features of the catalysts Cr / SBA-15 / Al_2O_3 / FeCrAl. Licheng Liu [14] reported 68.1 % ethane conversion and 53.4 % ethylene yield and 55.6 % at 700 °C.

The catalytic behavior varied according to the support nature. In this reaction, the Cr_2O_3/SiO_2 catalyst performed very well. The loading of Cr_2O_3 also impacted activity of catalyst; 8 wt. % SiO_2 /Cr_2O_3 catalyst generated an 55.5 % ethylene yield at 61.0 % conversion of ethane at 650 °C. Characteristics indicated that the nature of the support influenced the chromium oxide distribution on the surface chromium species' support and structure. In addition, Ithas reported that an appropriate structure was of great importance in order to increase the performance of catalyst. Heteroatom-Incorporated in the framework of various mesoporous materials, as, for example HMS, SBA-15[17-18] and MCM-41[15], high selectivity and activity for light alkanes was demonstrated. Particularly, the two-dimensional SBA-15 was the most commonly used catalyst support. Co-promoted $SiO_2/Mn/Na_2WO_4$ catalysts have been developed and used for C_2H_6 carbon dioxide reaction. Techniques XRD and XPS have been used to study the framework of new and post-reacted catalysts. With the rise in C_2H_6/CO_2, the carbon dioxide conversion continuously increased from 14.70% to 45.10%, while the selectivity and

corresponding C_2H_4 yield decreased sharply from 92.90 % and 51.60 %to 45.40 % and 25.20 % respectively and help with the quick desorption of C_2H_4 from the surface of the catalyst [19].

Xuejun Shi et al. researched [20] catalysts prepared with a relevant aqueous concentration solution of Cr and Ce nitrates by co-impregnation of pure SBA-15. 55 % ethane transformation and 96% selectivity of ethylene were achieved with a catalyst of 700 ℃ over 5.0Cr–10Ce / SBA-15. The C_2H_6 conversion reduced from original 46.40 % to 23.60 % above 5Cr / SBA-15 as well as from 55.5 % to 45.6 % over 5Cr–10Ce /SBA-15. The evident energy activated for ethylene was 96.70–110.70 kJ/mol of the catalysts, which is in agreement with Mimura 's values published previously [20].

Table 2.2: Activity of Chromium based Catalysts for ODH of ethane:

S.No	Catalyst Name	T(℃)/h	X-C_2H_6	S-C_2H_4	Y-C_2H_4	Feed	Ref
1.	5Cr–10Ce/SBA-15	700/(12h)	55.0	96.0	33.9	1:3	[26]
2.	Ce-based monolithic catalystsSBA-15/Al_2O_3/FeCrAl	750/ (1130h)	63.9	87.2	55.7	1:4	[27]
3.	Na_2WO_4/Co(2)-Mn/SiO_2(Co loading)	750/(10h)	60.3	90.7	54.7	1:5	[28]
4.	5%Cr/SiO_2	700	30.7	96.5	29.6	1:7	[29]
5.	Cr_2O_3//SiO_2	650	56:1	92.9	52:1	1:5	[30]
	5wt.% Cr_2O_3//Al_2O_3		19:2	96.5	18:5		
	5 wt.% Cr_2O_3/ZrO_2		57:3	60.4	34:6		
6.	Cr_2O_3	650 (550-650)	22.5	87.0	19.6	1:5	[31]
	Cr_2O_3/SiO_2		56.1	92.9	52.1		
	Cr_2O_3/ SO_4 –SiO_2		67.2	81.8	55.0		
7.	9Fe–9Mn/Si-2	800/(150h)	68.6	92.3		1:1	[32]
8.	Cr_2O_3/SBA-15	675 /(16h)	61.2	82.2	50.3	1:6	[33]

Chromium based catalysts supported by silica and non silica materials are most suitable for oxidative dehydrogenation of ethane due to their high catalytic activity. Metal oxide or silica supported chromium catalysts showed excellent performance for the dehydrogenation of

ethane with carbon dioxide as oxidant. These catalysts were normally prepared by fully dispersing Cr species on supports with high surface areas [23] .The main supports include inorganic oxides like SiO_2, ZrO_2, Al_2O_3, TiO_2 and mesoporous materials like SBA-15, SBA-16, MSU-x and MCM-41. The Chromium loading and the properties, structures of different supports greatly influence the oxidation state, redox status, and dispersion of chromium species on the support.

2.2. Kinetic modeling simulation:

2.2.1. Kinetics studies on ODH of ethane:

Even though ODH of ethane has been known since 1980's most investigations focused on development of catalysts. Very few papers related to kinetics are available. Various kinetic models were reported in the literature for the light alkanes ODH to olefins [21].

Though there is a common perception regarding propane ODH, that was successfully modeled by using classical Mars–van Krevelen (MVK),redox mechanism [22,23], and there is some controversy with regard to ethane ODH. After the earlier works of on mix of oxides Mo–V – Nb [34], a lattice oxygen intervention has been proposed for production of ethylene and mechanism of redox has been proposed. In addition, data of kinetic obtained from catalysts of vanadium oxide have been satisfactorily adapted with rate equations as well as parameters based on actual Mars–van Krevelen mechanism or the mixture of both Langmuir-Hinshelwood expressions for CO_2 formation and Mars–van Krevelen mechanism for ethylene formation.However, Lunsford and Solymosi have proposed a different mechanism for molybdenum catalysts, who proposed a mechanism that would consider the intervention of O−species in the step determination instead of the MVK reaction pattern; that is, Ethane activation includes hydrogen minimalism from O− to further give radicals of ethyl that further respond on the surface with oxygen species. Kaddouri et al 2004[35] conducted kinetic studies using both ethane feed and propane on $NiMoO_4$ and did show that ODH of ethane depended on partial oxygen pressure, while ODH of propane were not. In addition, they noted that ethylene was formed only in the apparent molecular oxygen involvement with a maximum concentration before declining when the feed of the oxygen was switched off. They therefore proposed that while propane ODH is obtained through the lattice oxygen involvement, ethane ODH ethylene is obtained through mild oxidation from O-adsorbed species. Schuurman et al., 1997 [36]. He concluded by conducting TAP experimentation on NiO and recommended that only the ODH of ethane response to nickel includes a parallel- consecutive CO_2 production scheme and ethane is permanently adsorbed and activated through O-species. Despite of the

studies mentioned above, appropriate kinetic model development is still a major concern for the research groups.

Mathematical modeling approach is the normally used mathematical tool to optimize and examine a process. In addition, modeling could also be used before experimental testing to optimize operating parameters present in the scaleup process. The Carbon dioxide use as a soft oxidant in alkanes' oxidative dehydration can reduce CO_2 emissions. Ni-Nb-O catalyst [34] was used to investigate the oxidative dehydrogenation of ethane using CO_2. Heracleous, et al in a static bed reactor is considered for ODH of ethane modeling studies. Diffusion limitations in the catalyst particle is studied and found to have minimal effect on conversion and three different kinetic models were developed to describe the propane ODH reaction. Langmuir Hinshelwood Hougen Watson model describes the ODH process well when compared to Eley Rideal and MVK model. The model parameters are estimated using Levenberg Marquardt Algorithm and thermodynamically validated using Boudart Criteria. Among the LHHW models, Surface reaction model satisfies the Boudart Criteria and model results are well suited to the experimental data.

Ethane ODH is examined with a 10 wt % VO_x backed on C-Al_2O_3 in oxygen - free atmosphere. Reactivity experiments showed that the formulated ODH catalyst shows an ethane conversion of 6.5–27.6 % and an ethylene selectivity of 57.6–84.5 % in 550–600 °C. The formulated catalyst is stable even after ten repetitive ethane pulses. Thus this shows the important function of the lattice oxygen in maintaining the ODH XRD, the absence of V_2O_5 high volume surface species as well as high scattering of VO_x on the surface of the support. The XRD outcomes are in pact with the literature published with vanadia catalysts supported by C-Al_2O_3 with alike VO_x loads.

The VO_x stage is present primarily as polyvanadate or amorphic vanadate. In addition, XRD showed that none of the species are formed because of the communication between the V_2O_5 and the support given by Al_2O_3.NH_3-TPD demonstrates that adding vanadium to c-Al_2O_3 reduced bare c-Al_2O_3 acidity to 6.77 ml NH_3/g from 14.39 ml NH_3/g.

Ethylene oxidative dehydrogenation (ODH-Et) is taken to investigation with a high activity and selectivity mixed oxide MoVTeNb. Experiments are carried out using a combination of ethane, nitrogen and oxygen as feedstock under temperatures between 400 °C and 480 °C, partial ethane and oxygen pressures between 5.0 to 24.2 kPa and the space-time between 10 and 140 g cat•h•mol ethane. Selectivity of ethylene varies between 76 % to 96 %, with conversion range of ethane from 17 % to 85 %. Ethylene conversion in a series of experiments, which is at 440 °C feeding ethylene rather than ethane is between 3 and 14 % and CO_x is only

the product to be reacted. LHHW kinetics shows the best possible ability to characterize the remarks, being a potential representation for the ODH-Et reactors theoretical design in future research. Carbon Dioxide ODH is a new process between C_2H_6 and C_2H_4. Most recent investigations paid attention on the improvement and development of catalysts. Some papers dealt with kinetics. Cr-Mn / SiO_2 catalyst kinetic equation was suggested by Krylov and his colleagues [22-23]. Valenzuela and others examined the Carbon dioxide dehydrogenation kinetics of C_2H_6 over CaO-CeO_2 and CeO_2 systems and discovered that the energies activated are between 30 to 40 kcal / mol as well as reaction orders placed between 0.55-0.95 % for C_2H_6 [24] Xu et al. examined ethane carbon dioxide ODH kinetics for Cr / Si-2 catalysts and gained a 55.5 kJ / mol activation energy [25].

2.3. Observations from the literature survey:

The following points may be taken into consideration while pursuing research on the ethane ODH, particularly with Carbon dioxide as the oxidant.

1. Mixed oxide supported Cr_2O_3 catalysts may be given high priority as there were no studies on these catalysts.
2. When silica was found to be the best support, studies could be extended to understand the influence of mesoporous silica for Cr_2O_3.
3. No detailed studies are available on reaction and reactor modeling.
4. Heat and mass transfer of reactants into the catalyst particle has to be studied to check whether the model is diffusion or reaction controlled and also whether the catalyst inside the reactor is operating in isothermal or non-isothermal condition.
5. No systematic kinetic studies identifying the order of the reaction and activation energy is reported particularly after fitting the reaction data to various models like Eley-Rideal, MVK and LHHW models.
6. It is necessary to check their statistical and thermodynamic consistency.

2.4. Motivation for the study:

From the literature it has been found that most of the research work has been concentrated on a variety of single oxide supported catalysts but there is ample scope to investigate the performance of mixed oxide support. It is generally accepted that a mixed oxide support has an edge over its component single oxides as support in combining their good textural and mechanical properties. The dependence of catalytic activity on the distribution of CrO_x and the structure of Cr species on the surface of mixed oxide has not been reported so far.

It is noticed that sulfation of silica has a positive effect on the catalyst while strong basic promoters (alkali metal oxides) suppress the catalytic activity. It is required to study the

influence of sulfate modification of silica supported (i.e SBA-15 & SBA-16) Chromium oxide catalysts in view of their beneficial effects in controlling the aggregation phenomena. Not much literature is available on mixed oxide supports and sulfate modified silica supports and kinetic modeling for oxidative dehydrogenation of ethane especially using CO_2 as oxidant.

Hence it is concluded that still more investigations (experimental & modeling) are required to improve the performance of silica and non silica supported chromium catalysts for ODH of ethane process.

2.5. Objectives of the thesis work:

The present work was taken up with the following broad objectives:

- Synthesis of chromia catalysts using non-silica (ZrO_2, Al_2O_3 and Al_2O_3-ZrO_2) and silica based (SiO_2, SBA-15, SBA-16) supports.
- Characterization of catalysts by techniques like BET-Surface Area, Temperature Programmed Reduction (H_2-TPR), X-ray diffraction studies (XRD), Fourier Transform Infrared spectroscopy (FTIR) and laser Raman to identify their physic-chemical properties.
- Performance evaluation of the prepared catalysts in a down flow fixed bed reactor for their activity towards ODH of ethane to ethylene by means of Carbon dioxide as an oxidant.
- Identify the best catalyst that offers maximum ethylene selectivity and ethane conversion.
- To study the mass and heat transfer limitations during the kinetic evaluation.
- Kinetic modeling of the ODH process and to identify the best model that fits the experimental data.
- Finding the optimum process parameters for the ODH of ethane process using Response Surface Methodology.

REFERENCES:

1. Concepcion, P., Navarro, M. T., Blasco, T., Nieto, J. L., Panzacchi, B., & Rey, F. (2004). Vanadium oxide supported on mesoporous Al_2O_3: Preparation, characterization and reactivity. Catalysis today, 96(4), 179-186.
2. Lisi, L., Ruoppolo, G., Casaletto, M. P., Galli, P., Massucci, M. A., Patrono, P., & Pinzari, F. (2005). Vanadium-metal (IV) phosphates as catalysts for the oxidative dehydrogenation of ethane. Journal of Molecular Catalysis A: Chemical, 232(1-2), 127-134.
3. Zhang, Z., Han, L., Chai, R., Zhang, Q., Li, Y., Zhao, G,& Lu, Y. (2017). Microstructured CeO_2-NiO-Al_2O_3/Ni-foam catalyst for oxidative dehydrogenation of ethane to ethylene. Catalysis Communications, 88, 90-93.
4. Woods, M. P., Mirkelamoglu, B., & Ozkan, U. S. (2009). Oxygen and nitrous oxide as oxidants: Implications for ethane oxidative dehydrogenation over silica− titania-supported molybdenum. The Journal of Physical Chemistry C, 113(23), 10112-10119.
5. Ward, M. B., Lin, M. J., & Lunsford, J. H. (1977). The oxidative dehydrogenation of ethane by nitrous oxide over molybdenum oxide supported on silica gel. Journal of Catalysis, 50(2), 306-318.
6. Held, A., Kowalska, J., & Nowińska, K. (2006). Nitrous oxide as an oxidant for ethane oxydehydrogenation. Applied Catalysis B: Environmental, 64(3-4), 201-208.
7. Talati, A., Haghighi, M., & Rahmani, F. (2016). Impregnation vs. coprecipitation dispersion of Cr over TiO_2 and ZrO_2 used as active and stable nanocatalysts in oxidative dehydrogenation of ethane to ethylene by carbon dioxide. RSC Advances, 6(50), 44195-44204.
8. Mimura, N., Takahara, I., Inaba, M., Okamoto, M., & Murata, K. (2002). High-performance Cr/H-ZSM-5 catalysts for oxidative dehydrogenation of ethane to ethylene with CO_2 as an oxidant. Catalysis Communications, 3(6), 257-262.
9. Wang, S., Murata, K., Hayakawa, T., Hamakawa, S., & Suzuki, K. (1999). Oxidative dehydrogenation of ethane by carbon dioxide over sulfate modified Cr_2O_3/SiO_2 catalysts. Catalysis letters, 63(1-2), 59-64.
10. Talati, A., Haghighi, M., & Rahmani, F. (2016). Oxidative dehydrogenation of ethane to ethylene by carbon dioxide over $Cr/TiO_2–ZrO_2$ nanocatalyst. Effect of active phase and support composition on catalytic properties and performance. Advanced Powder Technology, 27(4), 1195-1206.

11. Wang, D., Xu, M., Shi, C., & Lunsford, J. H. (1993). Effect of carbon dioxide on the selectivities obtained during the partial oxidation of methane and ethane over Li+/MgO catalysts. Catalysis letters, 18(4), 323-328.
12. Talati, A., Haghighi, M., & Rahmani, F. (2016). Oxidative dehydrogenation of ethane to ethylene by carbon dioxide over $Cr/TiO_2–ZrO_2$ nanocatalyst. Effect of active phase and support composition on catalytic properties and performance. Advanced Powder Technology, 27(4), 1195-1206.
13. Shi, X., Ji, S., Wang, K., & Li, C. (2008). Oxidative dehydrogenation of ethane with CO_2 over novel $Cr/SBA-15/Al_2O_3$/FeCrAl monolithic catalysts. Energy & Fuels, 22(6), 3631-3638.
14. Liu, L., Li, H., & Zhang, Y. (2006). A comparative study on catalytic performances of chromium incorporated and supported mesoporous MSU-x catalysts for the oxidehydrogenation of ethane to ethylene with carbon dioxide. Catalysis today, 115(1-4), 235-241.
15. Du, G., Lim, S., Yang, Y., Wang, C., P fefferle, L., & Haller, G. L. (2006). Catalytic performance of vanadium incorporated MCM-41 catalysts for the partial oxidation of methane to formaldehyde. Applied Catalysis A: General, 302(1), 48-61.
16. Lin, C., Tao, K., Yu, H., Hua, D., & Zhou, S. (2014). Enhanced catalytic performance of molybdenum-doped mesoporous SBA-15 for metathesis of 1-butene and ethene to propene. Catalysis Science & Technology, 4(11), 4010-4019.
17. Capek, L., Bulánek, R., Adam, J., Smoláková, L., Sheng-Yang, H., & Cicmanec, P. (2009). Oxidative dehydrogenation of ethane over vanadium-based hexagonal mesoporous silica catalysts. Catalysis Today, 141(3-4), 282-287.
18. Lin, C., Tao, K., Yu, H., Hua, D., & Zhou, S. (2014). Enhanced catalytic performance of molybdenum-doped mesoporous SBA-15 for metathesis of 1-butene and ethene to propene. Catalysis Science & Technology, 4(11), 4010-4019.
19. Nakagawa, K., Kajita, C., Okumura, K., Ikenaga, N. O., Nishitani-Gamo, M., Ando, T., & Suzuki, T. (2001). Role of carbon dioxide in the dehydrogenation of ethane over gallium-loaded catalysts. journal of Catalysis, 203(1), 87-93.
20. Shi, X., Ji, S., & Wang, K. (2008). Oxidative dehydrogenation of ethane to ethylene with carbon dioxide over Cr–Ce/SBA-15 catalysts. Catalysis letters, 125(3-4), 331-339.
21. Mimura, N., Okamoto, M., Yamashita, H., Oyama, S. T., & Murata, K. (2006). Oxidative dehydrogenation of ethane over Cr/ZSM-5 catalysts using CO2 as an oxidant. The Journal of Physical Chemistry B, 110(43), 21764-21770.

22. Argyle, M. D., Chen, K., Bell, A. T., & Iglesia, E. (2002). Effect of catalyst structure on oxidative dehydrogenation of ethane and propane on alumina-supported vanadia. Journal of Catalysis, 208(1), 139-149.
23. Krylov, O. V., Mamedov, A. K., & Mirzabekova, S. R. (1995). The regularities in the interaction of alkanes with CO_2 on oxide catalysts. Catalysis Today, 24(3), 371-375.
24. Krylov, O. V., Mamedov, A. K., & Mirzabekova, S. R. (1995). Oxidation of hydrocarbons and alcohols by carbon dioxide on oxide catalysts. Industrial & engineering chemistry research, 34(2), 474-482.
25. Valenzuela, R. X., Bueno, G., Corberán, V. C., Xu, Y., & Chen, C. (2000). Selective oxidehydrogenation of ethane with CO_2 over CeO_2-based catalysts. Catalysis today, 61(1-4), 43-48.
26. Xu, L. Y., Lin, L. W., Wang, Q. X., Yan, L., Wang, D. B., Liu, W. C., ..& Arena, F. (1998). A new route for C_2H_4 production by reacting C_2H_6 with CO_2 over a catalyst of chromium oxide supported on silicalite-2 type zeolite.
27. Wang, S., Murata, K., Hayakawa, T., Hamakawa, S., & Suzuki, K. (2001). Effect of promoters on catalytic performance of Cr/SiO_2 catalysts in oxidative dehydrogenation of ethane with carbon dioxide. Catalysis letters, 73(2-4), 107-111.
28. Watson, R. B., Lashbrook, S. L., & Ozkan, U. S. (2004). Chlorine modification of Mo/silica-titania mixed-oxide catalysts for the oxidative dehydrogenation of ethane. Journal of Molecular Catalysis A: Chemical, 208(1-2), 233-244.
29. P.Thirumala Bai ,Manokaran, V., Saiprasad, P. S., & Srinath, S. (2015). Studies on Heat and Mass Transfer Limitations in Oxidative Dehydrogenation of Ethane Over Cr_2O_3/Al_2O_3 Catalyst. Procedia Engineering, 127, 1338-1345.
30. Kumar, a. s. h., & prasad, p. (2014). Cracking and oxidative dehydrogenation of ethane to ethylene: process and intensification options. Industrial Catalysis and Separations: Innovations for Process Intensification, 287.
31. Jianqiang Zhu, Song Qin, Songtao Ren, (2009). $Na_2WO_4/Mn/SiO_2$ catalyst for oxidative dehydrogenation of ethane using CO_2 as oxidant. Catalysis Today 148 310–315.
32. Xin Ge, Mingming Zhu, (2002).Catalytic performance of silica-supported chromium oxide catalysts in ethane dehydrogenation with carbon dioxide. React.Kinet.Catal.Lett. Vol. 77, No. 1, 103-108,
33. Shaobin Wang, (2000). Dehydrogenation of ethane with carbon dioxide over supported chromium oxide catalysts. Applied Catalysis A: General 196 1–8.

34. Shaobin Wang, (1999). Oxidative dehydrogenation of ethane by carbon dioxide over sulfate-modified Cr_2O_3/SiO_2 catalysts. Catalysis Letters 63 59–64.
35. Heracleous, E., & Lemonidou, A. A. (2006). Ni–Nb–O mixed oxides as highly active and selective catalysts for ethene production via ethane oxidative dehydrogenation. Part I: Characterization and catalytic performance. Journal of Catalysis, *237*(1), 162-174.
36. Kaddouri, A. (2004). CH bond activation in the presence or absence of oxygen or nitrous oxide. Reaction Kinetics and Catalysis Letters, 82(2), 401-409.
37. Schuurman, Y., Ducarme, V., Chen, T., Li, W., Mirodatos, C., & Martin, G. A. (1997). Low temperature oxidative dehydrogenation of ethane over catalysts based on group VIII metals. Applied Catalysis A: General, 163(1-2), 227-235.

CHAPTER –3

EXPERIMENTAL DETAILS

3.0. EXPERIMENTAL DETAILS:

This section of the present thesis work illustrates the outlines of the well-established principles and methods adopted with respect to catalyst preparation, their characterization by various techniques and evaluation in oxidative dehydrogenation of ethane to ethylene.

3.1. Construction of catalyst:

The catalysts utilised in the process were produced by adopting two major methods namely precipitation and impregnation. The general descriptions of these methods are given below.

3.1.1. Production of catalyst by impregnation:

In this approach a definite solution containing familiar amount of precursor makes contact with appropriate solid support. The adsorption ability of the support, the impregnation period and temperature are the parameters that affect the active metals to bind with the support surface. Wet impregnation and incipient wetness impregnation are the two methods used in catalyst preparation. They can be varied relying on the quantity of the known solution. In wet impregnation, solution is taken in excess quantity. Following certain duration of time the surplus amount of solid is isolated by evaporation and then followed by drying which allows the solid to set apart. In the incipient wetness impregnation method the amount of assigned solution is equal or somewhat less than the supports pore volume.Fig.3.1 & 3.2 [4]

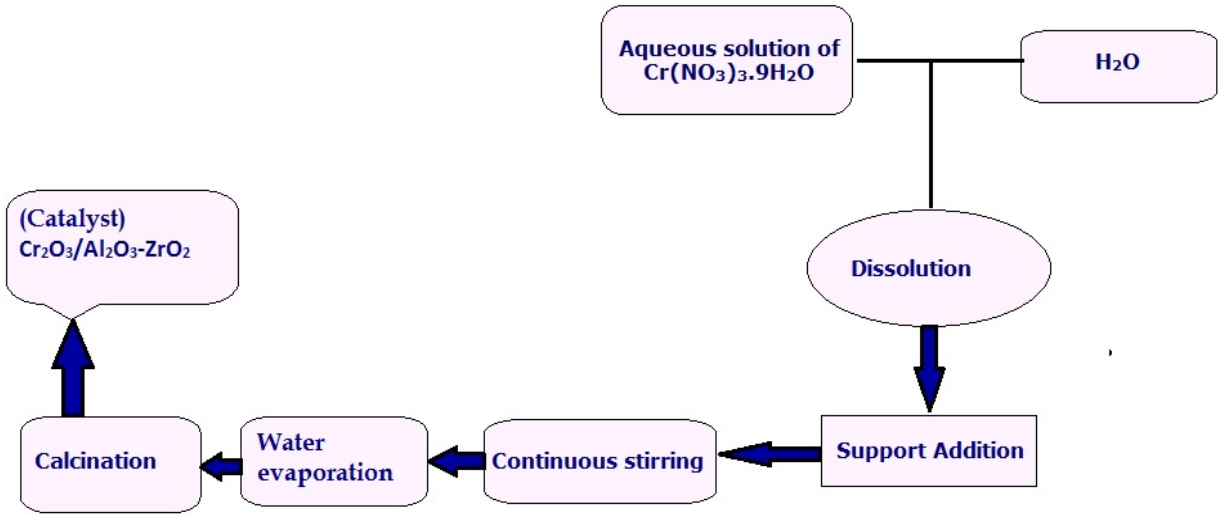

Figure.3.1. Flow diagram for Impregnation Method

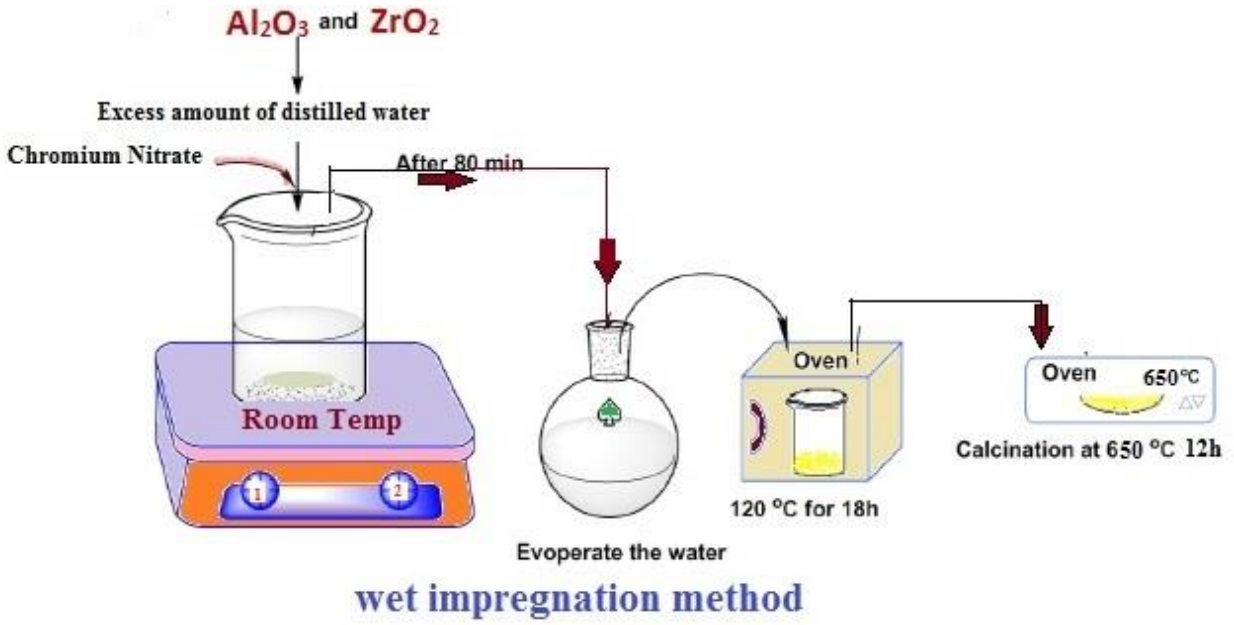

Figure.3.2. Experimental procedure for Wet impregnation method

3.1.2. Precipitation:

In this method the metal salts are allowed to dissolve in water and the precipitation process takes place by the steady addition of precipitating agent like ammonium hydroxide or sodium carbonate at room temperature until the pH reaches the assigned value. The precipitate thus acquired is cleaned with distilled water, dried overnight at a temperature range of 100-120 ℃. [4] Fig 3.3.

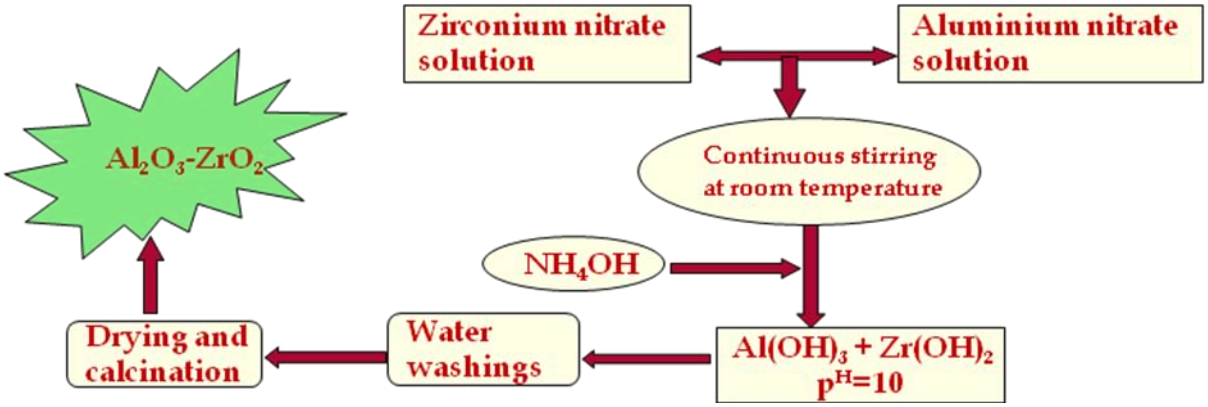

Figure.3.3: Flow diagram for Precipitation method

3.1.3. Co-Precipitation:

In co-precipitation method association of the catalyst components is attained by the generation of very minute or mixed crystallites consisting of the required constituents. pH is adjusted to the assigned level and is uniform throughout the process. The low solubility and

untroubled decomposition makes hydroxides and carbonates more preferable for this process and they are less toxic in nature. Factors that alter the properties of precipitated catalyst are shown in Fig 3.4 [3].

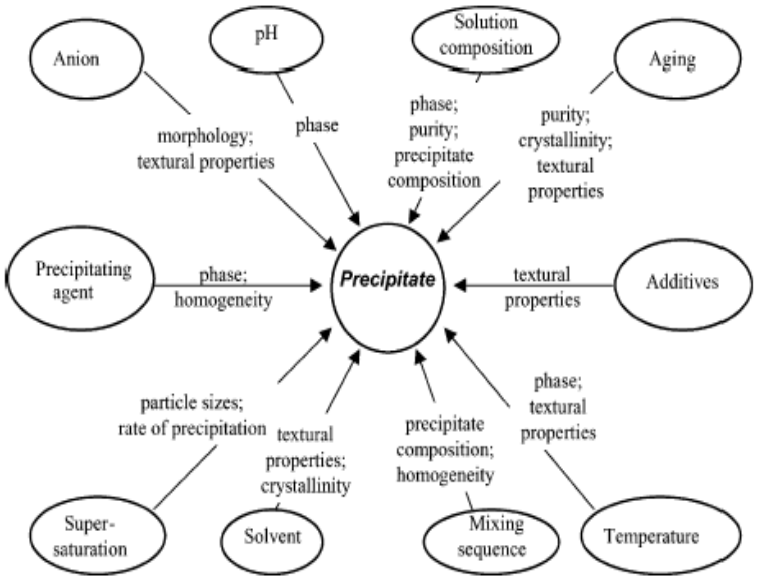

Figure.3.4. Factors influencing the properties of precipitated catalysts

3.1.4. Hydrothermal method:

In this process precursor solution, in occupancy of an alkali, is autoclaved at a definite temperature for certain time. Diluted solution of precursor and KOH are mixed and arranged in Teflon-lined stainless-steel autoclave reactor [3]. It is maintained at 70 - 200℃ for a residence time of 10 to 24 hours depending upon process and then it is air-cooled to room temperature. The acquired precipitate is collected by filtration process then it is washed thoroughly and it is dried (Fig 3.5).

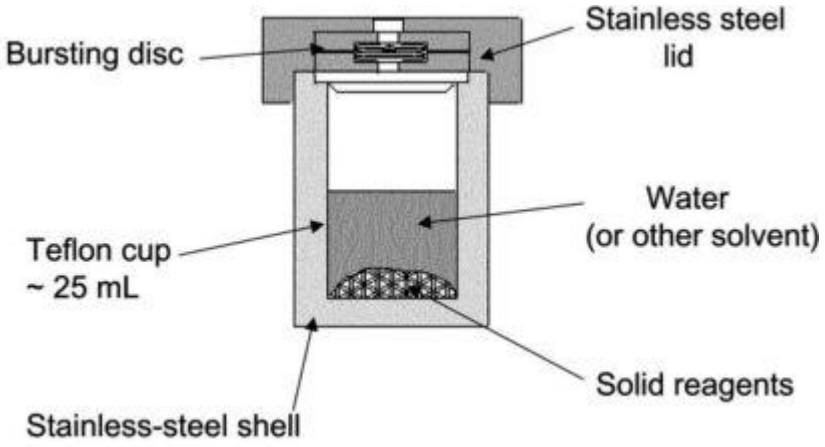

Figure.3.5. Hydrothermal method

3.1.5. Further treatment of the solid mass:

After the completion of precipitation or impregnation process the catalyst is normally treated with the following operations.

3.1.5. (A). Drying:

In drying operation the solid gets free from the solvent. Crystalline solid masses get mostly benefitted from drying but it is a complex process for aggregated lumpy mass (flocculate) and hydrogels that contains 90 % water. In this scenario the elimination of water molecules allows the texture to collapse and therefore required precautions should be taken while drying high porous materials. A support with high adsorption ability (high porosity), drying conditions will have no effect on the uniform dispersion of the active component. The carriers having low adsorption ability (low porosity), these parameters greatly influence the texture and the properties of the resulting catalysts. The evaporation rate should be slow and reversible so that it allows even redistribution of the active components on the surface of support [1, 3].

3.1.5. (B). Calcination:

Calcination allows heating of the material without the evolution of a liquid phase product. The temperatures in calcination are usually greater than compared to other reaction processes. In this process, various transformations like degradation of the impregnated metal salt into oxides, interaction among active constituents and surface of the support, coalescing of the support and condensation of the hydroxyl groups take place. During calcination the catalyst also solidifies into a final form, for example, amorphous into crystalline, therefore the surface and mechanical properties of the catalyst are derived mainly in this process.

3.1.6. Methodology of catalyst preparation adopted in the present work

In the present work the following different methods of preparation were adopted to prepare chromia on silica, SBA-15 and non-silica (Al_2O_3–ZrO_2) supported catalysts.

Commercially available Al_2O_3 was considered as a support. Hydrolysing the aqueous solution of $Zr(O)(NO_3)_2$ by using $8H_2O$ with ammonium hydroxide by maintaining a pH of 10 produced ZrO_2. Co-precipitation is the method used to prepare the mixed oxide Al_2O_3–ZrO_2 support in the molar ratio 1:1 by mixing ammonium hydroxide solution with mixed aqueous solution of $Zr(O)(NO_3)_2.8H_2O$ and $Al(NO_3)_3.9H_2O$ till the pH value of 10 is achieved. The precipitate was separated by filtration, washed thoroughly using deionized water and later dried at 120 ℃ for 12 h in air oven and calcined finally at 650 ℃ for 6 h. The catalysts were

prepared by using impregnation method with 15 wt. % Cr_2O_3 on the above supports taking assigned quantities of $Cr(NO_3)_3.9H_2O$. After drying for 12h at 120 ℃, the catalyst masses were sent to calcination process at 650 ℃ for 6 h. By keeping the Cr_2O_3 content uniform (15 wt%) in all the catalysts, the term 15 wt. % is used in appointing the catalysts during the following discussion. SBA-15 was produced according to the procedure by taking 20 g of triblock copolymer (P 123, Aldrich) that was dispersed in a mixture of 465 g of distilled water and 137.5 g of 35% hydrochloric acid (M/s. Loba Chemie). 44g of tetraethyl orthosilicate (TEOS, Aldrich) was then added under uniform stirring at 40 ℃ and the resultant mixture was subjected to the hydrothermal treatment at a temperature of 100 ℃ for duration of 24 h. The acquired slurry was sent to filtration process, dried in air at 110 ℃ for 12 h and then sent to calcination in air at 550 ℃ for 4 h. The Cr_2O_3/SBA-15 catalyst with 5 wt. % Cr_2O_3 (denoted as Cr/SBA-15) was developed by impregnating the support with demanded amount of aqueous chromium nitrate (Wako Chemicals). Aqueous ammonium sulphate of required quantity was used to modify (by wet impregnation) the SBA-15 support such that the SO_4 was 6%. The sample is termed as S.SBA-15. The Cr/S.SBA-15 was prepared with 5 wt. % Cr_2O_3 on the sulphate modified support following the same procedure for Cr/SBA-15 catalyst. For the above three samples, the impregnation step was carried out by drying at 120 ℃ and calcined at 700 ℃ for 4 h. Fig 3.2 [5].

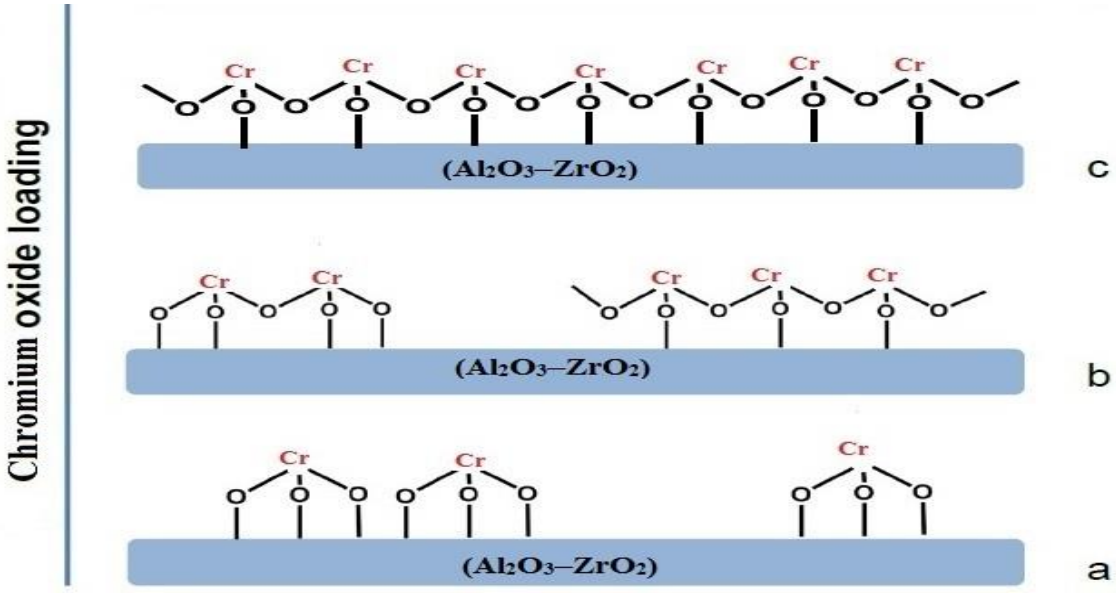

Figure.3.6. Chromium metal loading on mixed oxide catalyst with load variations

3.2. Catalyst characterization:

3.2.1. BET surface area:

The catalytic oxidative dehydrogenation of ethane took place in a fixed-bed reactor. The design details of the fixed bed reactor are given below. A fixed bed reactor system with a microprocessor-based control was setup with the following provisions. On-line data acquisition and processing of data, mass flow controllers for gas feeds, a metering pump for the liquid feed and a gas chromatograph for the on-line sample collection and analysis.

$$\frac{P}{V_a\,(P_o - P)} = \frac{1}{V_m \cdot C} + \frac{C-1}{V_m \cdot C} \cdot \frac{P}{P_o} \qquad \text{- - - - (3.1)}$$

Where

P_o = saturated vapour pressure of the adsorbent

P = equilibrium adsorption pressure

V_m = volume of adsorbate required to form a monolayer coverage

V_a = volume (in ml) adsorbed at STP at pressure P

C = constant related to heat of adsorption

A graph drawn between P/Va (P_o-P) versus relative pressure of P/P_o which is a straight line with slope of (C–1)/(V_mC) and intercept of 1/(V_mC), respectively. Knowing the values of slope and intercept allows calculation of V_m.

$$\frac{P}{V_{ads}(P_0 - P)} \quad Vs \quad \frac{P}{P_0} \qquad \text{- - - - (3.2)}$$

Will be a straight line (within the range of P/P_o: 0.05-0.30) with slope of (C-1)/V_mC and intercept of 1/V_mC. By considering these values of intercept and slope V_m can be determined and further, specific surface area is calculated as follows:

$$\text{Specific surface area } \left(\frac{m^2}{g}\right) = \frac{V_m \times N_A \times A_m}{22414 \times W} \qquad \text{- - - - (3.3)}$$

Where

N_A = Avogadro number (6.023×10^{23})

V_m = Monolayer volume in ml at STP

W = Weight of the catalyst in g

A_m = Cross sectional area of adsorbate molecule (16.2 Å for N_2 molecule)

Surface area can be calculated using all conventional glass high vacuum system at liquid nitrogen (77K) temperature by nitrogen adsorption process. A systematic representation of the apparatus used is shown in Figure.4. A catalyst of known weight is taken in a glass sample tube and fused to the high vacuum system and evacuated to 10-6 Torr vacuum at 423 K to ensure that no pre-adsorbed gas remains on the catalyst surface. To get the value of dead volume experiment was carried out at liquid nitrogen temperature using helium gas in successive steps by quantifying the volume engaged at different pressures. After complete removal of helium gas at low pressures such as 10-6 Torr, nitrogen gas was adsorbed in the same way as explained above. The volume of N_2 adsorbed (V_{ads}) was obtained from the difference in the volumes of nitrogen and helium introduced into the sample tube at the same equilibrium pressures. From the measured values of P, P_o and V_{ads}, specific surface area of the catalyst was investigated by BET equation.

3.2.2. Introduction to Powder X-ray diffraction (XRD) :

XRD is an important technique for knowing the characteristics of catalysts and investigates both qualitative and quantitative phase changes. It gives the information about the crystallinity of the specific components, and allows identification of ensemble size of the components in the catalyst. This analysis gives information about the presence of foreign atoms of an active component in its crystal lattice, lattice constants, structure of the substance, and the transition of different phases. X-ray diffractometer consists of a circular table with a stationary X-ray source and a moving detector, usually a proportional counter, which records reflected beam intensity which is a function of the reflected angle 2θ. Diffraction patterns of powders are compiled in the powder diffraction file search manual. In the XRD technique, to observe the intensity of scattering radiations relating to scattering angle 2, the Bragg's peaks are measured for which fixed wavelength (λ) is chosen as the incident. The d' spacing is estimated from the peaks using the Bragg's equation.

$$n\lambda = 2d \sin(\theta) \qquad - - - - (3.4)$$

Here,

n = Order of reflection (1, 2, 3.....etc.)

λ = Wave length of the X-ray radiation

d = Spacing between two successive planes

θ = The angle between the scattered radiation and the catalyst plane.

The diffractograms of the catalysts obtained from the diffractometer are with different peak heights of which the strongest intense peak is designated as d1 and also taken as 100% intense peak. The remaining peaks are designated as d2, d3, d4 etc., corresponding to the order of their intensities. There are four routine steps to identify the compound and its phase. The proper Hanawalt group for d_1 is located in the numerical index. The values of d_2, d_3 and d_4 etc., are next found in the group. The d values sought for d_1, d_2, d_3, etc., were then matched with the reported values followed by a comparison of relative intensities. Based on the intensities as well as 'd' values, identification of phase and confirmation is attained with reference to the compound data card in the ASTM file. All the XRD results were recorded on a Rigaku Diffractometer with the use of Ni-filtered CuKα radiation (λ = 1.5405 A^o) which are reported in this thesis.

3.2.3. Temperature programmed reduction:

In recent years, TPR is the most extensively used physio–chemical techniques for the characterization of solid materials and also metal supported catalysts. It is used to find the efficient reduction conditions. It is highly reactive to sentient and will rely on its reducibility under investigation. It has the ability to monitor frequently the successive reactions of species with increasing the temperature. Thus, it gives information about the metal – metal, metal – support interactions as well as the state of dispersion of metallic component in catalysis, since reduction conditions depends on all these parameters.

The main idea of this technique is to monitor the reactions of the metal catalyst with the gaseous environment on the surface (or) in bulk volume by carrying out a continuous analysis of the gas phase. In TPR experiment, solid or catalyst is filled in a reactor tube on which a reducing gas is allowed to get in contact with it. Thermal conductivity detector (TCD) is used to examine the effluent gases. This study gives details about interactions between metal oxide and support, zeolites-metal ions valence state and catalyst supports and the identifying formation of alloy in bimetallic catalysts.

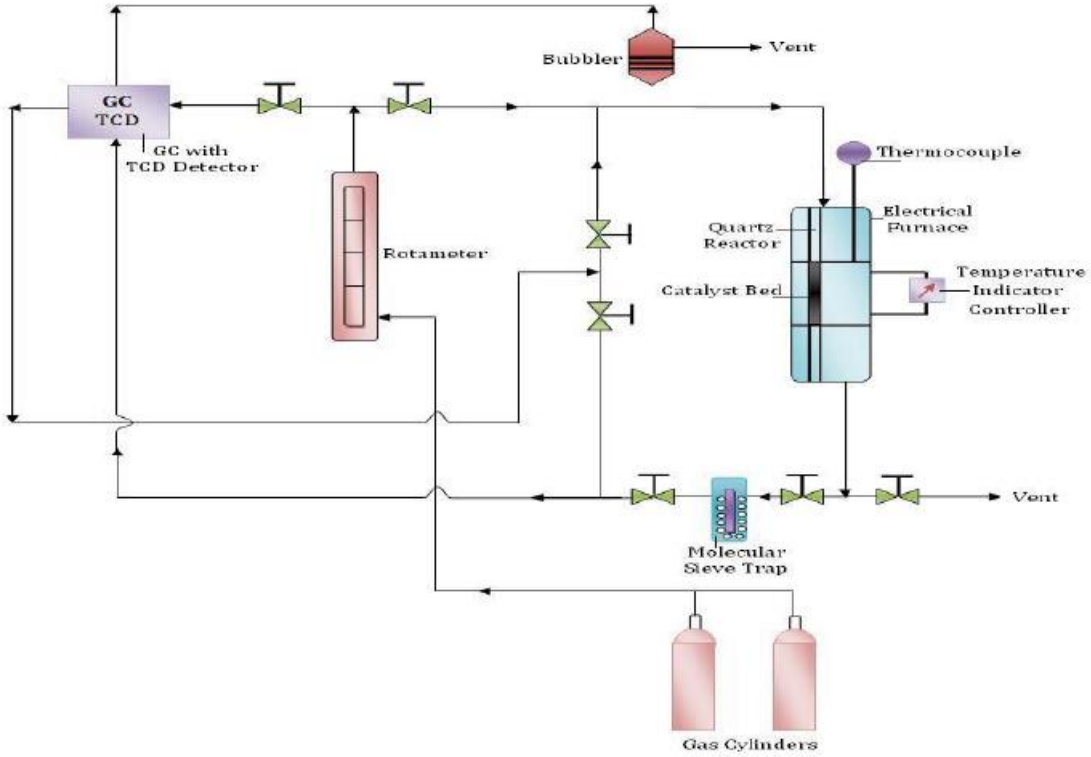

Figure.3.7. Schematic diagram of TPR

In this thesis, the TPR experiment to estimate the reduction behaviour of the catalysts were carried out at a flow of 5 % H_2/Ar mixture gas and maintaining the total flow rate at 60 mL/min including with a change in temperature of 10 °C/min. The catalysts were pre-treated with helium gas at 200 °C for duration of 2 h.

Thermal conductivity detector helps in notifying the consumption of Hydrogen. Fig 3.7 shows the schematic representation of the TPR set up.

.

3.2.4. X-ray photoelectron spectroscopy:

X-ray photoelectron spectroscopy (XPS) is a popular approach to emphasize the chemical information. This spectroscopic technique is used to measure the elementary composition along with electronic state and chemical state within a material. The chemical constitution of solids with a depth of 20 Å can be investigated by using XPS. X-ray photoelectron spectroscopy is conducted by exposing the sample material to radiation with a beam of mono energetic soft X-rays and material has been analysed for energy through the electrons emitted. Al Kα (1486.6 eV) or Mg Kα (1253.6 eV) X-rays are conventionally used. The penetrating power of these photons in a solid is of limited order of 1-10 mm. Photoelectric effect allows the interaction between the photons and the atoms present on the surface region which results

in the emission of the electrons. The kinetic energy (KE) of these electrons is calculated by using the below equation:

$$KE = h\vartheta - BE - \varphi s \qquad \text{- - - - (3.5)}$$

There are several ions from various atoms which correspond to a variation in the kinetic energies of the electrons. The samples used for analysing the XP spectra were registered in a Shimadzu (ESCA 3400) spectrometer by using the excitation source, Mg Kα (1253.6 eV) radiation. Later the binding energy of the adventitious carbon (C 1s) was set at 284.6 eV to charge the catalyst samples. This analysis was carried out at ambient temperature and pressure varying between 10-6 Pa. A precision of ±0.1 eV was maintained while estimating the binding energies of the electrons. Quantification of atomic ratios was achieved by estimating the elemental peak areas, a subsequent Shirley background subtraction and correcting using atomic sensitivity factors supplied by the instrument manufacturer [1,2].

3.2.5. Raman spectroscopy:

Raman spectroscopy can be used to identify broad range of solid, liquid and gaseous components. It eliminates usage of sample preparation, since it is not required. In this process mono chromatic light casts upon the trial sample and a spectrometer is utilised to investigate the light that is dispersed by the trial sample. Usually in absorption or any of the scattering processes, photons will be able to interact with the matter only at their molecular phase. Scattering can take place both elastically or in elastically. Moreover, elastic processes are commonly referred as Rayleigh scattering, whereas the inelastic processes are referred as Raman scattering. The electric field component of the scattering photon perturbs the electron cloud of the molecule and may be regarded as exciting the system to a 'virtual' state. Raman scattering usually takes place whenever the system supplies the energy to the photon and thus decaying of the system to vibrational energy levels occurs. The Raman shift can be defined as the frequency shift which relates the energy difference between the incident photon and the dispersed photon. The Raman shift generally takes place as an up-shift or down-shift relying on whether the system loses or acquires the energy where the down-shifted components are referred as the Stokes lines and the up-shifted constituents corresponds to anti-Stokes lines. A graph drawn between the total numbers of photons detected and the Raman shift will fetch us a Raman spectrum. Various materials consist of several vibrational modes, and thus vary in their Raman spectra and assists in identifying the material. In liquids and gases the material is made up of the vibrational energy levels of the independent molecules whereas Crystals consists of molecules with definite vibrational energy levels. Photons are characterized by the macroscopic vibrational modes.

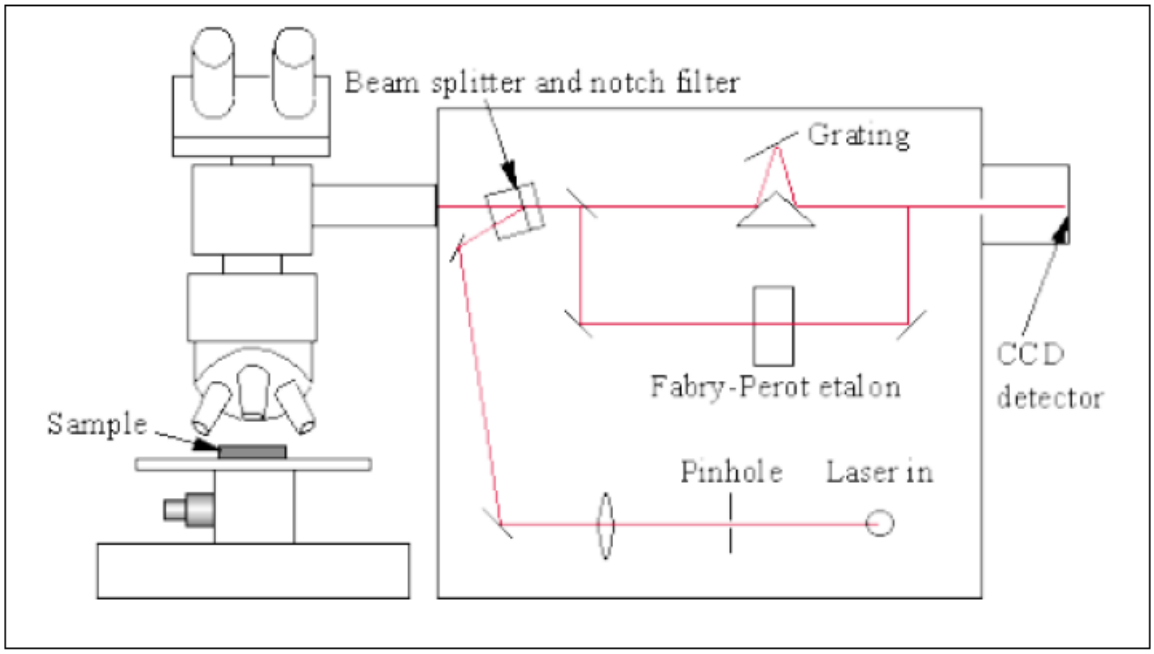

Figure.3.8. Schematic representation of Raman spectrometer

The high monochromatic nature and beam fluxes allow the laser to function as a photon source in the above Raman spectrometer. The Raman effect is generally weak since compared to the Rayleigh dispersed component the Stokes lines are usually105 times weaker. In Raman spectrometer microscope allows the laser beam to focus on small spot (<1-100 μ t) which helps in understanding the characteristics of the material. L to the sample proceeds backwards into the spectrometer through the microscope optics. A charge coupled device (CCD) detects the shifted radiation and data acquisition and curve fitting are processed in the system. The above mentioned factors allow us to know the sensitivity and accuracy of the Raman spectroscopy method [3, 5].

3.2.6: Particle size distribution:

Customary-sized sieves (1000μm to 5μm) are owned to acquire the designated size distribution of the catalyst. The top sieve consists of the allocated quantity of catalyst which is measured precisely. Then this catalyst particles are sieved down and the quantity of catalyst particles in the sieves are measured. This method was performed frequently to maintain the precision of the results [5, 4].

3.3. Experimental evaluation of catalysts and the calculation methodology:

3.3.1. Activity Measurement:

Figure.3.9. ODH reactor system

The catalytic oxidative dehydrogenation of ethane took place in the reactor as described in fig.3.9. The design details of the fixed bed reactor are given below. The reactor system with a microprocessor-based control was setup with the following provisions. On-line data acquisition and processing of data, mass flow controllers for gas feeds, a metering pump for the liquid feed and a gas chromatograph for the on-line sample collection and analysis.

The specifications for the individual equipment were as follows:

a) Mass flow controllers (MFCs):
   i. Mass flow controllers were provided for ethane, helium, nitrogen and oxygen.
   ii. Flow rates of the gases: C_2H_4: 10-500 mL/min; O_2: 10-500 mL/min; He: 10-50mL/min.
   iii. MFCs with in-let and outlet line filters.
   iv. Operating pressure was ambient (1atm).

b) Reactor: Made of stainless steel, length: 300mm, inner diameter: 10 mm, Electrical heating with two zone split type furnaces; programmable temperature controllers with variable heating rates, for the two furnaces; A thermo well of 6 mm outer diameter incorporated in the reactor with O-ring and nut fitting facility; Two bed temperature indicators. Maximum temperature of operation: 900 ℃, suitable thermocouples.

c) Reactor pressure safety valve was set at 2 bar, pressure gauge at inlet and outlet maximum range 2.5 atm and a pressure transmitter.

d) Non-return valves (NRVs) in each gas inlet and outlet (0-5 atm) and to the liquid feed line.

e) Reactor downstream: Condenser with cooling jacket.

f) On-line control and data acquisition system for the above reactor set-up.

g) Six MFCs and two programmable temperature controllers, bed temperatures at two points, outlet gas temperature.

h) All the above hardware connected to a PC based control system with suitable SCADA software.

i) Analytical: A two port gas chromatograph with on-line sample collection and analysis and a PC based data acquisition and processing system with the required software.

j) Skid mounted reactor system:

Figure.3.10. NUCON 5765 Online Gas chromatography system

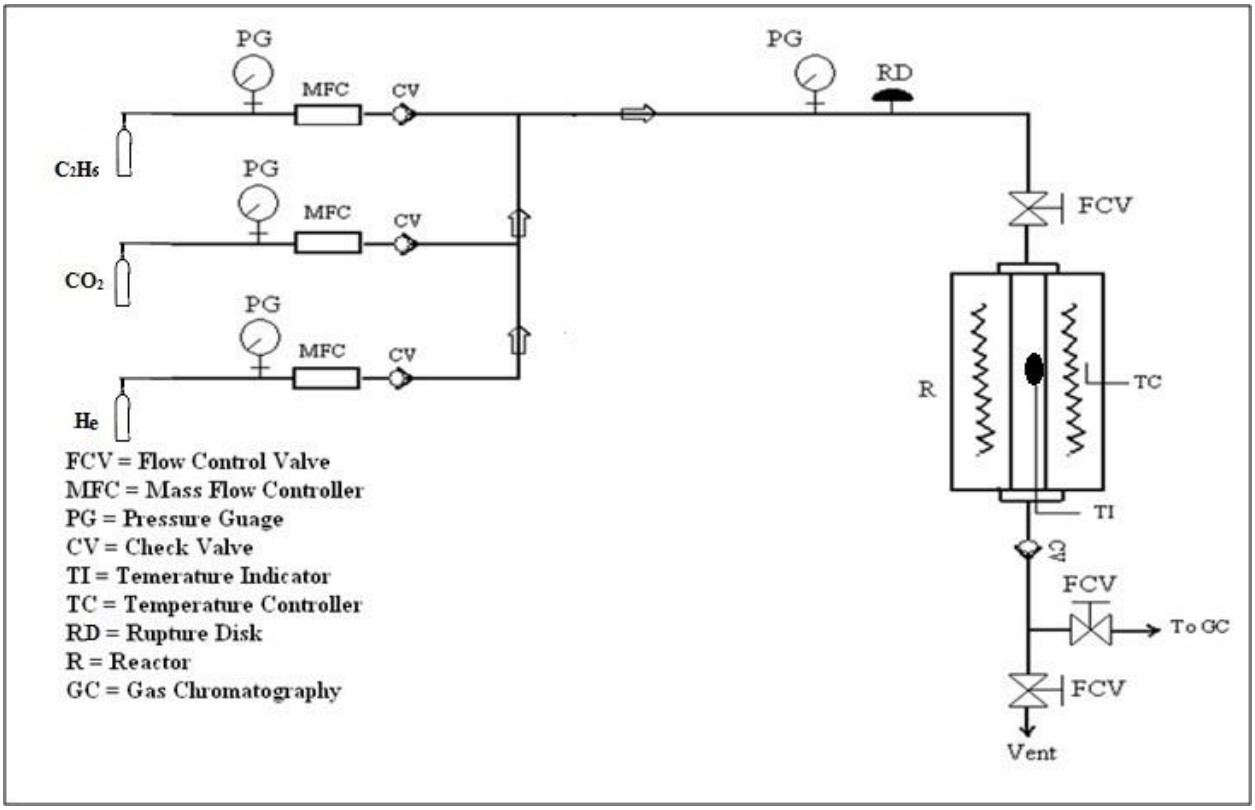

Figure.3.11.Schematic diagram of ODH experimental setup

3.3.2. Calculation procedure:

$$\text{Conversion of ethane } X_{C_2H_6} = \frac{\text{moles of ethane reacted}}{\text{moles of ethane fed}} \quad (3.6)$$

$$X_{C_2H_6} = 1 - \frac{2*n_{C_2H_6}}{2*n_{C_2H_6}+2*n_{C_2H_4}+n_{CH_4}} \quad (3.7)$$

$$\text{Conversion of } CO_2 X_{CO_2} = \frac{\text{moles of } CO_2 \text{ reacted}}{\text{moles of } CO_2 \text{ fed}} \quad (3.8)$$

$$X_{CO_2} = 1 - \frac{n_{CO_2}}{n_{CO_2}+n_{CO}} \quad (3.9)$$

$$\text{Selectivity of ethylene } S_{C_2H_4} = \frac{\text{No of moles of ethylene formed}}{\text{No of moles of methane formed}} \quad (3.10)$$

$$S_{C_2H_4} = \frac{2*n_{C_2H_4}}{2*n_{C_2H_4}+n_{CH_4}} \quad (3.11)$$

$$\text{Yield of ethylene } Y_{C_2H_4} = \frac{\text{No of moles of ethylene formed}}{\text{Total no of moles of products formed}} \quad (3.12)$$

Ethane conversion (X C_2H_6) and selectivity to ethane (S C_2H_4) are defined as:

XC_2H_6 (%) = (moles of C_2H_6 converted * 100) / (moles of C_2H_6 in feed).

SC_2H_4 (%) = (moles of C_2H_4 in outlet gas* 100) / (moles of C_2H_6 in feed).

CO_2 conversion (X CO_2) and selectivity to CO (SCO) are defined as:

X CO_2 (%) = (moles of CO_2 converted *100) / (moles of CO_2 in feed).

S CO (%) = (moles of CO in outlet gas *100) / (moles of CO_2 in feed).

REFERENCES:

1. Srilatha, K., Lingaiah, N., Prasad, P. S., Devi, B. P., & Prasad, R. B. N. (2011). Kinetics of the esterification of palmitic acid with methanol catalyzed by 12-tungstophosphoric acid supported on ZrO_2. Reaction Kinetics, Mechanisms and Catalysis, 104 (1), 211-226.
2. Baidya, T., van Vegten, N., & Baiker, A. (2011). Selective Conversion of Ethane to Ethene via Oxidative Dehydrogenation Over Ca-doped ThO_2 Using CO_2 as Oxidant. Topics in Catalysis, 54(13-15), 881.
3. P. Thirumala Bai, K. S. Rajmohan, P. S. Sai Prasad, S. Srinath. (2019).Chapter 7 Oxidative Dehydrogenation of Ethane to Ethylene Over Metal Oxide Catalysts Using Carbon Dioxide", Springer Nature America, Inc,.
4. Ramesh, Y., P. Thirumala Bai, B. Hari Babu, N. Lingaiah, K. S. Rama Rao, and P. S. Sai Prasad. (2014)."Oxidative dehydrogenation of ethane to ethylene on Cr_2O_3/Al_2O_3–ZrO_2 catalysts: the influence of oxidizing agent on ethylene selectivity", Applied Petrochemical Research,
5. Bai, P. T., Srinath, S., Upendar, K., Sagar, T. V., Lingaiah, N., Rao, K. R., & Prasad, P. S. (2017). Oxidative dehydrogenation of ethane with carbon dioxide over Cr_2O_3/SBA-15 catalysts: the influence of sulfate modification of the support. Applied Petrochemical Research, 7(2-4), 107-118.
6. Sreevardhan Reddy, S. (2007)"Beneficial role of SiO_2 plugging in $AlCl_3$ heterogenized plugged hexagonal templated silica (PHTS) for the isopropylation of m-cresol", Catalysis Communications.

CHAPTER -4

RESULTS & DISCUSSION
- METAL OXIDE SUPPORTED CHROMIA CATALYSTS

4.1.0. General:

Xinjie Zhang et.al [1] have been studied six Al_2O_3 supports, designated as S1–S6, prepared by using different aluminum precursors with different procedures for O_2 as oxidant. Wang et al [2] investigated that the loading of Cr_2O_3 also affects the activity with the optimal amount of 8 wt%. However, recent studies have focussed on the utilisation of CO_2 as the oxidant for the ODH of ethane. The following paragragraphs describe the results obtained on this process using single and mixed oxide supported chromia catalysts.

4.1.1. Al_2O_3 supported Cr_2O_3 Catalyst- Preparation:

Commercially available alumina was used as a support for the preparation of the catalyst. The catalysts with 5-20 wt% Cr_2O_3 on Al_2O_3 were prepared by adopting conventional wet impregnation method. The procedure was as follows.

The required quantity of Cr $(NO_3)_3.9H_2O$ was dissolved in minimum amount of water and this solution was added to the Al_2O_3 support with constant stirring. Excess water was removed on a water bath, and the catalyst masses were dried in an air oven at 120 ℃ for 12 h (Fig 4.1).

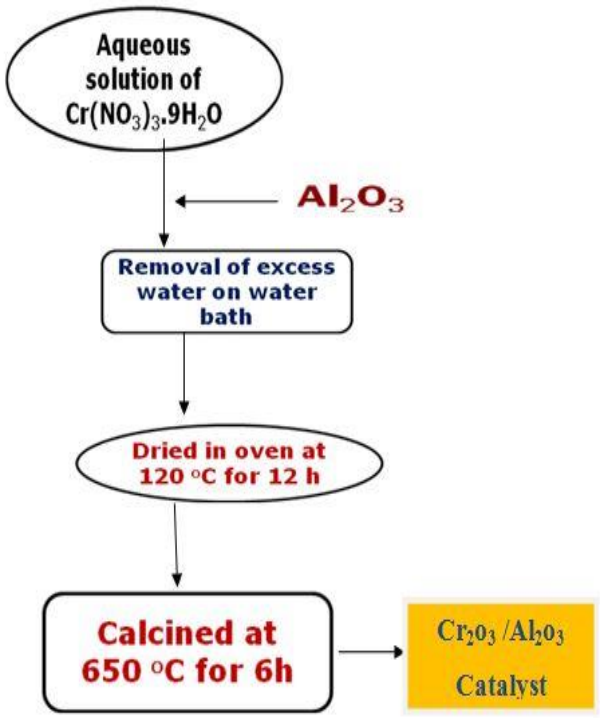

Figure.4.1. Flow diagram for preparation of Al_2O_3 supported Cr_2O_3 catalysts

4.1.2. Characterization of the Catalyst:

Different characterization methods were employed to know physico –chemical properties and composition of the catalyst material.

4.1.2. (A).BET Specific Surface area:

Specific areas of 5-20 wt% Cr_2O_3/ Al_2O_3 catalysts are presented in Table.4.1. In all the supports Al_2O_3 have highest surface area (205), 5 -20 wt% Cr_2O_3/ Al_2O_3 catalyst has surface areas of 110 to 192 m^2/g with addition of Chromium on Al_2O_3 surface area decreased gradually up to 20 wt% Cr_2O_3/ Al_2O_3 (110).

Catalyst	**Surface Area of Catalyst (m^2/g)**	**Support Surface Area (m^2/g)**
5 wt% Cr_2O_3/Al_2O_3	192	205
10 wt% Cr_2O_3/Al_2O_3	173	205
15 wt% Cr_2O_3/Al_2O_3	152	205
20 wt% Cr_2O_3/Al_2O_3	110	205

Table.4.1. Specific Surface areas of 5-20 wt% Cr_2O_3/ Al_2O_3 catalysts

It could be observed from the surface area values that there is a marginal decrease of surface area with increasing chromia loading up to 15 wt%, this is due to clogging of alumina pores by chromia species [3]. Significant reduction in surface area is noticed in 20 wt% Cr_2O_3/ Al_2O_3 catalyst due to formation of crystalline Cr_2O_3 species, similar kind of observation was made by Cherian et al [4] and this observation was supported by XRD results of this work where crystalline Cr_2O_3 observed at higher loadings.

4.1.2. (B).X-ray diffraction (XRD):

The XRD patterns of Cr_2O_3/Al_2O_3 catalysts with different loadings calcined at 650 ℃/6h are presented in Fig.4.2. All the catalysts exhibited two characteristic peaks at 2θ of 45.8° and 66.8° corresponding to γ-Al_2O_3 (JCPDS 29-0063), the intensity of these peaks decreased with increase in Cr_2O_3 loading, this might be due to the surface coverage of alumina by chromium species. One could notice from Fig.4.2 that different type of chromium oxide species are formed on alumina

surface. The XRD results recommend that the chromium can be stabilized on alumina in different oxidation states ranging from +5 to +6 at lower loadings, on increasing the chromium content to above 10 wt%, chromium can be stabilized with its highly stable oxidation state +3 in addition to its higher oxidation states.

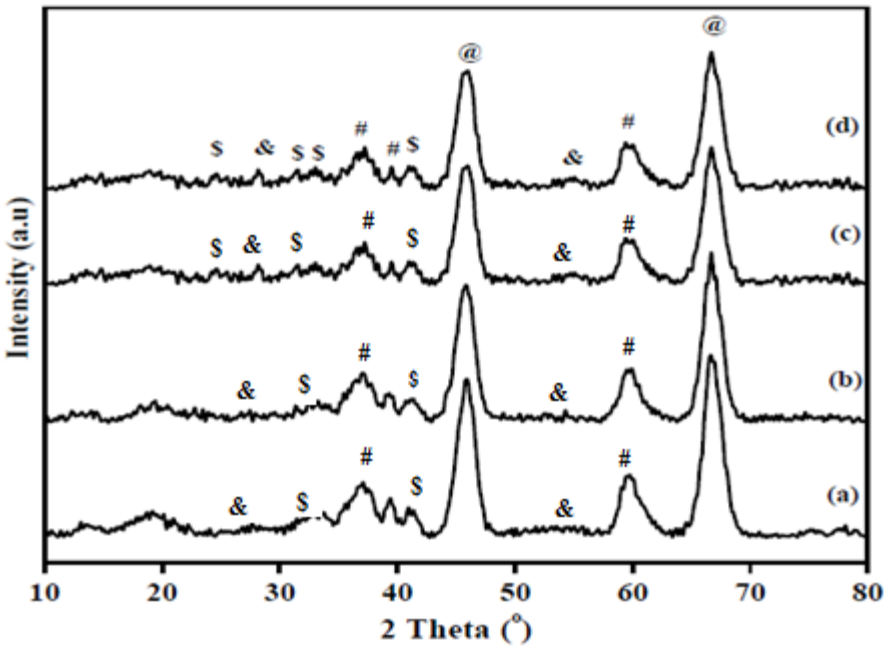

Figure.4.2. XRD patterns of catalysts (a) 5% Cr_2O_3/Al_2O_3 (b) 10%Cr_2O_3/Al_2O_3 (c) 15% Cr_2O_3/Al_2O_3 (d) 20% Cr_2O_3/Al_2O_3; (@) (at) Al_2O_3, (#) (*hash*) CrO_3 (@) Al_2O_3, (#) (*hash*) ZrO_2 tetragonal,($) (dollar) Cr_2O_5 and (&) (and) Cr_2O_3

The XRD patterns of 5-20% Cr_2O_3/Al_2O_3 catalysts with different loadings calcined at 650 ℃/6h are presented in Fig.4.2. All the catalysts exhibited two characteristic peaks at 2θ of 45.8º and 66.8° corresponding to γ-Al_2O_3 (JCPDS 29-0063), the intensity of these peaks decreased with increase in Cr_2O_3 loading, this might be due to the surface coverage of alumina by chromium species. One could notice from Fig.4.2 that, different type of chromium oxide species (Cr_2O_5, Cr_2O_3) are formed on alumina surface. The XRD results recommend that the chromium can be stabilized on alumina in different oxidation states ranging from +5 to +6 at lower loadings, on up increasing the chromium content to above 10 wt%, chromium can be stabilized with its highly stable oxidation state +3 in addition to its higher oxidation states. This suggests that the phase and dispersion of chromium species mainly depends on the surface area, nature of support and

chromium content. It has been informed that the molecular structure of chromium oxide species strongly depends on the surface hydroxyl chemistry and support surface. The acid-base properties of a support also play a major role in the chromium dispersion and its anchoring capacity with the support [6].

The support with high PZC value (Al_2O_3 basic hydroxyl groups) showed high anchoring capacity which led to high dispersion of chromium oxide species.

4.1.2. (C). Temperature Programmed Reduction profiles of the catalysts:

Temperature Programmed Reduction (TPR) was performed in a flow of 5% H_2/Ar mixture gas at a flow rate of 30 ml/min with a temperature ramp of 10 ℃/min. The TPR profiles of alumina supported chromium catalysts with varying loadings (5-20 wt%) calcined at 650 ℃/6h are given in Fig.4.3.Only single stage reduction was exhibited by all the catalysts in the range between 379 to 415 ℃. It has been reported in the literature [4, 5] that the single stage reduction occurs due to the reduction of Cr^{+6} to Cr^{+3}.

5wt% Cr_2O_3/Al_2O_3 catalyst showed the reduction temperature (T_{max}) centered at 415 ℃. This value shifted towards lower temperature (379 ℃) when the content of Cr_2O_3 increased to 15 wt% and remained constant above 15wt% loading, these results are in good agreement with the earlier reports [4,5,6].

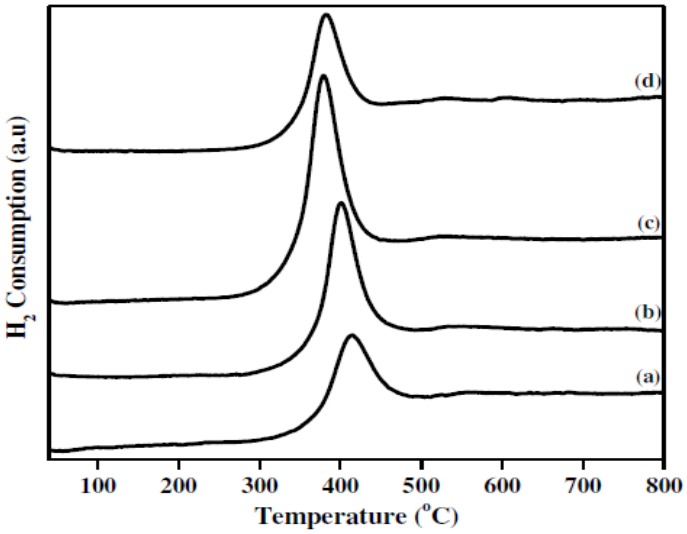

Figure.4.3. TPR profiles of catalysts calcined at 650 ºC/ 6h (a) 5% Cr_2O_3/Al_2O_3 (b) 10% Cr_2O_3/Al_2O_3 (c) 15% Cr_2O_3/Al_2O_3 and (d) 20% Cr_2O_3/Al_2O_3

At lower loadings oxygen is strongly bound to the support due to strong chromium-support interactions. It requires higher temperature for reduction, whereas in higher loadings chromium-support interactions become weaker due to the accumulation of chromia. They consume hydrogen comparatively at lower temperatures to undergo reduction [5,6]. Zaki et al [7] described the reduction behavior of chromium coated alumina catalysts. The chromium can be stabilized in two different kinds of species; polychromates and monochromates. The polychromate species exposed on crystalline chromia reduce at lower temperatures and the monochromate species directly anchored to the support reduce at higher temperatures might be due to the formation of monochromate like species, whereas low reduction temperature is observed in the higher loadings might be due to the formation of polychromate like species.

4.1.3. Performance evaluation of Cr_2O_3/Al_2O_3:

The prepared catalyst was evaluated in a fixed bed down flow reactor as explained in Sec 4.1.1 for ODH of ethane. Initially the effect chromium loading was evaluated to determine the optimum loading of Chromium, further the effect of temperature was evaluated for optimum loading catalyst to obtain maximum conversion and selectivity of ethane and ethylene respectively.

4.1.3. A. Effect of Cr_2O_3 loading:

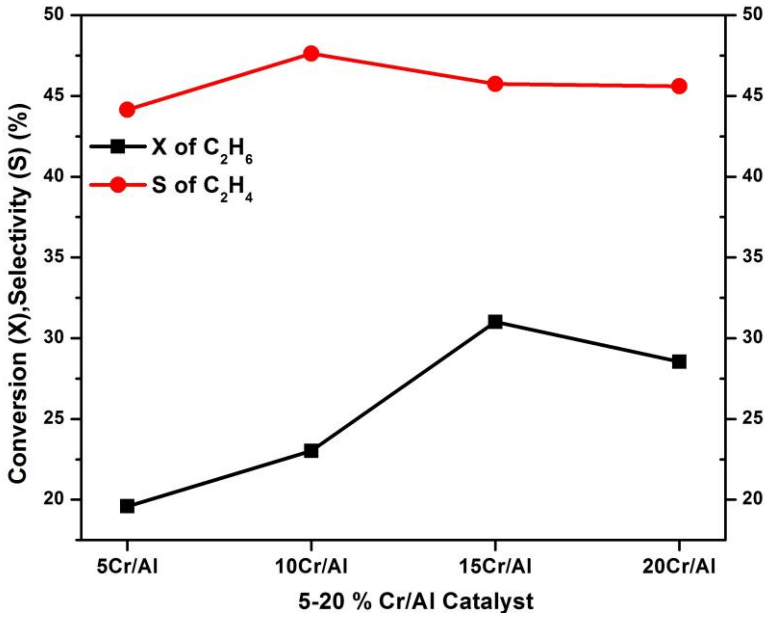

Figure.4.4. Effect of Chromium loading for ODH of Ethane with CO_2

Fig 4.4 shows the effect of various % loadings of Cr on Al_2O_3 support for ODH of ethane at 650 ℃. The conversions of ethane were increased with increase in loading up to 15 wt% and suddenly decrease when weight % of Chromium increased to 20%. This may be due to high agglomeration of active metal on support. Among them 15 wt% Cr_2O_3/Al_2O_3 catalyst exhibited best catalytic activity with conversions of ethane and CO_2 around 28% and 15% % and ethylene selectivity of 46%. Higher activity of 15 wt% Cr_2O_3/Al_2O_3 is proved by the presence of higher dispersion of chromium species on support by TPR.

4.1.3. (B). Effect of Temperature:

The effect of temperature on conversions of ethane and CO_2 at optimum loading (15 wt% Cr_2O_3/Al_2O_3) of catalyst is shown in Fig.4.5. The conversion of reactants i.e CO_2 and ethane both increases with increase in temperature up to 650 ℃ and there is a small variation from 600 to 650 ℃.

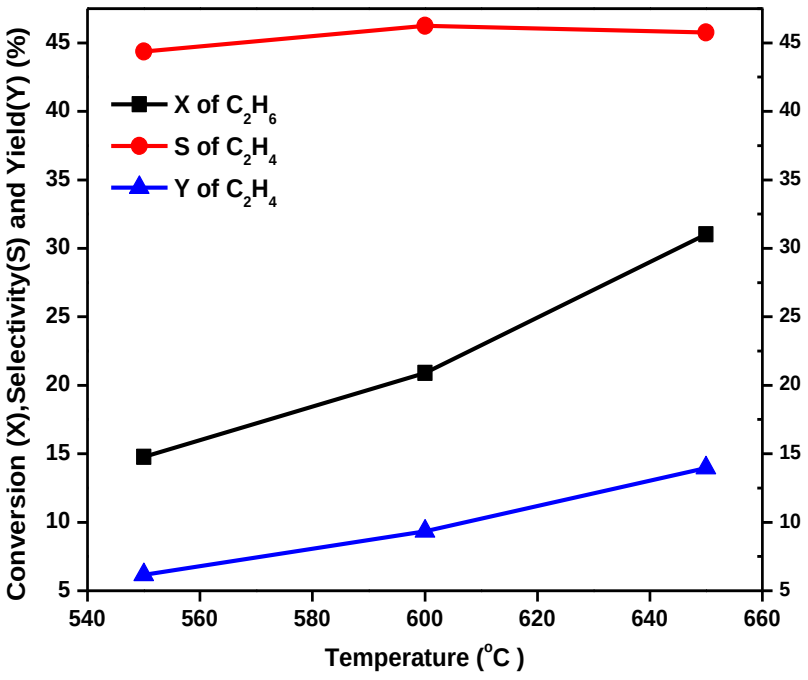

Figure.4.5. Effect of temperature of 15 wt% Cr_2O_3/Al_2O_3

The selectivity of ethylene increases slightly with respect to temperature up to 600 ℃ and remain constant till 650 ℃. The redox cycles of Cr^{+6} to Cr^{+3} may increase with rise in temperature might be responsible to attain high catalytic activity at 650 ℃.

4.2.0. Studies on ZrO_2 supported Cr_2O_3 catalyst:

4.2.1. ZrO_2 supported Cr_2O_3 Catalyst- Preparation:

As explained in sec 4.1.2 ZrO_2 support is added in place of Al_2O_3 support to synthesize the 15 wt % Cr_2O_3/ZrO_2 catalyst as shown in Fig 4.6. The optimum loading of chromium i.e 15% is used for the preparation further catalysts.

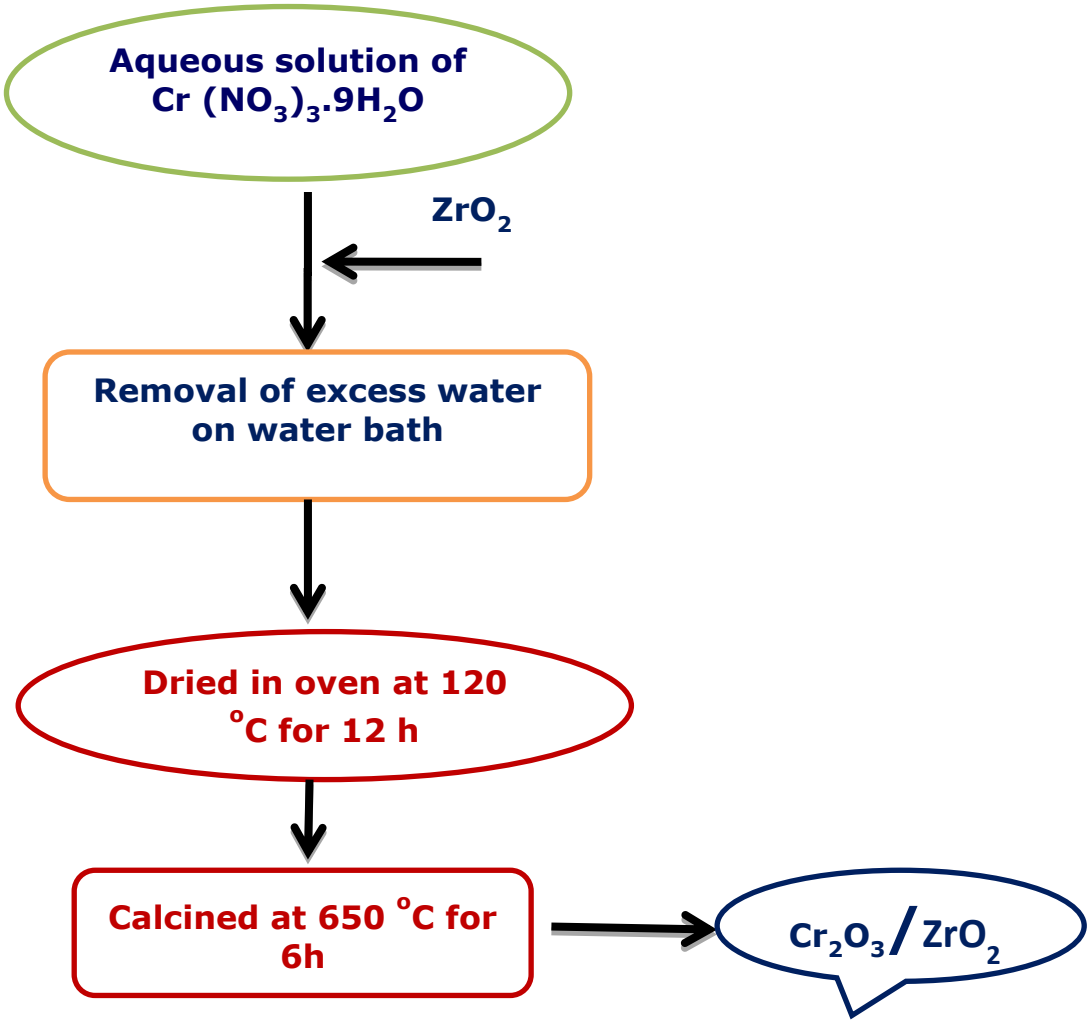

Figure .4.6. Flow diagram for preparation of ZrO_2 supported Cr_2O_3 Catalyst

4.2.2. Characterization of Catalyst:

Various characterization techniques used for the determination of properties and compositions are presented in detail here.

4.2. 2. (A) .X-ray diffraction (XRD):

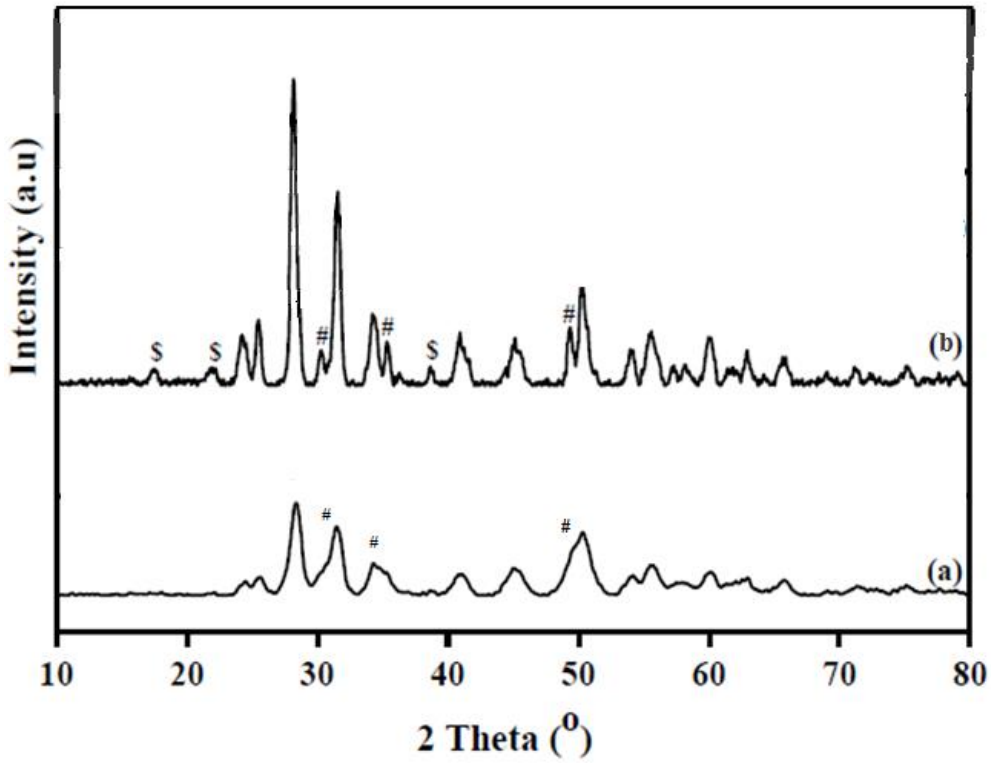

Figure.4.7. XRD patterns of catalysts calcined at 650 ºC/ 6h (a) ZrO_2 (b) 15% Cr_2O_3/ZrO_2

(#) (astrik) ZrO_2 tetragonal,($) (dollar) Cr_2O_5

Fig.4.7 presents the XRD patterns of the 15 wt% Cr_2O_3 supportedZrO_2 and ZrO_2 catalysts. Zirconia support only exhibits monoclinic phase, whereas Cr_2O_3 supported zirconia exhibited the tetragonal phase of ZrO_2 along with the monoclinic phase of **(#)** ZrO_2 and crystalline Cr_2O_3**,**($) Cr_2O_5. Metastable tetragonal phase of zirconia was observed in the 15 wt% Cr_2O_3/ZrO_2 catalyst. This is due to the interaction of Cr_2O_3 with ZrO_2 support.

4.2. 2. (B).Temperature programmed reduction (TPR):

Fig.4.8 displayed the TPR profile of 15 wt% Cr_2O_3 /ZrO_2 catalysts. The catalysts showed two stage reduction peaks between 320-470 ℃ and 480-625 ℃. This kind of observations were well

reported for the Cr_2O_3/ZrO_2 catalysts, the first peak is attributed to reduction of Cr^{+5} to Cr^{+3} and the second reduction peak could be ascribed to reduction of Cr^{+6} to Cr^{+2} [8] [9], But one cannot ruled out that the higher temperature reduction peak observed for the pure Cr_2O_3, might be due to the reduction of bulk chromia species to lower than +3 oxidation states [10].

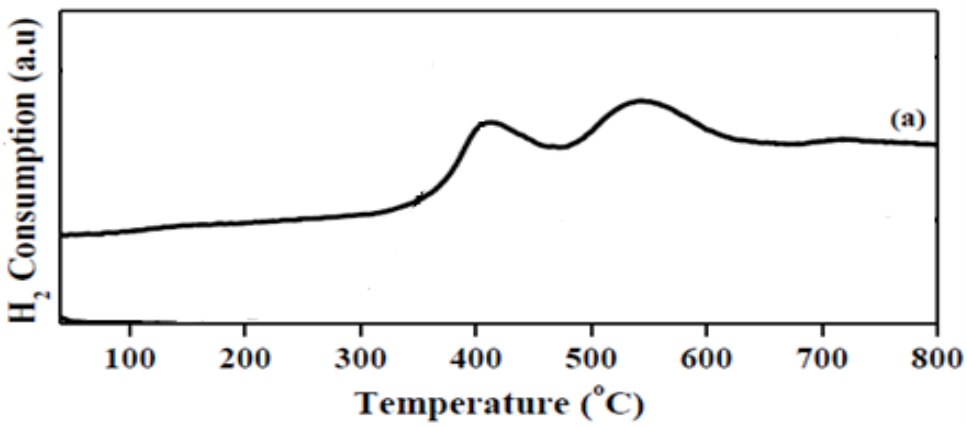

Figure.4.8. TPR profiles of catalysts calcined at 650ºC/ 6h (a) 15% Cr_2O_3/ZrO_2

4.2.3. Performance evaluation of Cr_2O_3/ZrO_2:

4.2.3. (A). Catalytic Evaluation and measurement:

The ZrO_2 supported Cr_2O_3 catalyst was evaluated in a fixed bed down flow reactor as explained in chapter 3, for ODH of ethane. The product gas stream was analyzed by a on-line Nucon 5765GC. Catalytic activity of single oxide i.e ZrO_2 supported chromium catalysts are shown in Fig.4.9.It can be seen that the conversion of CO_2 and ethane both increases with increase in temperature. 15wt% Cr_2O_3/ZrO_2 catalyst showed 41.6 % ethane, 37.3 % CO_2 conversions with 35.9 % ethylene selectivity, as it is expected, this catalysts showed high conversions of ethane and CO_2 compared to alumina supported chromium catalyst.

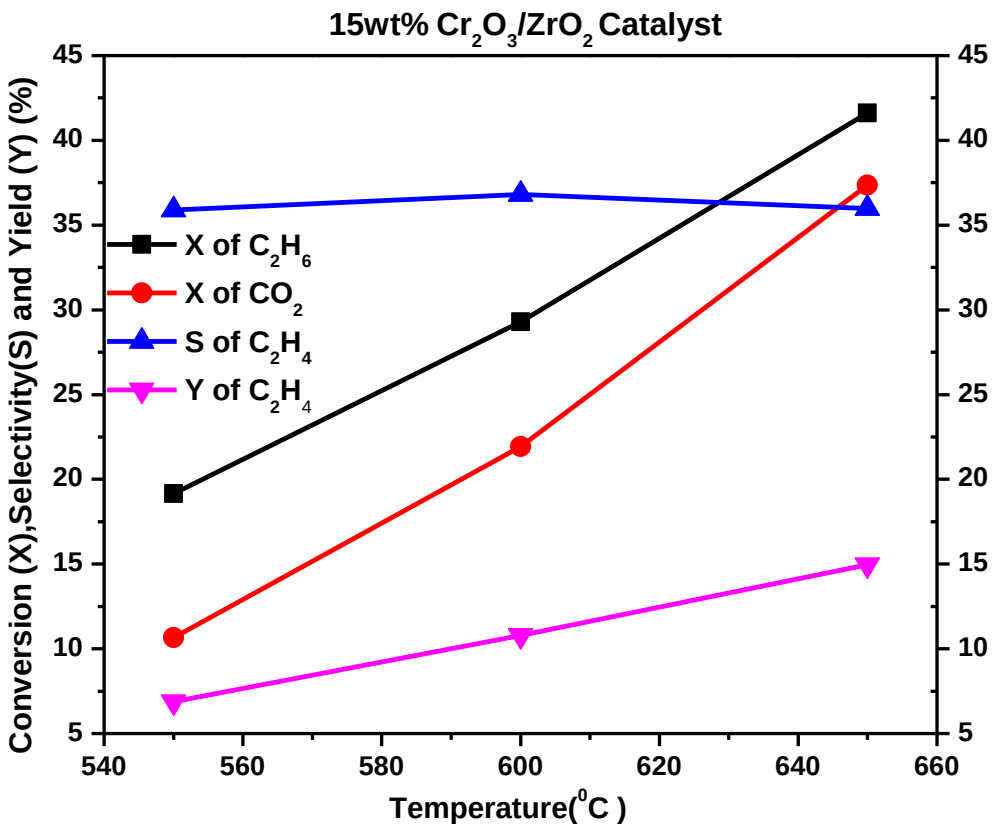

Figure.4.9. Effect of Temperature on catalytic activity of 15 wt% Cr_2O_3/ZrO_2

4.3.0. Studies on Mixed oxide supported Chromium Catalyst:

From the literature it has been found that most of the research work has been concentrated on a variety of single oxide supported catalysts but there is ample scope to investigate the performance of mixed oxide support. It is generally accepted that a mixed oxide support has an edge over its component single oxides as support in combining their good textural and mechanical properties. The dependence of catalytic activity on the distribution of CrO_x and the structure of Cr species on the surface of mixed oxide has not been reported so far. In view of this it is proposed to study the performance of mixed supported chromium catalyst for ODH of ethane.

4.3.1. Preparation of mixed oxide supported catalyst:

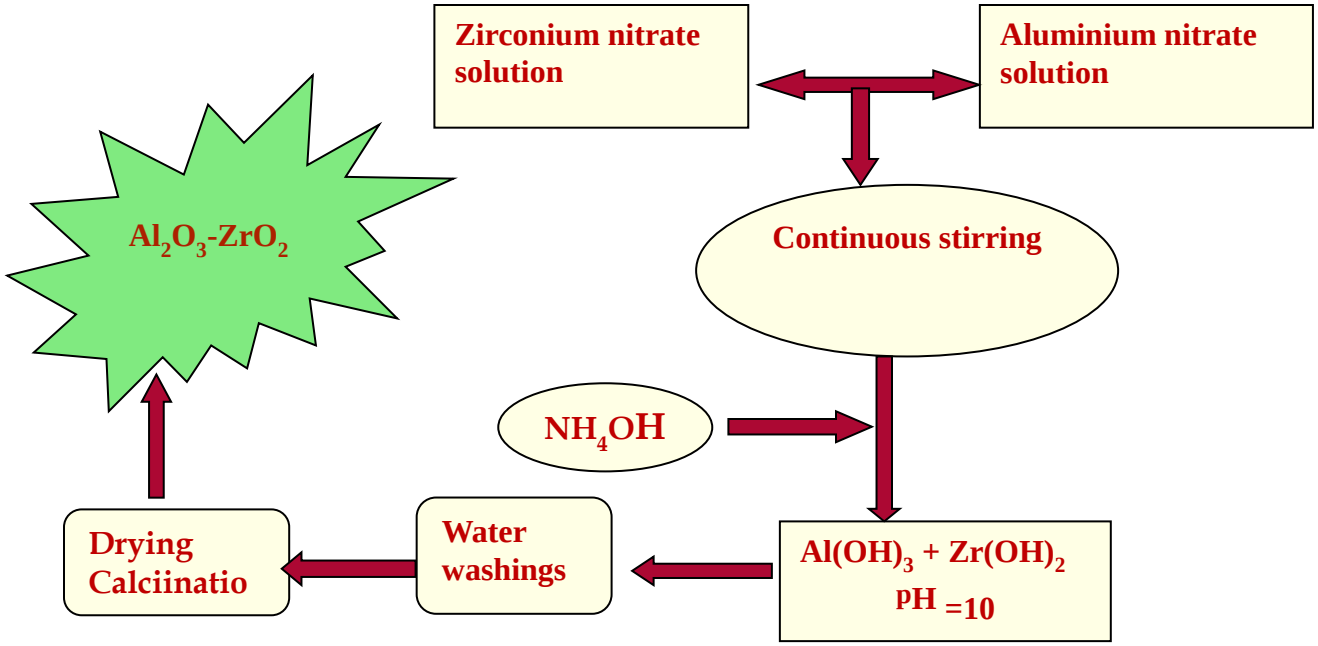

Figure.4.10. Flow diagram for preparation of Mixed oxide supported Cr_2O_3 catalyst

Co-precipitation method was used to prepare the Al_2O_3–ZrO_2 mixed Oxide support (molar ratio 1:1) by adding ammonium hydroxide solution to a mixed aqueous solution of $Zr(O)(NO_3)_2\,8H_2O$ and $Al(NO_3)_3 9H_2O$ until the pH reached a value of 10. The precipitate was filtered off and thoroughly washed with deionized water several times. Then it was dried at 120 ^oC for 36 h in air oven and calcined at 650 ^oC for 6 h. The same method was used to prepare alumina-zirconia mixed oxide with different molar ratios (1:3 and 3:1).

The catalysts with 15 wt% Cr_2O_3 on Al_2O_3–ZrO_2 mixed Oxide support were prepared by adopting conventional impregnation method. The procedure was as follows. The required quantity of Cr $(NO_3)_3.9H_2O$ was dissolved in minimum amount of water and this solution was added to the Al_2O_3 support with constant stirring. Excess water was removed on a water bath, and the catalyst masses were dried in air oven at 120 ℃ for 12 h. Finally 15 wt% Cr_2O_3 on Al_2O_3–ZrO_2 mixed Oxide support were prepared and also chromium supported Al_2O_3–ZrO_2 with different molar compositions were prepared.

4.3.2. Characterization of Catalyst:

The prepared catalysts of different compositions of mixed oxide were characterized by different techniques described below to know the composition and physico –chemical properties.

4.3.2. (A). X-ray diffraction (XRD):

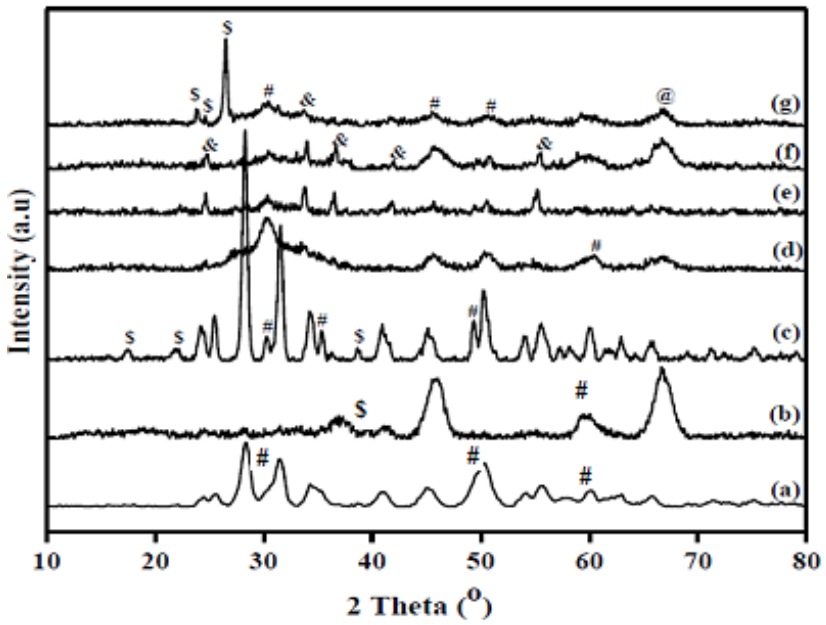

Figure.4.11. XRD patterns of catalysts calcined at 650 ºC/ 6h (a) ZrO_2 (b) 15% Cr_2O_3/ Al_2O_3- (c) 15% Cr_2O_3/ZrO_2 (d) 15% Cr_2O_3/ Al_2O_3-ZrO_2 (1:1)(e) 15% Cr_2O_3/ Al_2O_3-ZrO_2 (1:3) (f) 15% Cr_2O_3/ Al_2O_3-ZrO_2 (3:1) (g)15% Cr_2O_3 /Al_2O_3-ZrO_2 (1:1) used; (@) ZrO_2 tetragonal,($) Cr_2O_5 and (&)Cr_2O_3.

Fig.4.11. presents the XRD patterns of the 15 wt% Cr_2O_3 supported Al_2O_3, ZrO_2 and Al_2O_3- ZrO_2 catalysts. XRD patterns of pure ZrO_2 are also shown for the sake of comparison. Zirconia support only exhibits monoclinic phase, whereas Cr_2O_3 supported zirconia exhibited the tetragonal phase of ZrO_2 along with the monoclinic phase of ZrO_2 and crystalline Cr_2O_3, Cr_2O_5. Metastable tetragonal phase of zirconia was observed in the 15 wt% Cr_2O_3/ ZrO_2 catalyst. This is due to the interaction of Cr_2O_3 with ZrO_2 support, while other three mixed oxide supported chromium catalysts exhibit only tetragonal ZrO_2 phase. Monoclinic phases of ZrO_2 were not detected in the mixed oxide supported catalysts because of the protective effect of Cr^{+3}, which prevents the phase transformation of ZrO_2 from tetragonal to monoclinic phase [11] and the addition of alumina to

zirconia also delays the phase transformation from metastable tetragonal zirconia to monoclinic phase, this may be due to the phase segregation of alumina and ZrO_2. Similar kind of observation was reported previously [12, 13]. 15 wt% Cr_2O_3/Al_2O_3-ZrO_2 (1:1) does not exhibit any diffraction lines belong to crystalline Cr_2O_3. It infers that the chromium oxide species are in highly dispersed state, where as these species are clearly seen in other two mixed oxide supported catalysts. The XRD pattern of the 15wt% Cr_2O_3/Al_2O_3-ZrO_2 (1:1) catalyst exhibited peaks corresponding to Cr_2O_5 along with crystalline Cr_2O_3 phases.

4.3.2. (B).Temperature programmed reduction (TPR):

Fig.4.12.displayed the TPR profiles of 15wt% Cr_2O_3 supported Al_2O_3, ZrO_2, and Al_2O_3-ZrO_2 catalysts. All catalysts showed single stage reduction except 15wt% Cr_2O_3/ZrO_2 catalysts, which exhibits two broad reduction peaks between 320-470 ℃ and 480-625 ℃. This kind of observations were well reported for the Cr_2O_3/ZrO_2 catalysts, the first peak is attributed to reduction of Cr^{+5} to Cr^{+3} and the second reduction peak could be ascribed to reduction of Cr^{+6} to Cr^{+2} [14,15]. But one cannot ruled out that the higher temperature reduction peak observed for the pure Cr_2O_3, might be due to the reduction of bulk chromia species to lower than +3 oxidation states [16].

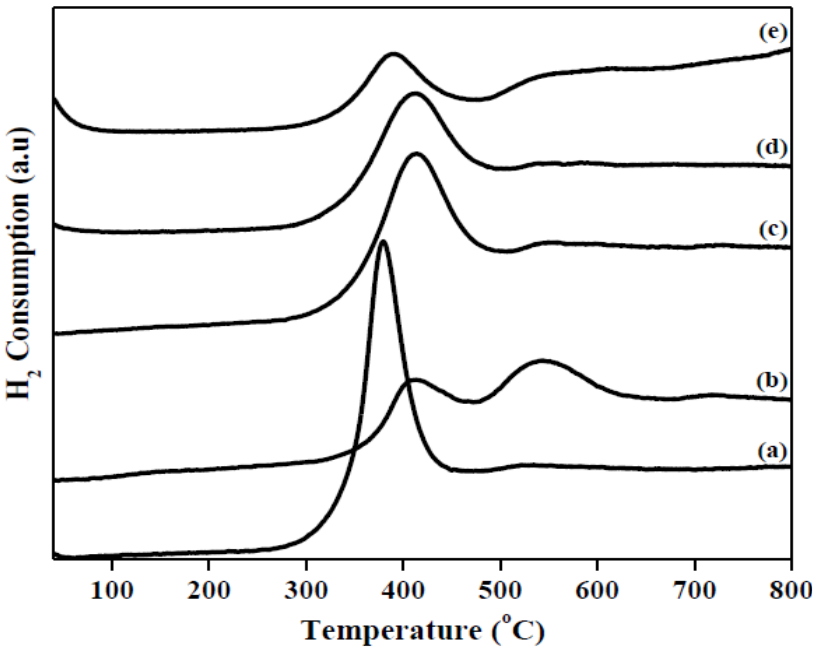

Figure.4.12.TPR profiles of catalysts calcined at 650°C/ 6h (a) 15% Cr_2O_3/Al_2O_3 (b) 15% Cr_2O_3/ZrO_2 (c) 15% Cr_2O_3/Al_2O_3-ZrO_2 (1:1) (d) 15% Cr_2O_3/Al_2O_3 -ZrO_2 (1:3) (e) 15% Cr_2O_3/Al_2O_3-ZrO_2 (3:1).

Al_2O_3-ZrO_2 mixed oxide supported chromium catalysts showed only one reduction peak and does not undergo further reduction even though these catalysts contains ZrO_2. The T_{max} of these catalysts changes with varying the mixed oxide composition. High alumina content in the mixed oxide support moves the T_{max} towards lower temperatures. From the above discussion one can conclude that the chromium species stabilized on alumina undergo single stage reduction, while zirconia support induces the two stage reduction. One can assume from the TPR peaks of 15 wt%Cr_2O_3/ZrO_2 that the monoclinic phase of ZrO_2 encourages the two stage reduction of chromium species which is not acknowledged in the mixed oxide supported catalysts, where the monoclinic ZrO_2 phase formation was not appeared. Furthermore, the addition of alumina to zirconia stabilizes the ZrO_2 in its metastable tetragonal phase which diminishes the further reduction of chromium species at higher temperatures.

4.3.2. (C).X-Ray photoelectron spectroscopy (XPS):

X-ray photoelectron spectroscopy has been used to know not only chemical state of the elements but also changes in the concentration of the catalysts during the reaction. Table.4.2. presents the core level binding energies of Cr 2p, Al 2p, and Zr 3d of some of the catalysts used in this study. Two binding energy values can be found in all the supported chromium catalysts for Cr $2p^{3/2}$ with slight shift in their binding energy values, first binding energy at 576.3 (±0.2) eV can be attributed to Cr^{+3} species and the second at 578.5 eV can be ascribed to Cr^{+6}, these findings were well established in the previous literature [17, 18].

The BE of Al $2p^{3/2}$ is observed at 75.3 (±0.3) eV indicates that the aluminum is in +3 oxidation state, whereas the BE values of Zr $3d^{5/2}$ exhibited at 182.8 (±0.2) eV slightly higher to pure ZrO_2 generally observed at 182.1 eV this could be due to the change in the co-ordination number of zirconium by the formation of Zr-O-metal or Zr-O-support bond [19]. The binding energies (Cr $2p^{3/2}$) of the spent catalysts showed slightly lower values compare to fresh catalyst, which indicates that the reaction condition brought some changes in the chemical environment of Cr species might be due to carbon deposition [20] likewise the binding energies of Al 2p and Zr 3d showed lower values in the used catalyst.

Table.4.2. Binding Energies of Cr based catalysts:

Catalyst	Binding Energies(eV)			
	Cr $^{2p3/2}$		Al $^{2p3/2}$	Zr $3d^{5/2}$
	Cr^{+3}	Cr^{+6}		
15 wt% Cr_2O_3/Al_2O_3	575.5	577.6	76.6	181.6
15 wt% Cr_2O_3/ZrO_2	575.2	577.3	-	-
15 wt% Cr_2O_3/Al_2O_3-ZrO_2 (1:1)	575.4	577.4	75.0	182.0
15 wt% Cr_2O_3/Al_2O_3-ZrO_2 (1:1) used	575.1	577.7	76.3	181.6

4.3.2. (D).C_2H_4 temperature programmed desorption (TPD):

Fig.4.13.showed the ethylene TPD profiles of 15 wt% Cr_2O_3 / Al_2O_3 -ZrO_2 (1:1) catalyst treated at 650 ℃ under two different oxidising atmospheres (C_2H_6+ CO_2 and C_2H_6+ O_2). This study revealed the important information regarding the selectivity of ethylene when the reaction conducted in presence of CO_2 and O_2. It is well known that the ODH of ethane in presence of CO_2 yield high ethylene selectivity than O_2.

In this work it was noticed that the amount of ethylene desorption was found to be low when the catalyst exposed to ethane and CO_2 mixture compared to catalyst exposed to ethane and O_2. From the above results one can notice that the desorption of ethylene from the catalysts surface was easy, when the reaction conducted in presence of oxygen, hence one can assume that the easy desorption of ethylene induces the secondary oxidation (i.e. ethylene to carbon oxides) so that the selectivity of ethylene was low when reaction conducted in presence of O_2.

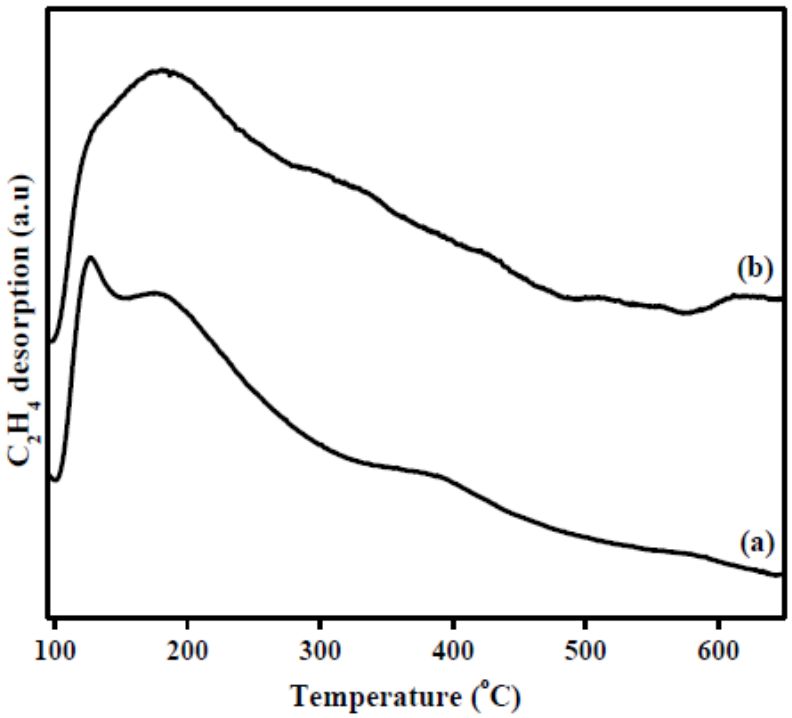

Figure.4.13. C_2H_4 temperature programmed desorption profiles of 15 wt% Cr_2O_3/Al_2O_3-ZrO_2 (1:1) catalyst treated at 650 ℃ for 1h (a) C_2H_6 + CO_2 treated (b) C_2H_6+ O_2 treated.

On the other hand the catalyst exposed to ethane and CO_2 release low amount of ethylene from the catalyst surface which cannot undergo further oxidation. Therefore the catalyst exposed to ethane and CO_2 yield high selectivity to ethylene when compared to ethane and O_2 [23].

4.3.3. Oxidative dehydrogenation of ethane catalytic activity measurements:

Catalytic activity of single and mixed oxide supported chromium catalysts are shown in Fig.4.14. 15wt% Cr_2O_3/Al_2O_3-ZrO_2 (1:1) catalyst showed 36% ethane (Fig 4.16),29 % CO_2 conversions with 56% ethylene selectivity, as we expected, this catalysts showed high conversions of ethane and CO_2 compare to alumina supported chromium catalyst but shown less activity than zirconia supported chromium catalyst, whereas the ethylene selectivity has been substantially increased to 56%. It is well known that the acidic ions boosts the catalytic activity while the basic ions inhibits the dehydrogenation of ethane [21] it is believed that the lower catalytic activity of 15 wt% Cr_2O_3/Al_2O_3 is due to strong basicity of alumina support. The addition of zirconia to alumina in the support distinctly changes the catalytic activity this is due to presence of highly dispersed chromium oxide species (probably in higher oxidation states) on Al_2O_3-ZrO_2 (1:1) support. The

appearance of crystalline Cr_2O_5 phases in used catalyst XRD supports that the single reduction peak in TPR is due to reduction of Cr^{+5} to Cr^{+3}, this redox couple might be the reason for high ethylene selectivity bared by this catalyst.

4.3.4. Effect of Al_2O_3-ZrO_2 support composition:

The conversion of ethane and CO_2 decreases with increase in Al_2O_3-ZrO_2 composition. Catalyst with high ZrO_2 composition shows higher CH_4 selectivity while higher Al_2O_3 composition has higher C_2H_4 selectivity. Catalyst with equal amounts of Al_2O_3/ZrO_2 shows higher catalytic activity. Fig.4.14 displayed the variation in catalytic activity with changing Al_2O_3-ZrO_2 support composition. The conversion of both ethane and CO_2 decreased with change in composition of Al_2O_3-ZrO_2, but significant variation in selectivities of ethylene and methane has been observed. The Al_2O_3-ZrO_2 support with high ZrO_2 content exhibited low ethylene and high methane selectivity, while Al_2O_3-ZrO_2 with high Al_2O_3content behave exactly opposite to it. But both the catalysts with high zirconia and alumina content displayed lower activity than the catalyst with equal amount of Al_2O_3 and ZrO_2 in support. Such kind of behavior may possible in these catalysts, which can be clarified from the XRD results in which Cr_2O_3 crystalline phases are observed in the mixed oxide support with high alumina and zirconia content, however these phase are not identified in the XRD of 15wt% Cr_2O_3 / Al_2O_3-ZrO_2 (1:1). From this we can understand that the amorphous chromium oxide species are highly active and useful to get respectable ethylene selectivity.

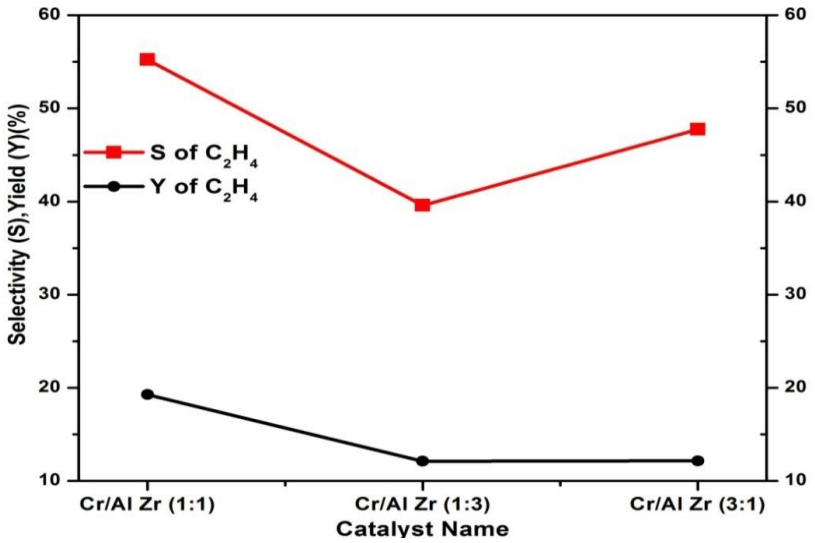

Figure.4.14. Effect of catalyst support composition on Conversion and selectivity

4.3.5. Effect of oxidizing agent on catalytic activity:

Fig 4.15 presents the effect of oxidizing agent on ODH of ethane. The conversions of ethane is higher when O_2 is used as oxidizing agent compared to CO_2 in 15 wt% Cr_2O_3/Al_2O_3-ZrO_2 (1:1) but the ethylene selectivity is higher when CO_2 is used as oxidizing agent. The higher conversion of ethane when O_2 is used as oxidizing agent is due to secondary oxidation of ethane to CO_2.

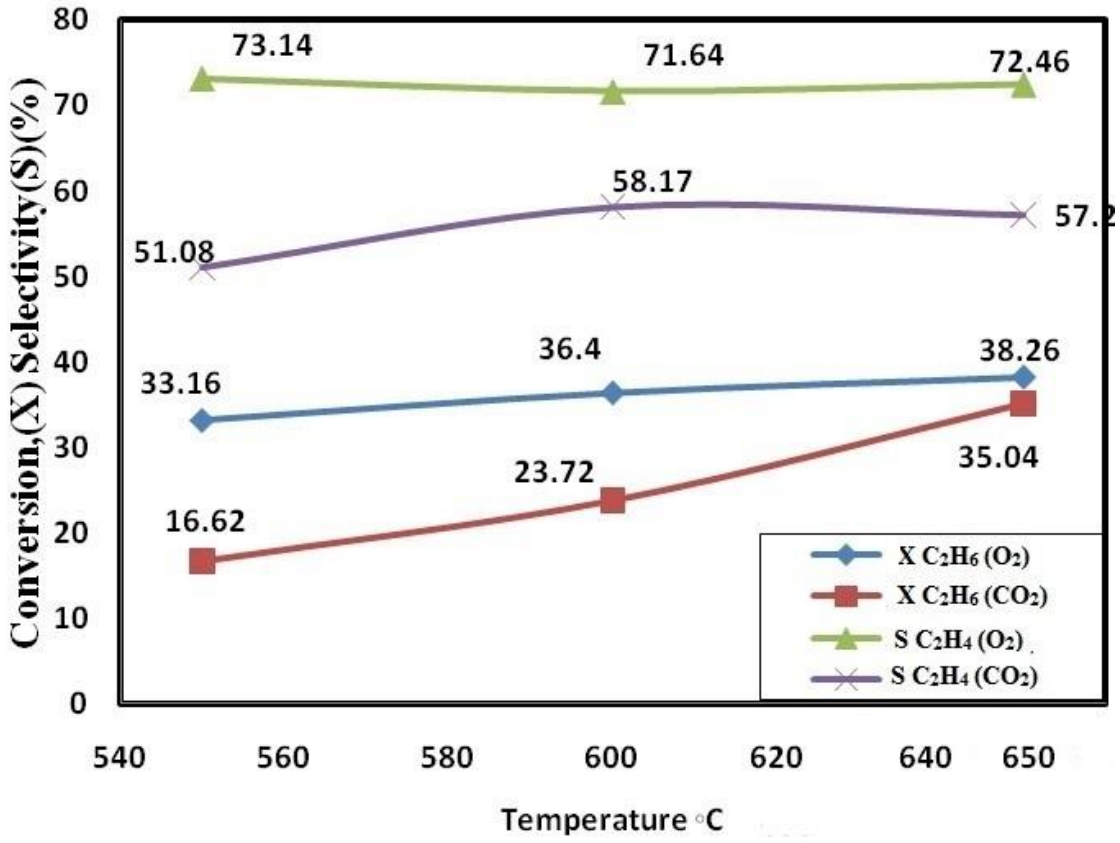

Figure.4.15. Effect of oxidizing agent on conversion and selectivity

4.3.6. Effect of catalyst particle size:

For different sizes of 15 wt% Cr_2O_3/Al_2O_3-ZrO_2 (1:1) catalysts the conversion of ethane and CO_2 is found at a temperature of 650^0C for a flow rate of C_2H_6:CO_2:He = 15 :15: 30 (60 ml/min) and at a pressure of 1atm. It is observed from the Fig 4.16 that the conversion of ethane and CO_2 both remains unchanged with increase in particle size up to 600 μm and it decreases with further increase in particle size. The internal diffusion resistance for different catalyst size is found by Weisz Prater criterion [22] and size is chosen for which internal resistance is negligible.

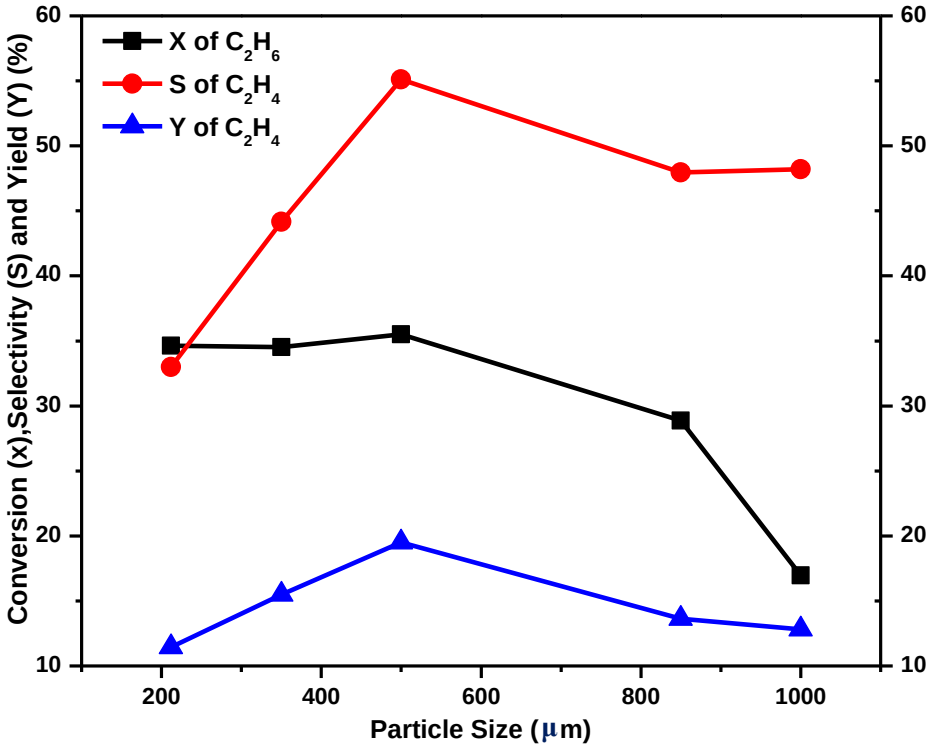

Figure.4.16. Effect of particle size of the 15wt% Cr_2O_3/Al_2O_3-ZrO_2 (1:1) Catalyst

4.3.7. Effect of Temperature:

The catalytic activity of 15 wt% Cr_2O_3/Al_2O_3-ZrO_2 (1:1) at different temperatures is presented in Fig 4.17. The conversions of both ethane and CO_2 increases with increase in temperature while the selectivity of ethane is constant around 57% at 650 ℃. As explained in the previous sections the conversion is high for the equal composition when compared to the change in compositions of the individual oxide supports.

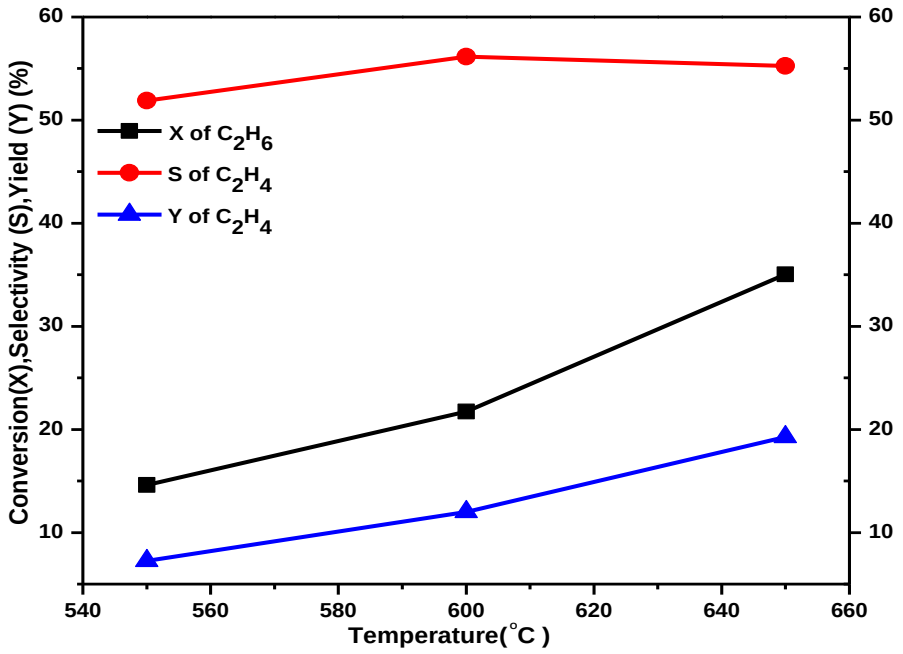

Figure.4.17. Effect of Temperature on Conversion and selectivity in 15 wt%Cr_2O_3/Al_2O_3-ZrO_2 (1:1) Catalyst

4.3.8. Effect of weight on catalytic activity:

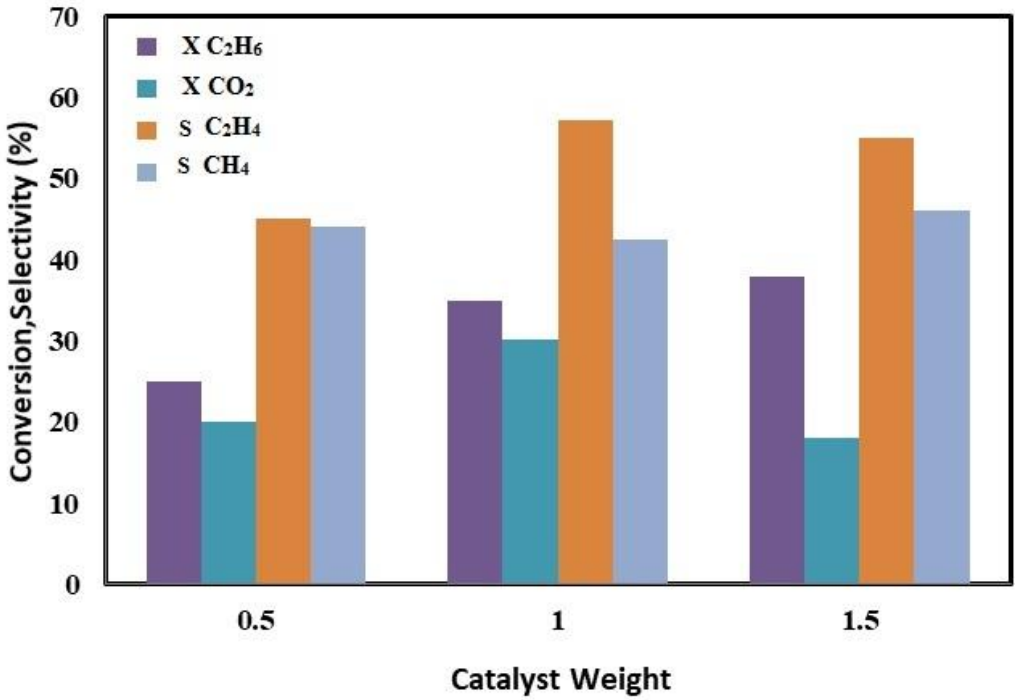

Figure.4.18. Effect of weight on catalytic activity of 15 wt% Cr_2O_3/Al_2O_3-ZrO_2 (1:1)

Fig.4.18 shows the variation in catalytic activity with changing weight of catalyst. The conversion of both ethane and CO_2 increased with increase in weight of catalyst, similar trend in selectivities of ethylene has been observed while the trend differs with methane.

4.3.9. Effect of CO_2 flow variation:

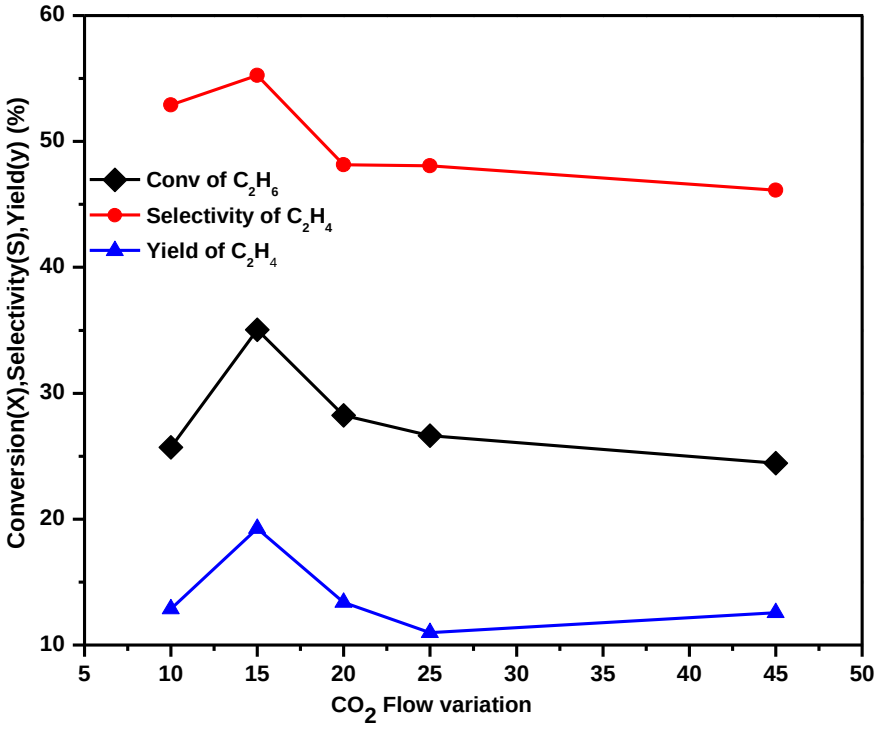

Figure.4.19. Effect of CO_2 flow variations (ml/min)

Fig 4.19 presents the effect of CO_2 flow on performance of 15 wt% Cr_2O_3/Al_2O_3-ZrO_2 (1:1) catalyst. The flow of oxidant is varied in such a way that the total flow remains constant by adjusting the inert gas flow rate and maintaining the constant flow of reactant i.e ethane. It can be seen from the Fig 4.19 that the conversion of ethane and selectivity and yield of ethylene are increased with increase in oxidant flowrate up to 15 mi/min, but further increase in flow of oxidant results in decrease in all three parameters. The conversion is maximum at C_2H_6: CO_2: He = 15:15:30 flow conditions.

4.3.10. Non Silica supported chromium based catalyst comparison:

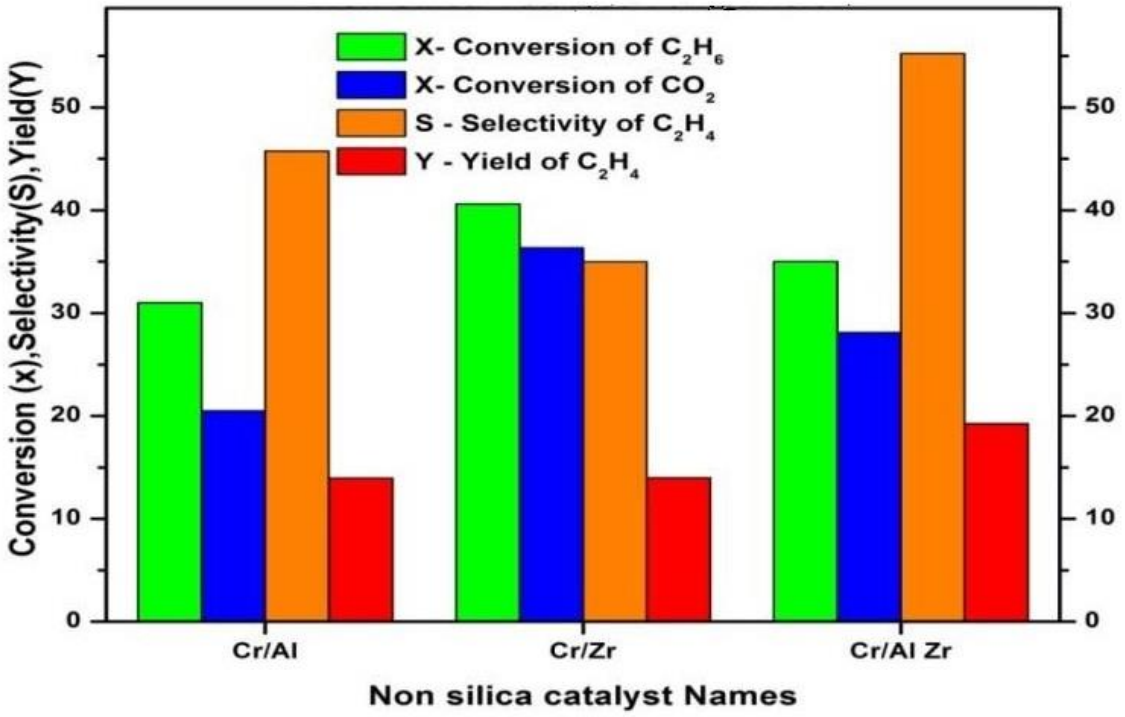

Figure.4.20. Effect of non-silica support comparison

Fig 4.20 presents the effect of non-silica supported chromium based catalysts for ODH of ethane. The comparison is made between the best catalysts of single oxides and mixed oxides. 15 wt% Cr_2O_3/Al_2O_3 catalyst showed best catalytic activity among the alumina supported chromium catalysts with 32% ethane, 21% CO_2 conversions with 46% ethylene selectivity. 15 wt% loading is necessary to obtain reasonable ethane and CO_2 conversions.15 wt% Cr_2O_3/ZrO_2 catalyst displayed high conversions to ethane (42%) and CO_2 (37%) with less ethylene selectivity (36%), while 15 wt% Cr_2O_3/Al_2O_3-ZrO_2 (1:1) catalyst showed best catalytic activity among all the catalysts used in this work with 36% ethane, 29% CO_2 conversions with 56% ethylene selectivity. Among all the Al_2O_3-ZrO_2 supported chromium catalysts with 1:1 Al_2O_3-ZrO_2 composition showed best catalytic activity. The selectivity of ethylene is mainly depending on the oxidising atmosphere used in the reaction medium. Cr^{+6}, Cr^{+5} and Cr^{+3} species are active for oxidative dehydrogenation of ethane with CO_2.

REFERENCES:

1. Zhang, X., Liu, J., Jing, Y., & Xie, Y. (2003). Support effects on the catalytic behavior of NiO/Al_2O_3 for oxidative dehydrogenation of ethane to ethylene. Applied Catalysis A: General, 240(1-2), 143-150.

2. Wang, S., Murata, K., Hayakawa, T., Hamakawa, S., & Suzuki, F. (2000). Dehydrogenation of ethane with carbon dioxide over supported chromium oxide catalysts. Applied Catalysis A: General, 196(1), 1-8.

3. Grzybowska, B., Słoczyński, J., Grabowski, R., Wcisło, K., Kozłowska, A., Stoch, J., & Zieliński, J. (1998). Chromium oxide/alumina catalysts in oxidative dehydrogenation of isobutane. Journal of Catalysis, 178(2), 687-700.

4. Cherian, M., Rao, M. S., Yang, W. T., Jehng, J. M., Hirt, A. M., & Deo, G. (2002). Oxidative dehydrogenation of propane over Cr_2O_3/Al_2O_3 and Cr_2O_3 catalysts: effects of loading, precursor and surface area. Applied Catalysis *A: General*, *233*(1-2), 21-33.

5. Wang, S., Murata, K., Hayakawa, T., Hamakawa, S., & Suzuki, F. (2000). Dehydrogenation of ethane with carbon dioxide over supported chromium oxide catalysts. Applied Catalysis A: General, 196(1), 1-8.

6. Weckhuysen, B. M., Wachs, I. E., & Schoonheydt, R. A. (1996). Surface chemistry and spectroscopy of chromium in inorganic oxides. Chemical Reviews, 96(8), 3327-3350.

7. Zaki M.I, Fouad N.E, Bond G.C, Tahir S.F. 'Temperature-programmed reduction of calcined chromia-coated alumina and silica catalysts: probing chromium (VI)-oxygen species', Therrnochimica Acta 285 (1996) 167-179.

8. Cutrufello M.G, Rossi S, Ferino I, Monaci R, Rombi E, Solinas V,Preparation,characterisation and activity of chromia–zirconia catalysts for propane dehydrogenation', Thermochimica Acta 434 (2005) 62–68.

9. Wang, S., Murata, K., Hayakawa, T., Hamakawa, S., & Suzuki, K. (2001). Oxidative dehydro-isomerization of n-butane over anion-promoted Cr_{2O3}/ZrO_2 catalysts. Energy & fuels, 15(2), 384-388.

10. Grzybowska B, Sloczynki J, Grabowski R, Wcislo K, Kozlowska A, Stoch J,Zielinski 'Chromium Oxide/Alumina Catalysts in OxidativeDehydrogenation of Isobutane', J. Catal. 178 (1998) 687-700.

11. Liotta, L. F., Venezia, A. M., Pantaleo, G., Deganello, G., Gruttadauria, M., & Noto, R. (2004). Chromia on silica and zirconia oxides as recyclable oxidizing system: structural and surface characterization of the active chromium species for oxidation reaction. Catalysis today, 91, 231-236.

12. Klimova, T., Rojas, M. L., Castillo, P., Cuevas, R., & Ram ŕez, J. (1998). Characterization of Al_2O_3-ZrO_2 mixed oxide catalytic supports prepared by the sol-gel method. Microporous and mesoporous materials, 20(4-6), 293-306.

13. Li, G., Li, W., Zhang, M., & Tao, K. (2004). Characterization and catalytic application of homogeneous nano-composite oxides ZrO_2–Al_2O_3. Catalysis today, 93, 595-601.

14. Cutrufello M.G, Rossi S, Ferino I, Monaci R, Rombi E, Solinas ,Preparation,characterisation and activity of chromia–zirconia catalysts for propane dehydrogenation', Thermochimica Acta 434 (2005) 62–68.

15. Wang, S., Murata, K., Hayakawa, T., Hamakawa, S., & Suzuki, K. (2001). Oxidative dehydro-isomerization of n-butane over anion-promoted Cr_2O_3/ZrO_2 catalysts. Energy & fuels, 15(2), 384-388

16. Grzybowska B, Sloczynki J, Grabowski R, Wcislo K, Kozlowska A, Stoch J,Zielinski 'Chromium Oxide/Alumina Catalysts in OxidativeDehydrogenation of Isobutane', J. Catal. 178 (1998) 687-700.

17. Wang S, Murata K, Hayakawa T, Hamakawa S, Suzuki K. Dehydrogenation ofethane with carbon dioxide over supported chromium oxide catalysts', Appl.Catal. A: Gen. 196 (2000) 1-8.3.

18. Denga S, Huiquan Li, Songgeng Li, Yi Zhang. 'Activity and characterization of modified Cr_2O_3/ZrO_2 nano-composite catalysts for oxidative dehydrogenation of ethane to ethylene with CO_2', Journal of Molecular Catalysis A: Chemical 268 (2007) 169–175.

19. Reddy B.M, Chowdhury B, Smirniotis P.G. An XPS study of the dispersion of MoO3 on TiO_2–ZrO_2, TiO_2–SiO_2, TiO_2–Al_2O_3, SiO_2–ZrO_2, and SiO_2–TiO_2– ZrO_2 mixed oxides', Appl. Catal. A: Gen. 211 (2001) 19-30.

20. Xuejun Shi, Shengfu Ji, Kai Wang, and Chengyue Li. 'Oxidative Dehydrogenation of Ethane with CO_2 over Novel Cr/SBA-15/Al_2O_3/FeCrAl Monolithic Catalysts', Energy & Fuels 22 (2008) 3631–3638

21. Wang S, Murata K, Hayakawa T, Hamakawa S and Suzuki K. 'Oxidative dehydrogenation of ethane by carbon dioxide over sulfate-modified Cr2O3/SiO2 catalysts', Catalysis Letters 63 (1999) 59–64.

22. Bhasin M.M, McCain J.H, Vora B.V, Imai T, Pujado P.R. Applied Catalysis A Gen. 221(2001) 397-405.

23. Ramesh, Y., Bai, P. T., Babu, B. H., Lingaiah, N., Rao, K. R., & Prasad, P. S. (2014). Oxidative dehydrogenation of ethane to ethylene on Cr_2O_3 / Al_2O_3 -ZrO_2 catalysts: the influence of oxidizing agent on ethylene selectivity. Applied Petrochemical Research, 4(3), 247-252.

CHAPTER -5

RESULTS & DISCUSSION

SILICA SUPPORTED CHROMIA CATALYSTS

5.0. General:

SiO_2 is the most favoured support for the chromia catalysts. 5-8 wt % Cr_2O_3/SiO_2 catalysts have exhibited excellent performance [6,11]. However, the aggregation of CrO_x on SiO_2 is found to negatively influence the catalyst behaviour, particularly during the reaction on Cr-Si-2 molecular sieve catalyst [12]. SBA-15 is later found to be a convenient support to overcome the problem of aggregation [13]. Wang et al. studying the chromium oxide catalysts brought out the advantages of sulfate modification of the silica support during the oxidative dehydration of ethane, particularly in the presence of CO_2 [14]. The presence of promoters with high basicity like alkali metal oxides suppressed the reactivity of silica supported catalysts [15]. Sulfate modification of zirconia was tried in studies related to oxidative dehydrogenation of ethane (ODH) to achieve better results [16]. An intensive observation of the literature revealed that though the benefits were elaborated, the reasons for the better performance of the sulfate modified catalysts were not reported. Particularly, the influence of sulfate modification of the support in Cr_2O_3/SBA-15 had not been studied. In this thesis an attempt was made to understand the reasons responsible for increase in activity and selectivity in the case of Cr_2O_3/SiO_2 catalysts and mesoporous Cr_2O_3/SiO_2 (SBA-15) because of sulfate modification of the support.

5.1. Silica Supported Chromia Catalyst preparation:

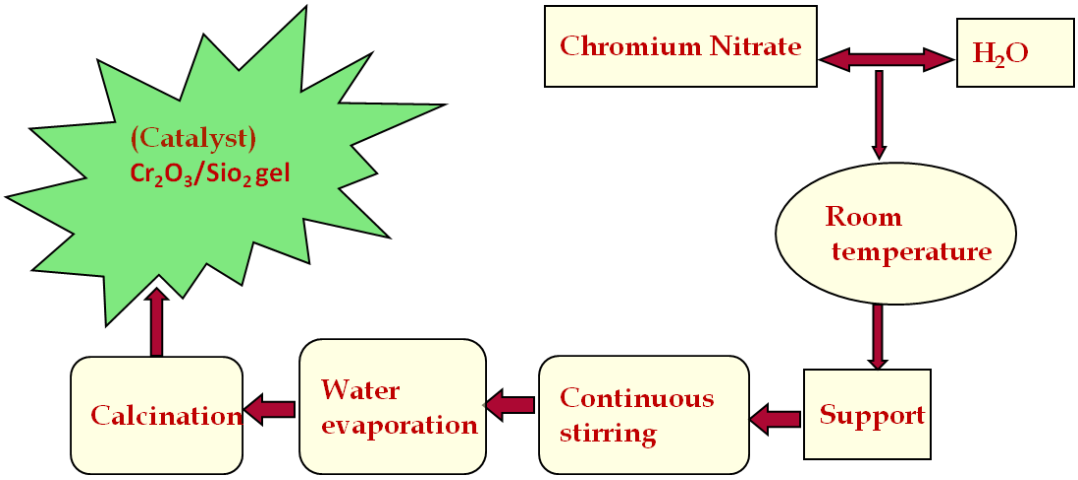

Figure.5.1. Impregnation of Silica supported Chromia catalyst

5.1.1. Catalysts Characterization:

For the determination of pore volume, BET surface area, and average pore diameter nitrogen adsorption/desorption at liquid nitrogen temperature was adopted, using the BET and BJH equations, respectively. SMART SORB 92/93 instrument was used for this purpose. The samples dried at 150 ℃ for 2 h were used for the analysis. X-ray diffraction patterns of the catalysts were recorded on an Ultima-IV diffractometer. Nickel-filtered Cu Kα radiation (λ= 1.54 Å) was used. Phase identification was carried out by comparing the data with those given in JCPDS files. H_2-TPR studies were carried out using a lab-made apparatus. 50 mg of catalyst samples were fixed in a reactor made of quartz. They were treated in a mixture of 10 % H_2, balanced by Ar supplied at 30 mL/min. The rate of heating was 5 ℃/min in the temperature region of 30-800 ℃. Before starting the run, the catalyst was pre-treated under inert argon atmosphere at 300 ℃ for a period of 2 h. For the monitoring of hydrogen consumption a TCD equipped gas chromatograph (Varian, Model 8301) was used. The catalyst samples were also analysed by UV-Vis DRS spectroscopy using a GBC Cintra 10e spectrometer collecting the data in the region of 200-800 nm. A mixture of 15 mg of the catalyst and the remaining dry KBr were mixed, made into a pellet to collect the FT-IR spectra. A Perkin Elmer instrument supplied by M/s. Spectrum GX, USA was used. A K-5 Alpha model of M/s Thermo instruments was used for XPS studies. At a vacuum of 1×10^{-9}torr, the Cr2p and O1s core level spectra were secured under Al Kα radiation (photon energy = 1253.6 eV). The carbon (C 1s) peak with a BE of 284.6 eV was considered for charge correction. A Lab Ram HR800UV Raman spectrometer (Horiba Jobin-Yvon) containing a confocal microscope provided the Raman spectra, for which a liquid-nitrogen cooled CCD detector was employed. Inductively coupled plasma optical emission spectroscopy (ICP-OES, Instrument Model:Varian 725ES) was adopted for the chemical analysis of the chromia containing samples. TEM analysis was carried out on a JEOL supplied 100S microscope, for which the samples were prepared by suspending about 1 mg catalyst in 1 ml of ethanol followed by subjecting it to sonication for 10 min.

5.1.1. (A). Scanning Electron Microscopy (SEM):

The SEM pictures of 5%Cr_2O_3/SiO_2 (denoted as Cr_2O_3/SiO_2) and 5%Cr_2O_3/6%Sulphated SiO_2 (denoted as $Cr_2O_3/S.SiO_2$) are shown in Fig.5.2. For SiO_2 support the particles had spot like morphology due to the aggregation of particles (picture not shown for brevity) and

stacking of particles on one another. Cr_2O_3 addition changed the particle morphology. Cr_2O_3/SiO_2 and $Cr_2O_3/S.SiO_2$ catalysts exhibited a well dispersed Cr_2O_3 phase on SiO_2.

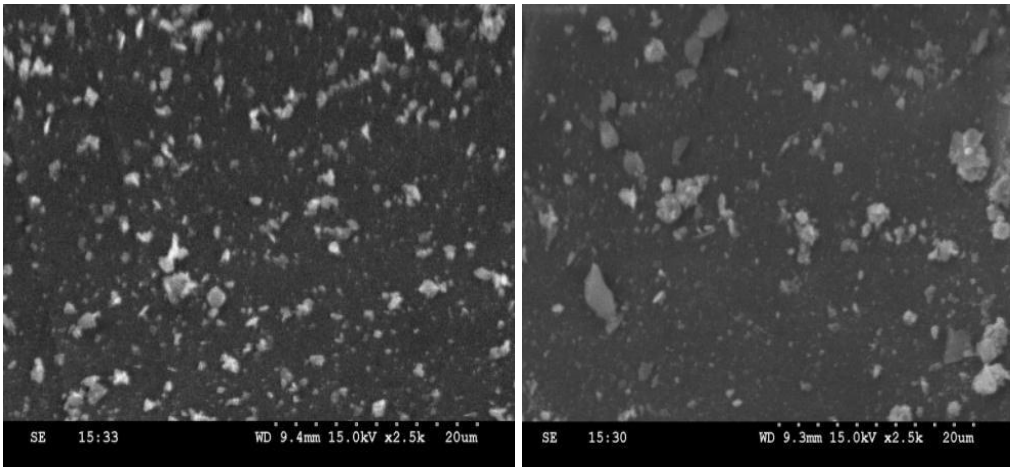

Figure.5.2. SEM pictures of (a). Cr_2O_3/SiO_2 & (b). $Cr_2O_3/S.SiO_2$ catalysts

5.1.1. (B).TPR profiles of the catalysts*:*

H_2-TPR profiles of Cr_2O_3/SiO_2, $Cr_2O_3/S.SiO_2$ and Cr_2O_3 alone samples are shown in Fig.5.3.No reduction peak was seen for silica support in the entire range of temperature. A peak with its maximum at 550 ^oC only appeared representing weak reduction in the case of bulk Cr_2O_3. This corresponds to the reduction of chromium in its highest oxidation state of Cr^{6+} [4]. In the case of Cr_2O_3/SiO_2 the $Cr^{6+} \rightarrow Cr^{3+}$reduction peak shifted to higher temperature, as already reported [3, 5, 6].

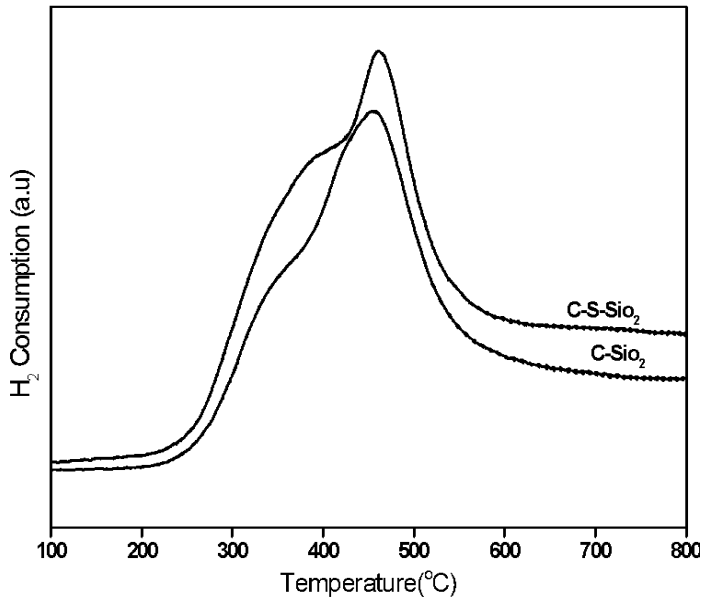

Figure.5.3. TPR profiles of Cr_2O_3/SiO_2 & $Cr_2O_3/S.SiO_2$

5.1.1. (C).X-Ray diffraction:

Powder XRD is an extremely beneficial characterization technique to find out the crystalline phases of solid materials. This technique is widely used in the heterogeneous catalysis to find out the phases and their crystalline planes responsible for the activity. Wang et al. recorded the patterns of SiO_2 and $S.SiO_2$ supported Cr_2O_3 catalysts. Both the catalysts exhibited diffraction peaks corresponding to Cr_2O_3. However, the peak intensities of Cr_2O_3 decreased and shifted in their positions in the case of $Cr_2O_3/S.SiO_2$ Fig.5.4.

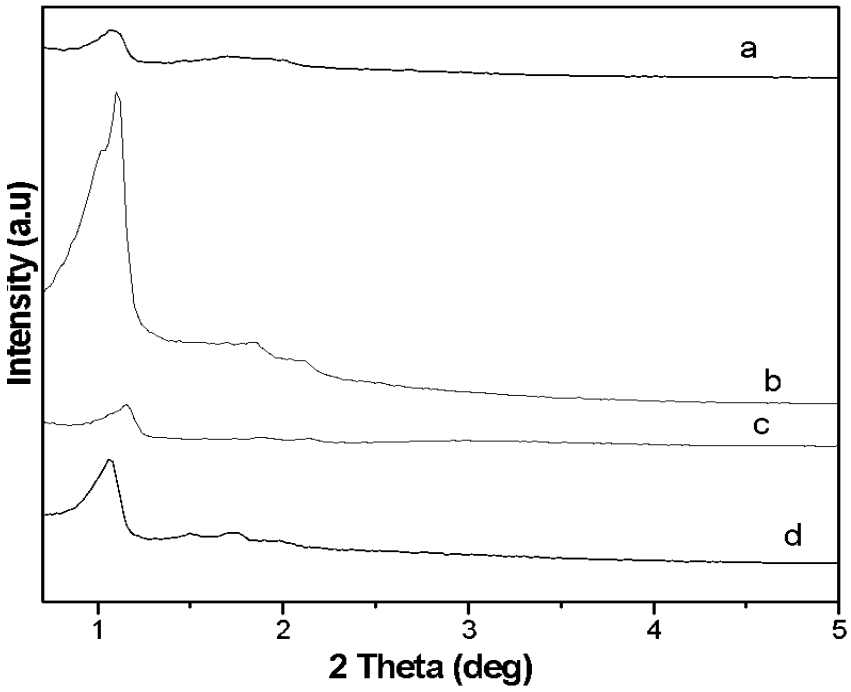

Figure.5.4. XRD patterns of (a) $Cr_2O_3/S.SiO_2$; (b) $Cr_2O_3.SiO_2$; (c) $S.SiO_2$ and (d) SiO_2

5.1.2. Temperature effect on activity:

In the case of $Cr_2O_3/S.SiO_2$, having optimum Cr_2O_3 loading and sulphate modification, the reaction temperature played a significant role on ethane and CO_2 conversions. The results are displayed in Fig 5.5.(A). Increase in temperature increased the conversions up to 650 ℃. Beyond this temperature, there was a small variation up to 675 ℃. Ethylene selectivity followed the

same trend as conversion. The Cr^{+6} to Cr^{+3}redox cycle might be responsible for the initial increase up to 650 ℃ and maintenance of high catalytic activity at 675 ℃.

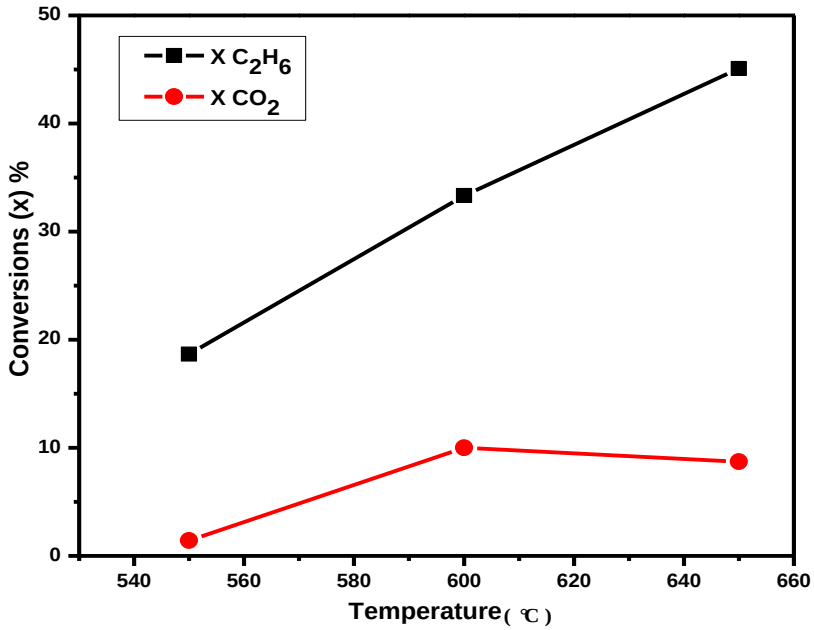

Figure.5.5. (A).Activity for Chromium on silica gel catalyst

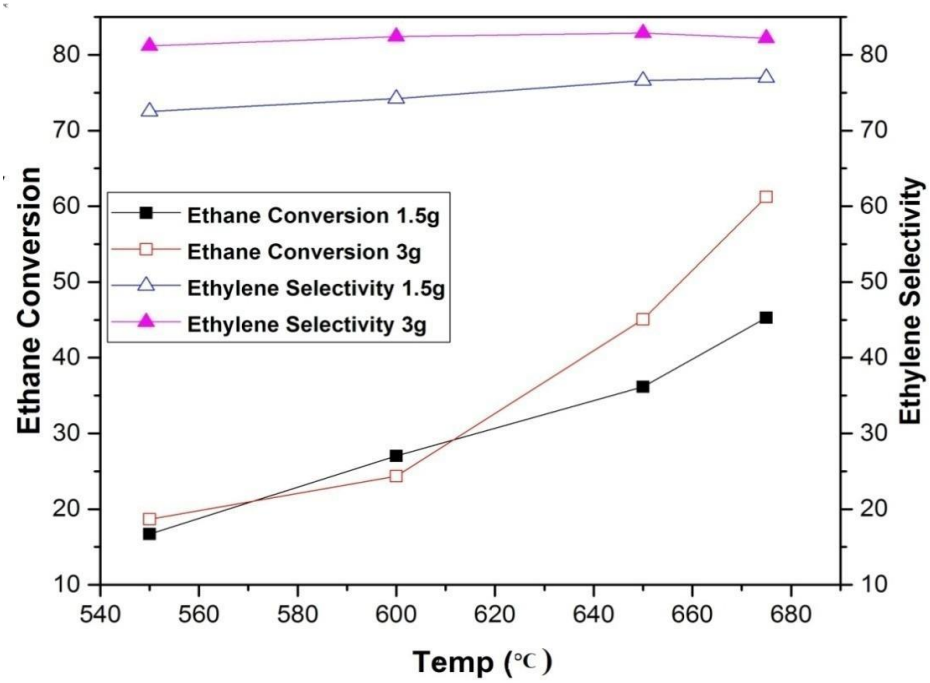

Figure.5.5.(B). Ethane conversion and ethylene selectivity on 1.5g, 3g of Cr_2O_3/S.SiO_2 catalyst

Change in weight of catalyst changed conversion and selectivity as shown in Fig.5.5. Conversion of ethane and ethylene selectivity increased with increasing temperature in both cases. With a catalyst weight of 1.5g 73%- 75% selectivity of ethylene was achieved at 675 ℃. The conversion also increased. When the weight of catalyst was doubled, i.e 3g, the selectivity further increased reaching a value of 80%. Simultaneously, there was an increase in conversion of ethane from 20% to 60 % with increasing temperature.

5.1.3. Summary:

SiO_2, used for this study, was proved as a promising support for the catalyst with suitable characteristics. $Cr_2O_3/S.SiO_2$ was better than Cr_2O_3/SiO_2 in terms of reactant conversions and product selectivity. At 45% ethane and 10% CO_2 conversions, the ethylene selectivity reached 76%. Thus the importance of sulphate modification was brought forward.

5.2. Studies on Cr_2O_3 / SBA-15 catalyst:

5.2.1. Preparation of catalysts:

The synthesis of SBA-15 was carried out adopting the procedure already reported in the literature [17]. Typically,P123 triblock copolymer (20 g) dispersed in a mixture of (465 mL) of distilled water and 35 % hydrochloric acid (M/s. Loba Chemie,137.5 g) was added to 44 g of tetraethyl orthosilicate (Aldrich). Continuous stirring (1 h at 40 ℃) was followed by filtration of the resultant slurry, its drying(at 110 ℃ for 12 h) and calcination of the solid for 4 h at 550 ℃ . Required quantity (6 wt.% sulphate) of aqueous ammonium sulfate solution was used to impregnate known quantity of SBA-15 to prepare6 wt.% sulphated SBA-15 (denoted as S.SBA-15). 5 wt. % Cr_2O_3/SBA-15 (Cr/SBA-15) and 5 wt. % Cr_2O_3/sulfated SBA-15 (Cr/S.SBA-15) were prepared by support impregnating the with necessary quantities of aqueous chromium nitrate (Wako Chemicals) solution (Fig 5.6). For all the catalysts, drying at 120 ℃ and calcinations at 700 ℃ for 3h were common [17].

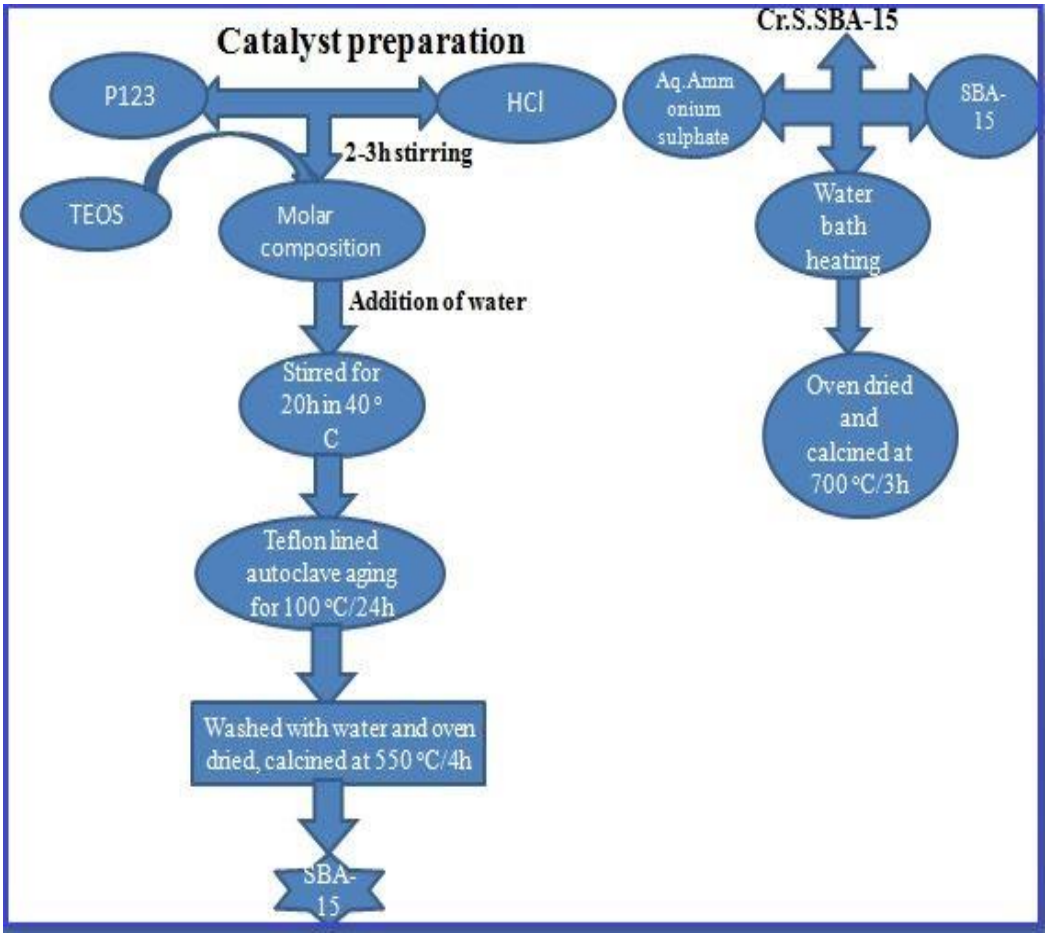

Figure.5.6.SBA15 Catalyst preparation by Hydrothermal method

5.2.2 .Catalysts Characterization:

Surface area was estimated by using BET equation. Pore volume and average pore diameter were obtained from BJH equations. Required data for the above were secured by nitrogen adsorption on a SMART SORB 92/93 instrument. The samples were pre-dried at 150 ℃ for 2 h and the adsorption/desorption was followed using nitrogen at liquid nitrogen temperature. Rigaku Corporation supplied Ultima-IV diffractometer was used for collecting the XRD data. The parameters were: nickel-filtered Cu Kα radiation (λ= 1.54 Å), steps of 0.045 °, count time of 0.5 s and 2θ range of 0 to 80°. JCPDS files were referred for fixing the crystalline phases. For the H_2-TPR studies the samples (50 mg) were taken in a quartz reactor, reduced under 10 % H_2/Ar gas mixture at a flow rate of 30 mL/min with a heating rate of 5 ℃/min up to 800 ℃. Before the TPR run, the catalysts were pretreated in argon flow at 300 ℃ for 2 h. Hydrogen consumption

was monitored using thermal conductivity detector of a gas chromatograph (Varian, 8301). The UV-V is DRS, FTIR, Raman and XPS analyses of the samples were carried out as described above. The chemical composition of the chromia samples, the ICP-OES technique was adopted using a Varian 725ES instrument. The morphology of the samples was obtained from a JEOL 100S transition electron microscope. 1 mg catalyst was suspended in 1 mL of ethanol and placed on a copper grid coated with carbon film.

5.2.2. (A).Textural properties of the catalysts:

The estimated values of BET surface area, pore volume and pore diameter along with the Cr_2O_3wt % of the catalysts are reported in Table 1. Surface area and pore volume decreased after sulfation of SBA-15, which further decreased after the addition of CrO_x to SBA-15. This decrease might be due to the extra-framework CrO_x species formed in the support, as also reasoned by Zhang et al. [19].However, the prior addition of sulfate ion to the support reduced the loss in surface area due to CrO_x addition.

Catalysts	**S_{BET}(m^2/g)**	**V_p (cm^3/g)**	**D_{BJH} (nm)**	**Cr_2O_3 (wt%)**
SBA-15	506	0.681	6.6	--
S.SBA-15	462	0.671	6.5	--
Cr/S.SBA-15	435	0.648	5.9	4.92
Cr/S.BA-15	417	0.645	5.8	4.85

Table.5.1: Textural characteristics of the supports and catalysts

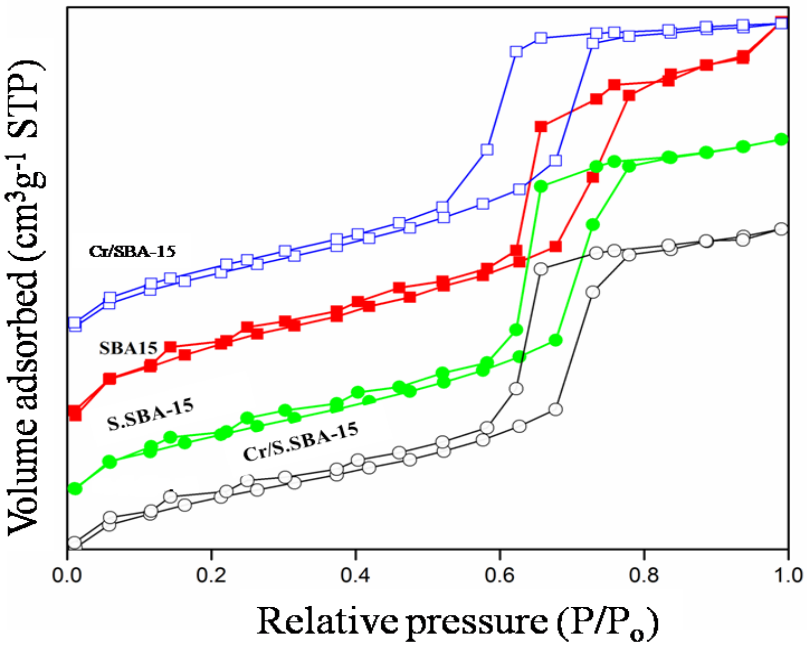

Figure.5.7.N_2 adsorption/desorption isotherms of the supports and catalysts

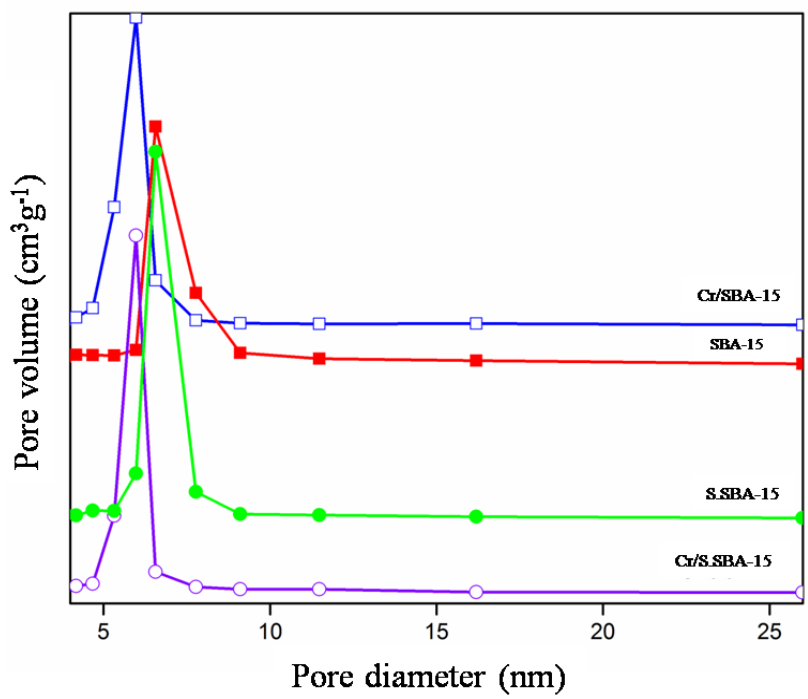

Figure.5.8.Pore size distribution of the supports and catalysts

Pore size distribution data of the samples are shown in Fig.5.8. The hysteresis loop was of H1-type confirming the mesoporous structure SBA-15[18]. Capillary condensation within uniform mesopores was visible, as observed by a sharp inflection in the pore region of 0.6–0.8. The isotherms of Cr/SBA-15 and Cr/S.SBA-15 also show similar patterns revealing the intactness of

the hexagonally ordered structure. The nonclosure of the adsorption and desorption patterns can be seen from the figure, which may b explained as follows. As Esparza et al. [21] have reported, SBA-15 materials may contain some amount of intra-wall pores that can possibly interfere adsorption/desorption phenomenon. In addition to this, a sort of pore-blocking effect occurs if the cross section of the pore varies along its length. Normally, a pore of a given diameter releases its condensate completely at a particular relative pressure. In the case of SBA-15 the emptying of pore takes place progressively. The decrease in pore volume may be due to partial blockage of the mesopores of SBA-15 with the CrO_x species. During this process partial pore wall collapse might be responsible for the decrease of the pore diameter, as reported by Shi et al. [20]. The phenomenon of nonclosure of adsorption and desorption can be observed from the isotherms which can be explained as follows.

5.2.2. (B).X-ray Diffraction:

Fig.5.9 (A) displays the low angle XRD patterns of support SBA-15, sulphate modified support SBA-15 supports and the unmodified and sulfate modified catalysts. The peaks corresponding to 2θ values of 0.98, 1.74, and 2.00° can be indexed as (100), (110), and (200) reflections [18]. The addition of CrO_x to SBA-15 showed a slight right shift towards high 2θ region, whereas sulphate modification of SBA-15 demonstrates no deviation. The shift in the case of Cr/SBA-15 catalyst may indicate partial substitution of Si with Cr species in the SBA-15 frame work. However, the shift in the peak position that indicates the increase in unit cell constant may be considered trivial in the case of Cr/SBA-15, as opined by Charan et al. [22]. Instead, the shift in (100) peak may be attributed to the blockage of SBA-15 framework because of CrO_x interaction [22].

XRD patterns obtained in the wide angle are shown in Fig.5.9.(B). The presence of amorphous silica in SBA-15 was revealed by a broad peak between 15–30 º [20]. The diffraction patterns CrO_x containing catalysts show peaks at 2θ = 24.38, 33.50, 36.16, 41.42, 50.18, 54.84, 63.42 and 65.10 ° ascribed to the presence of crystalline Cr_2O_3 (JCPDS No.: 84-1616) [23].The intensities of these peaks are lower in Cr/S.SBA-15 catalyst than those of Cr/SBA-15. It means a better CrO_x dispersion in the modified catalyst. Thus, the addition of sulfate ion obviously enhanced the chromium species dispersion in Cr/S.SBA-15.

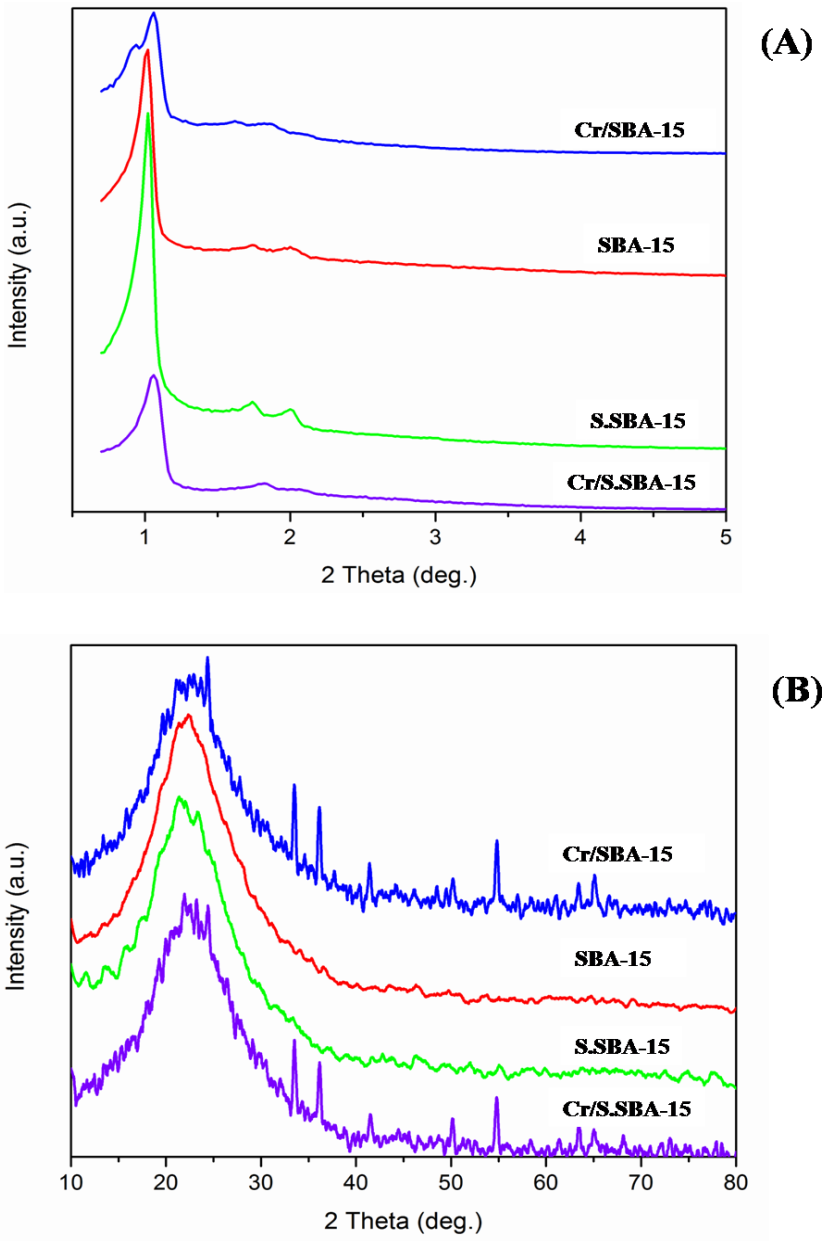

Figure.5.9. XRD patterns of the supports and catalysts; (A) Low angle and (B) Wide angle

5.2.2. (C).FT-IR results:

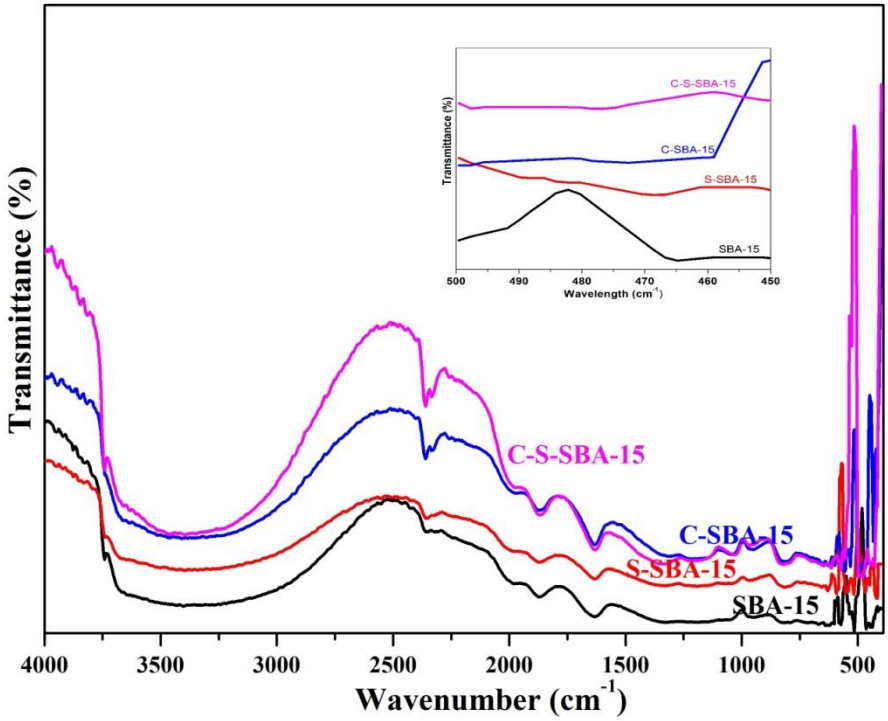

Figure.5.10. FT-IR spectra of supports and catalysts

The FT-IR spectra generated are shown in Fig.5.10 The vibrational bands at 3400, 1632-1640, 1055-1213, 958, 805-809, 566-575 and 460-489 cm^{-1} represent the surface silanols; Si-O-Si, Si-O and the hydrated Si-O groups [24]. The spectra demonstrate the symmetric stretching modes of Si–O–Si groups (796 cm^{-1}), bending vibration of Si–O–Si groups (455 cm^{-1}) and the defective Si–OH groups (967 cm^{-1} and 3398 cm^{-1}) [24].The high wavelength (3567 cm^{-1}) absorption bands are due to –OH stretching in intermolecular water. The band at 1,080 cm^{-1}denotes the presence of internal Si–O asymmetric stretching and the one at 1,227 cm^{-1} correspond to external asymmetric stretching. Si–O symmetric stretching was also seen by the peak at 800 cm^{-1} due to SiO_4 vibrations [25] in the SBA-15. SBA-15 has a covalent frame work with predominantly stabilized and isolated $(O)_3$-Si–OH and geminal $(O)_2$-Si–$(OH)_2$ silanol groups on its surface. These surface graft with chromia [22]. The presence of extra framework hydrated CrO_x species on the pore surface was visible by the bands at 573 and 620 cm^{-1}[22, 23]. Especially, the intense band at 573 cm^{-1} in the sample indicates the existence of Cr-polycation. A close observation of intensities of the bands at 550 and 620 cm^{-1} seen in Cr/SBA-15 and Cr/S.SBA-15 catalysts

indicate that there is a decrease in intensity of 550 cm^{-1} band after sulfate modification. Thus, there is a more prevalence of hydrated CrO_x species in the latter indicating better dispersion [24].

5.2.2.(D).Temperature Programmed Reduction:

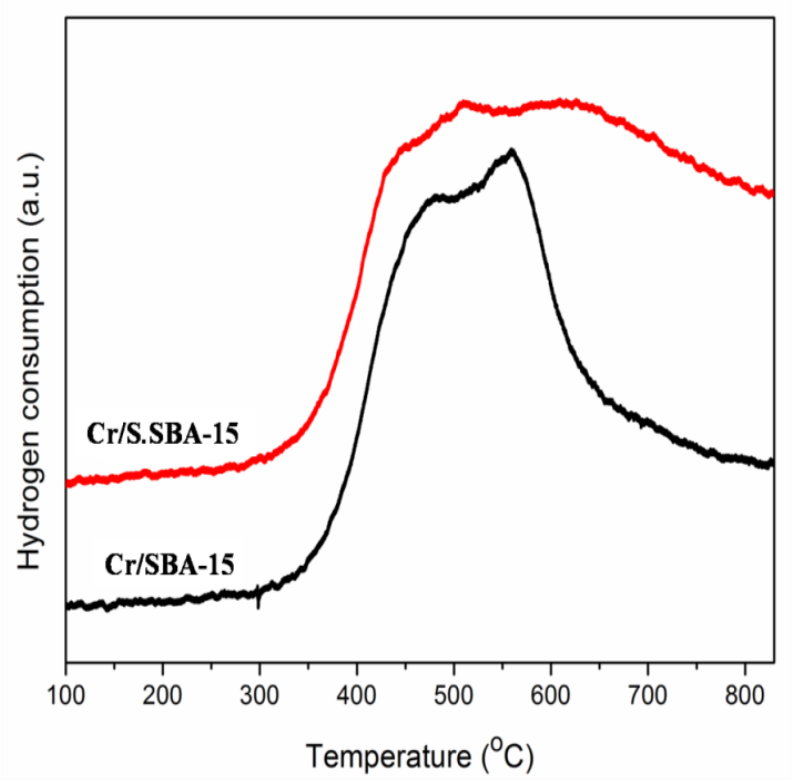

Figure.5.11. TPR profiles of the SBA15 catalysts

TPR analysis provides valuable information regarding the redox property of a catalyst. The TPR profiles of the CrO_x containing catalysts are displayed in Fig.5.11. Several differences in H_2-TPR analysis of CrO_x are reported in the literature [23].Preparation method, calcination temperature and nature of support material determine the nature of interaction of CrO_x with support. Depending the nature of interaction either dispersed mono or polychromates are formed on the surface. Different reduction profiles of CrO_x could be seen based on these species formed because of the strength of interaction between CrO_x and SBA-15. Cr/SBA-15 shows a strong reduction band at 550 ℃ with shoulder at 450 ℃ due to the reduction of $Cr^{6+} \rightarrow Cr^{3+}$ [26, 26].Sulfate modification has shifted the reduction maxima to higher temperatures. Higher reduction temperature observed in Cr/S.SBA-15 compared to that of Cr/SBA-15 suggests stronger interaction between the active component and the support leading to better dispersion of CrO_x species in the former case [15].

Earlier studies revealed that the chromium exists in various oxidation states in supported chromia materials, in which Cr^{6+} and Cr^{3+} are prominent during the redox processes in the catalytic ODH of alkanes [14,29,30]. Grafted and the soluble Cr^{6+} species are formed on the surface, as reported by Cavani et al. [31] Grafted Cr^{6+} species demonstrates greater interaction with the support and in turn is difficult to be reduced than the latter species. The intense peak appearing between 374 and 397 ℃ represents to reduction of soluble Cr^{6+} species. The high temperature 510 ℃ peak is due to the reduction of the grafted Cr^{6+} species.

5.2.2. (E).UV-DRS results:

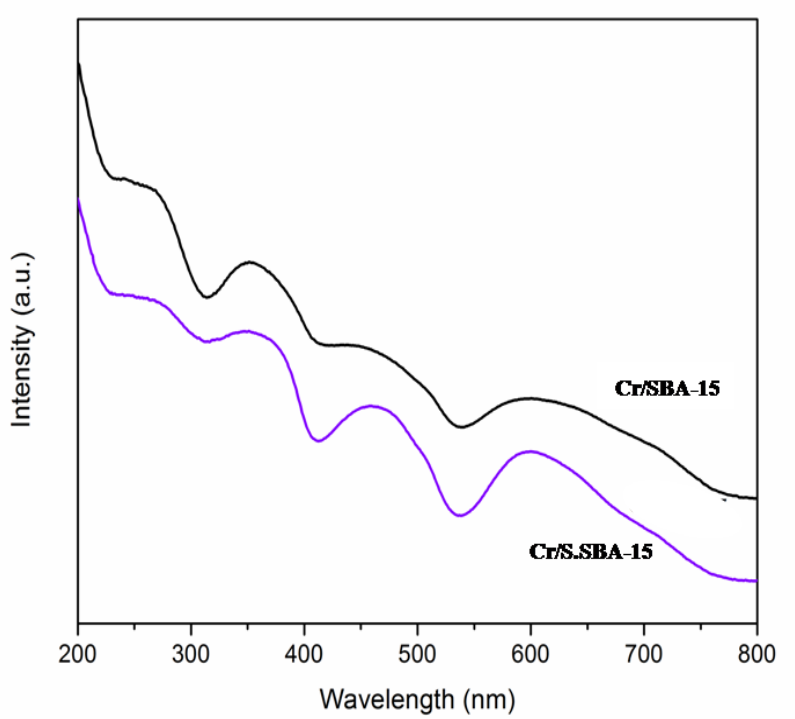

Figure.5.12. UV-DRS bands of the catalysts

The UV-Vis DRS patterns (Fig.5.12) have shown absorbance bands at 250, 350, 450 and 600 nm. According to literature the lower wavelengths at 250, 350 and 450 nm are due to the presence of monochromatic Cr^{6+} species. 250 and 350 nm bands are due to the charge transfer spectra of d-d transitions from 1A11T2 transitions of tetrahedral Cr-oxide. 450 nm bands are due to the symmetric forbidden nature of transitions from 1A1 1T1 of tetrahedral Cr-oxides. On the other hand the 600 nm bands are due to the symmetric transitions of A2gT2g octahedral

coordinated Cr^{3+} in Cr_2O_3 clusters [27, 32]. So, the mono- and polychromatic Cr^{6+} species are dominant in Cr/S.SBA-15.

5.2.2. (F).XPS results:

O1s XPS: Fig.5.13 Shows the O1s spectra of all catalysts. The peaks observed correspond to the BE varying in the range of 534 – 536 eV for O1s. SBA-15 shows peaks at 534.3 and 535.8 eV, the addition of sulfate ion shows a high BE value than the parent SBA-15 indicating the interactions of sulfate with SBA-15. CrO_x addition to SBA-15 showed a left shift in the BE values describing their stronger interaction with SBA-15. The shift in O1s peak towards lower BE is due to the creation of of CrO_x domains on Cr/SBA-15 [23]. This indicates high interaction of CrO_x with the support S.SBA-15.

Cr2p XPS: The results of Cr2p XPS studies are presented in Fig.5.14. The study establishes the formation of Cr^{6+} species in both the Cr containing catalysts. The asymmetric peaks between BE of 575–580 and 585–589 eV gave rise to two sets; one with BEs at 577 and 579 eV and the other at 586 and 588 eV. The former can be assigned to Cr^{3+} ions whereas the latter to Cr^{6+} ions. Thus, the simultaneous presence of Cr^{3+} and Cr^{6+} ions was confirmed, as also reported in the literature [32, 33]. The peaks assigned to Cr^{6+} are more intense than those of Cr^{3+} indicating the dominance of Cr^{6+}, as also evidenced by the UV-Vis DRS studies. Sulfate ion addition helps promote chromium with higher oxidation states [34].Since XPS is a surface technique it is not possible to estimate the overall quantity of Cr^{6+} and Cr^{3+} species. However, a surface Cr^{6+}/Cr^{3+} ratio >1 can be discerned from the analysis which is preferable for the catalyst to show higher activity. These results corroborate with the XRD results.

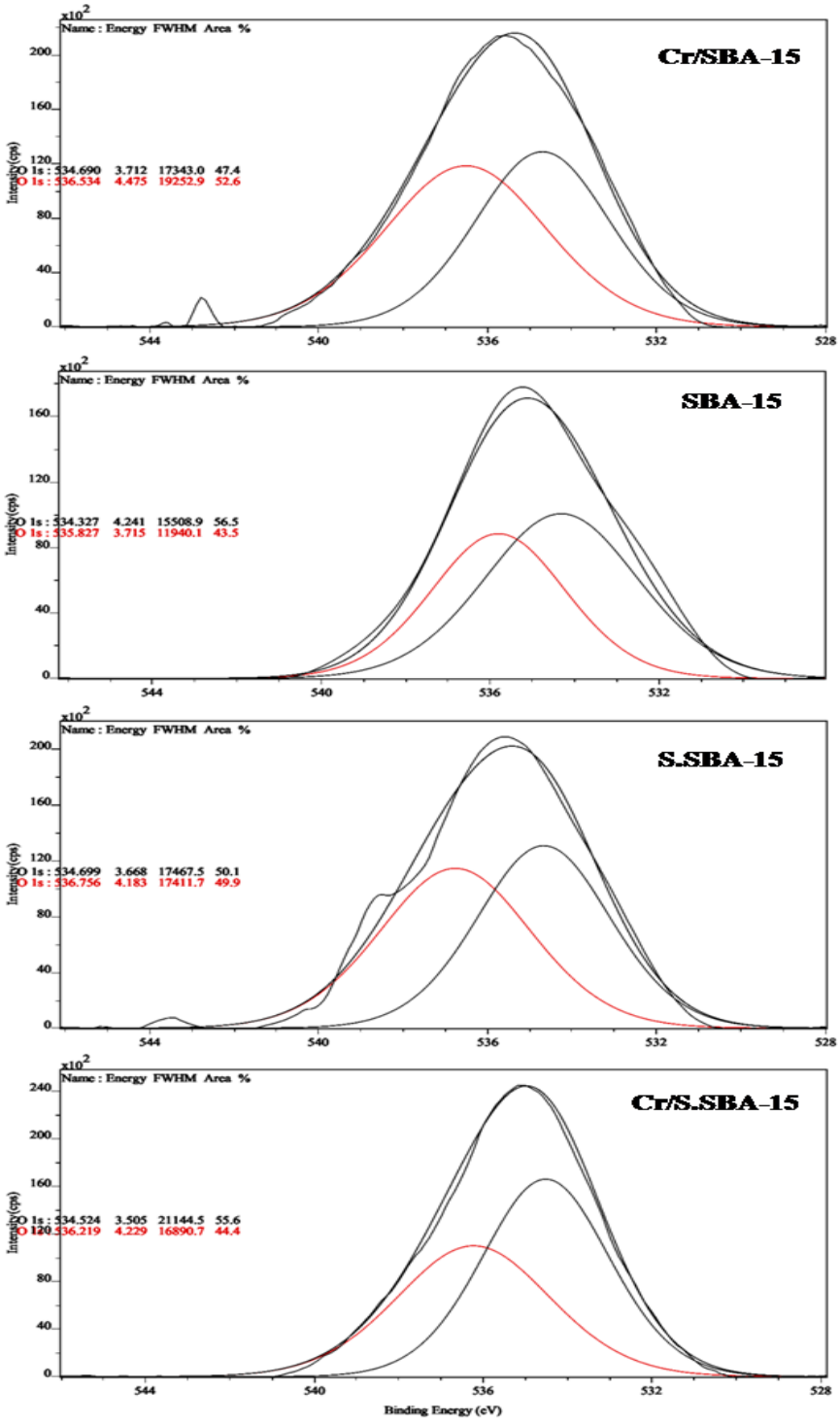

Figure.5.13. O 1s XP spectra of the SBA15 supported catalysts

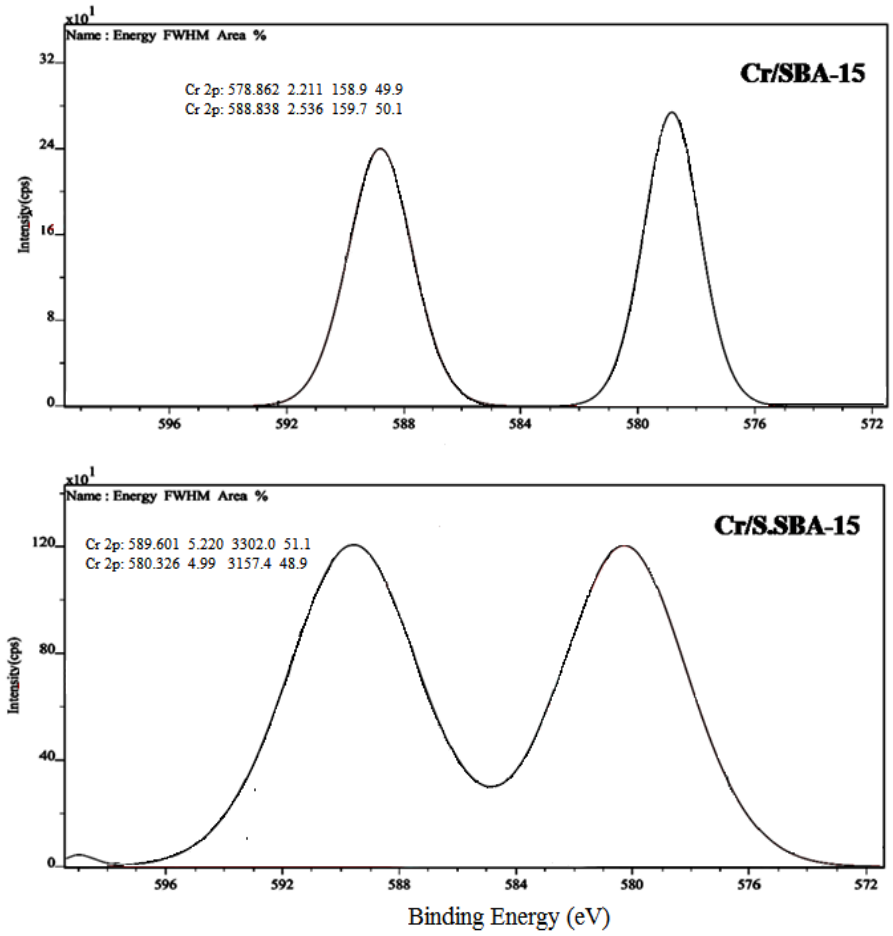

Figure.5.14. Cr 2p XP spectra of the SBA-15 supported catalysts

5.2.2. (G). Laser-Raman:

Raman spectra of catalysts are presented in Fig.5.15. Typically three kinds of Cr species, i.e. isolated (monochromate), polychromate, and crystalline Cr_2O_3 are seen in supported chromia catalysts. The Raman spectrum of SBA-15 shows three bands at 497, 607 and 977 cm^{-1} assigned to cyclic tetrasiloxane rings, cyclic trisiloxane rings and the Si–OH stretching, respectively [35]. It can be seen that the spectra of chromium incorporated samples exhibit a band at 987 cm^{-1} assigned to the υ_s(O=Cr=O) stretching, the other at 394 cm^{-1} due to δ(O=Cr=O) bending, and finally, the band at 1014 cm^{-1} referred to υ(O=Cr=O) stretching, as reported by Dines et al during their DFT calculations [36]. Cr/SBA-15 shows several Raman bands appearing at 219, 306, 344, 394, 449, 505, 543, 601, 669, 747, 818-859, 915, 1014 and 1145 cm^{-1}.

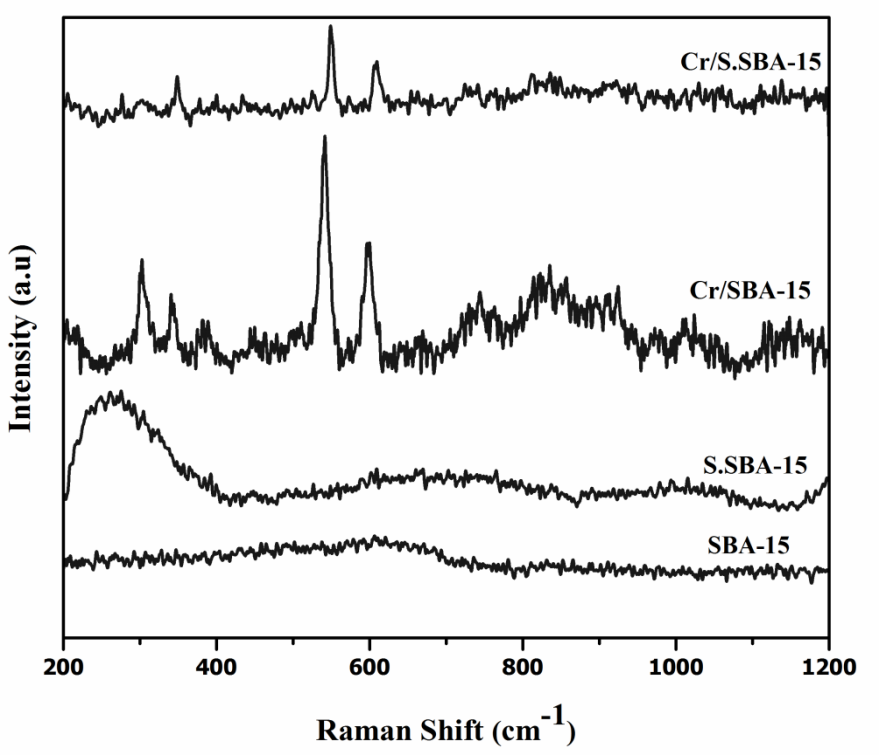

Figure.5.15.Raman spectra of the SBA15 and SO_4^- catalysts

The Raman spectrum of Cr/S.SBA-15 shows bands at 353, 551, 606, 725, 814, 833, 908-945, 1057 and 1141 cm^{-1}, in which the band at 353 cm^{-1} could be ascribed to Cr^{6+} [37]. The peaks observed at 396, 929-949 cm^{-1} are attributed to monochromatic Cr^{6+} species [37, 38]. The Cr^{6+} species is known by the Raman bands at 896 (weak), 970 (strong), and 1061 (weak) cm^{-1}[23] and the difference in the band shifts of 970 $cm^{-1}$and 980 cm^{-1} is due to Cr–O stretching of monochromate species in Cr-SBA-15 [32, 39].The peaks in the range 690-1017 cm^{-1} are due to the polychromatic Cr^{6+} species from the oligomerization [32, 37].Incorporation of sulfate ions in SBA-15 support is more favourable to formation of Cr^{6+} ion species than the unmodified one. These results corroborate the XRD analysis.

5.2.2. (H). ICP-OES results:

The composition of Cr_2O_3 present in the modified SBA-15 samples was determined by ICP-OES technique. The acquired results are presented in Table 5.1. These values are found to be very close to the theoretical values.

5.2.2.(I). TEM Analysis:

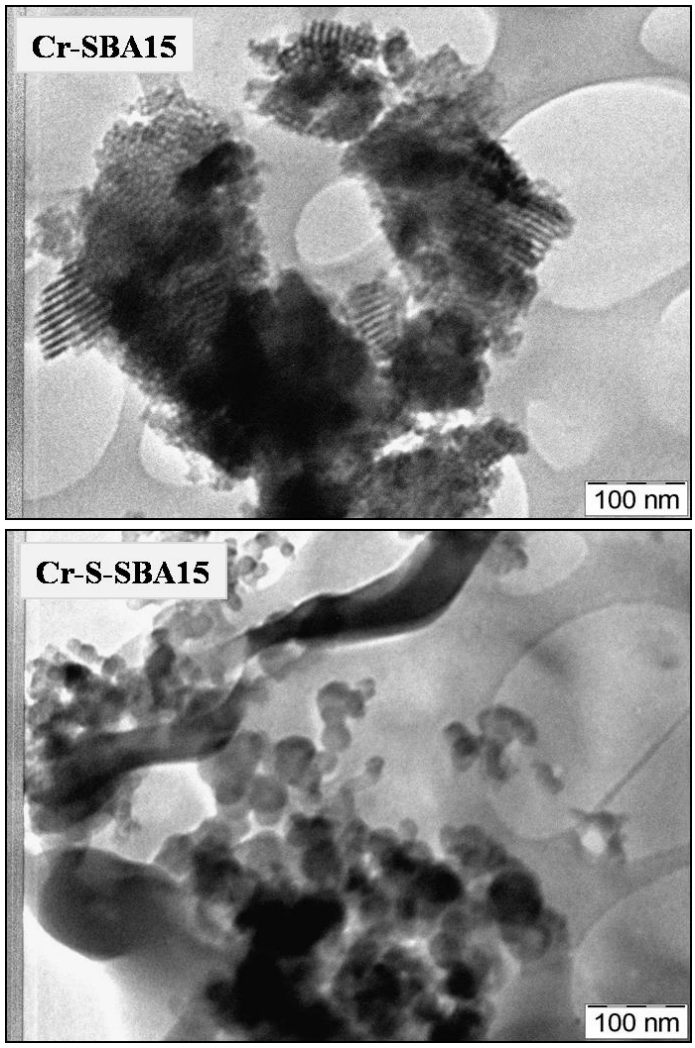

Figure.5.16.TEM images of the catalysts

The TEM micrographs of the Cr/SBA-15 and Cr/S.SBA-15 catalysts shown in Fig.5.16.reveal the hexagonal structure of SBA-15. The average crystal size of sulfate modified catalyst was found to be 120 nm (Cr/S.SBA-15), whereas that for Cr.SBA-15 catalyst was 240 nm. From the above results, it can be concluded that modification with sulfate ion leads to decrease in crystal size.

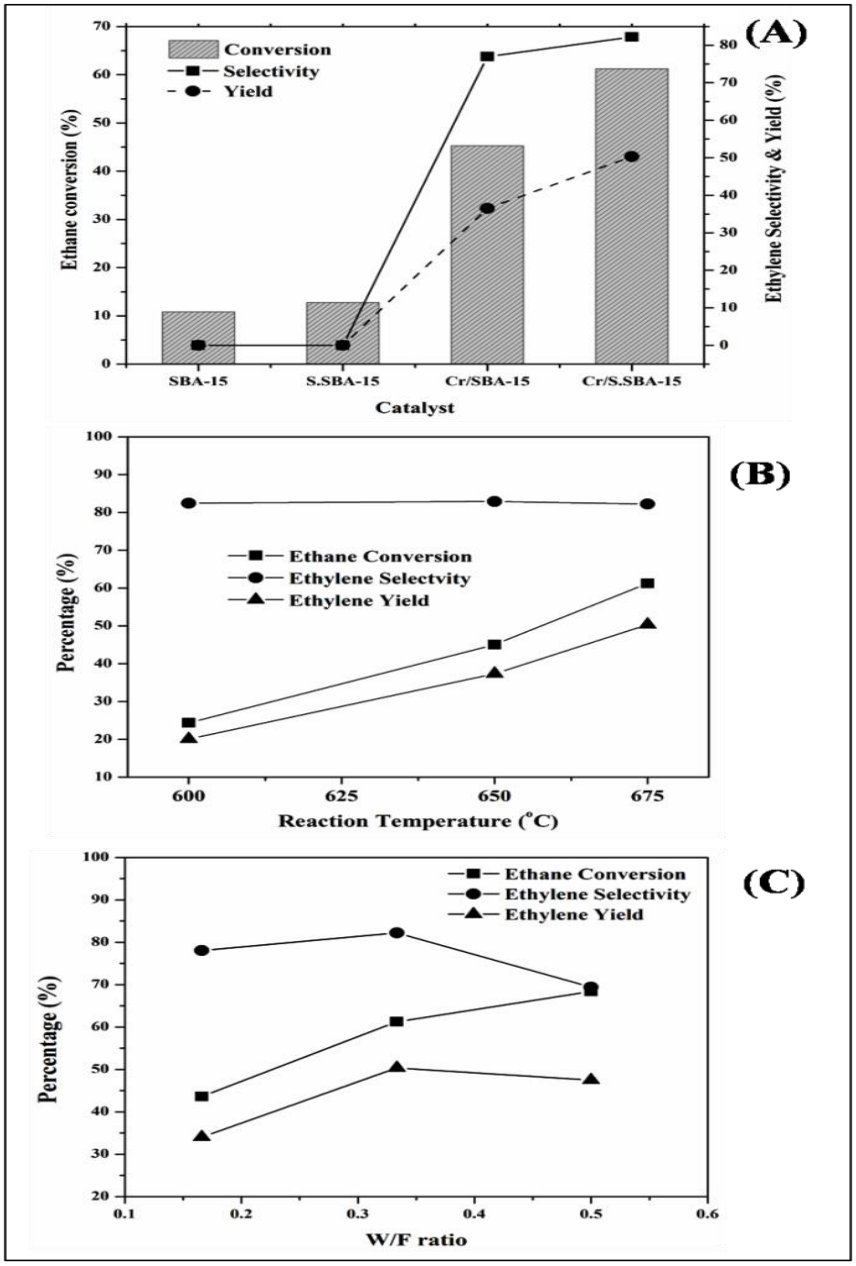

Figure.5.17. (A) Activity of the catalysts; (B) Effect of reaction temperature on the activity of Cr/S.SBA-15 catalyst; (C) Catalytic performance of Cr/S.SBA-15 at different W/F ratios (Temperature-675 ℃; Flow rate: 9 mL/min Ethane + 54 mL/min CO_2 + 27 mL/min He)

5.2.3. Catalytic activity:

All the catalysts were evaluated for their ODH performance using CO_2 as the oxidant. The CrO_x containing catalysts showed (Fig.5.17A) high conversion of ethane and high ethylene selectivity and yield compared to the bare SBA-15 and S.SBA-15 supports. Cr/S.SBA-15

showed the highest conversion (61.2 %) and selectivity (82.2 %) in the series, with ethylene yield reaching 50.3 %, the same for Cr/SBA-15 are obtained as 45.3, 76.9 and 36.5 %, respectively. Thus, sulfate modification had a distinct influence of the performance of the catalysts. Better dispersion of Cr species on the sulfated sample might have increased ethane activity by facilitating more number of active sites, as also reported by Wang et al [15].

The high oxidation state chromium species play a key role in getting highcatalytic activity [40, 41]. Ge et al. [12] used ESR and UV-DRS to identify the active sites in the catalyst responsible for the ODH of ethane with CO_2. They established that the presence of Cr^{5+} or $Cr^{6+}$is significant for the reaction. Cr^{6+} or Cr^{5+} was proposed to be the active species in Cr/H-ZSM-5 (SiO_2/Al_2O_3>190). Fridman et al. investigated CrO_x/Al_2O_3 catalysts for the dehydrogenation reaction and stated that the high oxidation states were responsible for the redox reaction [42, 43]. In the present catalysts also, the Cr^{6+} species seems to be responsible for the high activity. The Cr^{6+} species is initially reduced to Cr^{3+} species during the dehydrogenation of ethane. Subsequently, the reduced Cr^{3+} is re-oxidized to Cr^{6+} by CO_2, as described by the following equations [11].

$$\begin{aligned} C_2H_6 + Cr^{6+} = O \quad &\rightarrow \quad C_2H_4 + H_2O + Cr^{3+} \\ Cr^{3+} + CO_2 \quad &\rightarrow \quad CO + Cr^{6+} \end{aligned} \qquad (5.1)$$

According to literature, 8 wt. % Cr_2O_3/SiO_2 catalyst at 650 ℃ was excellent with 55.5 % ethylene yield and 61 % ethane conversion [7]. Ge et al.showed that 5 % Cr/SiO_2 gave 30.7 % ethane conversion and 96.5 % ethylene selectivity at 700 ℃. Cr^{5+} and/or Cr^{6+} were observed to be important for the reaction [12, 13]. Cr-Si-2 molecular sieve gave 45.5 % ethylene yield with 87.9 % selectivity at 650 ℃. 66.5 % ethane conversion and 99.5 % ethylene selectivity were reported on the 5wt. % Cr loaded monolithic FeCrAl alloy foil catalyst at 750 ℃ [14]. An enhancement in the activity was observed after Ce modification of Cr/SBA-15 catalyst. The Cr^{6+}–Cr^{3+} redox cycle was carried out by the sequential dehydrogenation of ethane and oxidation by CO_2 [20]. In the present investigation, FT-IR, UV-DRS, Raman and XPS investigations revealed that the surface Cr species were mainly Cr^{6+} in mono and polychromate forms, with a minor amount of Cr^{3+}. The TPR profiles reveal the facile redox nature of Cr^{6+} to Cr^{3+}.The performance of the present catalyst is also comparable with those reported in the literature, except for small discrepancies due to the variation in the reaction temperature or the definition adopted for arriving at parameters. Thus, we believe that the predominance of surface

Cr^{6+} species on the sulfate modified catalyst also seems to be responsible for the higher activity. The presence of more number of active Cr^{6+}species in the monolayer coverage area of CrO_x, having uniform dispersion on the support is responsible for the good performance of the catalyst. Higher oxidation state of chromium also leads to better performance.

The Cr^{6+}/Cr^{3+} ratio is also a significant factor in the ODH of ethane. Asghari et al [44] reported a direct correlation between this ratio and the activity in their studies on MCM-41supported Cr_2O_3 catalysts. The ratio increased up to 8% Cr where the activity was also maximum. According to Mimura et al. [11] Cr^{6+}/Cr^{3+}redox cycle plays a vital role in the CO_2 ODH of ethane over Cr/H-ZSM-5 catalyst. High dehydrogenation activity can be realized by the Cr redox cycle [14].

The effect of reaction temperature on the activity and selectivity of Cr/S.SBA-15 catalyst is shown in Figure.5.17 B. It may be observed that increase in reaction temperature increased the ethane conversion and the selectivity continued to be at its high value. 675 ℃ was the best temperature in the studied region.

Change in the ODH activity of Cr/S.SBA-15 with change in space velocity was studied at 675 ℃ temperature and the results are presented in Figure.5.17C. Increase in W/F increased the conversion of ethane and ethylene. Ethylene selectivity reached its maximum value at a W/F of 0.33.

5.2.4. Time on stream analysis on Cr/S.SBA-15 catalyst:

Cr/S.SBA-15 catalyst was further subjected to time on stream (TOS) studies for 16 h.The results are shown in Fig.5.18. This catalyst showed steady catalytic activity up to 16 h of reaction time. Apart from ethylene the formation of CO, CH_4 and H_2 was noticed in the product gas. Both the catalysts showed the same selectivity (14 %) for methane. The unmodified and sulfate modified catalyst showed variation in CO (6.6 % and 3.4 %, respectively) and H_2 (1.7 % and 0.7 %, respectively) compositions. The higher values for the CO and H_2 shown by Cr/SBA-15 compared to that of Cr/S.SBA-15 may be due to over-oxidation of the main product ethylene, as reported in the earlier publication [6].

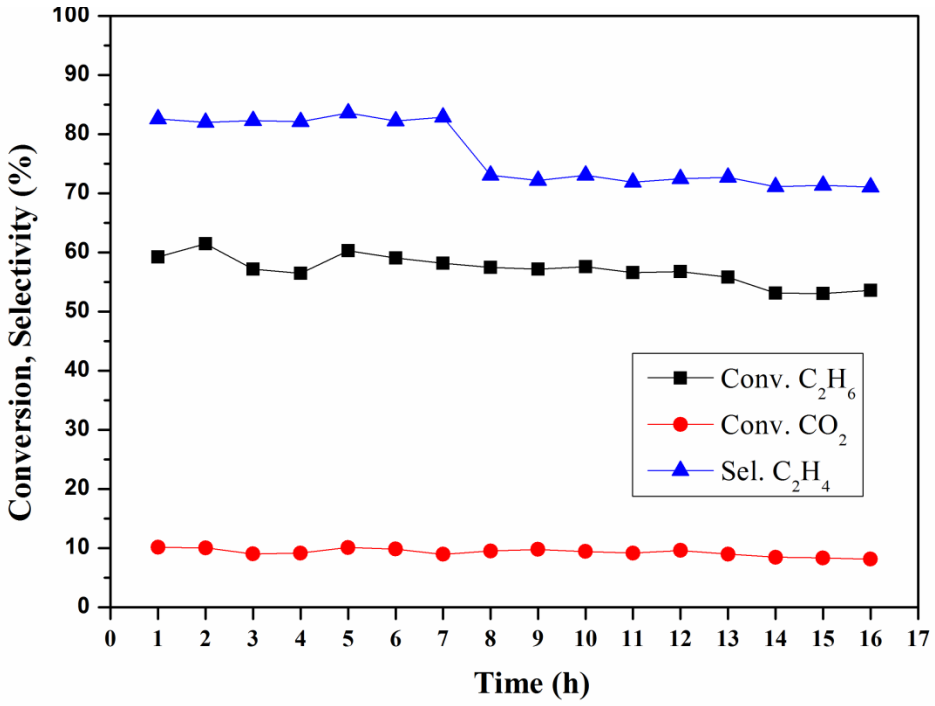

Figure.5.18. Time on stream (TOS) analysis on Cr/S.SBA-15 catalyst for 16h

5.2.5. Influence of Cr loading on the activity of Cr/S.SBA-15 catalyst:

The effect of loading was studied by taking 2.5, 5 and 7.5 wt% chromium in Cr/S.SBA-15. 5 wt% was found to be the optimum, the 5%Cr/S.SBA-15 showing the highest conversion (61.2 %) and selectivity (82.2 %) in the series, with ethylene yield reaching 50.3 % (Fig.5.19).

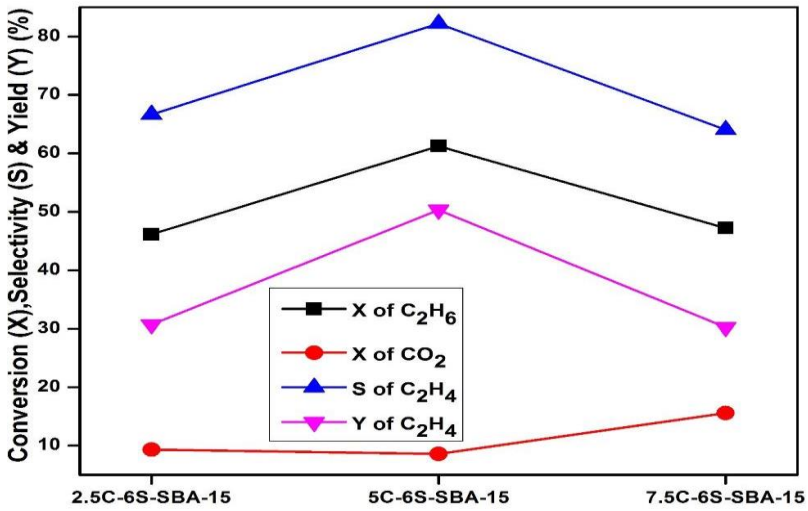

Figure.5.19. Chromium effect on Cr/S.SBA-15 catalyst

5.2.6. Effect of extent of sulphate modification in Cr/S.SBA-15:

Again, as shown in Fig.5.20, 6 wt.% sulphate modification was found to be the optimum.

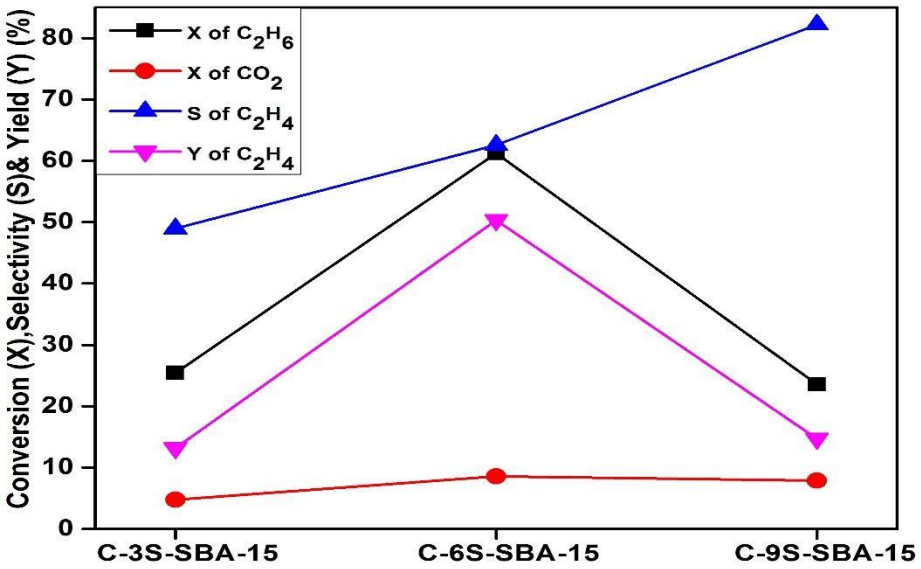

Figure.5.20. Effect of extent of sulphate modification in Cr/S.SBA-15 catalyst

5.2.7. .Effect of catalyst weight on the activity of Cr/S.SBA-15 catalyst

Study on change in the catalyst weight was made taking 1.5 and 3 g of Cr/S.SBA-15 catalyst. There was not much change in the CO_2 conversion, whereas ethane conversion showed a considerable variation, as shown in Fig.5.21.

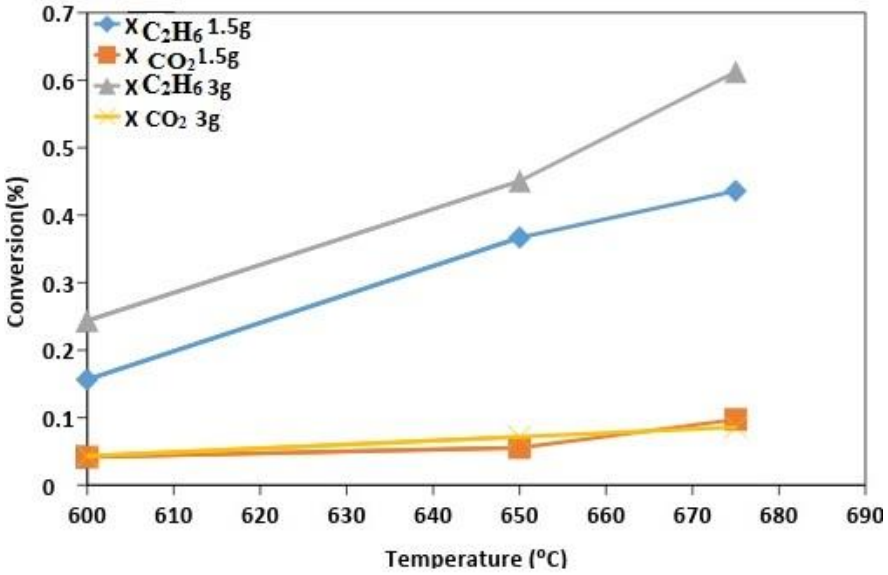

Figure.5.21. Effect of catalyst weight on C_2H_6 and CO_2 conversions

5.2.8. Summary:

The sulfate modified Cr/S.SBA-15 catalyst exhibits higher activity for the ODH with CO_2 compared to the unmodified catalyst. Sulfate modification affords higher dispersion of the Cr species. In both the catalysts, the Cr species exists in Cr^{6+} or$Cr^{5+}$and Cr^{3+} states. The addition of sulfate ion to the support SBA-15 remarkably changes the redox properties of the CrO_x species. A higher Cr^{6+}/Cr^{3+} ratio is observed in the case of Cr/S.SBA-15 catalyst.

5.3. Studies on Cr_2O_3/SBA-16 catalyst:

5.3.1. Preparation of SBA-16:

For the synthesis of SBA-16 the structure directing triblock copolymer surfactant (EO106PO70EO106,F127) was used. Tetraethylorthosilicate was selected as the silica source. Low concentration of acid and the absence of NaCl salt were the main features of the preparation. A solution with molar composition of TEOS: 0.00367 F127: 0.864 HCl: 100.231 H_2O was thoroughly stirred and the solution transferred to a Teflon vessel and kept at auto geneous pressure at 100 ℃ for a period of 24 h. After filtration, the solid was washed, dried at 80 ℃ in air, and finally calcined at 550 ℃ for 4 h at a heating rate of 3 ℃/min.

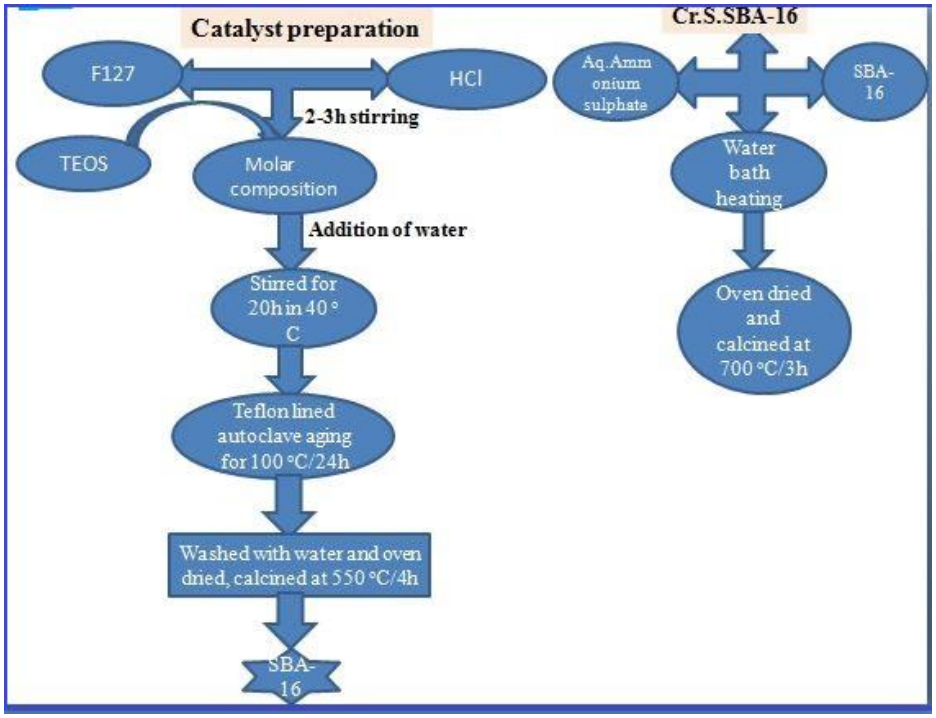

Figure.5.22.SBA16 and Cr.S.SBA16 catalyst preparation

5.3.2. Characterization of catalyst:

5.3.2. (A). X-ray diffraction:

The low angle and wide angle X-ray diffraction patterns of SBA-16,sulphated SBA-16 (denoted asS.SBA-16),Cr_2O_3/SO_4/SBA-16 (Cr/S.SBA-16) catalysts are presented in Fig.5.23.By means of a major (110) reflection and a minor (200) reflection SBA-16 showed its ordered cubic well defined structure. The structure with mesoporosity remained intact in S/SBA-16 and Cr/S.SBA-16. There was no collapse of the pore structure [13].

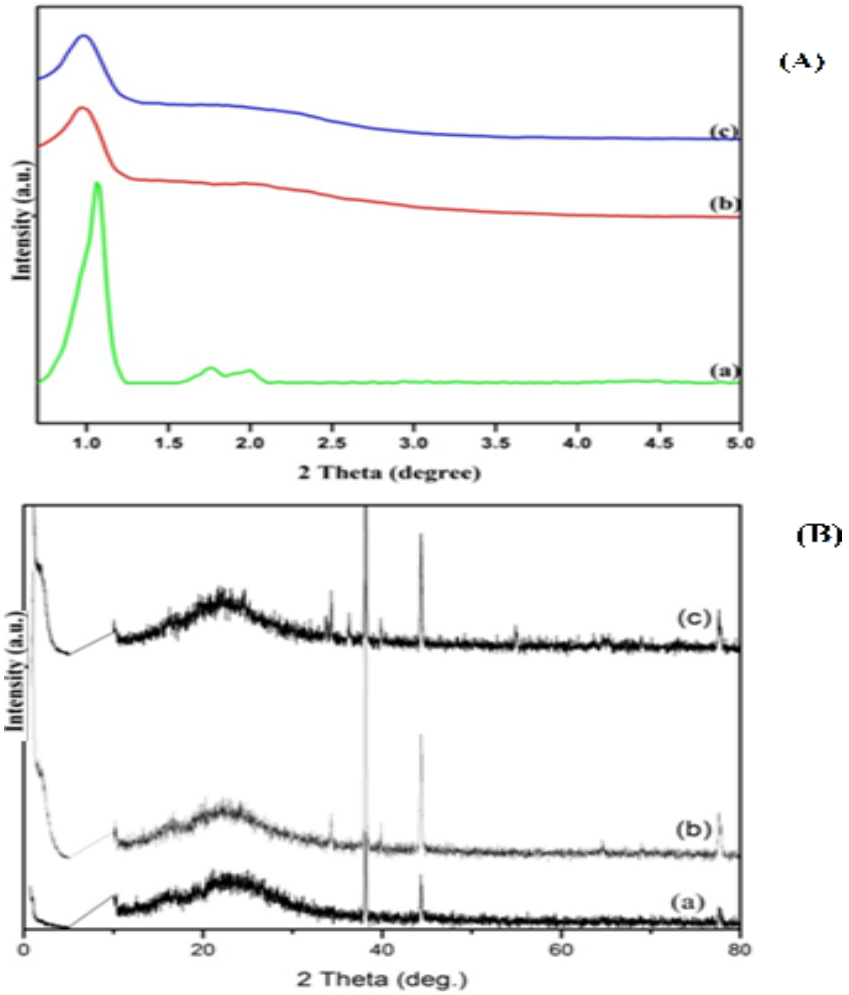

Figure.5.23.Low angle (A) and wide angle (B) XRD patterns of the catalysts (a) SBA-16 (b). S.SBA-16 (c). Cr/S.SBA-16

5.3.2. (B).Scanning Electron microscopy:

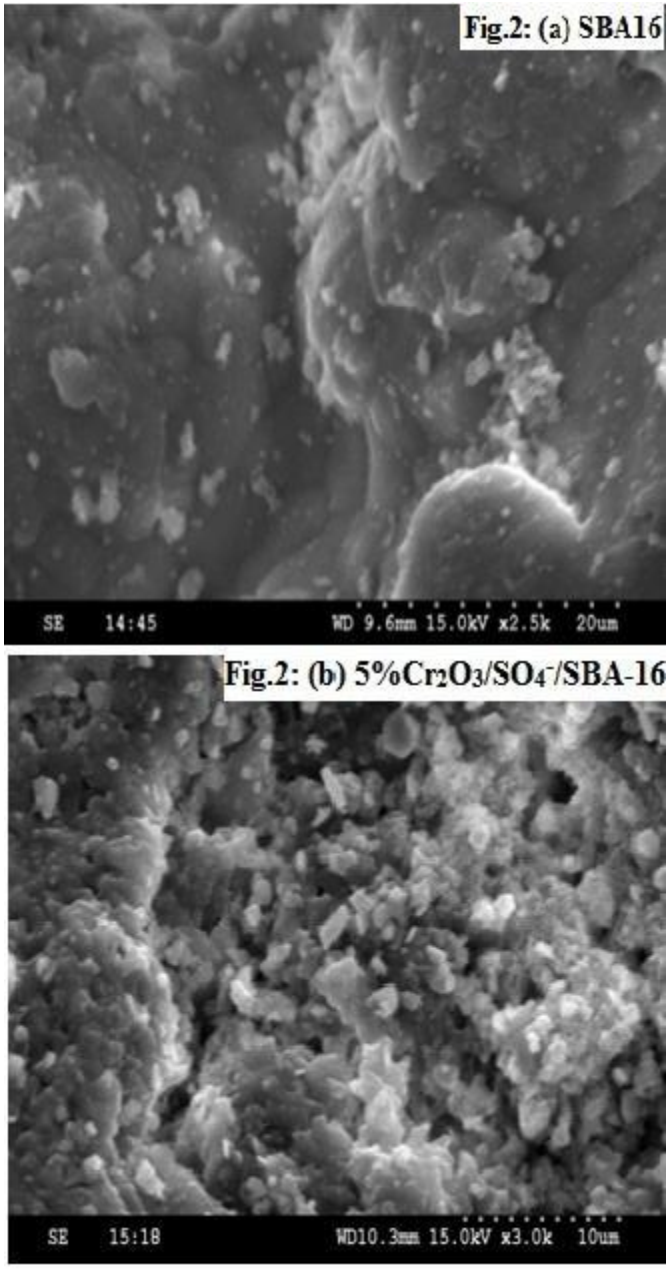

Figure.5.24. SEM images of (a). SBA-16 (b). Cr/S.SBA-16

SEM images of samples shown in Fig.5.24, evidence the presence of spherical particles in SBA-16. The particle size was smaller and well dispersed in Cr/S.SBA-16 Fig.5.24.(b). Some agglomerations resulting in the increase of the polydispersity, was also seen in Fig. 5.24(a).

5.3.2. (C).FT-IR spectra:

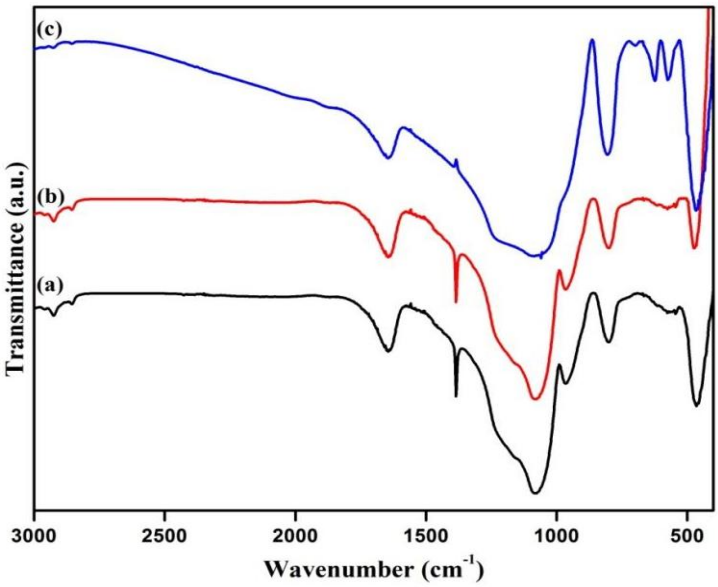

Figure.5.25. FTIR Spectra for (a) SBA-16 (b) S.SBA-16 (c) Cr/S.SBA-16

Typical bands of mesoporous silica can be seen in Fig.5.25 [14]. The bands at 2900,1055-1213, 958, 805-809, 566-575 cm^{-1} correspond to the surface silanols; Si-O-Si, Si-O and the hydrated Si-O groups [13]. In the case of Cr/S.SBA-16, the vibrations of δ (CH)-(CH_2) and δ (OH) were seen at 2938 $cm^{-1}$and at 1460 cm^{-1} and 1650-1630 cm^{-1}respectively [15].

5.3.2. (D). BET:

BET surface areas of SBA-16, S.SBA-16 and Cr/S.SBA-16 are shown in Table 5.1. SBA-16 had higher surface area than the others. Cr/S.SBA-16 catalyst showed the lowest surface area as well as pore volume.

Table.5.2: BET Surface area for SBA-16 samples

Catalyst	Surface Area (m^2/g)	Pore Diameter (nm)	Pore Volume (cm^3/g)
SBA-16	340.8	3.584	0.347
S/SBA-16	320.4	3.457	0.327
Cr/S.SBA-16	280.6	3.386	0.310

5.3.2. (E).Textural Properties Analysis:

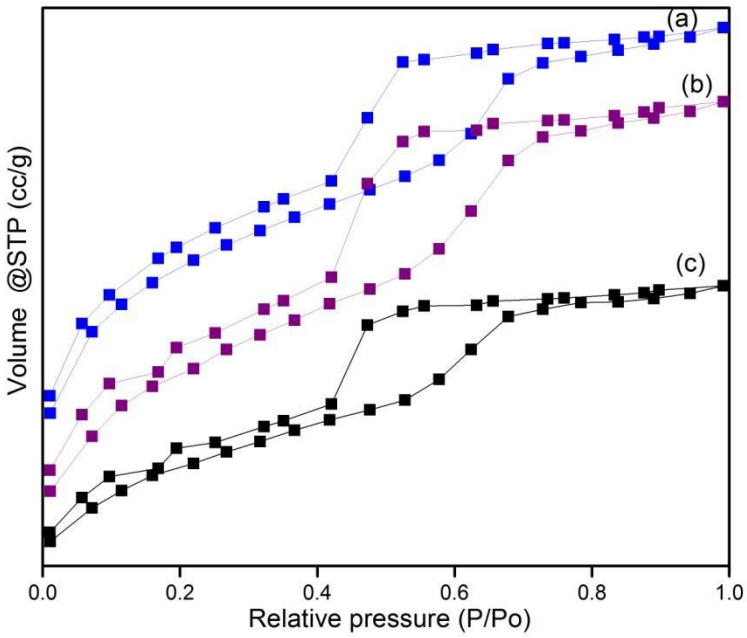

Figure.5.26.Pore volume distribution of (a) SBA-16 (b) S. SBA-16 and (c) Cr/S.SBA-16

From Table.5.1 it may be observed that the surface area and pore volume data are presented. The surface area decreased from 340 to 280 $m^2g^{-1}$with the addition of SO_4^- and Cr_2O_3. The pore volume distribution of SBA-16, as shown in Fig.5.26, was similar to that of supported SBA-16 catalyst.The differential curves are shown in Fig.5.27. Similarly to that of SBA-15, featuring type IV isotherm with uniform mesopores [16]. The pores were of inkbottle-type [17, 18]. However, the pore size distribution of S.SBA-16 was much wider, revealing destruction of pore arrangement present in parent SBA-16 material. According to literature the CrO_x species could have covered the inner walls of SBA-16 [19, 20, and 21] and increased the mesopore channels [22].

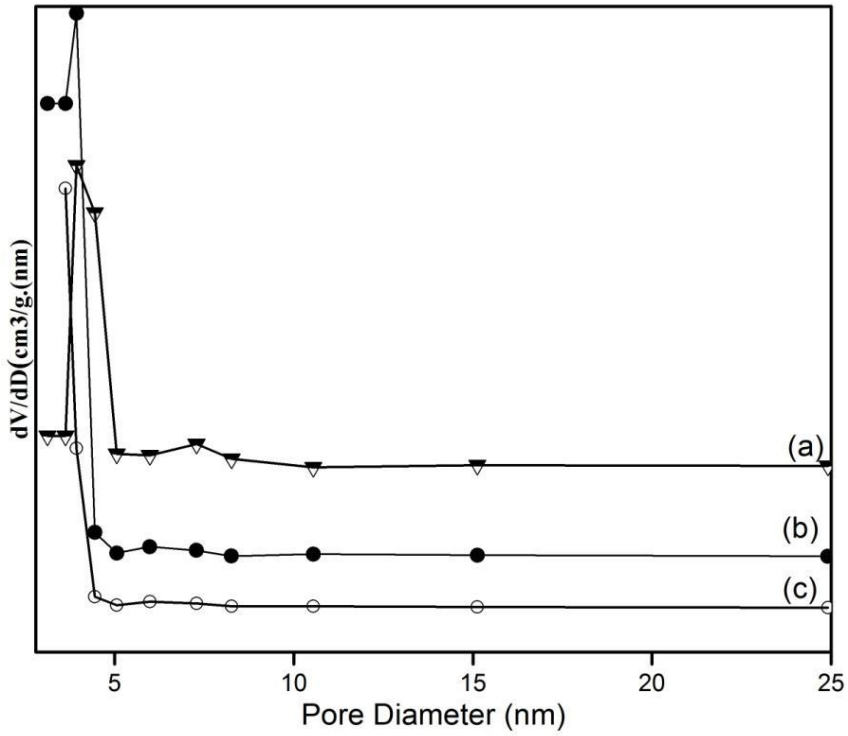

Figure.5.27.Differential pore size distribution curves of (a) SBA-16 (b) S.SBA-16 (c) Cr/S.SBA-16

5.3.2. (F).Raman Shifts:

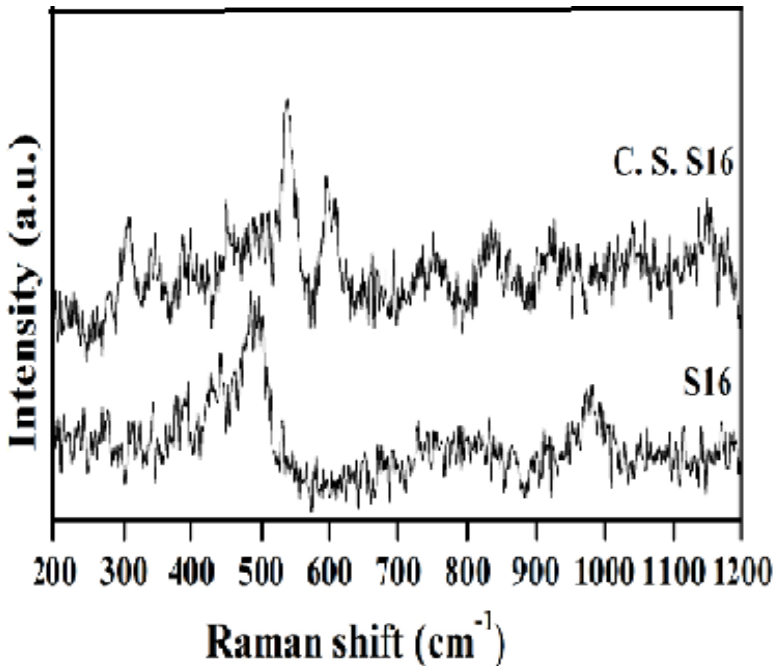

Figure.5.28. Raman shifts of SBA16, C.SO_4^{-}.SBA16

The materials were characterized by Fourier transformed Raman spectroscopy. The corresponding spectra are shown in Fig.5.28. The support exhibited siloxane bridges (950 cm^{-1}) and surface silanol groups (980 cm^{-1}) [23]. The band at 985 cm^{-1}represents the symmetric Cr=O stretching vibration [24], the intensity of the two broad bands increased with the chromium loading [25]. The SBA-16 possessed amorphous-like silica structure with a band at 494 cm^{-1}.

5.3.2. (H) TPR of SBA-16:

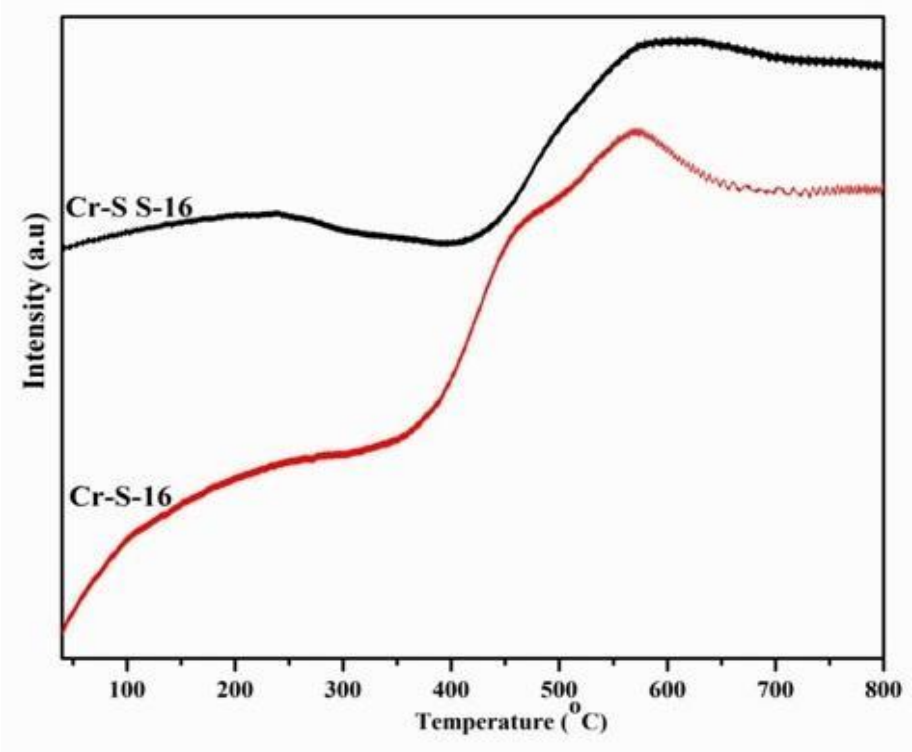

Figure.5.29. Temperature programmed reduction profiles of Cr/SBA-16 and Cr/S.SBA- 16

The TPR profiles of the catalysts are displayed in Fig.5.29. H_2-TPR analysis of CrO_x normally exhibits several discrepancies [26].Broad reduction peaks centered at 610 and 490℃ were detected. The weak peak at 280 ℃ for the Cr/S.SBA-16 sample is due to the reduction of Cr^{6+} to Cr^{3+} as well as the removal of a small amount of oxygen and species. The ones above 600 ℃ are due to Cr^{3+} to Cr^{2+} reduction [27]. Sulfate modification has shifted to reduction maxima to higher temperatures. The higher reduction temperature in Cr/S.SBA-16 in comparison with that of

Cr/SBA-16 suggests stronger interaction and thereby better dispersion of CrO_x species in the former [28].

5.3.3. Catalytic Activity:

The activity data on Cr/SBA-16 and Cr/S.SBA-16 are shown in Table.7 (ANNEXURE). From Fig.5.30,it can be noticed that SBA-16 catalyst did not show any activity. Acidic sites, in good number, were created after the addition of sulphate ion in SBA-16. The catalyst showed increased conversion of ethane. With the addition of 5 % $Cr_2O_3$to 6%SO_4^-/SBA-16 the catalyst showed remarkably enhanced activity (62% ethane, 10% CO_2 conversions with 71% ethylene selectivity).

ODH of ethane with CO_2 yielded higher ethylene selectivity. The behaviour of the catalyst can be explained based on the characterization results. The conversion of ethane was significantly enhanced with the increasing of reaction temperature.

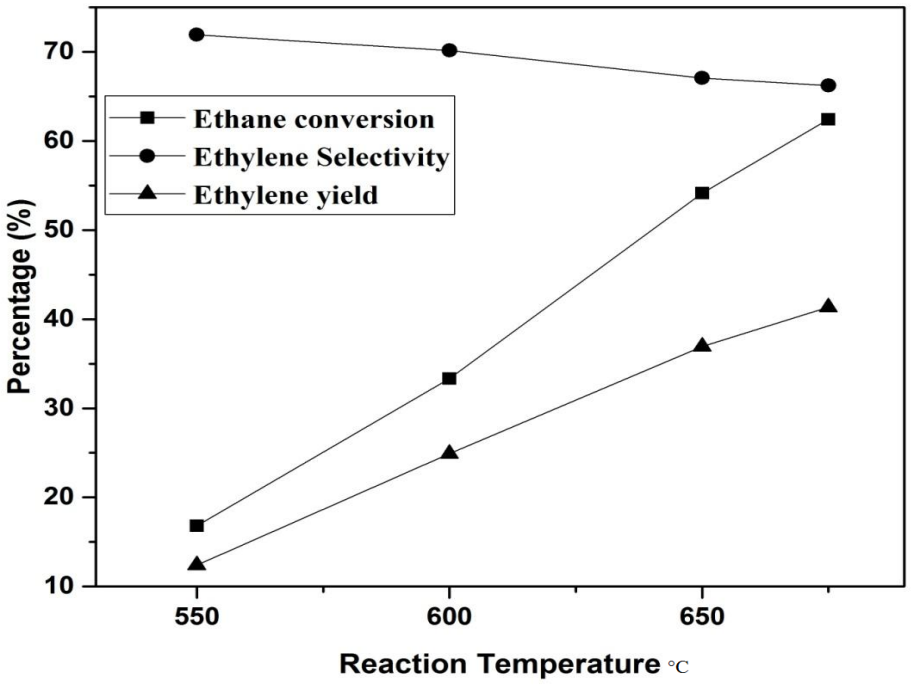

Figure.5.30. Conversion (X), Selectivity (S), Yield (Y) for C/S.SBA-16 catalyst.

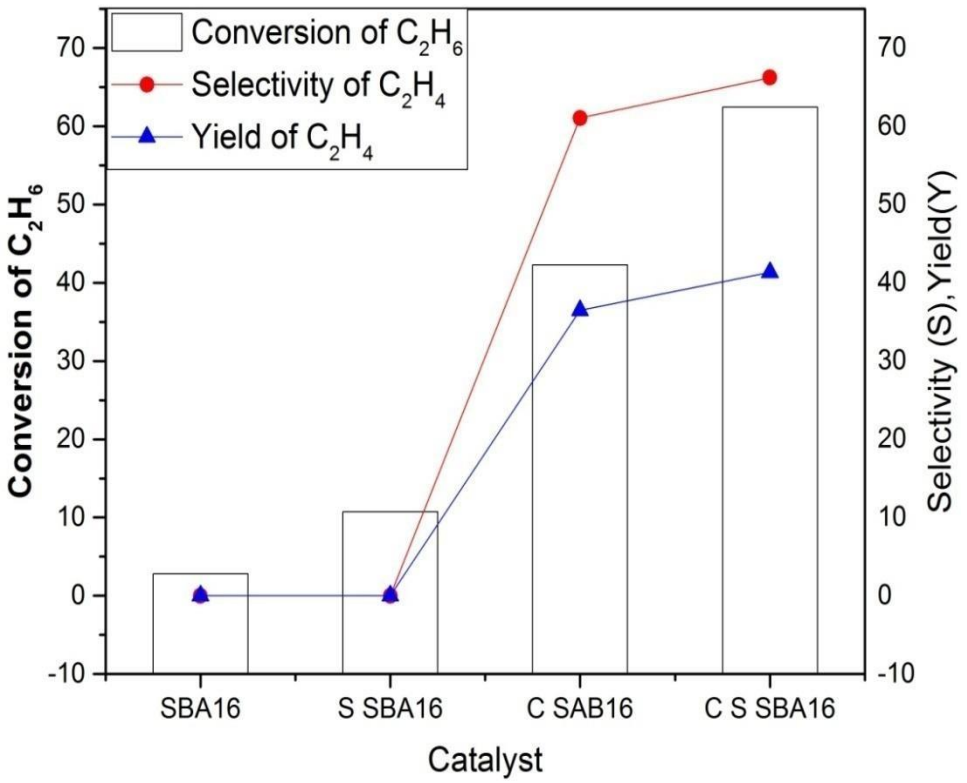

Figure.5.31.Conversion (X), Selectivity (S), Yield (Y) for SBA16 supported catalyst

A comparison of the activities of all the catalysts and supports is shown in Fig.5.31.Compared to the bare SBA-16 the ODH performance of CrO_x containing catalysts were high with higher conversion of ethane and ethylene selectivity and yield. Cr/S.SBA-16 showed the highest conversion (62.44 %) and selectivity (66.23 %) in the series, with ethylene yield reaching 41.35 %.The same for Cr/SBA-15 were 42.28, 76.98 and 36.5 %, respectively. Thus, sulfate modification has a distinct influence of the performance of the catalysts. Better dispersion of Cr species on the sulfated sample might have increased ethane activity by facilitating more number of active sites, as also reported by Wang et al [29].

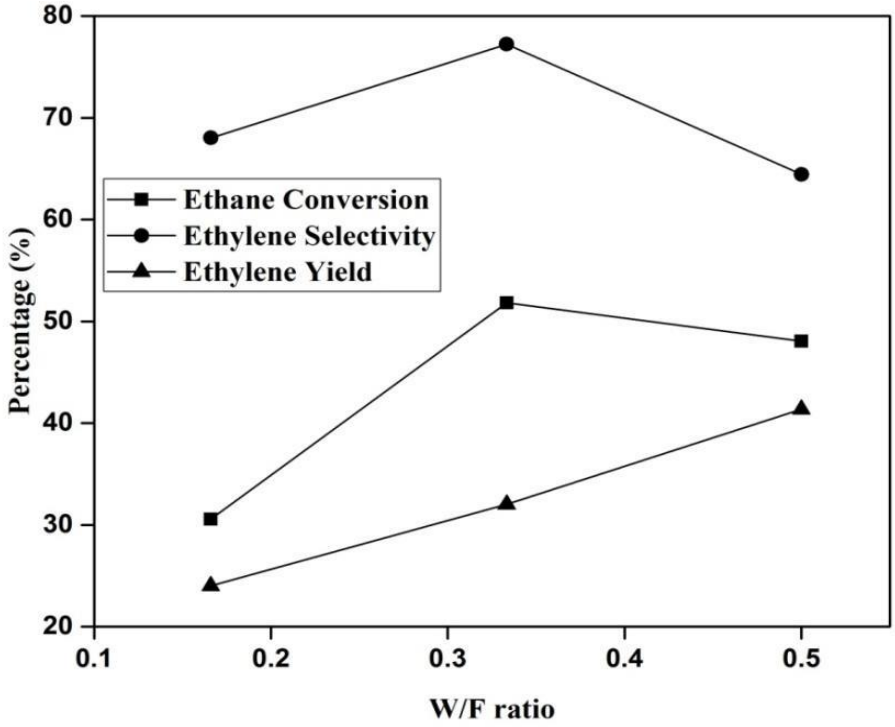

Figure.5.32.Catalytic performance of Cr/S.SBA-16 at different W/F ratios

The effect of space velocity on the ODH of ethane to ethylene activity of Cr/S.SBA-16was studied at 675 ℃ temperature and the results are disclosed in Fig.5.32. Upon increasing the W/F ratio the yield of ethylene increased because of decrease in conversion. However, the selectivity towards ethylene reached its maximum at a W/F of 0.33.

5.3.4. Summary:

The SBA-16 supported catalyst used for this study showed best catalytic activity among the SBA-16 and sulphated on SBA-16 giving 62% ethane conversion, 10% CO_2 conversions with 66% ethylene selectivity. From the FT-IR results it can be concluded that the chromium oxide was clearly incorporated on SBA-16. The superior activity of Cr/S.SBA-16 catalyst was due to high dispersion.

5.3.5. Comparison of activity of silica supported chromia catalysts.

As shown in Fig.5.33. Cr/S.SBA-15showed similar ethane conversion as that of silica gel supported catalyst (60 %) but its ethylene selectivity (83 %) was the highest in the series. The overall yield of ethylene was also the highest on this catalyst. The sulfate modification had a distinct influence of the performance of the catalysts. The dispersion of Cr species on the sulfated

sample might have increased ethane conversion by facilitating more number of active sites, also reported by Wang et al [26].

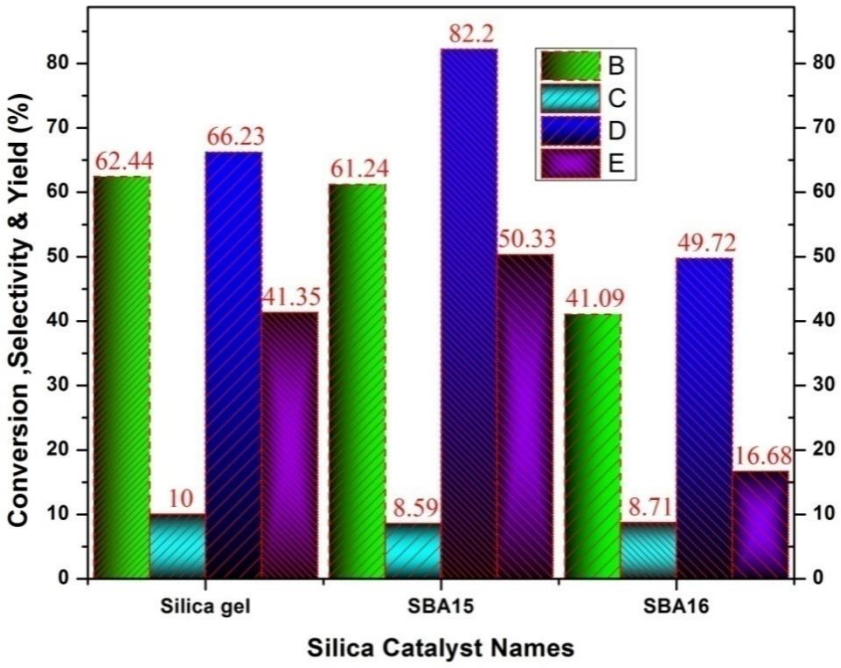

Figure.5.33. comparision of Silica catalysts (silica gel,SBA15,SBA16)

5.3.6. Comparision of Best Catalyst from Non Silica and Silica supported catalysts:

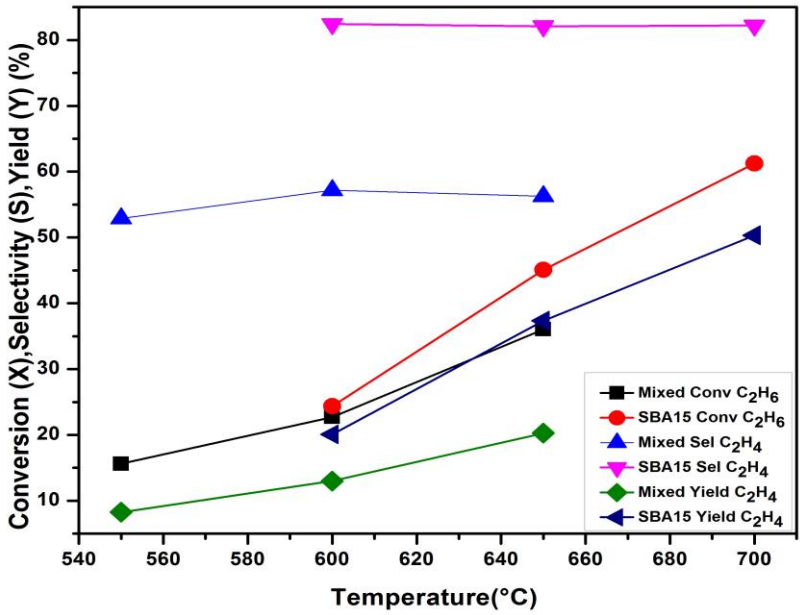

Figure.5.34. Temperature effect for best catalysts from Non Silica & Silica supported catalysts

Fig.5.34, illustrates the difference in the performance of the best catalysts selected from the studied non silica and silica supported catalysts. Sulfated SBA-15 supported Cr_2O_3 showed best performance when compared to other catalysts. The maximum conversion of 60% and selectivity of 83% were observed for chromium sulfated SBA-15, which are considered to be the maximum values among the all other catalysts studied.

REFERENCES:

1.Kresge, C. T., Leonowicz, M. E., Roth, W. J., Vartuli, J. C., & Beck, J. S. (1992). Ordered mesoporous molecular sieves synthesized by a liquid-crystal template mechanism. nature, 359(6397), 710.

2. Zhao, D., Feng, J., Huo, Q., Melosh, N., Fredrickson, G. H., Chmelka, B. F., & Stucky, G. D. (1998). Triblock copolymer syntheses of mesoporous silica with periodic 50 to 300 angstrom pores. science, 279(5350), 548-552.

3. Stevens, W. J., Lebeau, K., Mertens, M., Van Tendeloo, G., Cool, P., & Vansant, E. F. (2006). Investigation of the morphology of the mesoporous SBA-16 and SBA-15 materials. The Journal of Physical Chemistry B, 110(18), 9183-9187.

4.Van Der Voort, P., Benjelloun, M., & Vansant, E. F. (2002). Rationalization of the synthesis of SBA-16: Controlling the micro-and mesoporosity. The Journal of Physical Chemistry B, 106(35), 9027-9032.

5. Grudzien, R. M., Grabicka, B. E., & Jaroniec, M. (2006). Effective method for removal of polymeric template from SBA-16 silica combining extraction and temperature-controlled calcination. Journal of Materials Chemistry, *16*(9), 819-823.

6 Du, G., Lim, S., Yang, Y., Wang, C., Pfefferle, L., & Haller, G. L. (2006). Catalytic performance of vanadium incorporated MCM-41 catalysts for the partial oxidation of methane to formaldehyde. Applied Catalysis A: General, 302 (1), 48-61.

7. Čapek, L., Bulánek, R., Adam, J., Smoláková, L., Sheng-Yang, H., & Čičmanec, P. (2009). Oxidative dehydrogenation of ethane over vanadium-based hexagonal mesoporous silica catalysts. Catalysis Today, *141*(3-4), 282-287.

8. Lin, C., Tao, K., Yu, H., Hua, D., & Zhou, S. (2014). Enhanced catalytic performance of molybdenum-doped mesoporous SBA-15 for metathesis of 1-butene and ethene to propene. Catalysis Science & Technology, *4*(11), 4010-4019.

9. Lin, S., Shi, L., Yu, T., Li, X., Yi, X., & Zheng, A. (2015). Plug precursor assisted synthesis: A highly efficient method of tuning the acidic and structural properties of Al-SBA-15. Microporous and Mesoporous Materials, 207, 111-119.
10. Ying, F., Li, J., Huang, C., Weng, W., & Wan, H. (2007). Direct synthesis and superior catalytic performance of V-containing SBA-15 mesoporous materials for oxidative dehydrogenation of propane. Catalysis letters, *115*(3-4), 137-142.
11. Liu, J., Yu, L., Zhao, Z., Chen, Y., Zhu, P., Wang, C.,& Jiang, G. (2012). Potassium-modified molybdenum-containing SBA-15 catalysts for highly efficient production of acetaldehyde and ethylene by the selective oxidation of ethane. Journal of catalysis, 285(1), 134-144.
12. Grudzien, R. M., Grabicka, B. E., & Jaroniec, M. (2006). Effective method for removal of polymeric template from SBA-16 silica combining extraction and temperature-controlled calcination. Journal of Materials Chemistry, 16(9), 819-823.
13. Mureseanu, M., Reiss, A., Cioatera, N., Trandafir, I., & Hulea, V. (2010). Mesoporous silica functionalized with 1-furoyl thiourea urea for Hg (II) adsorption from aqueous media. Journal of hazardous materials, 182(1-3), 197-203.
14. Doadrio, J. C., Sousa, E. M., Izquierdo-Barba, I., Doadrio, A. L., Perez-Pariente, J., & Vallet-Reg ί M. (2006). Functionalization of mesoporous materials with long alkyl chains as a strategy for controlling drug delivery pattern. Journal of Materials Chemistry, *16*(5), 462-466.
15. Andrade, G. F., Soares, D. C. F., dos Santos, R. G., & Sousa, E. M. B. (2013). Mesoporous silica SBA-16 nanoparticles: synthesis, physicochemical characterization, release profile, and in vitro cytocompatibility studies. Microporous and Mesoporous Materials, *168*, 102-110.
16. Li, B., Yan, R., Wang, L., Diao, Y., Li, Z., & Zhang, S. (2014). SBA-15 supported cesium catalyst for methyl methacrylate synthesis via condensation of methyl propionate with formaldehyde. Industrial & Engineering Chemistry Research, 53(4), 1386-1394.
17. Han, Y. J., Watson, J. T., Stucky, G. D., & Butler, A. (2002). Catalytic activity of mesoporous silicate-immobilized chloroperoxidase. Journal of Molecular Catalysis B: Enzymatic, 17(1), 1-8.
18. Aburto, J., Ayala, M., Bustos-Jaimes, I., Montiel, C., Terr és, E., Dom ńguez, J. M., & Torres, E. (2005). Stability and catalytic properties of chloroperoxidase immobilized on SBA-16 mesoporous materials. Microporous and Mesoporous Materials, *83*(1-3), 193-200.

19. Hess, C., Hoefelmeyer, J. D., & Tilley, T. D. (2004). Spectroscopic characterization of highly dispersed vanadia supported on SBA-15. The Journal of Physical Chemistry *B*, *108*(28), 9703-9709.
20. Du, G., Lim, S., Pinault, M., Wang, C., Fang, F., Pfefferle, L., & Haller, G. L. (2008). Synthesis, characterization, and catalytic performance of highly dispersed vanadium grafted SBA-15 catalyst. Journal of Catalysis, 253(1), 74-90.
21. Schmidt, R., Hansen, E. W., Stoecker, M., Akporiaye, D., & Ellestad, O. H. (1995). Pore size determination of MCM-51 mesoporous materials by means of 1H NMR spectroscopy, N2 adsorption, and HREM. A Preliminary Study. Journal of the American Chemical Society, 117(14), 4049-4056.
22. Wang, L., Kong, A., Chen, B., Ding, H., Shan, Y., & He, M. (2005). Direct synthesis, characterization of Cu-SBA-15 and its high catalytic activity in hydroxylation of phenol by H_2O_2. Journal of Molecular Catalysis A: Chemical, 230(1-2), 143-150..
23. Das, N., Eckert, H., Hu, H., Wachs, I. E., Walzer, J. F., & Feher, F. J. (1993). Bonding states of surface vanadium (V) oxide phases on silica: structural characterization by vanadium-51 NMR and Raman spectroscopy. The Journal of Physical Chemistry, *97*(31), 8240-8243.
24. Went, G. T., Oyama, S. T., & Bell, A. T. (1990). Laser Raman spectroscopy of supported vanadium oxide catalysts. Journal of physical chemistry, 94(10), 4240-4246.
25. Du, G., Lim, S., Pinault, M., Wang, C., Fang, F., Pfefferle, L., & Haller, G. L. (2008). Synthesis, characterization, and catalytic performance of highly dispersed vanadium grafted SBA-15 catalyst. Journal of Catalysis, 253(1), 74-90.
26. Zhang, L., Zhao, Y., Dai, H., He, H., & Au, C. T. (2008). A comparative investigation on the properties of Cr-SBA-15 and CrO_x/SBA-15. Catalysis Today, 131(1-4), 42-54.
27. Zhu, Y., Sun, Y., Niu, X., Yuan, F., & Fu, H. (2010). Preparation of La-Mn-O perovskite catalyst by microwave irradiation method and its application to methane combustion. Catalysis letters, 135(1-2), 152-158.
28. Abbas, M. N. (2011). Modeling of porosity equation for water flow through packed bed Of monosize spherical packing. Journal of Engineering and Sustainable Development, 15(4), 205-226.
29. Wang S, Murata K, (1999),Oxidative dehydrogenation of ethane by carbon dioxide oversulfate-modified Cr_2O_3/SiO_2 catalysts. Catal Lett 63:59–64.

CHAPTER -6

KINETIC MODELING

6.0. KINETIC MODELING:

Oxidative dehydrogenation of ethane is thermodynamically favorable and it could be the one of the best alternative for production of ethylene in coming years. But as the reaction is very slow, it requires high performance and highly active catalysts to obtain the products. Supported chromium catalysts are highly active for ODH of ethane and are found to offer superior ethane and CO_2 conversions. The nature of chromium species formed and their distribution on the support surface play important role in the activity and selectivity of the catalyst. Number of authors has reported experimental and theoretical studies on ODH over a variety of catalysts but concerning detailed kinetics are relatively scarce and the mechanism of this reaction is far from being well understood.

6.1.0. Selection of the catalysts for detailed analysis:

It was established from the previous chapter that mixed oxide supports combine good textural and mechanical properties as they establish different types of interaction with the active component. The activity of the catalysts during ODH of ethane with CO_2 depended on the chromium loading. Catalyst with 15 wt% chromium loading was found to be optimum to obtain reasonable ethane and carbon dioxide conversions when compared to the other metal oxide supported chromium catalysts studied. Equal composition of metal oxides with 15 wt% chromium loading i.e Cr_2O_3/Al_2O_3-ZrO_2 (1:1) catalyst showed the best catalytic activity among all the catalysts tested in this study. The selectivity of ethylene mainly depended on the oxidizing atmosphere, which was clearly explained by the C_2H_4 temperature programmed desorption.

The performance of mixed oxide i.e Cr_2O_3/Al_2O_3-ZrO_2 (1:1) catalyst was evaluated at ambient pressure in a fixed bed down flow reactor by varying the temperature (550 – 650 ˚C), total flow rate, Catalyst weight as explained in 60 mL/min. The experimental data i.e ethane and carbon dioxide conversion, yield and selectivity values at different conditions were evaluated under steady state conditions.

Subsequently, the study was extended to identify mass and heat transfer effects to check whether the reaction was diffusion or reaction controlled and also whether the catalyst inside the reactor was operating in isothermal or non-isothermal conditions. After establishing the influences of mass and heat transfer, kinetic studies were carried out to know the order of the reaction and activation energy. Power law and other kinetic models namely, EleyRideal, LHHW and Mars van Krevelen models were checked for statistical and thermodynamic

consistency. Kinetics was developed using lab-scale catalytic experiments whereas reactor key transport parameters characterizing hydrodynamics, dispersive, conductive and interfacial heat as well as mass transport before phenomena were obtained from a previous study in the absence of chemical reaction. The results are reported in the following paragraphs.

6.1.1. Estimation of mass transfer effects in mixed oxide supported Cr_2O_3 catalysts.

Before evaluating the kinetic parameters for the ODH process it is required to estimate the heat and mass transfer effects in the catalyst during the reaction process to identify the reaction mechanism.

Considering the reactant gas and the catalyst pore size, Knudsen diffusion was considered for the analysis. The corresponding parameters are shown in Table 6.1.

Table 6.1: Parameters and their values for evaluating Knudsen diffusion

Parameters	Values
Temperature T, (K)	823,873,923
Pressure P,(Pa)	$1.013*10^{5}$
Diameter of gas molecule d_g (m)	$0.8384*10^{-9}$
Diameter of pore, d_p (m)	$6.9*10^{-9}$

6.1.1. (A). Diffusion effects on the heterogeneous reaction:

In heterogeneous catalytic reactions the diffusion of reactant gases from the bulk phase to surface of catalyst (i.e external diffusion) and from catalyst surface to the pores of catalyst (i.e internal diffusion) plays a vital role in determining the rate of reaction. These components of diffusion act as resistances affecting the rate of reaction. In the estimation of kinetics it is necessary to establish their influence. The procedure to establish their influence is described below.

Shell mass balance on catalyst Pellet:

Radius of spherical catalyst pellet = R_s

Spherical shell volume of thickness = ΔR

Mass balance at steady state over catalyst will be:

(Rate of diffusion of reactant into element) – (Rate of diffusion of reactant out of element) = Rate of disappearance of reactant within element due to reaction

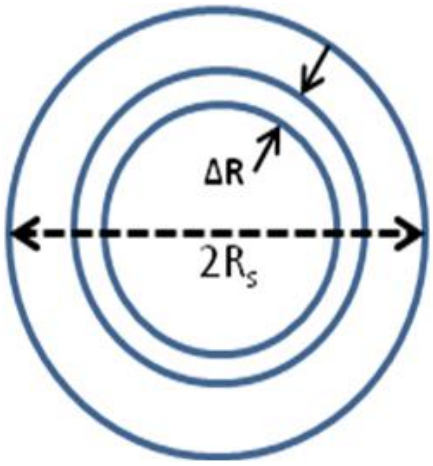

Figure.6.1.Catalyst Particle

Reaction Rate (per unit mass of catalyst) = k_1C

Reaction rate (per unit volume of catalyst) = $k_1C\rho_p$.

Where ρ_p is the density of pellet

$$[4\pi R^2 N_A]_r - [4\pi R^2 N_A]_{r+\Delta r} + \left[-r_A'\rho_c 4\pi R^2 \Delta r\right] = 0 \quad (6.1)$$

$$\frac{d(N_A r^2)}{dr} - r_A'\rho_c r^2 = 0 \quad (6.2)$$

The molar flux (N_A) of A by molecular diffusion is given by

$$N_A = -D_e \frac{dC_A}{dr} \quad (6.3)$$

Where D_e is effective diffusivity given by

$$D_e = \frac{D_{AB}\,\phi\,\sigma}{\tau} \quad (6.4)$$

The diffusivity of binary gas mixture is given by wilke lee equation [32] shown below

$$D_{AB} = \frac{10^{-4}(1.084 - 0.249\sqrt{\frac{1}{M_A}+\frac{1}{M_B}})T^{1.5}\sqrt{\frac{1}{M_A}+\frac{1}{M_B}}}{P_t(r_{AB})^2 f(\frac{kT}{\varepsilon_{AB}})} \quad (6.5)$$

Where

M_A, M_B = Molecular weight of gases

P_t = Total pressure

T = Temperature of gas mixture

r_{AB} = the collision diameter=$(r_A+r_B)/2$

$f(kT/\varepsilon_{AB})$ = the collision function

ε_{AB}= energy of molecular attraction=$\sqrt{\varepsilon_A \varepsilon_B}$

D_{AB} = bulk or Knudsen diffusivity of A in B

ϕ = pellet porosity and

σ = constriction factor.

The constriction factor σ accounts for the variation in the cross-sectional area that is normal to diffusion $\sigma = \frac{Maximum\ pore\ area}{Minimum\ pore\ area}$

The concentration profiles of various components when the Knudsen diffusion is significant are given by the following equation 6.6 [1].

Substitute equation 6.3 in 6.1

$$\frac{d^2}{dR^2} C_i + \frac{2}{R}\frac{d}{dR} C_i = \frac{\rho_{cat}}{D_{K,C_i}} r_i \qquad (6.6)$$

Boundary conditions:

At the Catalyst pellet center $\frac{dC}{dR} = 0 \quad \text{at } R = 0$ (6.7)

At outer surface $C = C_s \qquad R = R_s$ (6.8)

Where

C_i=Concentration of component i in gas mixture,

R = radius of the particle,

$D_{K,Ci}$ = Knudsen diffusivity of component i,

ρ_{cat}= density of catalyst,

r_i= rate of reaction of component i

The Knudsen diffusivity of component gas is found by Eq. 6.3

$$D_{K,i} = \frac{\varepsilon}{\tau}\frac{d_p}{3}\sqrt{\frac{8RT}{\pi m_i}} \quad (6.9)$$

Where ε = voidage of bed,

τ = Tortuosity of bed,

d_p= Diameter of catalyst particle,

T = Temperature

M_i = molar mass of component i.

The concentration profiles of components remain constant as Knudsen diffusion does not affect the intrinsic reaction rate.Concentration inside the reactor can be found by solving equation 6.6

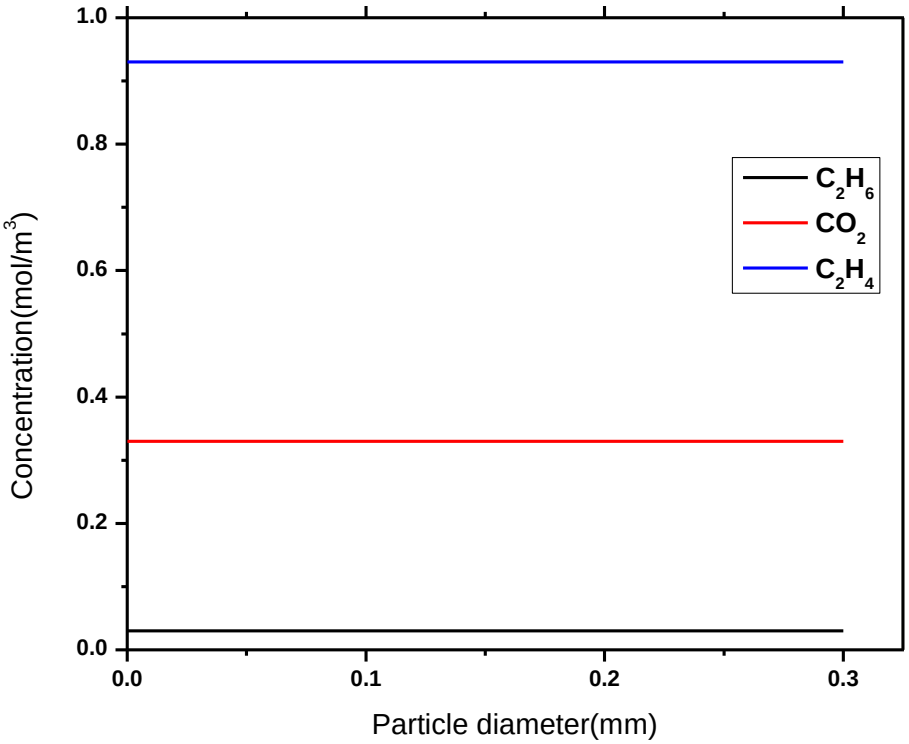

Figure .6.2. Concentration profile inside the catalyst

The concentration profiles of the gaseous components inside the catalyst particle can be determined by solving the equation 6.6 at boundary conditions. From the Fig 6.2 it can be seen that the concentrations of gases i.e ethane, carbon dioxide and ethylene are remains unchanged inside the radius of the catalyst. From the results it is concluded that the concentrations are same at both ends of the catalyst. It can be inferred from the graph that the reaction is not

diffusion controlled it is surface controlled. The same mechanism can be explained by determining the Weisz Prater criterion and Mears Criterion as discussed below.

A. Internal diffusion:

The effectiveness factor η is nearly equal to 1 when internal diffusion in the catalyst is negligible.

Weisz Prater criterion [2], stated in Equation 6.3 is used to check whether the reaction is diffusion limited.

$$C_{wp} = \frac{-r_A' \rho_c R^2}{D_e C_{As}} < 1 \qquad (6.10)$$

C_{wp} =Actual reaction rate/Actual diffusion rate

r_A' = Rate of reaction observed

ρ_c= Catalyst pellet density

R = Radius of the catalyst particle

D_e= Effective diffusivity of the particle

C_{As}= Concentration of A at the surface

$D_{A,i}$ = Diffusivity of A in the gas mixture into catalyst

The Internal diffusion equation is negligible when C_{wp} is <<1 and vice versa.

The values used in the above equation are given in Table 5.2 below.

Parameters	Values
r_A'(obs)	0.000872779(mol/g $_{cat}$.hr)
ρ_c	200 (Kg/m^3)
R	225 (μm)
D_e	2.33*10^{-5}(m^2/s)
C_{As}	3.303*10^{-3} (mol/lit)
Φ	0.13
T	2.02

Table.6.2. Parameters and their values for evaluating the Weisz-Prater criterion

Upon substitution of the above in Eq. 6.3, the value of C_{wp} was obtained as 0.0001 and from this it was inferred that the internal diffusion resistance was negligible in the above reaction.

B. External Diffusion:

Under steady state conditions the external diffusion of the reactants into the heterogeneous catalyst from bulk of fluid is equal to the rate at which reactants are consumed both within the catalyst and on the surface. Mears Criterion [2], as shown in Equation 5.4, was used to check whether the reaction was limited by external diffusion. The parameters and their values for evaluating the Mears criterion are given in Table 6.3.

$$C_m = \frac{-r_A' \rho_b R n}{K_C C_{Ab}} < 0.15 \qquad (6.11)$$

Where

- r_A = Rate of reaction per unit weight of catalyst

ρ_b = Catalyst bulk density ($\rho_b = (1-\phi)\,\rho_c$)

ϕ = Porosity of the bed,

ϕ = Volume of solid/Volume of catalyst bed

R= Radius of catalyst particle

n = Reaction order

K_c= Mass transfer coefficient

C_{Ab}= Bulk fluid Concentration of A

d = diameter of catalyst particle

Parameters	Values
r_A'	0.000872779(mol/g cat.hr)
ρ_c	200 (Kg/m^3)
R	225 (μm)
N	1
Φ	0.13
C_{Ab}	3.303*10^{-3} (mol/lit)
K_c	0.109 (m^3/m^2.s)

Table.6.3. Parameters and their values for evaluating Mears criterion

The value of C_m estimated was equal to 2.25*10^{-4}. As the value was < 0.15, the external diffusion resistance of the gases into the catalyst was considered negligible.

6.1.2. Heat transfer effects in the catalyst:

The following table (Table 6.4) gives the parameters used in establishing the isothermality prevailing in the reactor.

Temperature (°C)	**λ_f (KW/m.K)**	**λ_s (W/m.K)**
550	212.34	
600	216.24	32.49
650	221.54	

Table.6.4. Thermal conductivity of solid and gas mixtures at different temperatures

The value of λ_{eff} was found to be equal to 39.45 W/m. K. For the catalyst pellet as a whole the temperature gradient is given by Equation 6.5.

$$\Delta T_{Particle} = \frac{D_e(C_{As} - C_{A,centre})(-\Delta H_r)}{\lambda_{eff}} \qquad (6.12)$$

The temperature at the centre of the catalyst is maximum when $C_{A,centre}$ is equal to zero. Thus, the ΔT within the particle was evaluated as $1.122*10^{-5}$. So the catalytic reaction was considered operating under isothermal condition.

6.1.3. Temperature dependency of Reaction

The activity of ethane oxidative dehydrogenation can be kinetically represented in terms of the activation energy. Temperature dependency of the reaction can be expressed by Arrhenius law as shown below

Arrhenius law: $k = k_o * e^{\left(\frac{E_a}{RT}\right)}$

The integrated form of the Arrhenius equation has been considered to evaluate the temperature dependency of the reaction rate constant. In Fig.6.3 the logarithm of the rate constant is plotted as a function of the reciprocal of absolute temperature. The activation energy of the reaction can be obtained from the slope and pre-exponential factor from the intercept.

From the plot of ln k vs 1/T the values of activation energy (E_a) and pre exponential factor can be obtained.

$$k = k_o * e^{\left(\frac{E_a}{RT}\right)}$$

$$\ln(k) = \ln(k_0) - \frac{E_a}{R * T}$$

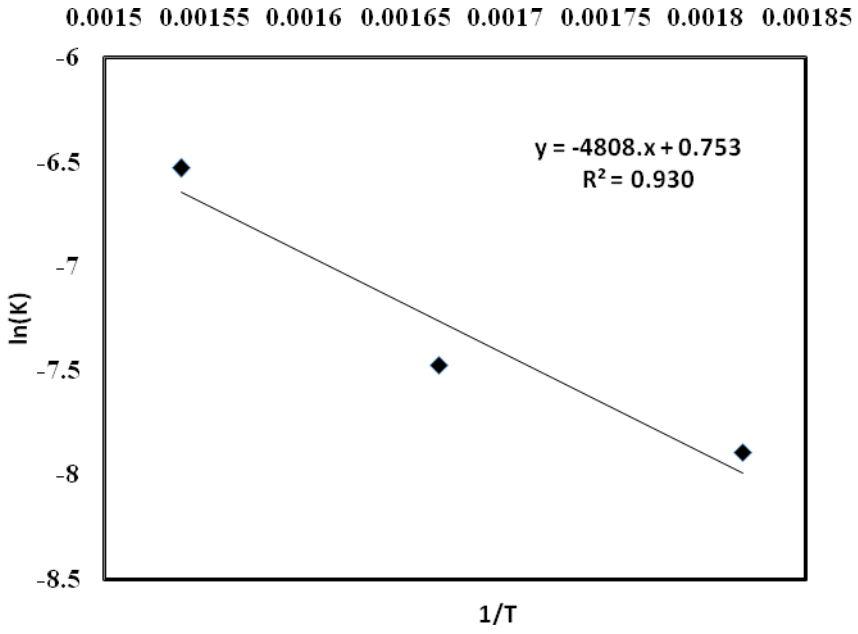

Figure .6.3. ln(Concentration) Vs ln (rate) for 15wt% Cr_2O_3 /Al_2O_3-ZrO_2(1:1) catalyst

From the above graph Pre exponential factor k_o =2.536

Activation Energy E_a = 39.141kj/mol

From the above Plot and the corresponding results it is understood the model is inadequate in fitting the experimental data.

6.2. Selection of kinetic models

To overcome the inadequacy of the above model, it is proposed to deal with different mechanism models like Eley-Rideal mechanism, Langmuir-Hinshelwood mechanism and Mars-Van Krevelen mechanisms for testing the catalytic data.

6.2.1. (A). Eley Rideal Model:

In Eley Rideal model one of the gaseous components adsorbs on the catalyst active site while the other component reacts from bulk gaseous phase. Based on the properties of catalyst surface the adsorbing component changes and the model is created. In this work ethane is assumed to be the adsorbed molecule while CO_2 reacts from the bulk gas phase.

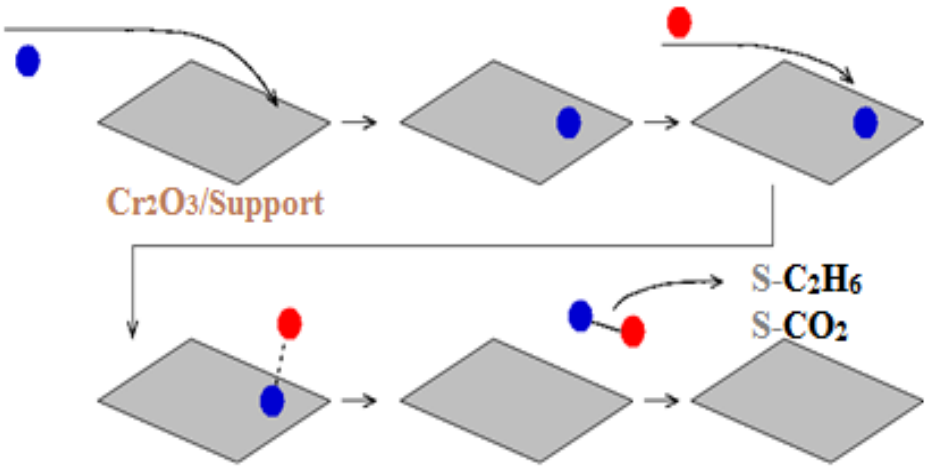

Figure.6.4. Eley Rideal mechanism

$$C_2H_6 + S \overset{K_{C_2H_6}}{\longleftrightarrow} [S - C_2H_6]$$

$$[C_2H_6 - S] + CO_2 \overset{k}{\rightarrow} C_2H_4 + CO + H_2O + S$$

$$[S - C_2H_6] = K_{C_2H_6}[C_2H_6][S]$$

$$r_{ER} = k[C_2H_6 - S]\,[CO_2]$$

$$C_T = [S] + [C_2H_6 - S]$$

$$[S] = \frac{C_T}{1 + K_{C_2H_6}[C_2H_6]}$$

$$r_{ER} = \frac{k\,K_{C_2H_6}[C_2H_6][CO_2]C_T}{1 + K_{C_2H_6}[C_2H_6]}$$

$$r_{ER} = \frac{K_{ER}K_{C_2H_6}[C_2H_6][CO_2]}{1 + K_{C_2H_6}[C_2H_6]}$$

Where C_T is the total concentration of active sites, [S] concentration of active site and parameters enclosed in square brackets is concentration of corresponding components.

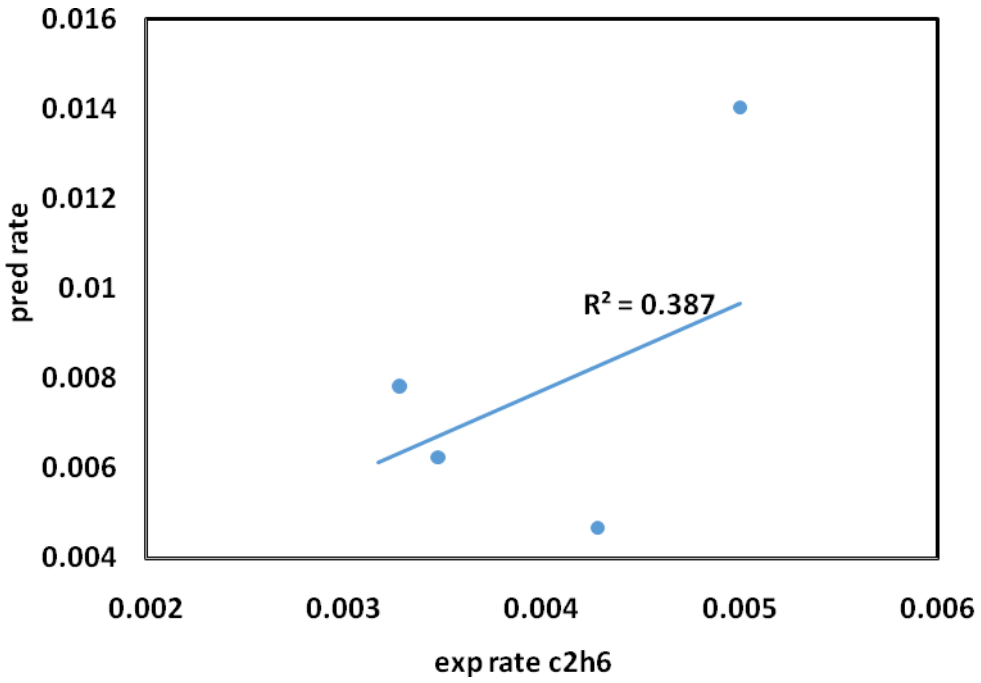

Figure.6.5. Parity plot at 650°C

From the parity plot (Fig 6.5) it can be understood that Eley Rideal mechanism is not suitable for the prediction of the experimental rates. The proposed reaction may not follow this mechanism

. 6.2.1. (B).Mars van Krevelen Mechanism:

In Mars van Krevelen mechanism the catalyst which is of metal oxide is reduced by hydrocarbon and catalyst is regenerated by O atoms from CO_2 which reoxidizes the catalyst.

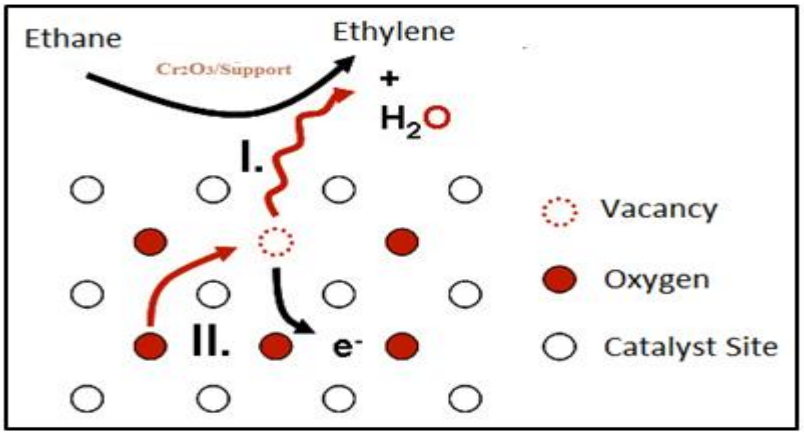

Figure.6.6. Mars van Krevelen mechanism

Based on the above phenomena the rate expression for the ODH of ethane reaction developed as follows:

$$[C_2H_6 - S] + [O - S] \overset{K_{red}}{\longleftrightarrow} C_2H_4 + H_2O + 2S$$

$$CO_2 + S \overset{K_{ox}}{\longleftrightarrow} CO + [O - S]$$

$$r_i = k_{red}\, \theta\, [C_2H_6]$$

$$r_o = k_{ox}\, (1 - \theta)[CO_2]$$

$$r_i = r_o$$

$$k_{red}\, \theta\, [C_2H_6] = k_{ox}\, (1 - \theta)[CO_2]$$

$$\theta = \frac{k_{ox}[CO_2]}{k_{red}[C_2H_6] + k_{ox}[CO_2]}$$

$$r_{MVK} = \frac{k_{red}k_{ox}[C_2H_6][CO_2]}{k_{red}[C_2H_6] + k_{ox}[CO_2]}$$

Where θ represents the fractions of active sites, components enclosed in square brackets are concentration of the species, S is the active site, K_{ox}, K_{red} are constants of oxidation and reduction steps respectively.

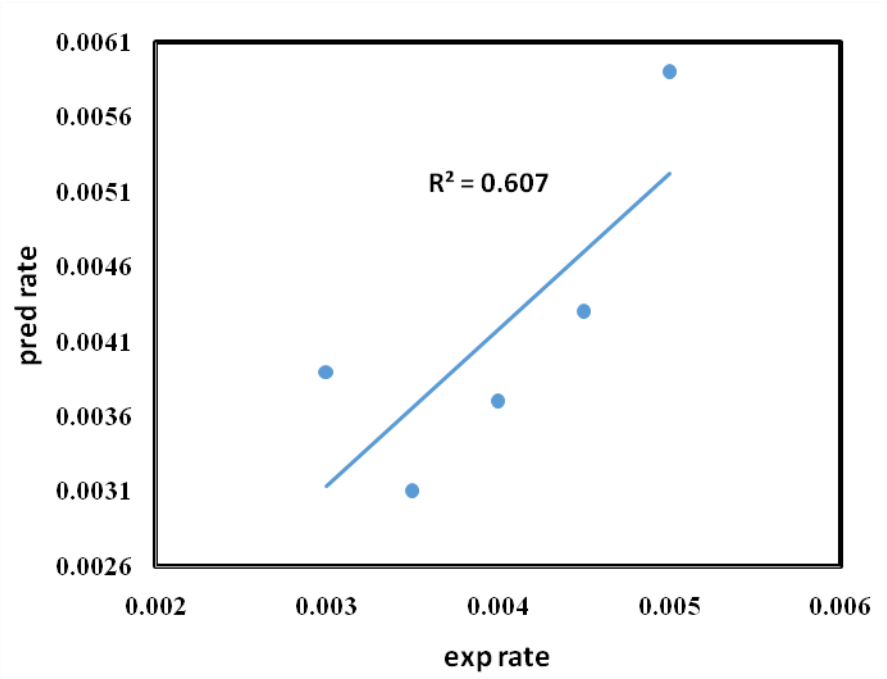

Figure.6.7. Parity Plot at 650 °C

The parity plot is drawn at 650 °C where the maximum conversion was obtained. The predicted rate from the developed rate expression eq.6.2 from MVK mechanism is not suitable to match the experimental rate.

6.2.1.(C). Langmuir Hinshelwood Hougen Watson (LHHW) model for kinetic evaluation:

The LHHW model for ODH of ethane over 15% Cr_2O_3/Al_2O_3-$ZrO_2$was formulated based on the following assumptions.

- The presence of a single type of active site over the entire catalyst surface.
- Competitive adsorption of reactants and products over the catalyst surface.
- Molecular adsorption of reactant gases.
- Surface reaction as the rate controlling mechanism.

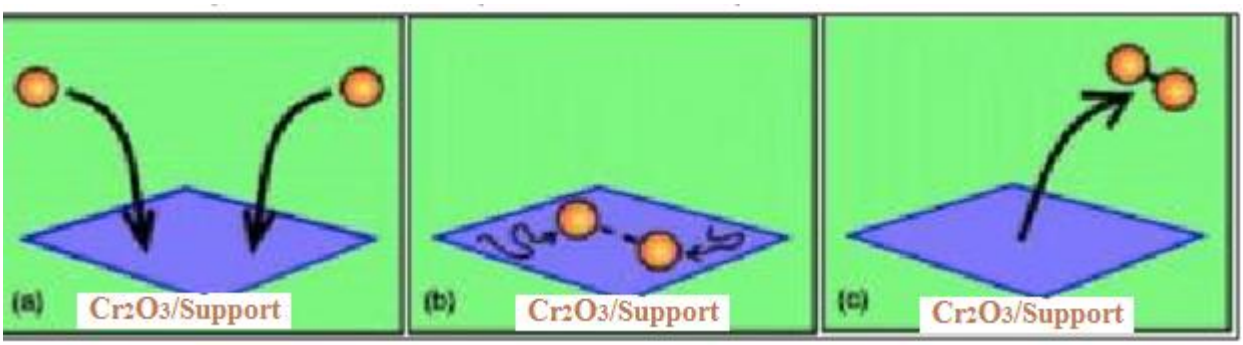

Figure.6.8. Langmuir Hinshelwood Hougen Watson (LHHW) mechanism

Based on this rate expression for rate equation developed as follows.

$$C_2H_6 + S \overset{K_{C_2H_6}}{\longleftrightarrow} [S - C_2H_6] \quad (6.13)$$

$$CO_2 + S \overset{K_{CO_2}}{\longleftrightarrow} [CO_2 - S] \quad (6.14)$$

$$[C_2H_6 - S] + [CO_2 - S] \overset{k}{\rightarrow} C_2H_4 + CO + H_2O + 2S \quad (615)$$

$$[S - C_2H_6] = K_{C_2H_6}[C_2H_6][S] \quad (6.16)$$

$$[CO_2 - S] = K_{CO_2}[CO_2][S] \quad (6.17)$$

$$C_T = [S] + [C_2H_6 - S] + [CO_2 - S] \quad (6.18)$$

$$[S] = \frac{C_T}{1 + K_{C_2H_6}[C_2H_6] + K_{CO_2}[CO_2]} \quad (6.19)$$

$$r_{LR} = k[C_2H_6 - S]\ [CO_2 - S] \tag{6.20}$$

$$= k\ K_{C_2H_6}[C_2H_6][S]K_{CO_2}[CO_2][S] \tag{6.21}$$

$$= \frac{k\ K_{C_2H_6}K_{CO_2}[C_2H_6][CO_2]C_T^2}{(1 + K_{C_2H_6}[C_2H_6] + K_{CO_2}[CO_2])^2} \tag{6.22}$$

$$r_{LR} = \frac{K_{LR}K_{C_2H_6}K_{CO_2}[C_2H_6][CO_2]}{(1+K_{C_2H_6}[C_2H_6]+K_{CO_2}[CO_2])^2} \tag{6.23}$$

Where C_T is the total concentration of active sites, [S] concentration of active site and parameters enclosed in square brackets are concentration of corresponding components.

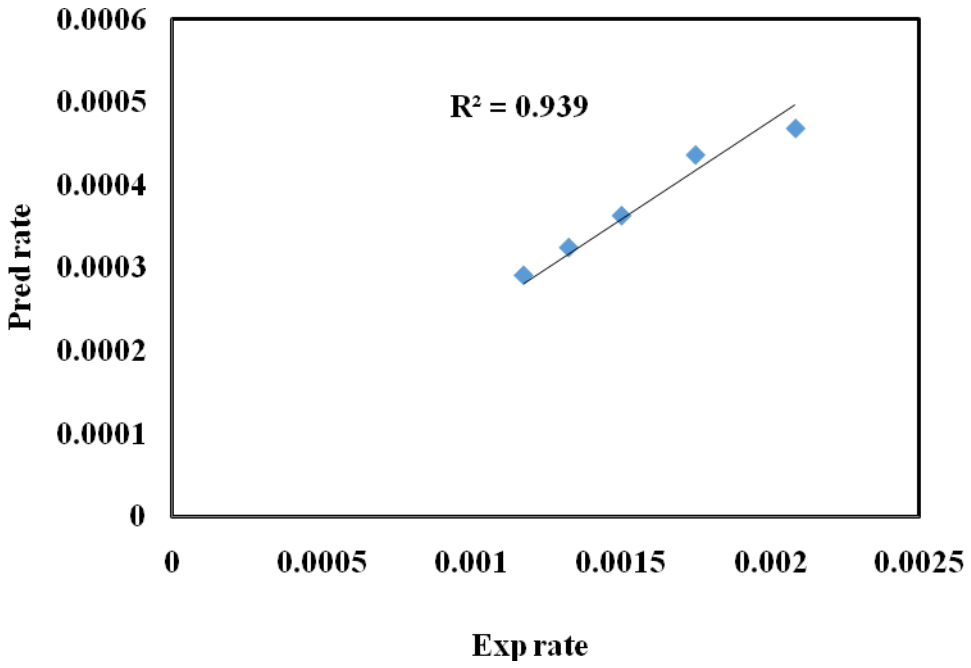

Figure.6.9. Parity plot at temp 550°C

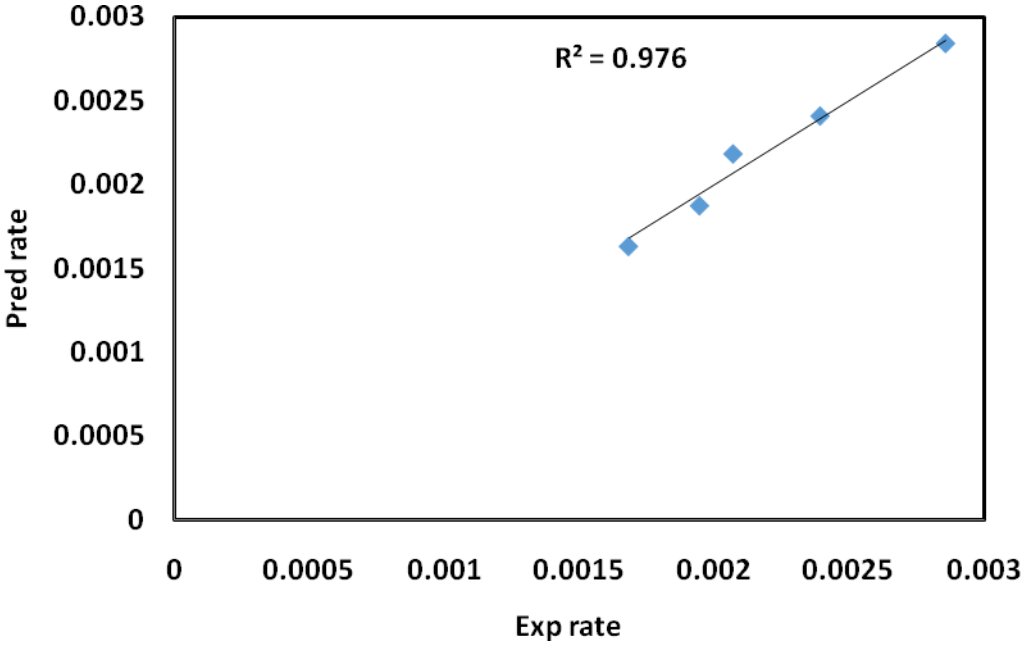

Figure.6.10. Parity plot at temp 600°C

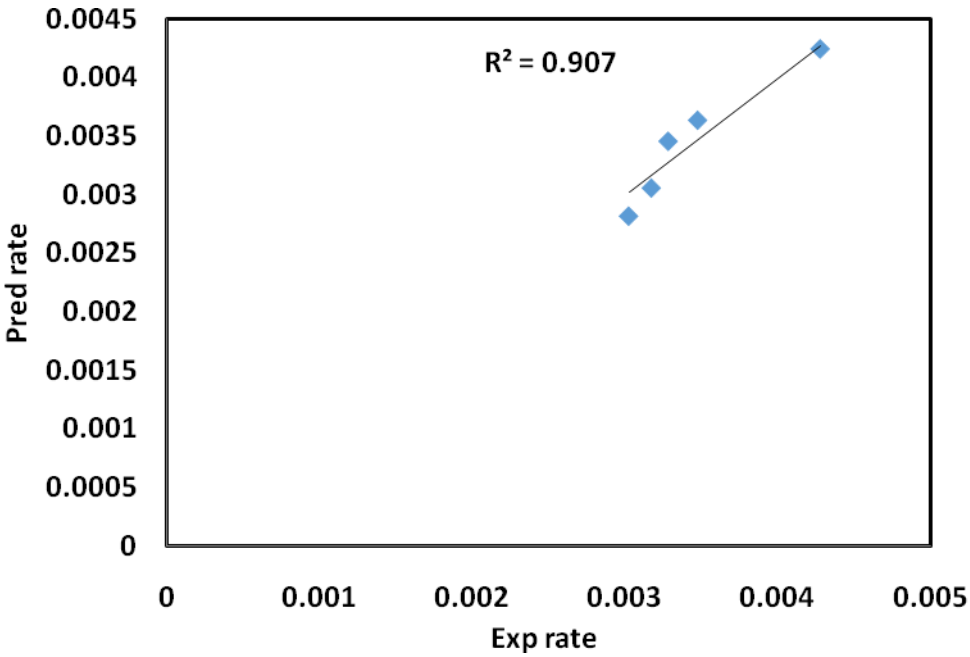

Figure.6.11. Parity plot at temp 650°C

Parity plots were drawn to validate the rate expression developed through LHHW mechanism. From the Plots 6.7 -6.9, it can be understood that the LHHW mechanism is perfectly suitable

for the proposed reaction for the selected catalyst. The regression coefficients are satisfactory for all three temperatures.

6.2.2. Finding the activation energy and kinetic constant:

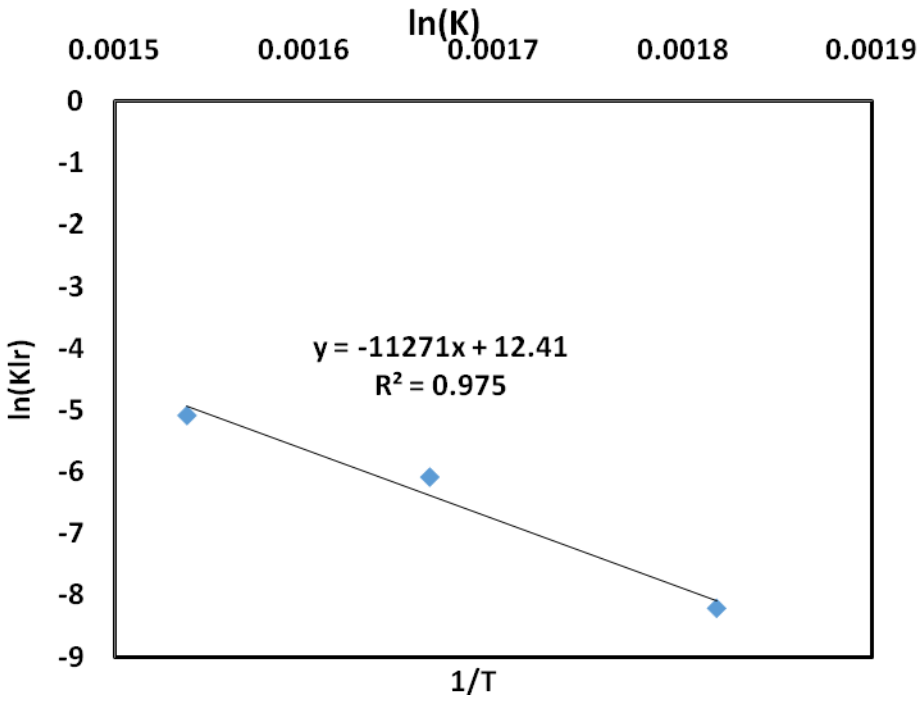

Figure.6.12. Plot for constant of the LHHW model

	Arrhenius model	LHHW model
Activation energy (J/mol)	39.14	7.29
Pre-exponential factor (mol/L-s)	0.0447	0.02687

Table.6.5. Activation energy & Kinetic constants

Activation energy calculated from Arrhenius model and LHHW model are shown in table. 6.5. The value obtained from the LHHW is less when compared to the Arrhenius model,

6.3. Parameter Estimation:

The parameter in the rate equations are estimated by using Levenberg Marquardt method which minimizes the following objective function.

$$obj\ Function = \frac{1}{n}\sum_{i=1}^{n}(r_{i,cal} - r_{i,exp})^2 \quad (6.24)$$

Where,

n = Number of experimental data,

r_{cal}= calculated reaction rate.

Marquardt Method:

Estimation in algebraic or differential equations which are nonlinear in the parameters can be performed by minimizing the objective function by methods such as steepest descent, Newton-Gauss, and Marquardt algorithm. These methods are explained elsewhere [10-12].Newton-Gauss and Marquardt methods are presented below.

Let a nonlinear model be expressed by

$$y_i = f(x_i,\beta) + \varepsilon_i \quad (6.25)$$

Where y_i are the dependent variables, x_i are the independent variables, β are the parameters, and ε are the experimental errors.

The minimization of the least squares criterion can be represented by

$$S(\beta) = \sum_{i=1}^{n}[y_i - f(x_i,\beta)]^2 \xrightarrow{\beta} min \quad (6.26)$$

To minimize the sum of squares of residuals the necessary conditions require taking the partial derivative of *S*(β) with respect to β and setting it equal to zero:

$$\frac{\partial S}{\partial \beta} = 0 \quad (6.27)$$

Because *f* is nonlinear with respect to the parameters, it is converted into a linear form by Taylor series around an estimated value of the parameter vector β:

$$f(x_i,\beta) = f(x_i,b_0) + \sum_{j=1}^{p}\left[\frac{\partial f(x_i,\beta)}{\partial \beta_i}\right]_{\beta=b_0} \Delta b_j + \cdots + \varepsilon \quad (6.28)$$

Where the Taylor series has been truncated after the second term. Above equation can be expanded into:

$$f(x_i,\beta) - f(x_i,b_0) = \sum_{j=1}^{p}\left[\frac{\partial f(x_i,\beta)}{\partial \beta_i}\right]_{\beta=b_0} \Delta b_j + \cdots + \varepsilon \qquad (6.29)$$

Equation mentioned above is linear in Δb_j and the improvement of the parameter values are obtained

From

$$\Delta b = (J^T J)^{-1} J^T r \qquad (6.30)$$

Where

$$r = \begin{pmatrix} f(x_i,\beta)-f(x_i,b_0) \\ \vdots \\ f(x_n,\beta)-f(x_n,b_0) \end{pmatrix} \Delta b = \begin{pmatrix} \Delta b_i \\ \vdots \\ \Delta b_n \end{pmatrix} J = \begin{bmatrix} \frac{\partial f(x_1,\beta)}{\partial \beta_1} & \cdots & \frac{\partial f(x_1,\beta)}{\partial \beta_n} \\ \vdots & \ddots & \vdots \\ \frac{\partial f(x_n,\beta)}{\partial \beta_1} & \cdots & \frac{\partial f(x_n,\beta)}{\partial \beta_p} \end{bmatrix} \qquad (6.31)$$

This procedure is called the Newton-Gauss method. This method works very well unless the model is highly nonlinear. But the linearization of nonlinear model may lead to such a large Δb that the method diverges [9].To overcome this, Marquardt developed a compromise between the method of steepest descent and the method of Newton-Gauss [13].Marquardt's compromise starts with a large value of λ, the Lagrangian multiplier, and the direction of search is close to that of steepest descent. λ is gradually decreased and the direction of search becomes that of Newton-Gauss. Mathematically Δb is determined using

$$\Delta b = (J^T J + \lambda I)^{-1} J^T r \qquad (6.32)$$

Where **I** is the unit matrix. It can be seen from equation above that the step size Δ**b**is inversely proportional to λ and λ determines the orientation of the search.

When λ is very large, previous equation reduces to

$$\Delta b = \lambda^{-1} J^T r \qquad (6.33)$$

The step size is very small and the search direction is that of the steepest descent.

When λ is very small

$$\Delta b = (J^T J)^{-1} J^T r \qquad (6.34)$$

The step size reaches the maximum and the search direction is that of Newton-Gauss.

6.3.1. Algorithm for ODH process:

1. For different loading of catalyst on the support at different temperature find at which ethane conversion is high and ethylene selectivity is high
2. For different partial pressures of ethane and CO_2 find the experimental rate of reaction is found by

$$\frac{dx}{-r_i} = W/F_i \qquad (6.35)$$

   x- Conversion of component i

   r_i- rate of reaction for component i

   W-weight of catalyst

   F_i-flow rate of component i
3. select a diameter of particle in a range of size for which internal diffusion is negligible. Also select W/ F_i ratio for the catalyst for which external diffusion is negligible. Hence assumption of surface reaction as controlling mechanism is reasoned.
4. Check different kinetic model for which experimental rate is fitting well with the predicted one.
5. Similarly for kinetic models such as LHHW, Eley Rideal and Mars van krevlen the parameters are found by non linear least square fitting. The algorithm employed is Levenberg Marquardt algorithm.
6. In present case LHHW (Molecular adsorption) fits the data perfectly.
7. The parameters obtained are checked with the Boudart criteria for thermodynamic consistency.

6.4. Validation of the model:

6.4.1. Thermodynamic validation:

Boudart and co-authors [13,14] have proposed well established rules for testing the suitability of the estimated parameter values in the final rate equations. In this work the adsorption enthalpies and entropies are tested by the constraint rules presented by Boudart et al.[14] and Boudart.[15] The following test procedure is guided by Mears and Boudart [14], Van Trimpont et al.[18], Xu and Froment [19], and Froment and Bischoff [20].

1. Thermodynamics requires the activation energy of reaction *i* to be greater than the heat of the reaction, $\Delta H_{r,i}$, for an endothermic reaction *i*. Therefore, the following relation must be obeyed.

$$E_i > \Delta H_{r,i}$$

The table below discussions shows that the activation energy of the reaction (163/KJ/mol) is greater than the heat of reaction (134 KJ/mol)

2. The heat of adsorption, ($-\Delta H_{a,i}$), has to be greater than zero, because the adsorption is exothermic. All the estimates of heat of adsorption satisfy this constraint.

3. The adsorption entropy has to satisfy

$$0 < |\Delta S_i| < S_g$$

Where S_g is the standard entropy of the gas, and ΔS_i is the entropy of the adsorbed molecule.

4. The last criterion is

$$41.8 < |\Delta S_i| < 51.0 - 0.0014\Delta H$$

Everett [21] obtained the above equality relation by the linear regression between standard entropy and enthalpy changes for physical adsorption on a gas-charcoal. This equation can be extended to chemisorptions [20]. Furthermore, Vannice et al [15] showed that it could be applicable to dissociative adsorption which was not included in the rule proposed earlier by Boudart et al.[14] The verification of this rule is shown in Table 6.6 below. The values obtained are within the range, hence the rule is satisfied.

Model		**C_2H_6**	**CO_2**
LHHW	$\Delta H_{a,i}$(kg-m^2/s^2)	4.0622204	9.32830
	ΔS_i(gr-m^2/S^2-K^{-1})	4.306652	11.96385
	S_g(J/gr-k)	255.28	257.28
	51-0.0014$\Delta H_{a,i}$	50.994	50.9869

Table.6.6. Thermodynamic parameters

6.5. Statistical evaluation:

The F statistic is the ratio of the explained variability (R^2) and the unexplained variability in the model ($1 - R^2$), each divided by the corresponding degrees of freedom. The larger the F statistic, the more useful the model.

To check for statistical consistency of model, F value of model which is the proportion of regression sum of mean square to residual error sum of mean square

$$F = \frac{\sum_i^M r_{i,exp}^2 - \sum_i^M (r_{i,exp} - r_{i,cal})^2 / M_p}{\sum_i^M (r_{i,exp} - r_{i,cal})^2 / (M - M_p)} \quad (6.36)$$

Wherer $_{i,exp}$ and $r_{i,cal}$ is the experimental and calculated rates of ethane and CO_2

ρ^2 is the key parameter calculated by

$$\rho^2 = 1 - \frac{\sum_i^M (r_{i,exp} - r_{i,cal})^2}{\sum_i^M r_{i,exp}^2} \quad (6.37)$$

M – Number of parameters, M_p- number of replicates.

The model is suitable when $\rho^2 > 0.9$, $F > 10F_{0.05}$ [21].The results for the statistical analysis is given below in Table 6.7.

Model	**ρ^2**	**F**	**$10F_{0.05}$**
LHHW(Molecular adsorption) for ethane	0.962	5578	29.375
LHHW(Molecular adsorption) for CO_2	0.9507	3510	18.47

Table.6.7 .LHHW statistical parameters

The values in the table show that kinetic model is statistically consistent.

REFERENCE:

1. Smith, J. M. (1998). Chemical engineering kinetics.
2. Octave levenspiel, Chemical Reaction engineering, 3rd edition, 2010.
3. Charles G.Hill, Introduction to chemical engineering & Reactor design, Johnwiley and sons,Singapore ,1977
4. Mohammed Nasif Abbas, Modeling of porosity equation For water flow through packed bed Of monosize spherical packing, Journal Of Engineering And Development, Vol. 15, No.4, Des 2011
5. Robert.E.Treybal, 'Mass Transfer Operations'3rd edition,1981.
6. R. H. Perry, D. W. Green, Perry's Chemical Engineers Handbook, McGraw-Hill, New York 1997.
7. R. Byron Bird , Warren E. Stewart , Edwin N. Lightfoot,'Transport Phenomena',2nd edition,1958.
8. Xu L, Lin L, Wang Q, Li Y, Wang D, Liu W. 'A new route for C_2H_4 production by reacting C_2H_6 with CO_2 over a catalyst of chromium oxide supported on silicalite-2 type zeolite', Stud. Surf. Sci. Catal. 119 (1998) 605-610.
9. Krylov O.V, Mamedov A.A, Mirzabekova A.K. 'The regularities in the interaction of alkanes with CO2 on oxide catalysts', Catal. Today 24 (1995) 371-375
10. Krylov, O. V, Mamedov A. K, Mirzabekova S. R.' Oxidation of Hydrocarbons and Alcohols by Carbon Dioxide on Oxide Catalysts' Ind. Eng.Chem. Res. 34 (1995) 474-482.
11. Froment, G. F. 'Model Discrimination and Parameter Estimation in Heterogeneous Catalysis'. AIChE J. 1975, 21, 1041-1057
12. Constantinides, A.; Mostoufi, N. Numerical Methods for Chemical Engineers with MATLAB Applications; Prentice Hall Inc.: Upper Saddle River, N. J., 1999
13. Edgar, T. F.; Himmelblau, D. M. Optimization of Chemical Processes, 2nd ed.; McGraw-Hill: New York, 2001
14. Marquardt, D. W.' An Algorithm for Least-Squares Estimation of Nonlinear Parameters'. J. Soc. Indust. Appl. Math
15. Boudart, M.; Mears, D. E.; Vannice, M. A. Ind. Chim. Belge. 1967, 32, 281 . 1963, 11, 431

16. Vannice, M. A.; Hyun, S. H.; Kalpakci, B.; Liauh, W. C. ‘Entropies of Adsorption in Heterogeneous Catalytic Reactions’. J. Catal. 1979**,** 56, 358
17. Boudart, M. ‘Two-Step Catalytic Reactions’. AIChE J. 1972, 18, 465
18. Mears, D. E.; Boudart, M. ‘The Dehydrogenation of Isopropanol on Catalysts Prepared by Sodium Borohydride Reduction’. AIChE J. 1966**,** 12, 313
19. Van Trimpont, P. A.; Marin, G. B.; Froment, G. F. ‘Kinetics of Methylcyclohexane Dehydrogenation on Sulfided Commercial Platinum Alumina and Platinum-Rhenium Alumina Catalysts’. Ind. Eng. Chem. Fund. 1986,25, 544-553
20. Xu, J. G.; Froment, G. F. ‘Methane Steam Reforming, Methanation and Water-Gas Shift .1. Intrinsic Kinetics’. AIChE J. 1989**,** 35, 88-96..
21. Everett, D. H. ‘The Thermodynamics of Adsorptions Part II. Analysis and Discussion of Experimental Data’. Trans. Faraday Soc. 1950**,** 46, 957.
22. Huang H J. Practical Computer Simulation of Chemical Processes (in Chinese). Beijing: Chem Ind Press, 2004. 246.

CHAPTER -7

OPTIMISATION USING RESPONSE SURFACE METHODOLOGY

7.0. RESPONSE SURFACE METHODOLOGY:

Response Surface Methodology (RSM) is a statistical technique used to find the optimum conditions for a process of interest. It is used to find the optimum conditions for the process of interest. In RSM a relationship is found between the variables involved in the process and the response variable which is usually unknown. The response can be represented either in the 3D space or as contour plots which helps to visualize the shape of the response surface. Contours are curves of constant response drawn in the xi, xj plane keeping all other variables fixed. Each contour corresponds to a particular height of the response surface.

In RSM the unknown relation is usually identified between the variables involved in the process and the response variable. When the relationship between the variables involved and the response is approximated by using low order approximations such as linear functions of independent variables the model is said to be a first order model.

Optimum conditions of process variables can be found using steepest ascent or descent method. In this method the search is moved in the direction normal to the contours of response variable y and the experimental response is observed for changes. This process gives the optimum conditions of independent variables with several additional experiments. In the present study, the independent variables which affect the response (ethane conversion, ethane selectivity and methane selectivity) are the reaction temperature and volumetric flow rates of CO_2.

7.1. Results on RSM analysis:

As discussed in section 5.3 the experimental data obtained for the performance of mixed oxide i.e. 15wt% Cr_2O_3/Al_2O_3-ZrO_2 (1:1) was used for RSM analysis. Because the Catalyst with 15 wt% chromium loading was found to be optimum to obtain reasonable ethane and carbon dioxide conversions when compared to the other metal oxide supported chromium catalysts studied. RSM was performed to obtain the optimum parameters for maximum conversion of reactants i.e. ethane and selectivity of the product i.e. ethylene. By using the RSM methodology the following interaction plots for ethane conversion (X_{C2H6}), ethane selectivity (S_{C2H4}) and methane selectivity (S_{CH4}) were obtained (Figs. 7.1 (A - C). It is known that the conversion of ethane increases with increasing temperature while the selectivity towards ethylene, the desired product decreases [2]. From the following graphs it can be found that the optimum conditions to get higher conversion of ethane is at a higher temperature of 650°C and the volumetric flow rate of CO_2 at 15 mL/min. Also the selectivity of ethylene is maximum at temperature of 600° C and volumetric flow rate of CO_2 at 15 mL/min.

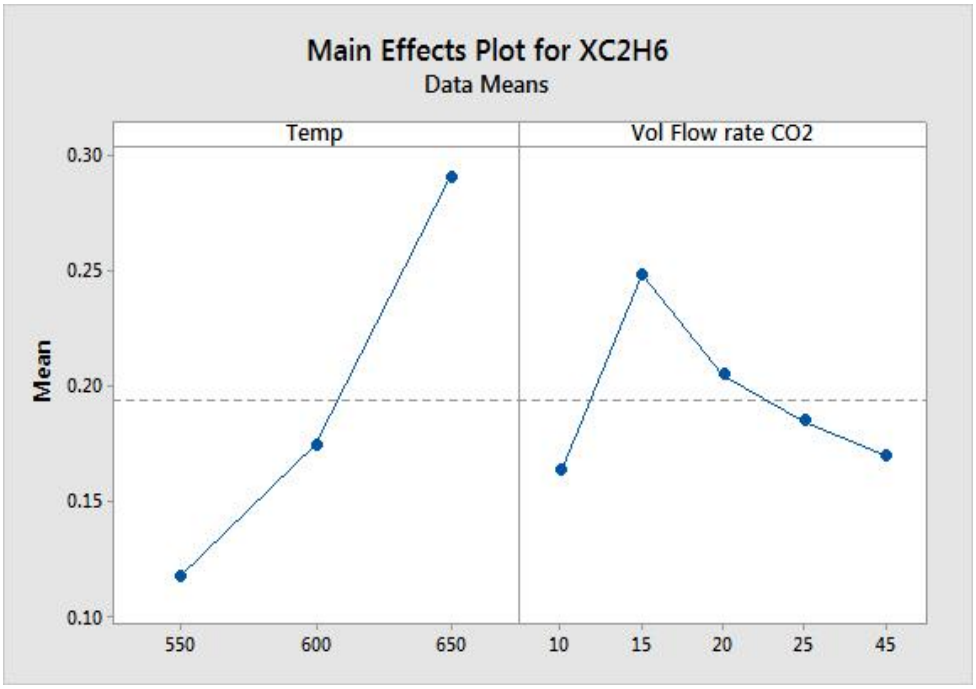

7.1.(A)

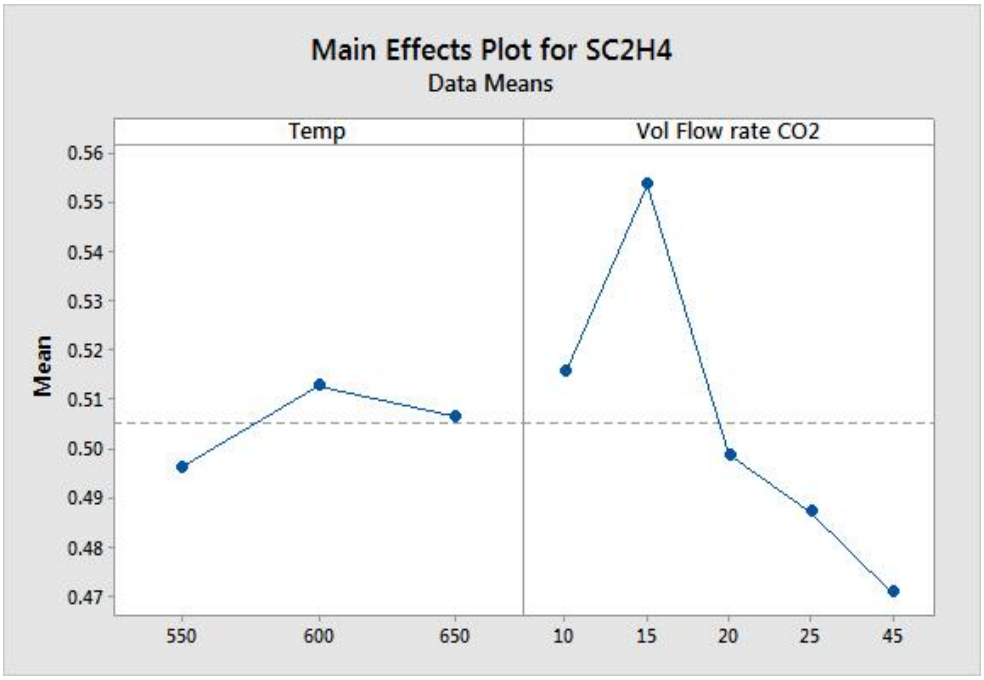

7.1.(B)

Figure .7.1. (A- B). Plots showing the main effects for various responses

The main effects plots show that conversion is a function of temperature but the selectivity of ethylene increases up to 600 °C and then decreases.

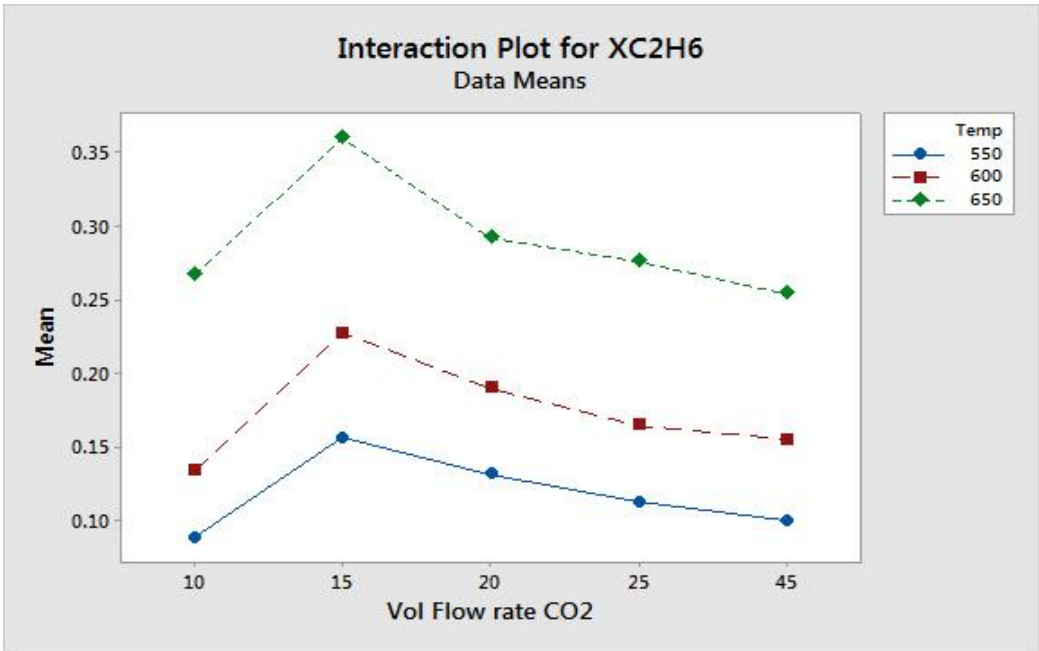

7.2.(A)

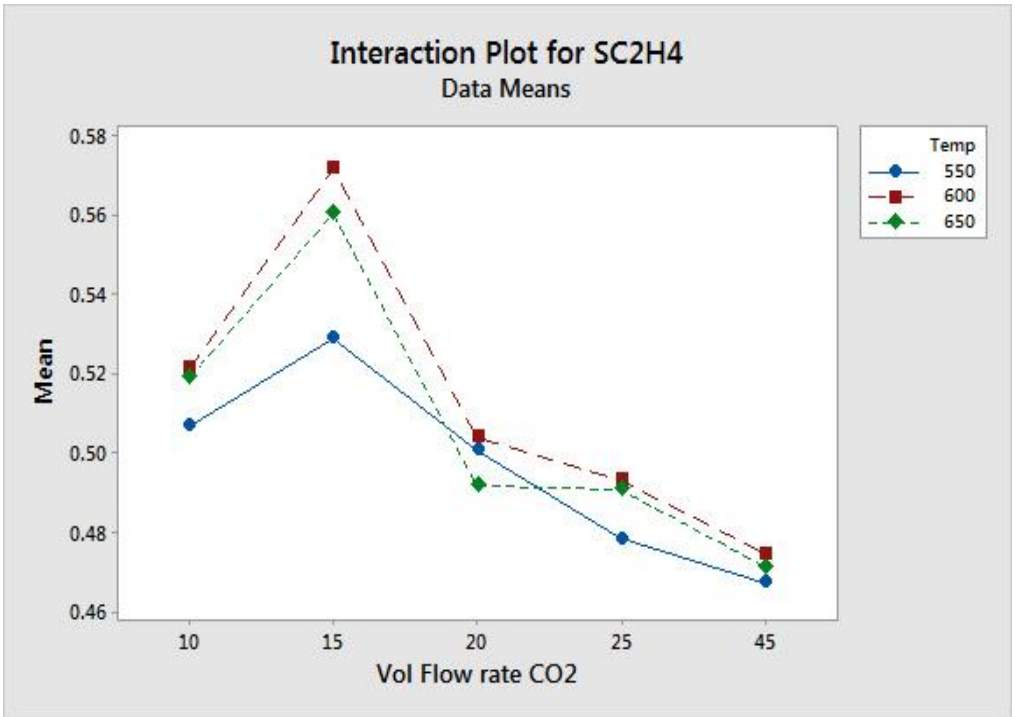

7.2. (B)

Figure.7.2. (A-B). Interaction plots for various responses

The interaction plots and their responses show that all the responses are in parallel with higher factor levels. It is shown that there are no interaction effect between the two factors, temperature and volumetric flow rate of CO_2.

7.2. Design of variables by RSM:

Two independent variables i.e Temperature (X_1), and flow rate (X_2) and the conversion was selected as the response variable (Y) of the ODH of ethane with selected catalyst i.e. 15wt%

Cr_2O_3 / Al_2O_3-ZrO_2 (1:1) . For each variable, the experimental range and central point are tabulated in Table 7.1. Box-Behnken [4] experimental design (BBD) gave fifteen sets of experimental runs according to the standard with two process variables at three levels. For design of experiments MINITAB tool was employed to analyze the data.

Table 7.1: Coded variables:

Independent variables	Coded	Actual factor levels		
		-1	0	1
Temperature	X_1	550	600	650
Flow rate	X_2	10	25	45

The results obtained from BBD method from fifty four sets of experiments are tabulated which are in good agreement with the experiment values.

Table 7.2. Results comparison obtained from BBD method

S.no	Experimental Conversion	Predicted conversion
1	0.0812	0.1
2	0.1349	0.14
3	0.263	0.274
4	0.2016	0.212
5	0.290167	0.302
6	0.4152	0.405
7	0.1332	0.101
8	0.2001	0.198
9	0.3012	0.297
10	0.1005	0.112
11	0.1667	0.153
12	0.2515	0.243
13	0.0847	0.019
14	0.1628	0.15
15	0.2515	0.24

The following are the **Analysis** of variance (**ANOVA**) results for ethane conversion, ethylene selectivity [3].

Table.7.3: ANOVA results for ethane conversion

Source	DF	Adj SS	Adj MS	F-Value	P-Value
Model	5	0.007863	0.001573	2.50	0.110
Linear	2	0.007277	0.003639	5.78	0.024
Temp	1	0.000171	0.000171	0.27	0.614
Vol Flow rate	1	0.007106	0.007106	11.29	0.008
Square	2	0.000605	0.000302	0.48	0.634
Temp*Temp	1	0.000416	0.000416	0.66	0.437
Vol Flow rate*Vol	1	0.000189	0.000189	0.30	0.597
2-Way Interaction	1	0.000057	0.000057	0.09	0.770
Temp*Vol Flow rate	1	0.000057	0.000057	0.09	0.770
Error	9	0.005667	0.000630		
Total	14	0.013530			

From the above table it can be found that the linear terms in volumetric flow rate, quadratic terms and interactions do not influence the response, ethane conversion, as the p value is greater than the significant value 0.005.

Table.7.4. ANOVA results for ethylene selectivity

Source	DF	Adj SS	Adj MS	F-Value	P-Value
Model	5	0.081166	0.016233	13.03	0.001
Linear	2	0.063106	0.031553	25.32	0.000
Temp	1	0.062140	0.062140	49.86	0.000
Vol Flow rate	1	0.000967	0.000967	0.78	0.401
Square	2	0.004804	0.002402	1.93	0.201
Temp*Temp	1	0.002934	0.002934	2.35	0.159
Vol Flow rate*Vol	1	0.001870	0.001870	1.50	0.252
2-Way Interaction	1	0.000340	0.000340	0.27	0.614
Temp*Vol Flow rate	1	0.000340	0.000340	0.27	0.614
Error	9	0.011217	0.001246		
Total	14	0.092383			

From the above table it may be found that the linear terms in volumetric flow rate, quadratic terms and interactions do not influence the response in ethane conversion as the p value is greater than the significant value 0.005.

7.3. Regression analysis and surface responses:

Multiple nonlinear regression analysis is carried out for different responses (i.e ethane conversion, ethylene selectivity and methane selectivity) as a function of independent variables [1] (Temperature, Oxidant flow rate (CO_2)) is given by Eq. 6.3.

$$y = \beta_0 + \sum_{i=1}^{n} \beta_i x_i + \sum_{i=1}^{n} \beta_{ii} {x_i}^2 + \sum_i \sum_j \beta_{ij} x_i x_j \; i < j \text{- - - -} \quad \text{(Eq. 6.3)}$$

The linear effects are represented by β_i, quadratic effects by β_{ii} and interactions between the factors by β_{ij}. The parameters values listed in the table below are estimated from experimental data (95% Confidence Interval) by nonlinear regression.

Table.7.5.Parameter values estimated for various response surface models

Parameter	Ethane Conversion	Ethylene Selectivity
β_0	3.24	-1.15
β_1	-0.01229	0.00556
β_2	0.0101	-0.00105
β_{11}	0.000012	-0.000004
β_{22}	-0.000091	0.000029
β_{12}	-0.00001	-0.000004

The figures below show various contour and surface plots for response variables as a function of independent variables.

The contour plots of conversion of ethane show that it increases with increase in temperature and the corresponding maximum obtained value. The contour plots represent the range of conversion, selectivity of ethylene with respect to variation in temperature. Different colors in the plots represent different ranges for the results at different temperatures.

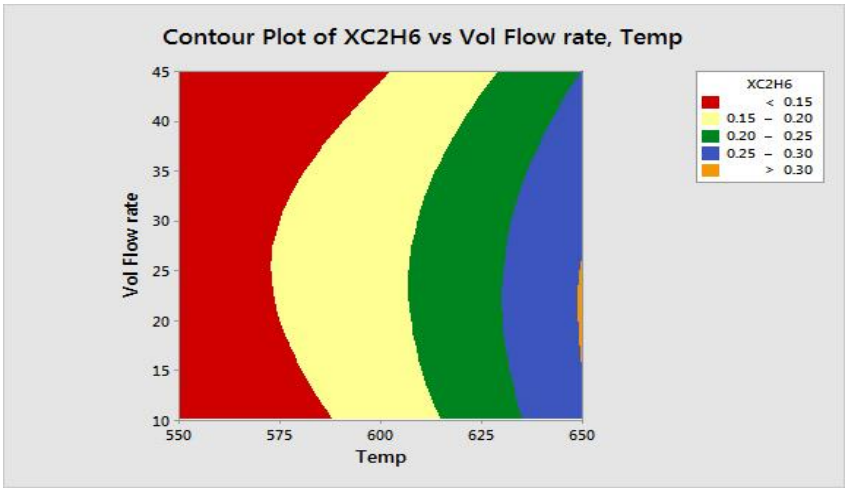

7.3.(A)

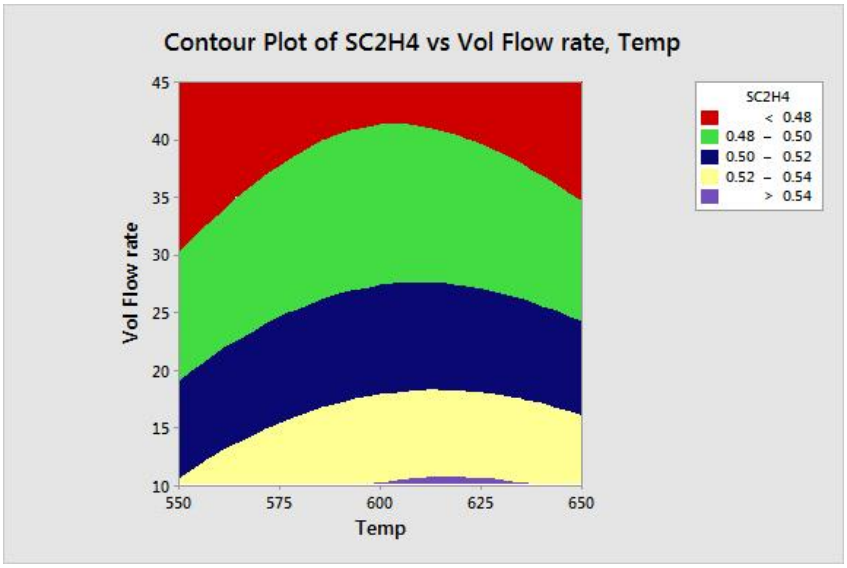

7.3.(B)

Figure 7.3(A - B): Contour plots for various responses

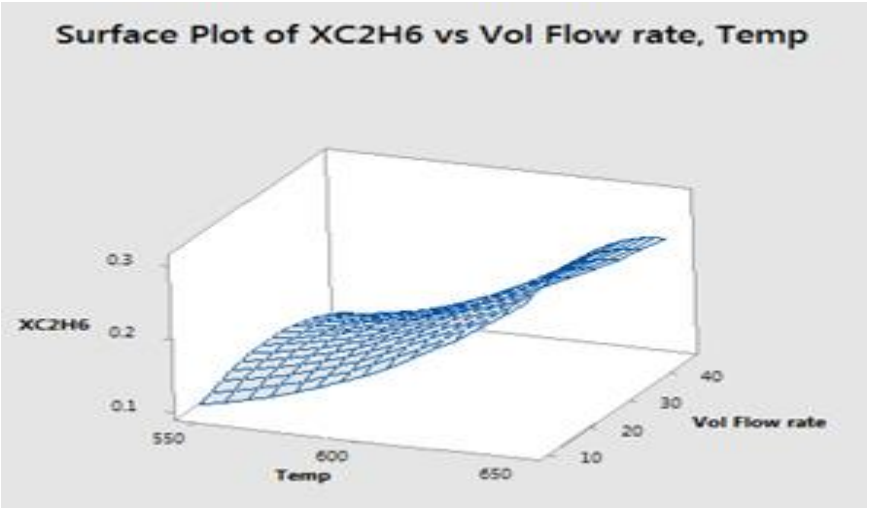

7.4.(A)

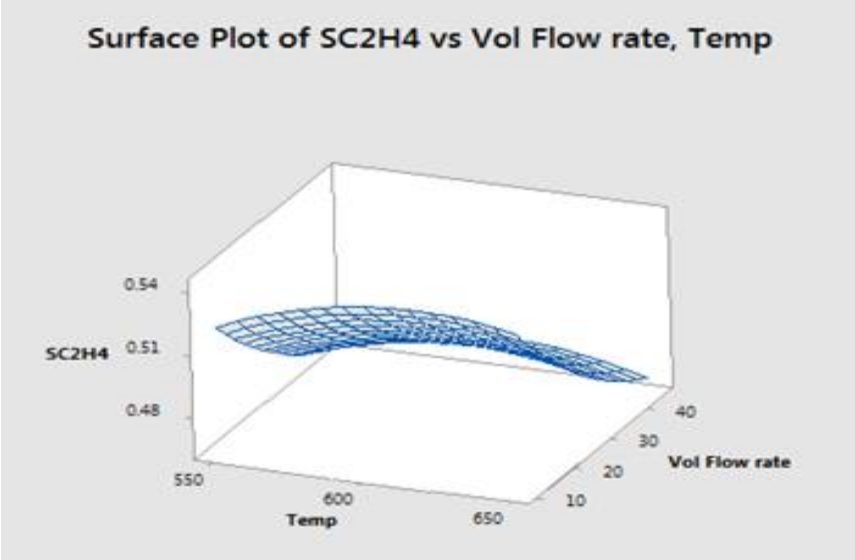

7.4.(B)

Figure.7.4 (A-B): Surface plots for various responses

The surface plots represent the responses i.e. conversion of ethane, selectivity of ethylene for the effect of temperature and flow rates. At different temperatures and flow rates the corresponding conversion 7.4 (A), ethylene selectivity 7.4 (B) can be obtained from the said graphs.

The plot below combines the effects of both factors at which optimum conditions are achieved in the reactor for the given operating conditions. The optimization plot contains the lower and upper limit of factors and the red line shows where the composite desirability is high for the given operating conditions. Optimization of the overall responses will be evaluated by composite desirability (D). Desirability has a range of zero to one. For an ideal case; zero indicates that one or more responses are outside their acceptable limits. The blue dotted line shows the values of factors at optimum conditions. The red line can be adjusted in such a way that the composite desirability is high. In the present study, the desirability ratio is 0.6963 for the operating conditions of temperature of 650 °C and the flow rate of 10 mL/min.

7.4. Optimization of ODH of ethane process parameters:

The optimum process parameters for the ODH of ethane reaction are obtained by numerical optimization using MINITAB tool. For the selected two independent variables, the response variable i.e ethane conversion was set to maximize the value within the range of variables provided. About 52 solutions were obtained using the Tool, and the solution with highest desirability and maximum conversion was chosen to be verified by experiments. The optimal conditions, predicted value and the experimental value (average of three measurements) of conversion are tabulated and the predictions are in good agreement with experiment values.

Variables	Temperatur	Flow rate	X-C_2H_6	S-C_2H_4
Experimental	650 ℃	15	29.54	49.5
Predicted	615.65 ℃	19.19	27	50

Table.7.6.Model validation and optimal condition for the ODH of ethane reaction for selected catalyst

7.5. Summary:

The oxidative dehydrogenation of ethane using $CO_2$was carried out in a packed bed reactor with silica and non silica supported chromium based catalysts. The experimental results obtained by using mixed oxide supported chromium based catalysts (i.e 15% Cr_2O_3/Al_2O_3-ZrO_2) were analyzed by ANOVA to determine optimum values. The effect of reaction temperature and the volumetric flow rate of CO_2 for various responses were studied using ANOVA and it was found that linear terms in volumetric flow rates of CO_2 (mL/min), quadratic terms and interactions did not influence the response variable (Ethane conversion, Ethylene Selectivity) significantly. Also the optimum conditions for ethane conversion was found as 650 ℃, the volumetric flow rate of CO_2 at 15 mL/min and for ethylene selectivity the optimum conditions were temperature at 600 ℃ and volumetric flow rate of CO_2 at 15 mL/min. The response surface methodology was formulated for different independent variables (Temperature, Volumetric Flow Rate of CO_2) and the corresponding surface plots and contour plots were plotted to check for optimum conditions for the process and it was found that they agreed well with the experimental results.

REFERENCES:

1. Rashidi, S., Bovand, M., & Esfahani, J. A. (2015). Structural optimization of nanofluid flow around an equilateral triangular obstacle. Energy, 88, 385-398.
2. Routray, K., & Deo, G. (2005). Kinetic parameter estimation for a multiresponse nonlinear reaction model. AIChE journal, 51(6), 1733-1746.
3. Valente, J. S., Quintana-Solórzano, R., Armendáriz-Herrera, H., Barragán-Rodríguez, G., & López-Nieto, J. M. (2013). Kinetic study of oxidative dehydrogenation of ethane over MoVTeNb mixed-oxide catalyst. Industrial & Engineering Chemistry Research, 53(5), 1775-1786.
4. Chandane, V. S., Rathod, A. P., Wasewar, K. L., & Sonawane, S. S. (2017). Esterification of propionic acid with isopropyl alcohol over ion exchange resins:Optimization and kinetics. Korean Journal of Chemical Engineering, 34(1), 249-258.

CHAPTER -8

CONCLUSIONS & SCOPE FOR FUTURE WORK

8.0. CONCLUSIONS AND SCOPE FOR FUTURE WORK

The experimental results obtained from the investigation demonstrated the efficiency of chromia based catalysts for the oxidative dehydrogenation of ethane using CO_2 as oxidant. The important conclusions drawn from this study are listed below.

- The nature of the support has a significant influence on the structure, surface area, type of CrO_x species formed, redox and acid-base properties of chromia catalysts.
- Cr_2O_3 based catalysts supported on different oxide carriers and silica materials, i.e Al_2O_3, ZrO_2, and their mixed metal oxides, SBA-15, SBA-16 and silica gel displayed different catalytic performance in the ODH reaction.
- The activity and selectivity over metal oxide and silica material supported chromia catalysts varied with the active species Cr_2O_3 composition (5-20 wt%). There was considerable difference in the chromium oxide species formed and the surface enrichment of chromium in the near-surface region.
- Carbon dioxide as an oxidant offers higher ethylene selectivity compared to oxygen.
- 15 wt% loading is necessary to obtain reasonable ethane and CO_2 conversions.
- 15 wt% Cr_2O_3/Al_2O_3 catalyst showed best catalytic activity among the alumina supported chromium catalysts with 32% ethane, 21% CO_2 conversions with 46% selectivity.
- 15 wt% Cr_2O_3/ZrO_2 catalyst displayed high conversions to ethane (42%) and CO_2 (37%) with less ethylene selectivity (36%).
- Among all the mixed Al_2O_3-ZrO_2 supported chromium catalysts the support with 1:1composition is advantageous in terms of attaining best activity i.e 36% ethane, 29% CO_2 conversions with 56% ethylene selectivity.
- The characterization results revealed that the chromium can be stabilized on supports with its higher oxidation states along with its highly stable oxidation state (Cr^{+6}, Cr^{+5} and Cr^{+3}) and also inferred that the redox couples (Cr^{+6}/Cr^{+5} to Cr^{+3}) are responsible for ethane dehydrogenation using carbon dioxide.
- The catalytic activity and selectivity over metal oxide and silica material supported chromium based catalysts with varying compositions were found to depend strongly on the nature of support and chromium oxide species formed and the surface enrichment of chromium in the near-surface region.

- The sulfate-modified Cr/S.SBA-15 catalyst exhibits higher activity for the ODH with CO_2 compared to the unmodified catalyst.
- Sulfate modification affords higher dispersion of the Cr species. In both the catalysts, the Cr species exists in $Cr^{6+}$and Cr^{+3} states.
- The addition of sulfate ion to the support SBA-15 remarkably changes the redox properties of the CrO_x species. A higher Cr^{6+} / Cr^{+3} ratio is observed in the case of Cr/S.SBA-15 catalyst.
- The ODH of ethane using CO_2 was kinetically modeled by various models using the mixed oxide supported chromia catalyst and it was found that the ethane and CO_2 decomposition rates best fitted the LHHW (Langmuir-Hinshelwood) mechanism when compared to other models (i.e. Eley-Rideal mechanism, Mars-van Krevelen). The parameters obtained from the model were checked for thermodynamic and statistical consistency.
- The response surface methodology was formulated for different independent variables and the corresponding surface plots and contour plots were plotted to check for optimum conditions and the obtained optimum values are in good agreement with the experiment values.

8.1. SCOPE FOR FUTURE WORK

There is a large scope to continue the present work. Some of the possibilities for future work are listed below.

- Synthesis of nano composites and mesoporous based catalysts using different synthesizing methods like hydrothermal, sol-gel method.
- Application of the nano composite and mesoporous based catalysts to ODH of ethane to improve the activity and selectivity.
- Application of other metal oxide based catalysts to the ODH of ethane with CO_2.
- Studies methane coupled reactions
- The work will be extended to the ODH of ethane to ethylene using N_2O as an oxidant over the same catalyst.
- Modeling and simulation of fixed bed reactor for ODH process.

RESEARCH PUBLICATIONS

JOURNAL PAPERS:

1. **P.Thirumala Bai,** Rajmohan K.S. P.S Sai Prasad, S. Srinath, **"Oxidative Dehydrogenation of Ethane to Ethylene over Metal Oxide Catalysts using Carbon Dioxide"** Book Chapter "CO_2 Separation, Purification And Conversion to Chemicals and Fuels"-Chapter7.page:93-117.(2018) doi.org/10.1007/978-981-13-3296-8_7, **Springer Publications.**
2. **P.Thirumala Bai,**S.Srinath**, "Oxidative Dehydrogenation of Ethane to ethylene over chromium on zirconia catalyst"** International Journal of Advances in Science Engineering and Technology, Vol-6, Iss-2, Spl. Issue-1 May-2018, IJASEAT-IRAJ- doi-12200 Page 24-27.
3. **P.Thirumala Bai**, V.Manokaran, P.S.Sai Prasad, S.Srinath **"Studies on heat and Mass transfer Limitations in oxidative Dehydrogenation of Ethane over Cr_2O_3/Al_2O_3 catalyst.** Proceedia Engineering127(2015)1338-1345.**Elsevier Publications**.

4. **P. ThirumalaBai** S. Srinath • K. Upendar • T. V. Sagar • N. Lingaiah • K. S. Rama Rao • P.S. SaiPrasad **"Oxidative dehydrogenation of ethane with carbon dioxide over Cr_2O_3 / SBA-15 catalysts: The influence of sulfate modification of the support** ",Applied Petrochemical Research, December 2017, Volume7, Issue 2–4, pp 107–118,**Springer Publications**.
5. Y. Ramesh, **P. Thirumala Bai**, B. Hari Babu, N. Lingaiah, K. S. Rama Rao, P. S. Sai Prasad,**Oxidative dehydrogenation of ethane to ethylene on Cr_2O_3/Al_2O_3-ZrO_2 catalysts: The influence of oxidizing agent on ethylene selectivity.** Applied Petrochemical Research 2014, Volume 4, No 3, pp 247–252. **Springer Publications**.

CONFERENCE PROCEEDINGS:

1. P.Thirumala Bai, P.S.Sai Prasad, S.Srinath "Catalytic Evaluation of ODE by Effect of Chromium on sulphated Silica catalyst" 20th International Conference of International Academy of Physical Sciences (CONIAPS XX) July14-16, 2017 young scientist award presentation.

2. P.Thirumala Bai, P.S.Sai Prasad, S.Srinath "Oxidative Dehydrogenation of Ethane to Ethylene over Cr_2O_3 on SBA16 catalyst" Published in the proceedings of International Conference on Trend Setting Innovations in Chemical Sciences &Technology - Applications in Pharma Industry TSCST-API 2015, 16-18, December 2015, JNTU Hyderabad.

3. P.Thirumala Bai, S.Srinath, P.S.Sai Prasad "Kinetic studies of the Oxidative Dehydrogenation of Ethane to Ethylene over a Cr_2O_3 on mixed oxide catalytic system" Published in the proceedings of International Conference ICMST 2016 at Kerala 5 -8,June 2016.

4. P.Thirumala Bai, V.Manokan, S.Srinath, P. S. Sai Prasad "Catalytic Evaluation of Oxidative Dehydrogenation of Ethane by Effect of Chromium Silica Catalyst" CHEMCON 2016 to be held at Chennai.

5. P.Thirumala Bai, T.Vishnu Kumar ,T.Vikram Sagar, S.Srinath, N.Lingaiah, P.S.Sai Prasad Kinetic Studies on Oxidative Dehydrogenation of Ethane with CO_2 on Cr_2O_3/Nb_2O_5 catalyst. Published in the proceedings of CHEMCON 2015 IIT Guwahati.

CATALYTIC ACTIVITY TABLES:

Catalyst Names	Input				output				
	Particle Size	React Flow (mL/min) (C_2H_6:CO_2:He)	Cr_2O_3 Loading	Temp ℃	X-C_2H_6 (%)	X-CO_2 (%)	S-C_2H_4 (%)	S-CH_4 (%)	Y-C_2H_4 (%)
Cr_2O_3/Al_2O_3	1000µm	15+15+30	5	650	20.12	11.37	45.79	55.15	9.58
			10	650	23	14.46	48.67	50.37	12.18
			15	650	31.96	21.58	47.15	52.25	15.36
			20	650	29.35	17.56	45.61	52.89	14.85
Cr_2O_3/ ZrO_2			15	650	41.52	38.05	35.67	14	41.52
Cr_2O_3/Al_2O_3-$ZrO_2$11	1000µm	15+15+30	15	650	35.04	28.11	56.84	44.76	21.07
Cr_2O_3/Al_2O_3-$ZrO_2$13				650	31.33	21.50	41.19	58.71	12.2
Cr_2O_3/Al_2O_3-$ZrO_2$31				650	26.0	21.03	48.95	51.85	12.16
Cr_2O_3/Al_2O_3-$ZrO_2$11	1000µm	15+10+35	15	650	26.30	20.74	52.00	49.09	13.76
		15+15+30		650	36.24	27.01	55.94	43.77	20.37
		15+20+25		650	30.12	18.80	50.16	51.34	14.78
		15+25+20		650	25.15	10.19	46.72	53.11	11.19
		15+45+0		650	25.15	10.19	46.72	53.11	11.19
Cr_2O_3/Al_2O_3-$ZrO_2$11	1000µm	15+15+30	15	650	16.97	16.97	48.19	49.81	12.8
	850µm			650	28.86	18.71	47.96	50.04	13.62
	500µm			650	35.51	25.13	55.12	42.88	19.50
	350µm			650	34.53	25.53	44.16	54.38	15.5
	212µm			650	34.62	25.92	32.99	65.01	11.45

Table.1.Non Silica Metal Oxide Chromia Catalyst

CATALYTIC ACTIVITY TABLES:

Table.2. 15% Cr_2O_3/ Al_2O_3-ZrO_2 (1:1) CO_2 flow variations:

Flow rate: 60 mL Catalyst wt: 1g Catalyst: 15% Cr_2O_3/ Al_2O_3-ZrO_2 (1:1)
Conditions: Feed: Ethane, CO_2 Temperature: 550^0C - 650^0C Pressure: 1bar

Catalyst	Temp	X-C_2H_6	X-CO_2	S-C_2H_4	S-CH_4	Y-C_2H_4	Y-CH_4
15%Cr_2O_3/Al_2O_3-ZrO_2(1:1)	550	7.82	2.54	49.68	48.32	3.47	3.35
C_2H_6:CO_2:He=15:10:35	600	12.39	7.27	51.12	46.88	5.98	5.41
	650	25.70	21.44	52.90	47.09	12.86	11.84
15% Cr_2O_3/Al_2O_3-ZrO_2 (1:1)	550	14.62	8.94	51.88	46.12	7.26	6.36
C_2H_6:CO_2:He=15:15:30	600	21.72	14.47	56.17	41.83	11.99	8.73
	650	35.04	28.11	55.24	42.76	19.27	14.77
15% Cr_2O_3/Al_2O_3-ZrO_2 (1:1)	550	12.12	7.07	49.07	48.93	5.57	5.55
C_2H_6:CO_2:He =15:20:25	600	18.03	11.45	49.38	48.62	8.58	8.44
	650	28.25	17.90	48.16	49.84	13.38	13.87
15% Cr_2O_3/Al_2O_3-ZrO_2 (1:1)	550	10.27	5.07	46.82	51.18	4.39	4.88
C_2H_6:CO_2:He =15:25:20	600	15.47	9.47	48.30	49.70	7.12	7.35
	650	26.63	14.57	48.07	49.93	12.56	13.07
15% Cr_2O_3/Al_2O_3-ZrO_2 (1:1)	550	8.95	3.26	45.73	52.27	3.65	4.30
C_2H_6:CO_2:He =15:45:0	600	14.48	5.49	46.45	51.55	6.34	7.13
	650	24.45	9.19	46.12	51.88	10.99	12.45

Table: 3. Oxidative dehydrogenation of ethane with CO_2 (Particle size):

Flow rate: 60 mL (15mL ethane + 15 mL CO_2 + 30 mL He)
Conditions: Feed: Ethane, CO_2 Temp: 550 ℃ - 650℃ Pressure:1bar Catalyst wt: 1g

Catalyst	Temp	X-C_2H_6	X-CO_2	S-C_2H_4	S-CH_4	Y-C_2H_4	Y-CH_4
15%Cr_2O_3/ Al_2O_3-ZrO_2 (1:1) Particle size=1000μm	550	9.47	5.02	48.046	51.954	4.55	4.92
	600	18.47	10.33	50.84	49.16	9.39	9.07
	650	17.97	17.97	49.19	50.81	13.8	14.25
15%Cr_2O_3/ Al_2O_3-ZrO_2 (1:1) Particle size=850μm	550	9.99	5.93	49.65	50.35	4.96	5.02
	600	18.03	9.69	49.36	50.64	8.90	9.13
	650	29.86	19.71	48.96	51.04	14.62	15.23

CATALYTIC ACTIVITY TABLES:

15%Cr_2O_3/ Al_2O_3-ZrO_2 (1:1) Particle size=500µm	550	14.38	10.85	51.81	48.19	7.45	6.93
	600	23.77	14.48	56.79	43.21	13.5	10.27
	650	36.51	26.13	56.12	43.88	20.50	16.01
15%Cr_2O_3/ Al_2O_3-ZrO_2 (1:1) Particle size=350µm	550	14.04	10.04	47.16	52.84	6.61	7.404
	600	22.9	12.29	48.03	51.97	11.0	11.9
	650	36.53	26.53	45.16	54.84	16.5	20.03
15%Cr_2O_3/ Al_2O_3-ZrO_2 (1:1) Particle size=212µm	550	14.21	10.26	29.55	70.45	4.2	10.01
	600	23.18	13.25	31.34	68.86	7.22	15.96
	650	36.62	26.92	33.99	66.01	12.45	24.17

Catalyst	**Temp ℃**	**X-C_2H_6**	**X-CO_2**	**S-C_2H_4**	**S-CH_4**	**Y-C_2H_4**	**Y-CH_4**	**C-Bal**
SBA-15	550	10.84	-	-	85.669	-	11.22	99.1
	600	14.44	3.57	-	82.74	-	11.94	95.4
	650	14.69	3.57	-	92.631	-	14.89	95.5
	700	10.83	4.46	-	92.10	-	11.23	95.7
SO_4-SBA-15	550	9.02	1.23	-	83.44	-	7.53	97.8
	600	3.74	0.31	-	78.60	-	2.94	99.4
	650	12.75	0.86	-	85.35	-	10.88	97.7
	700	12.75	1.54	-	91.92	-	11.72	97.2
Cr_2O_3/SBA-15	550	16.72	1.45	72.55	16.47	12.13	2.75	98.6
	600	27.05	2.90	74.25	15.29	20.08	4.13	97.1
	650	36.16	8.70	76.62	12.97	32.85	5.51	94
	700	45.28	7.25	76.98	14.61	36.50	6.93	93.8
Cr_2O_3/ SO_4 - SBA-15	600	24.37	4.29	82.43	14.3	20.08	3.5	96
	650	45.06	7.14	82.9	14.04	37.35	6.3	94
	700	61.24	8.59	82.2	14.3	50.33	8.7	97

Table.4. (i) SBA15 (ii) SO_4-SBA15 (iii) Cr_2O_3/SBA15 (iv) Cr_2O_3/ SO_4 -SBA15

CATALYTIC ACTIVITY TABLES:

Catalyst	T (℃)	Conversion		Selectivity			Yield			C-Bal
		C_2H_6	CO_2	C_2H_4	CH_4	CO	C_2H_4	CO	CH_4	
1.5g	600	15.64	4.17	75.12	16	8.8	11.25	1.3	2.5	98
	650	36.67	5.56	78.03	17.37	4.69	28.61	1.7	6.3	97
	675	43.59	9.72	78.03	17.68	4.29	34.03	1.8	7.7	95
3g	600	24.37	4.29	82.43	14.3	3.16	20.08	0.7	3.5	96
	650	45.06	7.14	82.9	14.04	3.05	37.35	1.3	6.3	94
	675	61.24	8.59	82.2	14.3	3.41	50.33	2.0	8.7	97
4.5g	600	28.69	6.38	74.75	17.9	6.59	21.45	1.8	5.15	95
	650	40.71	12.77	72.87	16.31	8.07	29.67	3.29	6.6	96
	675	68.38	15.96	69.42	15.53	7.43	47.47	5.08	10.62	91

Table.5. Catalyst weight variation for Cr_2O_3/ SO_4. SBA-15

Effects	Catalyst	Temp ℃	X-C_2H_6	X-CO_2	S-C_2H_4	S-CH_4	Y-C_2H_4	Y-CH_4	C-Bal
(3&9)Sulfate Effect Optimum 5% Cr_2O_3	$5Cr_2O_3/3SO_4$.SBA-15	600	7.43	1.59	-	82.14	-	6.10	97.4
		650	18.17	3.17	30.04	67.21	5.46	12.21	96.5
		675	25.45	4.76	48.97	46.34	13.19	12.21	95.7
	$5Cr_2O_3/9SO_4$.SBA-15	600	6.01	2.63	63.01	30.19	4.12	1.97	98.8
		650	17.64	5.26	66.75	28.01	11.77	4.97	95.4
		675	23.56	7.89	62.57	25.26	14.72	5.98	93.7
(2.5&7.5)Chromium Effect Optimum 6%SO_4	2.5% Cr_2O_3/ $6SO_4$. SBA-15	550	17.28	2.67	67.47	16.29	11.66	2.82	96.6
		600	32.30	4.00	67.13	16.68	21.68	5.39	95.1
		650	43.07	6.67	67.12	19.77	28.91	8.52	93.2
		675	46.15	9.33	66.65	19.07	30.72	8.80	91.0
	7.5% Cr_2O_3/ $6SO_4$. SBA-15	550	12.64	1.30	58.58	30.30	7.51	3.89	96
		600	24.99	6.49	60.93	28.35	15.57	7.25	94
		650	44.99	12.99	62.52	25.23	31.27	12.92	97
		675	47.21	15.56	64.04	19.91	30.24	9.40	95

Table.6. Cr_2O_3 and So^{4-} effects on Cr_2O_3/ SO_4 . SBA-15

CATALYTIC ACTIVITY TABLES:

Table.7: chromium oxide on sulfated SBA16 catalysts at 675 °C

T(℃)	X-C_2H_6	X-CO_2	S-C_2H_4	S-CO	S-CH_4	S-H_2	Y-C_2H_4	Y-CO	Y-CH_4	Y-H_2	C-Bal
550	16.80	1.43	71.93	5.48	22.58	-	12.39	0.94	3.89	-	98.4
600	33.33	4.29	70.16	5.55	24.30	-	23.95	2.52	8.30	-	95.8
650	54.16	8.57	67.08	6.98	23.95	2.33	36.95	3.78	12.97	1.25	91.2
675	62.44	10.00	66.23	6.72	19.62	2.22	41.35	5.89	15.59	1.93	90.0

Feed ratio: 1:6, Catalyst wt: 3g, Flows: 90 mL [9mL Ethane + 54 mL CO_2 + 27 mL He]

Catalyst	Temp ℃	X-C_2H_6	X-CO_2	S-$_2H_4$	S-CH_4	Y-C_2H_4	Y-CH_4	C-Bal
SBA16	550	9.84	-	-	75.5	-	12.97	95
	600	11.44	3.57	-	78.65	-	14.28	95
	650	11.69	3.57	-	79.67	-	13.75	95
	675	12.83	4.46	-	80.54	-	15.42	95
SO_4-SBA16	550	5.02	1.23	-	80.257	-	4.57	97
	600	6.74	0.31	-	84.57	-	3.51	99
	650	8.75	1.86	-	83.29	-	9.18	97
	675	10.75	1.54	-	85.47	-	10.42	97
Cr_2O_3/SBA16	550	17.72	1.45	72.55	56.74	12.13	3.41	98
	600	24.05	2.90	74.25	49.08	20.08	4.50	97
	650	33.16	8.70	76.62	59.87	32.85	5.65	94
	675	42.28	7.25	76.98	61.04	36.50	7.24	95
Cr_2O_3/ SO_4 - SBA16	550	16.80	1.43	71.93	36.58	12.39	4.8	96
	600	33.33	4.29	70.16	37.68	23.95	7.30	94
	650	54.16	8.57	67.08	35.47	36.95	10.97	96
	675	62.44	10.00	66.23	33.78	41.35	11.09	99

Table.8: SBA16 supported catalysts

CATALYTIC ACTIVITY TABLES:

weight	Temp ℃	Conversion		Selectivity			Carbon	
		C_2H_6	CO_2	C_2H_4	CH_4	C_2H_4	CH_4	
1.5g	600	20.84	5.47	65.12	15.4	10.25	3.1	98
	650	25.02	5.11	68.03	16.37	22.61	5.5	97
	675	30.57	6.17	68.03	16.08	24.03	6.7	95
3g	600	35.17	5.60	79.76	21.68	25	5	91
	650	46.20	7.87	72.08	22.71	26.57	6.57	92
	675	51.81	10.00	77.23	21.40	32.04	9.00	94
4.5g	600	33.33	4.29	60.16	37.68	23.95	7.30	94
	650	54.16	8.57	61.08	35.47	36.95	10.97	96
	675	48.04	10.00	64.45	33.78	41.35	11.09	99

Table.9. weight (1.5%-4.5%) variations of Cr_2O_3/6%SO_4^-/SBA-16

SAMPLE CALCULATIONS FOR ODH:

1. Wt: 3g Flow rate: 1:6 [9mL Ethane + 54 mL CO_2] 27mLHelium

Temp(ºC)	C_2H_6(mmol)	CH_4(mmol)	C_2H_4(mmol)	CO_2(mmol)
Room Temp	0.37	-	-	2.24
600	0.28	0.01	0.07	2.13
650	0.20	0.02	0.14	2.10
675	0.14	0.03	0.13	2.19

(a). Initial at room Temperature :

C_2H_6 (mmol) = {C_2H_6 GC count (11) / 302.3 const *5.05(off gas L/ hr)/500}*1000 =0.37

CO_2 (mmol) = {CO_2 GCcount (70) * 315.5 const * 5.05 (off gas L/ hr)/500}* 1000 = 2.24

At 600ºC C_2H_6 (mmol) = {C_2H_6 count (8) / 302.3 const *5.05(off gas L/ hr)/500}*1000 = 0.28

CO_2 (mmol) = {CO_2 count (67) /315.5 const * 5.05 (off gas L/ hr)/500}* 1000 = 2.13

CH_4 (mmol) = CH_4count (1.30) /1000.82const * 5.05 (off gas L/ hr)/500}* 1000 = 0.01

C_2H_4=CH_4count (2.25) /302.5const * 5.05 (off gas L/ hr)/500}* 1000 =0.07

Conversion of Ethane (C_2H_6) = [C_2H_6 (mmol) at room temp - C_2H_6 (mmol) at 600 ºC] / C_2H_6 (mmol) at room temp

= [0.37-0.28]/0.37 *100 = 24.324

Yield of C_2H_4 = [C_2H_4 (mmol) at 600 ºC/ C_2H_6 (mmol) at room temp] *100 = [0.07]/[0.37] *100 = 18.918

Selectivity of C_2H_4 = [Yield of C_2H_4 / Conversion of Ethane]*100 = [18.918]/[24.324] * 100 = 77.7

CATALYTIC ACTIVITY TABLES:

VII.Calibration:

Instrument calibration is an essential stage in most measurement procedures. It is a set of operations that establish the relationship between the output of the measurement system (e.g.,the response of an instrument) and the accepted values of the calibration standards (e.g., the amount of analyte present). A large number of analytical methods require for the calibration of an instrument. This typically involves the preparation of a set of standards containing a known amount of the analyte of interest, measuring the instrument response for each standard and establishing the relationship between the instrument response and analyte concentration. this relationship is then used to transform measurements made on test samples into estimates of the amount of analyte present, as calibration is such a common and important step in analytical methods, it is essential that analysts have a good understanding of how to set up calibration experiments and how to evaluate the results obtained.

(A).Ethylene:

mL/min	100	80	60	40	20	0
mmole	0.00446	0.003	0.002	0.001	0.0008	0

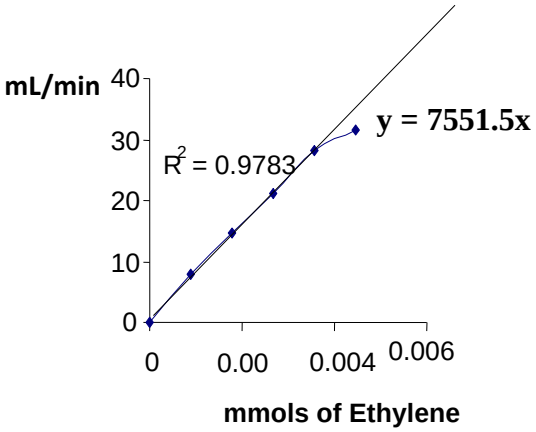

Figure.1. Scatter plot of instrument response data versus concentration

CATALYTIC ACTIVITY TABLES:

(B). Ethane:

ml/min	400	300	200	150	100	80	60	40	20	0
mmol	0.0178	0.0133	0.0089	0.066	0.004	0.0035	0.026	0.0017	0.0008	0

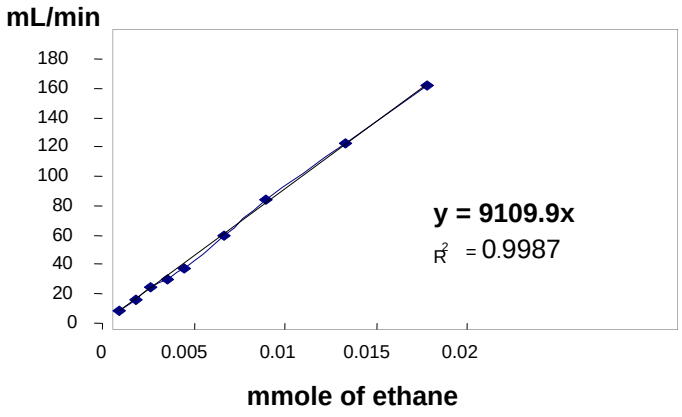

Figure.2. Scatter plot of instrument response data versus concentration

(C). Carbon dioxide:

ml/min	300	200	150	100	80
mmole	0.013	0.008	0.006	0.004	0.003

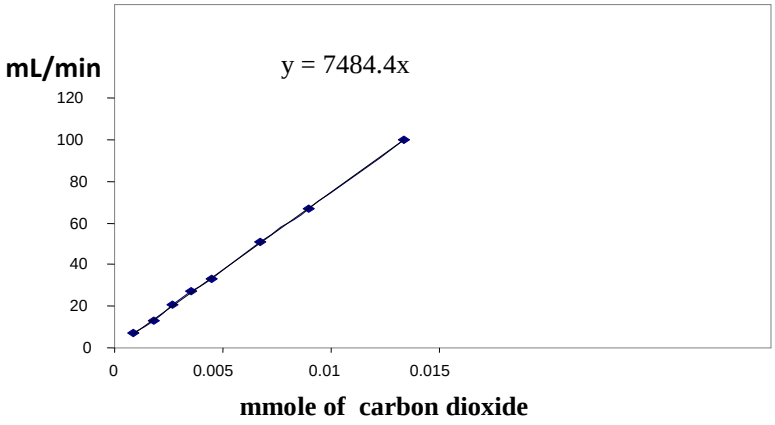

Figure.3. Scatter plot of instrument response data versus concentration

CATALYTIC ACTIVITY TABLES:

(D). Methane:

mL/min	0.5	0.6	0.7	0.8	0.9	1.0
mmole	11.6	17.1	21.7	34.3	40.4	46.9

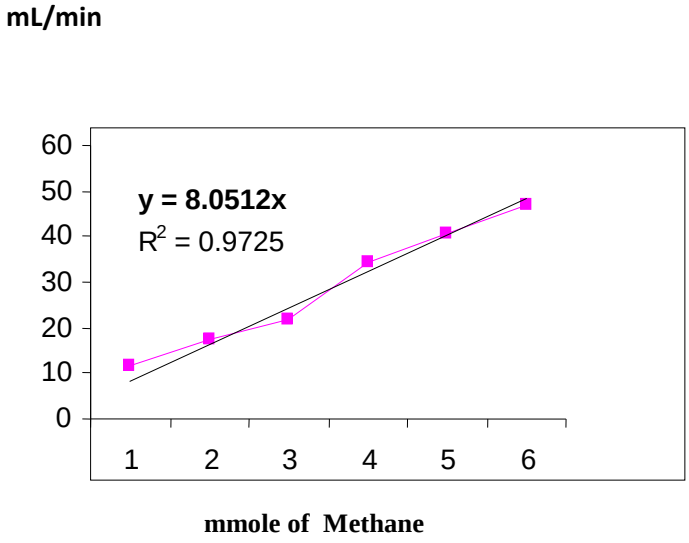

Figure.4. Scatter plot of instrument response data versus concentration